

# **Catalytic Behaviour of Ti Doping on Mg<sub>n</sub> Clusters and MgO Supported TiMg<sub>n</sub> Systems for Hydrogen Storage: A Density Functional Theory Investigation**

*Thesis*

Submitted in partial fulfillment of the requirements for the degree of

*Doctor of Philosophy*

by

*Soham Chatterjee*

2018PHXF0413P

*Under the Supervision of*

*Prof. Debashis Bandyopadhyay*



**BIRLA INSTITUTE OF TECHNOLOGY & SCIENCE PILANI**

**PILANI, RAJASTHAN, INDIA**

**2024**

**BIRLA INSTITUTE OF TECHNOLOGY AND SCIENCE, PILANI**

**CERTIFICATE**

This is to certify that the thesis entitled “Catalytic Behaviour of Ti Doping on  $Mg_n$  Clusters and MgO Supported  $TiMg_n$  Systems for Hydrogen Storage: A Density Functional Theory Investigation” and submitted by Soham Chatterjee, ID No-2018PHXF0413P for award of Ph.D. of the Institute embodies original work done by him under my supervision.

Dated:

Supervisor

(Prof. Debashis Bandyopadhyay)

Department of Physics

BITS, Pilani, Pilani Campus

Rajasthan-333031, India

*Dedicated to .....*

*My Parents*

## ACKNOWLEDGEMENTS

The author welcomes the opportunity to express his deep sense of gratitude and indebtedness to his supervisor Prof. Debashis Bandyopadhyay, Department of Physics, Birla Institute of Technology, Pilani for his able guidance, sympathetic cooperation, optimistic encouragement and overall supervision throughout the tenure of the work. The author is thankful to Prof. Rakesh Choubisa, Head of the Department of Physics, Birla Institute of Technology, Pilani for extending all the facilities for pursuing research. The author is sincerely thankful to his DAC members Prof. Anshuman Dalvi and Prof. Niladri Sarkar for their valuable suggestions and encouragement in pursuing the work. The author takes the occasion to express his heartfelt thanks to Prof. Navin Singh, Prof. Rishikesh Vaidya, Prof. Raj Kumar Gupta, Prof. Manjuladevi V., Prof. Jayendra Nath Bandyopadhyay, Prof. Kaushar Vaidya, and other Professors of the Department of Physics for their cooperation. Especially the author is grateful to Prof. V. Ramgopal Rao, VC, Prof. Sudhirkumar Barai, Director, Deans and Asso. Deans for their support and encouragement without which the dissertation would never be completed. The author is thankful to Mr. Rajiv Gaur and Mr. Shrikant Sharma for constant help all time. The author is thankful to the Department of Science and Technology, Government of India for providing partial financial assistance in carrying out the work. The author is thankful to the authorities of BITS for providing me institution fellowship for completing my research work.

Finally, the author expresses his gratitude to his parents without whose patience and unlimited sacrifices it would not be possible for him to think of any research work. Particularly he wishes to recall the affectionate supervision of his father Prof. Samarendra Nath Chatterjee who was instrumental with advice and suggestion to see the author successful in each and every step of his life.

**Soham Chatterjee**

Date

## ABSTRACT

---

The planet is now facing a possible catastrophic situation due to an imbalance between energy demand and energy supply on one side and ever-increasing environmental degradation on the other. World leaders, scientists and industrialists decided to switch over from fossil fuel to nonconventional, clean, environment-friendly sustainable energy sources like wind energy, solar energy, biomass energy, fuel cells etc. Due to the inherent problem of fluctuation of wind and solar energy production-sustainability, they are questionable for the attainment of a constant and steady supply from these renewable energy sources. Hydrogen emerges to be an alternative source of energy with a high energy density of  $\sim 142$  MJ/Kg, clean, environment friendly and at a competitive cost. The main challenge of hydrogen energy is due to storage and transportation. Compressed gas requires high pressure, high cost and high risk of leakage. Liquid hydrogen requires cryogenic temperature and high pressure. Solid state materials like Zeolites, MOFs, COFs, BN nanotubes, CWNT, SWNT etc. either suffer from low gravimetric density or requirement of low temperature and high pressure or non-reversibility, non-recyclability etc. issues. Magnesium hydrides offer favorable thermodynamic properties, high gravimetric density ( $\sim 7.6$  wt %), absorption at moderate temperature and pressure, safe and cost-effective but suffer from limited reversibility, high desorption temperature, and high activation barrier. With the advent of nanoclusters with their size-dependent tuning of thermodynamic and electronic properties, researchers hope for the possibility of effective hydrogen storage material with doped metal clusters.

The thesis systematically examined pure and Ti-doped (both endohedrally and exohedrally) magnesium clusters and their isomers from size  $n=2$  to 20 to find the global minimum structures. It reports that  $\text{TiMg}_8$  is a Magic cluster with a 20-electron cell closing structure with high stability and low reactivity. The  $\text{TiMg}_5$  emerges to be the most suitable cluster with all favorable hydrogen storage properties. Due to the catalytic effect of Ti doping the activation barrier drops by 32.8%, and gravimetric density increases from 1.63 wt.% for the pure  $\text{Mg}_5$  cluster to 3.45 wt.% for the  $\text{TiMg}_5$  cluster. MgO supported  $\text{TiMg}_5$  Cluster shows enhanced gravimetric density  $\sim 62.89$  wt.% with higher stability and greater recyclability due to catalytic effect of Ti doping and MgO support.

# TABLE OF CONTENTS

<i>Acknowledgements</i>	<i>IV</i>
<i>Abstract</i>	<i>V</i>
<i>Table of Contents</i>	<i>VI</i>
<i>List of Tables</i>	<i>XI</i>
<i>List of Figures</i>	<i>XII</i>
<i>List of Abbreviations</i>	<i>XV</i>
<b><i>1. Chapter-1-Introduction</i></b>	<b><i>1-31</i></b>
1.1. Preamble . . . . .	1
1.2. Energy Scenario today . . . . .	2
1.3. Hydrogen: The Alternative . . . . .	2
1.3.1. Prospects . . . . .	2
1.3.2. Challenges . . . . .	3
1.4. Solid State Hydrogen Storage Materials: The Challenges . . . . .	4
1.5. The possible solution: The Atomic Clusters . . . . .	6
1.5.1. Nanoparticles and nanoclusters . . . . .	7
1.5.2. Why do nanoclusters show unusual properties? . . . . .	7
1.6. Literature Survey: . . . . .	8
1.6.1. Literature Survey: Why Magnesium Clusters? . . . . .	8
1.6.2. Literature Survey: Why is Doping required? . . . . .	9
1.7. Research gap . . . . .	11
1.8. The Objectives of the Thesis . . . . .	11
1.9. The Mechanism . . . . .	11
1.9.1. Enhancement of stability and efficiency of hydrogen storage: Substrate Support . . . . .	13

1.10.	<i>Chapter wise Organization of the Thesis</i>	14
	<i>References</i>	17
<b>2.</b>	<b><i>Chapter-2-Methodology</i></b>	<b>32-52</b>
2.1.	<i>Introduction</i>	32
2.2.	<i>Theoretical Approach of Quantum Chemistry Calculations</i>	32
2.2.1.	<i>Quantum Theories and Ideas of Multielectron System</i>	32
2.2.2.	<i>Born-Oppenheimer Approximation</i>	34
2.2.3.	<i>Hartree Fock Theory</i>	36
2.2.4.	<i>Density Functional Theory</i>	38
2.2.4.1.	<i>Hohenberg-Kohn (H-K) Theorem</i>	38
2.2.4.2.	<i>The Second Hohenberg and Kohn (H-K) Theorem</i>	40
2.2.4.3.	<i>Kohn-Sham Equations</i>	41
2.2.5.	<i>Exchange Correlation Functional</i>	43
2.2.5.1.	<i>Local Density Approximation (LDA)</i>	43
2.2.5.2.	<i>Local Spin Density Approximation (LSDA).</i>	44
2.2.5.3.	<i>Generalized -Gradient Approximation (GGA)</i>	44
2.2.6.	<i>Basis Set</i>	45
2.2.7.	<i>Plane Wave Basis Set</i>	45
2.2.8.	<i>Self-Consistent Field (SCF)</i>	46
2.2.9.	<i>B3LYP</i>	47
2.3.	<i>Computational Methodology</i>	47
2.3.0.	<i>Gaussian'09, GaussView&amp; MultiWaveFunction</i>	47
2.3.1.	<i>Gaussian'09</i>	47
2.3.2.	<i>GaussView</i>	48
2.3.3.	<i>MultiWaveFunction</i>	48
	<i>References</i>	49

<b>3. Chapter-3-The Electronic Structures and Properties of <math>Mg_n</math> (<math>n=2-20</math>) Nanoclusters: A Density Functional Investigation</b>	<b>53-81</b>
3.1. Introduction . . . . .	53
3.2. Computational Methodology . . . . .	55
3.3. Results and Discussion . . . . .	56
3.3.1. Growth Pattern of Pure Magnesium Nanoclusters $Mg_n$ ( $n=2-20$ ) . . . . .	56
3.3.2. Relative Stability of Clusters . . . . .	60
3.3.2.1. Average Binding Energy and Stability of the Pure $Mg_n$ ( $n=2-20$ ). Clusters . . . . .	60
3.3.3. HOMO-LUMO gap . . . . .	63
3.3.4. Vertical Ionization Potential (VIP), Vertical Electron Affinity (VEA), Chemical Potential ( $\mu$ ) and Chemical Hardness ( $\eta$ ) . . . . .	65
3.3.5. HOMO-LUMO Orbital Study of Nanoclusters . . . . .	71
3.3.6. Molecular Electrostatic Potential and Total Electron Density Mapping . . . . .	71
3.4. Summary and Conclusions . . . . .	73
References. . . . .	76
<b>4. Chapter-4-Systematic Study of Ti Doped Magnesium (<math>TiMg_n</math>) (<math>n=2-20</math>) Clusters: A Density Functional Approach</b>	<b>82-129</b>
4.1. Introduction . . . . .	82
4.2. Computational Methodology . . . . .	85
4.3. Results and Discussion . . . . .	86
4.3.1. Growth Pattern of Magnesium Nanoclusters in Pure and Doped Form . . . . .	86
4.3.2. Relative Stability . . . . .	91
4.3.3. Electronic Properties . . . . .	96
4.3.3.1. HOMO-LUMO . . . . .	96
4.3.3.2. Reactivity Indicators . . . . .	98
4.3.4. Molecular Electrostatic Potential (MEP) and Total Electron Density Contours . . . . .	103



4.3.5. Mulliken Charge Distribution Between Ti Atom and Mg Atoms . . . . .	105
4.3.6. Electrostatic Dipole-moment and Polarizability of $TiMg_n$ Clusters . . . . .	106
4.3.7. Population Analysis . . . . .	107
4.3.8. Electron Localization Function (ELF) . . . . .	110
4.3.9. Critical Points (CP's) of $TiMg_8$ Cluster . . . . .	112
4.3.10. Nucleus Independent Chemical Shift (NICS) of $TiMg_8$ Cluster. . . . .	113
4.3.11. IR and Raman Spectra of the Doped Clusters . . . . .	115
4.4. Summary and Conclusions . . . . .	118
References . . . . .	120
<b>5. Chapter-5-Catalytic Effect of Ti Doping on Hydrogenation of <math>Mg_n</math> (<math>n=2-8</math>) Nanoclusters: A Density Functional Study</b>	<b>130-169</b>
5.1. Introduction . . . . .	130
5.2. Computational Methodology . . . . .	134
5.3. Results and Discussion . . . . .	135
5.3.1. The Structures . . . . .	135
5.3.1.1. Growth of Pure $Mg_n$ Clusters . . . . .	135
5.3.1.2. Growth of $Mg_{n-2}H$ ( $n=2-8$ ) . . . . .	137
5.3.1.3. Growth Pattern of $TiMg_n$ ( $n=2-8$ ) Clusters . . . . .	137
5.3.1.4. Growth Pattern of Hydrogenated $TiMg_n$ ( $n=2-8$ ) Clusters . . . . .	139
5.3.2. Thermodynamic and Electronic Properties of $Mg_{n-2}H$ and $TiMg_{n-2}H$ ( $n=2-8$ ) Nanoclusters . . . . .	140
5.3.3. Adsorption Energy ( $E_{ads}$ ) . . . . .	148
5.3.4. Chemisorption Energy . . . . .	149
5.3.5. Electron Localization Function (ELF) . . . . .	151
5.3.6. Mechanism of Catalytic Activity of Ti on Hydrogenation/Dehydrogenation of $TiMg_5$ Cluster . . . . .	154
5.3.7. Intrinsic Reaction Coordinate (IRC) . . . . .	155

5.4. Gravimetric Density of Hydrogen Storage . . . . .	157
5.5. Summary and Conclusions . . . . .	158
References . . . . .	161
<b>6. Chapter-6-Hydrogen Storage on MgO Supported TiMg<sub>n</sub> (n=2-6) Clusters: A First Principle Investigation</b>	<b>170-197</b>
6.1. Introduction . . . . .	170
6.2. Computational Methodology . . . . .	171
6.3. Results and Discussions . . . . .	172
6.3.1. Adsorption/ Desorption Energies . . . . .	177
6.3.2. HOMO-LUMO Gap . . . . .	178
6.3.3. Vertical Ionization Potential (VIP), Vertical Electron Affinity (VEA), Chemical Hardness ( $\eta$ ), and Chemical Potential ( $\mu$ ) . . . . .	179
6.3.4. Electron Localization Function (ELF) . . . . .	181
6.3.5. Hydrogen Dissociation and Drifting of Hydrogen Atoms to Reactive Sites . . . . .	185
6.3.6. Gravimetric Density Enhancement . . . . .	186
6.3.7. Binding Energy . . . . .	189
6.3.8. Relative Stability. . . . .	190
6.3.9. Reaction Energy and Activation Barrier Energy calculations . . . . .	190
6.4. Summary and Conclusions . . . . .	192
References . . . . .	194
<b>7. Chapter-7 Conclusions and Scope for Future Work</b>	<b>198-201</b>
<b>LIST OF PUBLICATIONS OF THE AUTHOR</b>	<b>202</b>
<b>LIST OF PRESENTATIONS</b>	<b>202</b>
<b>SEMINAR / WORKSHOP PARTICIPATED</b>	<b>203</b>
<b>BIOGRAPHY OF THE AUTHOR</b>	<b>204</b>
<b>BIOGRAPHY OF THE SUPERVISOR</b>	<b>205</b>

## **List of Tables**

<i>Table No</i>	<i>Title of Table</i>	<i>Page No</i>
<i>Table 3.1</i>	<i>Average bond length (Mg-Mg) for Mg<sub>n</sub> (n=2-20) pure clusters in (Å)</i>	<i>60</i>
<i>Table 3.2</i>	<i>Thermodynamic, Electronic and Chemical properties of Mg<sub>n</sub> (n=2-20) in eV.</i>	<i>69</i>
<i>Table 4.1</i>	<i>Comparison between the present work with experimental bond lengths and lowest frequency in different dimmers</i>	<i>86</i>
<i>Table 4.2</i>	<i>Average bond length and nearest neighbor distance in (Å)</i>	<i>90</i>
<i>Table 4.3</i>	<i>Average Binding energy per atom in eV, Fragmentation energy (FE) in eV and HOMO-LUMO gap in eV for Mg<sub>n</sub> and TiMg<sub>n</sub> (n=2-20) clusters.</i>	<i>95</i>
<i>Table 4.4</i>	<i>Vertical Ionization Potential (VIP) and Vertical Electron Affinity (VEA), Chemical Hardness (<math>\eta</math>) and Chemical Potential (<math>\mu</math>) in eV of TiMg<sub>n</sub> Clusters (Anion-Cation method).</i>	<i>102</i>
<i>Table 4.5</i>	<i>Variation of Charge transfer, Dipole moment, Polarizability and vibrational frequency of TiMg<sub>n</sub> with cluster size (n).</i>	<i>107</i>
<i>Table 4.6</i>	<i>Natural electronic configuration of Ti and Mg atoms in TiMg<sub>n</sub> (n=2-20).</i>	<i>109</i>
<i>Table 4.7</i>	<i>Frequency (cm<sup>-1</sup>) of IR and Raman spectra of TiMg<sub>n</sub> (n=1-12). The bold frequency values are the dominating mode in IR and Raman respectively</i>	<i>117</i>
<i>Table 5.1</i>	<i>Variation of av. BE (eV), Stability (eV), and HOMO-LUMO Energy Gap (eV)</i>	<i>144</i>
<i>Table 5.2</i>	<i>Variation of VIP, VEA, Chem. Pot., Chem. Hardness in eV with the size of the cluster</i>	<i>147</i>
<i>Table 6.1</i>	<i>Calculated data of various parameters associated with the supported clusters. All units are in eV.</i>	<i>186</i>
<i>Table 6.2</i>	<i>Comparative stability study in (eV) of Mg<sub>n</sub> clusters. All units are in eV</i>	<i>190</i>

## **List of Figures**

<i>Figure No</i>	<i>Title of Figure</i>	<i>Page No</i>
<i>Fig. 1.1</i>	<i>Pictorial view of the process of hydrogenation and dehydrogenation in hydrogen storage cluster systems.</i>	12
<i>Fig. 3.1</i>	<i>Optimized ground state structures of pure Mg<sub>n</sub> (n=2-20) clusters with point group symmetry. All the pink balls are Magnesium atoms.</i>	57
<i>Fig. 3.2</i>	<i>Variation of average binding energy per atom with cluster size.</i>	61
<i>Fig. 3.3</i>	<i>Variation of stability and fragmentation energy with cluster size.</i>	63
<i>Fig. 3.4</i>	<i>Variation of HOMO-LUMO gap with size of clusters.</i>	64
<i>Fig. 3.5(a)</i>	<i>Variation of VIP and VEA with cluster size for both anionic-cationic methods and Koopmans method.</i>	67
<i>Fig. 3.5(b)</i>	<i>Variation of VIP and VEA with cluster size (Koopmans method).</i>	68
<i>Fig. 3.6</i>	<i>Variation of chemical hardness and chemical potential with the size of cluster.</i>	68
<i>Fig. 3.7</i>	<i>HOMO and LUMO surface of pure Mg<sub>n</sub> cluster.</i>	70
<i>Fig. 3.8</i>	<i>MEP and total electron density of pure Mg<sub>n</sub> (n =2-20) clusters.</i>	72
<i>Fig. 4.1</i>	<i>Optimized global GS TiMg<sub>n</sub> (n=2-20) clusters.</i>	88
<i>Fig. 4.2</i>	<i>Variation of bond length (Ti-Mg and Mg-Mg) of TiMg<sub>n</sub> (n=2-20) clusters with cluster size (n).</i>	91
<i>Fig. 4.3</i>	<i>Average binding energy and embedding energy of global GS TiMg<sub>n</sub> (n=2-20) clusters.</i>	93
<i>Fig. 4.4</i>	<i>Second order changes in energy and fragmentation energy of TiMg<sub>n</sub> (n=2-20) clusters with cluster size (n).</i>	93
<i>Fig. 4.5</i>	<i>Representation of HOMO-LUMO surfaces of TiMg<sub>n</sub>.</i>	97
<i>Fig. 4.6</i>	<i>Variation of HOMO-LUMO energy gap of Mg<sub>n</sub> and TiMg<sub>n</sub> (n=2-20) clusters with cluster size (n).</i>	98
<i>Fig. 4.7(a)</i>	<i>Variation of VIP and VEA of TiMg<sub>n</sub> (n=2-20) clusters with cluster size (n). (Koopman)</i>	100
<i>Fig. 4.7(b)</i>	<i>Variation of VIP and VEA of TiMg<sub>n</sub> (n=2-20) clusters with cluster size (n). (Anion-cation method)</i>	100
<i>Fig. 4.8(a)</i>	<i>Variation of chemical hardness and chemical potential of TiMg<sub>n</sub> (n=2-20) clusters with cluster size (n) (Koopman)</i>	101
<i>Fig. 4.8(b)</i>	<i>Variation of chemical hardness and chemical potential of TiMg<sub>n</sub> (n=2-20) clusters with cluster size (Anion Cation Method)</i>	101

Fig. 4.9	Contour of electrostatic potential and electron density of $TiMg_n$ .	104
Fig. 4.10	Variation of average charge on Ti and on Mg atom in coulombs with cluster size ( $n$ ).	105
Fig. 4.11	Variation of electrostatic dipole moment and polarizability with cluster size ( $n$ ).	106
Fig. 4.12	Representation of ELF-2D map of $TiMg_8$ cluster.	111
Fig. 4.13	(a) represents (3, -1) bond critical point and (b) represents (3, -3) atomic critical points of $TiMg_8$ cluster.	113
Fig. 4.14	Variation of Nucleus-independent chemical shift (NICS) of $TiMg_8$ cluster with the distance from the center of the cluster.	114
Fig. 4.15	IR and Raman spectrum of different ground state isomer of $TiMg_n$ ( $n=1-12$ ).	116
Fig. 5.1	Optimized global minimum structures of pure, doped, $Mg_n-2H$ ( $n=2-8$ ) and $TiMg_n-2H$ ( $n=2-8$ ) clusters.	136
Fig. 5.2	Pictorial view of the growth pattern of $TiMg_n$ ( $n=2-8$ ) clusters.	138
Fig. 5.3	Pictorial view of the growth pattern of hydrogenated $TiMg_n$ ( $n=2-8$ ) clusters.	139
Fig. 5.4(a)	Binding energy variation of $Mg_n$ and $Mg_n-2H$ clusters.	141
Fig. 5.4(b)	Binding energy variation of $TiMg_n$ and $TiMg_n-2H$ clusters with cluster size.	142
Fig. 5.5(a)	The variation of stability of $Mg_n-2H$ and $Mg_n$ clusters.	143
Fig. 5.5(b)	The variation of stability of $TiMg_n-2H$ and $TiMg_n$ clusters with the growth of the clusters.	143
Fig. 5.6(a)	The variation of VIP and VEA of $Mg_n-2H$ and $Mg_n$ clusters.	145
Fig. 5.6(b)	The variation of VIP and VEA of $TiMg_n-2H$ and $TiMg_n$ clusters with the growth of the clusters.	145
Fig. 5.7(a)	The variation of Chem.Hard and Chem.Pot of $Mg_n-2H$ and $Mg_n$ clusters.	146
Fig. 5.7(b)	The variation of Chem.Hard and Chem.Pot of $TiMg_n-2H$ and $TiMg_n$ clusters with the growth of the clusters.	147
Fig. 5.8	Variation of $H_2$ adsorption energy with cluster size( $n$ ).	149
Fig. 5.9	The variation of chemisorption energy of $Mg_n-2H$ and $TiMg_n-2H$ with the growth of the clusters.	150
Fig. 5.10	Behavior of ELF (with contour) of $Mg_5$ , $Mg_5-2H$ , $TiMg_5$ , and $TiMg_5-2H$ .	153
Fig. 5.11	3D representation of ELF of $TiMg_5-2H$ .	153
Fig. 5.12	IRC path for the transition from reactant to product via transition state (TS) of $H_2+TiMg_5$ (reactant) to $TiMg_5-2H$ (product).	156
Fig. 5.13	Highest possible $H_2$ adsorption in $TiMg_5$ clusters systems.	157

Fig. 5.14	<i>The rejection of extra H<sub>2</sub> molecules by the cluster. Mg<sub>5</sub>-2H cannot adsorb one more H<sub>2</sub> molecule where TiMg<sub>5</sub> cluster is throwing the 4<sup>th</sup> hydrogen molecule away.</i>	158
Fig. 6.1	<i>Rectangular Mg<sub>18</sub>O<sub>18</sub> substrates.</i>	173
Fig. 6.2	<i>Other rejected substrates.</i>	173
Fig. 6.3	<i>Guess and optimized substrate supported pure Mg<sub>n</sub> and Mg<sub>n</sub>-2H clusters system.</i>	174
Fig. 6.4	<i>Guess and optimized substrate supported TiMg<sub>n</sub> and TiMg<sub>n</sub>-2H clusters system.</i>	175
Fig. 6.5	<i>Mg<sub>18</sub>O<sub>18</sub> substrate supported Mg<sub>n</sub>, TiMg<sub>n</sub>, Mg<sub>n</sub>-2H, TiMg<sub>n</sub>-2H clusters, E<sub>ads</sub> energy(eV) between the substrate and clusters Mg<sub>n</sub> and TiMg<sub>n</sub>; E<sub>ads-H</sub> energy between the supported clusters and adsorbed hydrogen.</i>	176
Fig. 6.6	<i>Variation of adsorption energy and HOMO-LUMO gaps of supported Mg<sub>n</sub>, Mg<sub>n</sub>-2H, TiMg<sub>n</sub> and TiMg<sub>n</sub>-2H clusters system.</i>	178
Fig. 6.7	<i>Variation of VIP and VEA of different supported clusters: (a) VIP of supported Mg<sub>n</sub> and Mg<sub>n</sub>-2H, (b) VIP of supported TiMg<sub>n</sub>, and TiMg<sub>n</sub>-2H, (c) VEA of supported Mg<sub>n</sub> and Mg<sub>n</sub>-2H, (d) VEA of supported TiMg<sub>n</sub>, and TiMg<sub>n</sub>-2H.</i>	179
Fig. 6.8	<i>Variation of <math>\mu</math> and <math>\eta</math> of different supported clusters: (a) <math>\eta</math> of supported Mg<sub>n</sub> and Mg<sub>n</sub>-2H, (b) <math>\eta</math> of supported TiMg<sub>n</sub>, and TiMg<sub>n</sub>-2H, (c) <math>\mu</math> of supported Mg<sub>n</sub> and Mg<sub>n</sub>-2H, (d) <math>\mu</math> of supported TiMg<sub>n</sub>, and TiMg<sub>n</sub>-2H.</i>	181
Fig. 6.9	<i>The nature of electron localization (ELF) of different pure Mg<sub>n</sub>, hydrogenated pure Mg<sub>n</sub>, Ti doped Mg<sub>n</sub> and hydrogenated Ti-doped Mg<sub>n</sub> clusters (n=2-6). ELF of the substrate supported TiMg<sub>5</sub>-2H from front and back side of the whole system.</i>	182- 184
Fig. 6.10	<i>Hydrogen adsorption and dissociation on the reactive surface of supported TiMg<sub>5</sub>. Different stages of drifting of the dissociated hydrogen atoms with atomic separation in Å are shown. ELF of supported TiMg<sub>5</sub>-2H at the final state.</i>	187
Fig. 6.11	<i>Highest possible H<sub>2</sub> adsorption in pure Mg<sub>5</sub>, TiMg<sub>5</sub>, and supported TiMg<sub>5</sub> cluster systems. Here, Mg atoms are colored by pink, oxygen atoms are shaded as green, Ti as blue and hydrogen as yellow.</i>	188
Fig. 6.12	<i>Repelling of additional hydrogen molecule beyond the dose limit. Here, Mg atoms are colored by pink, Ti as blue and hydrogen as yellow.</i>	189
Fig. 6.13	<i>The activation barrier energy for successive H<sub>2</sub> adsorption in bare TiMg<sub>5</sub> (blue) and substrate-supported TiMg<sub>5</sub> cluster systems (red).</i>	191

## *List of abbreviations*

<b>Abbreviation</b>	<b>Used for</b>
$\mu$	Chemical Potential
$\Delta_2$	Relative Stability
B3LYP	Becke, 3-parameter, Lee-Yang-Parr
BE	Binding Energy
CNT	Carbon Nano Tube
COFs	Covalent Organic Frameworks
CP	Critical Point
DFT	Density Functional Theory
DOS	Density of States
ECP	Effective Core Potential
EE	Embedding Energy
EJ	Exajoule
ELF	Electron Localization Function
FE	Fragmentation Energy
GGA	Generalized Gradient Approximation
GNF	Graphite Nano Fiber
HOMO	Highest Occupied Molecular Orbital
IEA	International Energy Agency
IRC	Intrinsic Reaction Coordinate
LCAO	Linear Combination of Atomic Orbitals
LDA	Local Density Approximation
LUMO	Lowest Unoccupied Molecular Orbital
MEP	Molecular Electrostatic Potential
MOFs	Metal Oxide Frameworks
MWCNT	MultiWalled Carbon Nano Tubes
$\eta$	Chemical Hardness
NBO	Natural Bond Orbital
NICS	Nucleus independent Chemical Shift
SCF	Self-Consistent Field
SWNT	Single Walled Nano Tubes
TED	Total Electron Density
TS	Transition State
VEA	Vertical Electron Affinity
VIP	Vertical Ionization Potential
WW	Wigner Witmer

# CHAPTER-1

## INTRODUCTION

### 1.1 Preamble

In the era of fast-growing civilization, the energy demand throughout the world is rising. According to the BP Statistical Review of world energy [1], the rising figure is ~ 5.8% in 2021. Fossil fuel remains the primary energy source covering about 82% of energy supplies and 90% of mobile transportation. The primary concern with the use of fossil fuels is climate change of the world. During consumption, fossil fuel releases CO<sub>2</sub>, NO<sub>x</sub> and SO<sub>x</sub> gases into the atmosphere, contributing to global warming and a non-habitable environment. The CO<sub>2</sub> level is now 50% higher than in the preindustrial age. World temperature rises ~1.1°C each year. The ancient prayer from Rikveda to the almighty is worth mentioning in this context

मधु वाता ऋतायते मधुक्षरन्ति सिन्धवः। माध्वीर्नः सन्त्वौषधीः॥

मधु नक्तमुतोषसि मधुमत्पार्थिवं रजः। मधुद्यौरस्तु न पिता॥

मधुमात्रो वनस्पतिर्मधुमाँ अस्तु सूर्यः। माध्वीर्गावो भवन्तु नः॥ शुक्त-90-ऋग्वेद॥ [2]

In English letters

*Madhu vātā ritāyate Madhu ksharanti sindavah,*

*Madhvīr nah santvoshadhīh.*

*Madhu naktam utoshasi Madhumat pāarthivam rajah,*

*Madhu dyaurastu nah pitā.*

*Madhumānno vanaspatih Madhumām astu sūryah,*

*Mādhvīr gāvo bhavantu nah. u Sukta 90-Rikveda u*

The “Sloka” of Rikveda is an absolute perception of a beautiful habitable planet. The “Sloka” is a prayer to the almighty for a pollution-free environment with clean air, water and soil, a prayer for a pollution-free sky and pure radiation from Sun, pollution-free fruits and vegetables from trees and vegetation, a prayer for mother nature’s biomedicines from plants



and herbs, and a prayer for milk from cows of its own natural quality. The “sloka” is an active realization of a habitable ecosystem for maintaining cosmic order and harmony.

The realization of the truth is reflected in the bold decisions of some countries. Many countries and international organizations have set the target for transitioning from fossil fuel to alternative, cleaner and sustainable energy sources to address the urgent challenges of climate change.

## ***1.2 The Energy Scenario Today***

According to BP statistical review [1], in 2019-2021, renewable energy production increased by 8 EJ (1 ExaJoule=108 J). Fossil fuel consumption has decreased by ~3% over the last five years. It is worth noting that India has committed to reducing its reliance on fossil fuels by transitioning to solar energy and wind energy by investing more in the sector. India has the world's highest installed solar power capacities, over 67 GW in 2023, wind power 44 GW in 2023, and biomass energy 10 GW. The developments in other sources are very low.

## ***1.3 Hydrogen: The alternative***

### ***1.3.1 Prospects***

One of the other significant sources of cleaner, nontoxic, environment-friendly, nonconventional energy source is hydrogen energy [3-6]. Hydrogen is not a source of fuel but an energy carrier. To develop a practically useable hydrogen fuel cell, firstly, hydrogen must be produced from water, bio-sources, or fossil fuels for storage. Secondly, a proper hydrogen storage system is required to store hydrogen. It is not only a challenge; the challenges that one has to face to make hydrogen fuel cell-driven vehicles include production, storage, transportation, and distribution. European Union considers hydrogen as a high-potential energy carrier for stationary and mobile transportation applications. International Energy Agency (IEA) has taken a leading global policy on hydrogen.

For mobile applications, critical demands of energy sources can be listed as

(i) lightweight (ii) competitive cost and availability (iii) high gravimetric and volumetric density (iv) first kinetics (v) proper thermodynamic properties (vi) low

temperature of dissociation (vii) easy activation (viii) reversibility and (ix) recyclability for a long time.

Hydrogen energy is getting attention as a potential energy source because of the following facts:

- (i) No emission: when used in a fuel cell, the only by-product is water and heat without any emission of pollutants that can adversely affect the climate.
- (ii) High energy density: Hydrogen has a high energy-to-weight ratio of about 142 MJ/Kg, about three times higher than the energy density of fossil fuel. High energy density implies storing a more significant amount in a small space. It makes hydrogen a good option for stationary and mobile transportation in vehicles.
- (iii) Versatility: Hydrogen can be produced from various sources. The flexibility makes it a potential solution for meeting energy needs among different sectors, including transportation, industry, and power generation.
- (iv) Durability: Hydrogen can provide a long-term energy solution as it can be produced from renewable energy sources and can be stored.

As of 2022, hydrogen energy has found a wide range of applications along with transportation, power generation, and industrial use. The most promising application is in fuel cells converting hydrogen into electricity with water and heat as by-products. Fuel cells are now used in cars, buses, trains, and airplanes.

### ***1.3.2 Challenges***

Hydrogen is a promising source of clean energy. It has the potential to replace fossil fuels, but a few challenges must be addressed.

- (i) Hydrogen is not readily available in nature. It is to be produced from other sources like fossil fuel reforming, biomass, nuclear/ solar thermo-chemical cycles, using solar, wind, hydro energy, or water using energy from fossil fuel or solar or wind energy. Mainly, it is produced in steam methane reforming (SMR), which is associated with the production of CO<sub>2</sub>. The Electrolysis method requires a lot of energy, which demands a high cost.

- (ii) Hydrogen storage is a big problem. Low-density hydrogen gas is to be compressed at high pressure of  $\sim 700$  bars or liquefied at a cryogenic temperature of  $\sim 20$  K, increasing its cost. New avenues for storing hydrogen are to be explored, viz., storing in solid-state materials.
- (iii) Hydrogen is inflammable. Storing and transportation or distribution is insecure. New technology development is required to distribute it safely.
- (iv) Hydrogen is currently more expensive than conventional fuels. New technology development is required to reduce the cost of storage and distribution.

#### ***1.4 Solid State Hydrogen Storage Materials: The Challenges***

The hydrogen storage techniques can be summarized into four categories

- (i) Compressed gas storage at high pressure  $\sim 700$  bars.
- (ii) Liquefied hydrogen storage at cryogenic temperature and high pressure.
- (iii) Physical adsorption in solid-state materials.
- (v) Chemical adsorption of solid-state materials.

High-pressure compressed gas storage in high-pressure tanks is currently used for mobile transportation systems. High cost and high risk of leaking from high-pressure tanks are the main challenges in expanding the technology. It also cannot provide high gravimetric density. The maximum gravimetric density achieved is  $0.042 \text{ Kg H}_2/\text{ Kg}$  [7-9].

Liquefaction of hydrogen is associated with a high energy requirement to produce a temperature of  $20\text{K}$  cooling system [10-12]. The hydrogen loss due to vaporization at room temperature is also a factor. It can provide high gravimetric density but at a high cost and leakage losses of hydrogen.

In physisorption, the hydrogen molecules get weakly adsorbed in solid state material surface by Weak Van der Waal forces. The technique provides highly competitive cost with respect to fossil fuel as it stores hydrogen at room temperature and relatively low pressure. Usually, porous materials of large surface area are used for physisorption. The materials have high storage density, longevity, recyclability, lightweight and fast charging-discharging kinetics. Zeolites, Metal-Organic Frameworks (MOF), Covalent Organic Frameworks (COF), and carbon materials viz fullerene, nanotubes and Graphene are studied extensively. Using

zeolites, it is reported that a maximum of 2.19 wt.% was obtained in CaX zeolites at 15 bar pressure and 77K can be achieved. Theoretical studies show that maximum gravimetric density with zeolites is limited to 2.086 wt.% [13-15].

The highest hydrogen storage capacity with MOFs reported is 7.5 wt.% at 77 K [16-18] and there is a direct correlation between hydrogen uptake and specific surface area. Here, the requirement of large surface area, sensitivity to the synthesis process and need for cryogenic temperature puts challenges for the industrialization of the MOFs and COFs systems.

Single-walled carbon nanotubes (SWNT), multi-wall carbon nanotubes (MWCNT), graphite nano fibres (GNF), etc. are among the nanotubes studied for hydrogen storage. It is reported that GNFs, SWNTs, and MWCNTs offer first kinetics and reversibility. The low hydrogen uptake capacity  $\sim 1.5$  wt.% per 1000 m<sup>2</sup>/g of specific area [19, 20] & requirement of cryogenic temperature puts a challenge for the materials for application as hydrogen storage systems. CNTs are often used as support material for low cost, high thermal stability, chemically inertness and lightweight material [21]

In the Physisorption technique, hydrogen molecules adsorbed on the reactive cluster surface and dissociates into hydrogen atoms. Then the hydrogen atoms diffuse to available reactive sites, and forms a bond with the reactive atoms present in the cluster by Chemisorption.

Metal hydrides provide a high storage density of  $\sim 6.5$  H atom/cc of MgH<sub>2</sub> compared to 0.99 H atoms/cc in hydrogen gas and 4.2 H atoms/cc in liquid hydrogen [3]. Metal hydrides are the most promising material for stationary and mobile applications. Magnesium-based other hydride materials viz. Mg<sub>2</sub>Ni, Mg-Co, Mg<sub>2</sub>FeTi, etc., are also studied [22-25].

Recently, complex metal hydrides have been studied extensively [26-28]. Usually, complex hydrides are studied with the formula A<sub>x</sub>Me<sub>y</sub>H<sub>4</sub>. The hydrides of Boron LiBH<sub>4</sub>, NaBH<sub>4</sub>, KBH<sub>4</sub>, Be(BH<sub>4</sub>)<sub>2</sub>, Mg(BH<sub>4</sub>)<sub>2</sub>, Ca(BH<sub>4</sub>)<sub>2</sub>, Al(BH<sub>4</sub>)<sub>2</sub> etc. are studied. It is reported that almost all complex Boron hydrides offer more than 5 wt.% of gravimetric density but suffer from poor hydrogen kinetics and high adsorption temperature.

Among the Aluminum complex hydrides LiAlH<sub>4</sub>, NaAlH<sub>4</sub>, KAlH<sub>4</sub>, Mg(AlH<sub>4</sub>)<sub>2</sub>, Ca(AlH<sub>4</sub>)<sub>2</sub>, Ca(AlH<sub>4</sub>)<sub>2</sub>, Li<sub>3</sub>AlH<sub>6</sub>, LiMg(AlH<sub>4</sub>)<sub>2</sub>, Na<sub>3</sub>AlH<sub>6</sub>, LiMgAlH<sub>6</sub>, etc are studied [29] extensively. Among the aluminum hydrides, NaAlH<sub>4</sub> partially fulfills the requirement for a hydrogen storage system, but its volumetric density falls too low after the first cycle. Some aluminum

hydrides are not reversible, and some others offer low hydrogen storage capacities, which are unsuitable for broad industrial applications.

The combination of Li-Mg-N-H systems cannot offer more than 5.5 wt.% at temperatures 150 °C to 200 °C, 100 MPa adsorption pressure, and 1 MPa desorption pressure [3]. They are not considered for broad industrial applications.

Compared to metal hydrides, the hydrogen storage capacity of complex hydrides is high. But due to ease of operation at NTP in the case of metal hydrides, these materials are considered more feasible for hydrogen storage from the application point of view.

### ***1.5 The Possible Solution: The Atomic Clusters***

Atomic clusters are promising alternatives for use as hydrogen energy storage systems because nanoclusters can exhibit unusual properties with change in size, viz. clusters of semiconductor atoms may show metallic properties and vice versa [30], clusters of nonmagnetic atoms may show magnetic behavior [31], a cluster of brittle material may show malleable character, a cluster of inert material atoms may exhibit reactivity and so on with a change of size of the cluster. Thus, clusters are the only way to be tuned to follow the pathway from physisorption to diffusion to chemisorption for hydrogen storage. Now, it is crucial to know what clusters are.

Clusters are assemblies of very few to 100's atoms comprising similar or dissimilar atoms, aggregated in such a way that they can form a definite crystal structure or a mixture of structures with some symmetry element. Their size varies from 1-10 nm.

There are marked differences between clusters and compounds or molecules. The molecules and compounds (CO<sub>2</sub>, CH<sub>4</sub>, O<sub>2</sub>, N<sub>2</sub>, inorganic and organic compounds) exist in nature at ambient conditions, whereas nanoclusters can exist only in a vacuum or inert environment. Compounds may exist with very few isomers with fixed composition, but a number of isomers of a cluster may be many, depending upon the structure and bonding. Isomers of clusters with the same composition may have different thermodynamic and chemical properties depending upon the geometry and symmetry of the cluster. Bonding of compounds may be ionic or covalent, whereas the cluster may be formed with varied bonding.

Both can be synthesized using various methods, including chemical reactions, self-assembly, and deposition techniques. Additionally, both types of materials can exhibit exciting properties that are not observed in their constituent elements or larger bulk forms, making them of interest for various applications in fields such as catalysis, electronics, and materials science.

### ***1.5.1 Nanoparticles and nanoclusters***

Nanoparticles and nanoclusters are nanoscale materials; nanoparticles are generally larger and have a more comprehensive range of shapes and structures, while nanoclusters are typically smaller and are composed of tiny atoms or molecules.

Nanoparticles typically have at least one dimension between 1 and 100 nanometers. They can be made from various materials, such as metals, metal oxides, and polymers, and can have a range of shapes and structures, including spheres, rods, and cubes. Nanoparticles are typically composed of a single material and have a well-defined structure. Nanoparticles are often used in various applications, including drug delivery, electronics, and catalysis.

On the other hand, nanoclusters are small groups of atoms or molecules that are typically less than 2 nm in size. They can be made from various materials, including metals, metal oxides, and semiconductors, and can have a range of structures, including crystalline and amorphous. Nanoclusters can exhibit unique properties due to their small size and high surface area, making them useful in catalysis, sensing, and biomedical imaging applications.

Both nanoparticles and nanoclusters exhibit unique physical and chemical properties that are distinct from those of bulk materials or individual atoms or molecules. These properties arise from the high surface-area to volume ratio of both nanoparticles and nanoclusters, resulting in many exposed atoms or molecules on the surface.

### ***1.5.2 Why do nanoclusters show unusual properties?***

The unusual properties of nanoclusters arise due to (i) the unusual surface-to-volume ratio of nanoclusters (ii) Molecular orbitals showing an energy gap between the highest occupied molecular orbital (HOMO) and lowest unoccupied molecular orbitals (LUMO). The

HOMO-LUMO gap varies with the cluster's structure and number of atoms. It determines the thermodynamic, electronic, and chemical properties of the cluster.

With the experimental confirmation of electronic shell structures from mass spectra [32, 33] and the theoretically established Jellium model in analogy with the nuclear shell model [34-36], atomic clusters may be considered separate entities with their own physical and chemical properties.

## **1.6 Literature Survey:**

### **1.6.1 Literature Survey: Why Magnesium Nanoclusters?**

An up-and-coming candidate is magnesium for mass-sensitive applications; it can store up to 7.6 wt.% of hydrogen. The metallic Mg has a hexagonal (space group: P63/mmc) crystal structure with lattice parameters  $a=b=3.2094 \text{ \AA}$  and  $c=5.2108 \text{ \AA}$ . It is one of the alkaline earth metals and the eighth most abundant material in the Earth's crust. It can be considered as a cheap material. Divalent Magnesium,  $[\text{Ne}] 3s^2$ , has a closed-shell electronic configuration and medium reactivity with the environment. A considerable energy gap exists between the ground state  $3s^2$  and the vacant  $3p$  state. Two Mg atoms interact weakly with binding energy  $0.0025 \text{ eV}$  compared to bulk material  $1.51 \text{ eV/atom}$ . These small-sized diatomic Mg clusters are weakly bonded by Van der Waals forces, while  $3p$  electron involvement in  $sp$  hybridization increases in larger clusters.

A huge number of theoretical investigations reported, using the Kohn-Sham Density Functional theory [34] with different exchange-correlation functional [37-52], Hartree-Fock Theory [35], Moller-Plesset (MP) perturbation theory [36], Moller-Plesset of fourth order MP4, etc. and their differences of results depending upon the method and basis set chosen. Thus, before proceeding further toward applications of Mg nanoclusters, it is worthy to perform a complete systematic study of pure Mg clusters using a proper method with a proper set of basis functions.

The interaction between Mg atoms increases in pure clusters with increased cluster size. The gap between the highest occupied molecular orbital (HOMO, here  $3s$ ) and the lowest unoccupied molecular orbital (LUMO,  $3p$ ) decreases. The evolution of structural growth of

Mg<sub>n</sub> clusters has been investigated by many researchers in the past [38-52]. The gap becomes negligibly tiny for higher-size clusters, reaching the metal work function and showing metallic characteristics [30, 38, and 42, 43]. F. Reuse et al. studied the geometry, stability, and electronic properties of small-sized (n=1-8) clusters using LDA approximation and concluded that Mg<sub>n</sub> clusters tend to form compact structures [39]. V. Kumar et al. [40] reported for (n=2-13), the base structure of Mg<sub>n</sub> clusters is trigonal and tetrahedral. Energetics and structural properties of Mg<sub>n</sub> (n=2-22) have been reported by Kohn et al. [41] using DFT and reported n=4, 10, and 20 are the most stable clusters as per the shell model. With the increase of the number of atoms in the cluster, metallic characteristics appear with an ionization potential of 3.64 eV, and the band gap becomes very narrow for clusters above n=18 are reported by Thomas et al. (n=3-35) and Lyalin et al. [44, 46]. Heidari et al. [47] reported for (n=10-56) as a theoretical counterpart of the experimental work of Diederich [48, 49], for (n=2-17). Detailed structure and bond length have been reported by Xia et al. [50], Dong Shen et al. [51] using kick's method of global minimum structures reported optimized stable structures. Janecek et al., using Langevin molecular dynamics, reported the nature and properties of Mg<sub>n</sub> and Na<sub>n</sub> for (n=2-30) [52], and Zhang et al. reported structure and electronic properties for (n=2-20) [53]. Experimental investigation of the stability of Mg<sub>n</sub> clusters up to 80 atoms using mass spectroscopy has been reported by Diederich et al. [48, 49] found the deviation of magic numbers in case of clusters and established them using spherical shell model. The conclusions arrived from these results (n=2-20) agree with the experimental results of mass spectroscopy and photoelectron spectroscopy [48, 49, 54-56].

### ***1.6.2 Literature Survey: Why is doping required?***

Pure magnesium clusters have limitations in terms of hydrogen storage, such as high desorption temperatures and slow kinetics. Among the nanoclusters with different compositions, transition metal-doped magnesium clusters have become one of the exciting systems in hydrogen storage. This is because the group II metal clusters possess some unique physiochemical tuning properties, tunable electronic properties, and the ability to transition from weakly bonded (Van der Waal type) small clusters to metallic characteristics in large clusters due to addition of Mg atoms. With the increase of size of a cluster, the s-p hybridization increases, and the non-additive many-body exchange interaction component



becomes significant. Another essential feature of Mg clusters is the rapid increase of binding energy per atom with the cluster size increase in the small range [54-56]. A physical process of charge transfer occurs after doping with a transition metal. The charge transfer process is responsible for cluster formation. There is a redistribution of charge density in the orbitals. The electronic charge transfers between the 4s, 3d, and 4p orbitals of transition metal and the 3s and 3d orbitals of Mg occur to stabilize the clusters. Due to the charge transfer mechanism, the average bond length also changes to form a stable cluster. TM doped clusters, the 4s and 3d orbitals of TM atoms form the core, and 4p has a minimal contribution. Similarly, in Mg, atoms 3s and 3p orbitals form the core showing strong sp hybridization while 3d, 4s, and 4p orbitals contribute very weakly.

The d-block elements exhibit vacant d-orbital, so they have variable vacancies. The vacancies of d-orbitals are very much helpful in storing hydrogen. The stored hydrogen can be released when needed at a particular temperature.

Xi et al. [60] reported electronic properties of strontium-doped  $Mg_n$  ( $n = 2-12$ ) clusters. Ni-doped  $Mg_n$  ( $n = 1-7$ ) clusters have been studied by Chen et al. [61] reported that the Ni atom starts trapped in cage clusters from  $n = 5$ . C. M. Li et al. [62] reported carbon-doped  $Mg_n$  ( $n = 1-12$ ) clusters and found that  $Mg_8C$  and  $Mg_{11}C$  are the most stable structures in endohedral doping. In another work, C. Li et al. [63] reported that Li-doped  $Mg_n$  ( $n = 2-11$ ) clusters  $LiMg_9$  with  $C_{4v}$  symmetry possess high stability and strong Li-Mg interaction. Zn-doped  $Mg_n$  ( $n = 1-5$ ) has been reported by Z. Li et al. [64], and claimed  $Mg_3Zn$  and  $Mg_3Zn_2$  are the most stable clusters. Zhu et al. [65] reported Pd-doped  $Mg_n$  ( $n = 2-20$ ) clusters with potential applications. Ge, Sn, and C doped  $Mg_n$  ( $n = 2-12$ ) has been studied by Zeng et al. [66] and found  $XMg_8$  ( $X = Ge, Sn, C$ ) is the most stable cluster always. Droghetti et al. [67] investigated the N-doped Mg system as a promising material for spintronics application. They reported that if MgN is possible to make, then MgO/MgN system will be a suitable system platform for tunnel junctions. Boruah et al. [68] studied 3d transition metal (TM) doped  $Mg_n$  ( $n = 2-10$ ) neutral and cationic clusters and reported  $TMMg_3$  as the most stable cluster. Husain et al. [69] reported TM (Sc, V, Fe, Co, Ni, Cu, Y, Zn, Nb) doping on  $Mg_5H_2$ . Transition metal (Fe, Co, Ni) doped  $Mg_n$  ( $n = 1-9$ ) clusters have been studied by Kong et al. [70].

## **1.7 Research Gap**

The first row of transition metals (Ti, V, and Cr) are exceptionally suitable dopant for alkaline earth metal clusters to achieve high gravimetric density and produce good hydrogen storage system [71-80]. The catalytic effect of Ti in hydrogenation reaction was first reported by Bogdanovic and Schwickardi [81]. The catalytic activity of Ti is different from other d-block elements in metal hydrides [82-86]. Experimental evidence shows  $\text{TiH}_2$  formation may offer effective catalytic activity [85, 86]. Kyoi et al. [87] experimentally studied  $\text{TiMg}_n$  hydrides. They have reported that  $\text{TiMg}_7$  is the most stable cluster. Ti is a suitable catalyst found in other studies. The Ti atoms occupy substitutional sites in the Mg lattice and act as catalysts to enhance the dissociation and adsorption of hydrogen molecules onto the cluster surface. This may lead to high stability, lower desorption temperatures and faster hydrogen uptake and release kinetics. Complete systematic studies on Ti-doped  $\text{Mg}_n$  clusters with exohedral and endohedral doping have yet to be reported regarding hydrogen storage. Impact of catalyst-substrate interaction on hydrogen storage with  $\text{Mg}_n$  clusters also not reported.

## **1.8 The Objectives of the Thesis**

From the discussions and literature search, it is evolved that the catalytic activity of Titanium doping on Magnesium clusters and its impact on hydrogenation/ dehydrogenation efficiency has yet to be systematically studied. The objectives of this thesis are:

- i). Systematic study of thermodynamic and chemical properties of pure Magnesium clusters,
- ii). Systematic study of Ti-doped Magnesium clusters and their hydrogen storage capacity in the framework of Kohn Sham density functional theory under effective core potential and B3LYP functional using 6-311G(d) basis set with Gaussian'09 package. The target is finding a high efficiency, clean, renewable, nontoxic environment-friendly energy storage system.
- iii). The last step is an attempt to enhance the stability and efficiency of hydrogenation/ dehydrogenation of Ti-doped Magnesium clusters using the catalytic effect of Titanium doping and substrate support.

## **1.9 The Mechanism**

The mechanism of solid-state hydrogen storage systems consists of two steps:

- (a) Hydrogenation: It includes (i) absorption of hydrogen molecules on the surface of the metal by weak van der Waals interaction (physisorption), (ii) dissociation of hydrogen molecule into atomic hydrogen, (iii) diffusion of the atomic hydrogen towards the reactive atoms of the cluster material (iv) chemical interaction of the hydrogen atom and the solid material by strong bonding (Chemisorption) (v) formation of metal hydride interface.

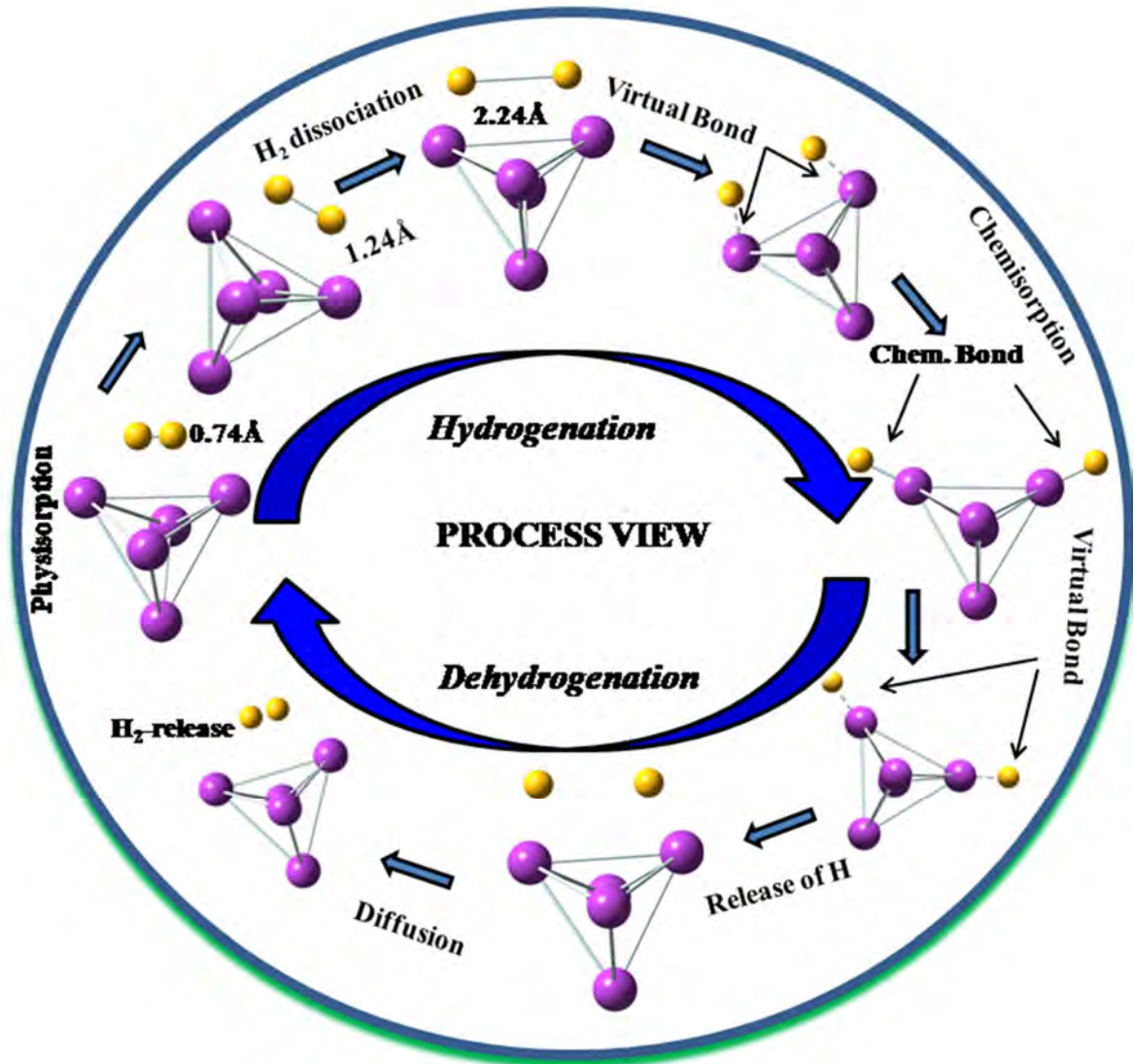


Fig. 1.1 Pictorial view of the process of hydrogenation and dehydrogenation in hydrogen storage cluster systems.

- (a) Dehydrogenation: The process includes (i) the release of hydrogen by metal hydride, (ii) diffusion of hydrogen atoms to the metal interface, (iii) recombination of hydrogen atoms to hydrogen molecules, and the release of hydrogen molecules.

During hydrogen intake by metal atoms, heat is evolved. As a result, the operating temperature enhances, reducing hydrogen intake and absorption rate. Since the hydrogen atoms are chemically bonded with Mg atoms, it requires higher detachment energy. So, releasing hydrogen atoms to form hydride requires heat (endothermic for Mg metal). Considering both hydrogenation (exothermic) and dehydrogenation (endothermic), the process becomes thermodynamically viable.

The pictorial view of the process of hydrogen storage and release of H<sub>2</sub> molecules in solid-state hydrogen storage cluster systems is presented in Fig. 1.1.

### ***1.9.1 Enhancement of stability and efficiency of hydrogen storage: Substrate support***

The catalytic activity of Ti doping on Mg<sub>n</sub> clusters was favorable in enhancing the hydrogen storage efficiency and kinetics [72, 74, 82, 85-87]. The main problems are with the system's stability during hydrogenation and dehydrogenation. To have optimum stability and hydrogen storage kinetics, atomic adsorption on support material has been reported in the recent past [88-91]. Another way of tuning the deciding parameters of hydrogen storage systems is by supporting the nanoclusters with a substrate. The interaction between the substrate material and the nanoclusters is reported by many researchers [92-109]. Some of the Graphene substrate supported clusters studied are: TM clusters (Ni<sub>n</sub>, Pd<sub>n</sub>, Pt<sub>n</sub>) [92, 94], Ti<sub>n</sub> [93], Fe<sub>n</sub>, Co<sub>n</sub>, Ni<sub>n</sub> [95, 96]. Ni<sub>n</sub> and Fe<sub>n</sub>, Au<sub>n</sub> [97]. L. Wang et al. [98] reported Graphene oxide substrate act as the ideal substrate. Other substrate materials include Ni<sub>n</sub> clusters on CeO<sub>2</sub> and TiO<sub>2</sub> substrate by Bo Han [99]. Os<sub>3-5</sub>, Ir<sub>2</sub>, Ir<sub>4</sub>, Rh<sub>6</sub> clusters on MgO and Al<sub>2</sub>O<sub>3</sub> substrate [100], Pt<sub>n</sub> clusters on ZrO<sub>2</sub> support [101], tungsten nanoclusters on Si substrate [102]. Carbon clusters on Ni (111) substrate [103]. Au<sub>n</sub> clusters on CeO<sub>2</sub>(111) substrate [104], Au<sub>n</sub> nanoclusters on MgO (111) substrate [105], Au<sub>n</sub>, Ag<sub>n</sub>, and Cu<sub>n</sub> nanoclusters on TiO<sub>2</sub> substrate [106], Cu<sub>n</sub> nanoclusters on Cu<sub>7</sub>SiO<sub>2</sub> substrate [107], Pt-Re nanoclusters on MgO (100) substrate [108], etc. Kantorovich et al. [109] reported theoretical and experimental work of Mg<sub>n</sub> clusters on the MgO surface. From the literature, it is seen that Graphene substrate, in many cases, yields good results. Also, MgO substrates can improve electronic properties on nanoclusters to achieve a hydrogen storage system. A substrate with a rectangular and a honeycomb structure of MgO substrate is reported by Zhang [110].

## ***1.10 Chapter-wise Organization of the Thesis***

### ***Chapter I: Introduction***

The chapter presents an overview of the present scenario of energy research, mainly hydrogen as an alternative source of clean, nontoxic, renewable and environment-friendly energy carrier and the present challenges of its implementation in mobile transportation systems. Different hydrogen storage methods, especially with an emphasis on solid-state hydrogen storage methods, are discussed with their challenges. A literature search indicates a promising alternative for highly efficient hydrogen storage is the nanoclusters of magnesium and the literature search advocates magnesium clusters with a suitable transition metal doping may be a promising solution.

### ***Chapter 2: Methodology***

This chapter briefly discusses the quantum mechanical development of Kohn Sham's density functional theory. The theoretical methods used for the calculations of the electronic structures and the computational methods have been discussed. This part can be categorized into two sections. The 1<sup>st</sup> section contains the concept of theories and the theoretical methods. In the 2<sup>nd</sup> section, the discussion on the computational approach, GAUSSIAN, Gauss View, and Multiwfn software are briefly discussed.

### ***Chapter 3: The Electronic Structures and Properties of Mg<sub>n</sub> (n=2-20) Nanoclusters: A Density Functional Investigation***

The chapter presents a systematic study of pure Mg<sub>n</sub> (n=2-20) nanoclusters within the Kohn Sham density functional theory using the Gaussian'09 package [111]. The clusters are optimized using B3LYP functional with a 6-311G (d) basis set. Growth of clusters, ground state structures, their symmetry elements, average bond length, Binding Energy (BE) per atom, second order change in energy or stability parameter, the gap between the highest occupied molecular orbital (HOMO) and lowest unoccupied molecular orbital (LUMO), the HOMO-LUMO orbitals, Vertical Ionization Potential (VIP), Vertical Electron Affinity (VEA), Chemical Potential ( $\mu$ ) and Chemical Hardness ( $\eta$ ) are studied. The Molecular Electrostatic Potential (MEP) and Total Electron Density (TED) contours are presented.

## ***Chapter 4: Systematic Study Of Ti Doped Magnesium (TiMg<sub>n</sub>) (n=2-20) Clusters: A Density Functional Approach.***

The chapter systematically studies Titanium doped Mg<sub>n</sub> (n=2-20) clusters using density functional theory using B3LYP functional and 6-311 G(d) basis set using Gaussian '09 package. The growth pattern of doped clusters, the ground state structures, the symmetry elements, and average bond lengths (Mg-Mg & Ti-Mg) are presented. The BE per atom. Stability parameters, Fragmentation energy (FE), HOMO-LUMO gap, VIP, VEA, Chemical Potential ( $\mu$ ) and Chemical hardness ( $\eta$ ) using both the anion-cation method and Koopmans method are presented. The HOMO-LUMO orbitals, Molecular electrostatic potential, and total electron density contour are studied. The Mullikan charge distribution, Polarizability, dipole moment, and vibrational frequencies are presented. From NBO (Natural Bond Orbital) analysis, the electronic configuration of the doped clusters is studied and included in the chapter. The Electron Localization Function (ELF) study and critical points of the most stable cluster (TiMg<sub>8</sub>) are presented in the chapter. The Nucleus independent chemical shift (NICS) is studied to check the aromaticity of the most stable nanocluster TiMg<sub>8</sub>. The IR and Raman spectra of the doped clusters are also presented.

## ***Chapter 5: Catalytic Effect of Ti Doping on Hydrogenation of Mg<sub>n</sub> (n=2-8) Nanoclusters: A Density Functional Study***

In this chapter, firstly, the optimized global minimum structures and their growth process are presented. The same computational technique is used: the Kohn Sham density functional theory with B3LYP functional, 6-311G (d) for magnesium and Ti atoms, and 6-311G (d, p) for hydrogen atoms. The thermodynamic, chemical, and electronic properties of the hydrogenated clusters (BE/atom, Stability, HOMO-LUMO gap, VIP, VEA,  $\eta$ ,  $\mu$ ) are presented. The variation of chemisorption energy with the size of the cluster is presented. The ELF for the most promising cluster (TiMg<sub>5</sub>) is studied. The catalytic activity of Ti on the doped cluster is studied by finding the reduction of activation barrier potential with the help of Intrinsic Reaction Coordinate (IRC) of pure hydrogenated and doped hydrogenated

clusters. The extra hydrogen storage capacity due to Ti doping and the gravimetric density of hydrogen storage is evaluated and presented in the chapter.

### ***Chapter 6: Hydrogen Storage on MgO Substrate Supported TiMg<sub>n</sub> (n=2-6) Clusters: A First Principle Investigation***

This chapter dealt with the enhancement of catalytic behavior and stability of the TiMg<sub>n</sub> clusters with the aid of MgO substrate support. In the first step, computation in the work is self-consistent-field (SCF) electronic structure calculations of all clusters within the density functional theory (DFT) framework. During the calculations, molecular orbitals (MO) are expressed as a linear combination of atom-centered basis functions for which the LanL2DZ inbuilt in the Gaussian'09 program package [111] is used. Spin-polarized calculations use the Becke three-parameter exchange and the Lee, Yang, and Parr generalized gradient approximation (GGA), famous as B3LYP functional.

The adsorption energy of the supported cluster ( $E_{\text{ads}}$ ), hydrogen adsorption energy by the supported clusters ( $E_{\text{ads-H}}$ ), HOMO-LUMO gap, vertical ionization potential (VIP), vertical electron affinity (VEA), chemical potential ( $\mu$ ) and chemical hardness ( $\eta$ ) are calculated. It is found that the supported TiMg<sub>5</sub> cluster enhances the clusters' thermodynamic stability and chemical reactivity compared to bare TiMg<sub>5</sub> due to the support. These properties make the substrate-supported TiMg<sub>5</sub> a sound system for hydrogen storage. The H<sub>2</sub> physisorption, splitting, diffusion, chemisorption, dissociation, and release of the H<sub>2</sub> molecule are verified in the supported TiMg<sub>5</sub> cluster system.

### ***Chapter 7: Summary and Future Scope***

This chapter summarizes the work done in the thesis. The direction for further studies that can be performed from the results obtained in the thesis are discussed.

## References

- [1] B. P. Statistical Review of World Energy. <https://www.bp.com/content/dam/bp/business-sites/en/global/corporate/pdfs/energy-economics/statistical-review/bp-stats-review-2022-full-report.pdf>
- [2] Krishna Dvaipayana Veda Vyasa, “The Rigveda”, (1500BCE), SLOKA 90.
- [3] P. Prabhukhot R, Wagh M. Mahesh, and A.C. Gangal, “A Review on Solid State Hydrogen Storage Material”, *Advances in Energy and Power*, **4(2)**, (2016), 11-22. <http://dx.doi.org/10.13189/aep.2016.040202>.
- [4] R. Nagar, S. Srivastava, S. Leo Hudson, L.A. Sandra, A. Tanna, M. Sharma, R. Achayalingam, S. Sonkaria, V. Khare, and S. S. Srinivasan, “Recent developments in state-of-the-art hydrogen energy technologies – Review of hydrogen storage materials”, *Solar Compass*, **5**, (2023), 100033. <https://doi.org/10.1016/j.solcom.2023.100033>.
- [5] S.Y. Lee, J.H. Lee, Y.H. Kim, J.W. Kim, K.J. Lee, and S.J. Park, “Recent Progress Using Solid-State Materials for Hydrogen Storage: A Short Review”, *Processes*, **10(2)**, (2022), 304. <https://doi.org/10.3390/pr10020304>
- [6] R. Zacharia, and S.U. Rather, “Review of Solid State Hydrogen Storage Methods Adopting Different Kinds of Novel Materials”, *Journal of Nanomaterials*, **2015(4)**, (2015), 1687-4110. <https://doi.org/10.1155/2015/914845>.
- [7] T.Q. Hua, H.S. Roh, and R.K. Ahluwalia, “Performance assessment of 700-bar compressed hydrogen storage for light duty fuel cell vehicles”, *Int. J. Hydrogen Energy*, **42(40)**, (2017), 25121–25129. <https://doi.org/10.1016/j.ijhydene.2017.0>.
- [8] E. Rivard, M. Trudeau, and K. Zaghbi, “Hydrogen Storage for Mobility: A Review”, *Materials*, **12(12)**, (2019), 1973. <https://doi.org/10.3390/ma12121973>
- [9] G. Sdanghi, G. Maranzana, A. Celzard, and V. Fierro, “Review of the current technologies and performances of hydrogen compression for stationary and



- automotive applications”, *Renew. Sustain. Energy Rev.*, **102**, (2019), 150–170. <https://doi.org/10.1016/j.rser.2018.11.028>.
- [10] J. Zheng, H. Zhou, C.G. Wang, E.Y. Ye, J.W. Xu, X.J. Loh, and Z.B. Li, “Current research progress and perspectives on liquid hydrogen rich molecules in sustainable hydrogen storage”, *Energy Storage Mater.*, **35**, (2021), 695–722. <https://doi.org/10.1016/j.ensm.2020.12.007>
- [11] Y.X. Zhao, M.Q. Gong, Y. Zhou, X.Q. Dong, and J. Shen, “Thermodynamics analysis of hydrogen storage based on compressed gaseous hydrogen, liquid hydrogen and cryo-compressed hydrogen”, *Int. J. Hydrogen Energy*, **44(31)**, (2019), 16833–16840. <https://doi.org/10.1016/j.ijhydene.2019.04.207>
- [12] G. Wei, and J. Zhang, “Numerical Study of the Filling Process of a Liquid Hydrogen Storage Tank under Different Sloshing Conditions”, *Processes* **8(9)**, (2020), 1020. <https://doi.org/10.3390/pr8091020>
- [13] H.W. Langmi, D. Book, A. Walton, S.R. Johnson, M.M. Al-Mamouri, J.D. Speight, P.P. Edwards, I.R. Harris, and P.A. Anderson, “Hydrogen storage in ion-exchanged zeolites”, *J. Alloys Compd.*, **404-406**, (2005), 637-642. <https://doi.org/10.1016/j.jallcom.2004.12.193>
- [14] J.G. Vitillo, G. Ricchiardi, G. Spoto, and A. Zecchina, “Theoretical maximal storage of hydrogen in zeolitic frameworks”, *Phys. Chem. Chem. Phys.*, **7(23)**, (2005), 3948-3954. <https://doi.org/10.1039/B510989B>
- [15] Z. Yang, Y. Xia, and R. Mokaya, “Enhanced Hydrogen Storage Capacity of High Surface Area Zeolite-like Carbon Materials”, *J. Am. Chem. Soc.*, **129(6)**, (2007), 1673-1679. <https://doi.org/10.1021/ja067149g>.
- [16] B. Panella, M. Hirscher, H. Putter, and U. Muller, “Hydrogen Adsorption in Metal-Organic Frameworks: Cu-MOFs and Zn-MOFs Compared”, *Adv. Funct. Mater.*, **16(4)**, (2006), 520-524. <https://doi.org/10.1002/adfm.200500561>

- [17] A.G. Wong-Foy, A.J. Matzger, and O.M. Yaghi, "Exceptional H<sub>2</sub> saturation uptake in Microporous Metal-Organic Frameworks", *J. Am. Chem. Soc.*, **128(11)**, (2006), 3494-3495. <https://doi.org/10.1021/ja058213h>
- [18] H. Furukawa, M.A. Miller, and O.M. Yaghi, "Independent verification of the saturation hydrogen uptake in MOF-177 and establishment of a benchmark for hydrogen adsorption in metal-organic frameworks", *J. Mater. Chem.*, **17(30)**, (2007), 3197-3204. <https://doi.org/10.1039/B703608F>
- [19] A. Zuttel, P. Sudan, Ph. Mauron, T. Kiyobayashi, Ch. Emmenegger, and L. Schlapbach, "Hydrogen storage in carbon nanostructure", *Int. J. Hydrogen Energy*, **27(2)**, (2002), 203-212. [https://doi.org/10.1016/S0360-3199\(01\)00108-2](https://doi.org/10.1016/S0360-3199(01)00108-2)
- [20] M. Hirsher, "Handbook of hydrogen storage: New materials for future Energy Storage", Weinheim : WILEY-VCH Verlag GmbH & Co. KGaA, 2009.
- [21] R. Vijay, R. Sundaresan, M.P. Maiya, and S.S. Murthy, "Application of nanostructured Mg-x wt% MmNi<sub>5</sub> (x=10-70) nanostructured composites in a hydrogen storage device", *Int. J. Hydrogen Energy*, **32(13)**, (2007), 2390-2399. <http://dx.doi.org/10.1016/j.ijhydene.2006.11.011>
- [22] H. Reardon, J.M. Hanlon, R.W. Hughes, A. Godula-Jopek, T.K. Mandal, and D.H. Gregory, "Emerging concepts in solid-state hydrogen storage: The role of nanomaterials design", *Energy Environ. Sci.*, **5(3)**, (2012), 5951-5979. <https://doi.org/10.1039/C2EE03138H>
- [23] A. Zaluska, L. Zaluski, and J.O. Strom-Oslen, "Structure, catalysis and atomic reactions on the nanoscale: a systematic approach to metal hydrides for hydrogen storage", *Appl. Phys. A*, **72**, (2001), 157-165. <https://doi.org/10.1007/s003390100783>
- [24] H. Imamura, K. Masanari, M. Kusuhara, H. Katsumoto, T. Sumi, and Y. Sakata, "High hydrogen storage capacity of nanosized magnesium synthesized by high energy ball milling", *J Alloys Compd.*, **386(1-2)**, (2005), 211-216. <https://doi.org/10.1016/j.jallcom.2004.04.145>

- [25] B. Sakintuna, F.L. Darkim, and M. Hirscher, "Metal Hydride Material for Solid Hydrogen Storage: A Review", *Int. J. Hydrogen Energy*, **32(9)**, (2007), 1121-1140. <http://dx.doi.org/10.1016/j.ijhydene.2006.11.022>
- [26] A. Zuttel, P. Wenger, S. Rentsch, P. Sudan, Ph. Mauron, and Ch. Emmengger, "LiBH<sub>4</sub> a new hydrogen storage material", *J. Power Sources*, **118(1-2)**, (2003),1-7. [https://doi.org/10.1016/S0378-7753\(03\)00054-5](https://doi.org/10.1016/S0378-7753(03)00054-5).
- [27] S. Orimo Y. Nakamori, and A. Zuttel, "Material properties of MBH<sub>4</sub> (M=Li, Na, and K)", *Mater. Sci. Eng. B*, **108(1-2)**, (2004), 51-53. <https://doi.org/10.1016/j.mseb.2003.10.045>
- [28] H.I. Schlesinger, H.C. Brown, and E.K. Hyde, "The Preparation of Other Borohydrides by Metathetical Reactions Utilizing the Alkali Metal Borohydrides", *J. Am. Chem. Soc.*, **75(1)**, (1953), 209-213. <https://doi.org/10.1021/ja01097a055>
- [29] B. Vishwanathan, and M.A. Scibioh, "Fuel Cells", Hyderabad : Univerisity Press, 2006.
- [30] J. Jellinek, and P.H. Acioli, "Magnesium clusters: structural and electronic properties and the size-induced nonmetal-to-metal transition", *The J. Phys. Chem. A*, **106(45)**, (2002), 10919-10925. <https://doi.org/10.1021/jp020887g>
- [31] E. Roduner, "Size matters: why nanomaterials are different", *Chem. Soc. Rev.*, **35(7)**, (2006), 583–592. <https://doi.org/10.1039/B502142C>.
- [32] S. Bjornhol, and J. Borggreen, "Electronic shell structure in clusters as reflected in mass abundance spectra", *Philosophical Magazine B (Taylor & Francis)*, **79(9)**, (1999), 1321-1342. <https://doi.org/10.1080/13642819908216974>
- [33] W.D. Knight, K. Clemenger, W.A. de Heer, W.A. Saunders, M.Y. Chou, and M.L. Cohen, "Electronic Shell Structure and Abundances of Sodium Clusters", *Phys. Rev. Lett.*, **52(24)**, (1984), 2141. <https://doi.org/10.1103/PhysRevLett.52.2141>

- [34] W. Kohn, and L.J. Sham, “Self-Consistent Equations Including Exchange and Correlation Effects”, *Phys. Rev.*, **140(4A)**, (1965), A1133– A1138. <https://doi.org/10.1103/PhysRev.140.A1133>
- [35] D.R. Hartree, “The Wave Mechanics of an Atom with a Non-Coulomb Central Field. Part I. Theory and Methods”, *Mathematical Proc. Cam. Philo. Soc.*, **24(1)**, (1928), 89-110. <https://dx.doi.org/10.1017/S0305004100011919>
- [36] V. Fock, “Approximation method for the solution of the quantum mechanical multi-body problem”, *Z. Physik*, **61**, (1930), 126-148. <https://doi.org/10.1007/BF01340294>
- [37] C. Møller, and M.S. Plesset, “Note on an Approximation Treatment for Many-Electron Systems”, *Phys. Rev.*, **46(7)**, (1934), 618–622. <https://doi.org/10.1103/PhysRev.46.618>
- [38] J. Akola, K. Rytkönen, and M. Manninen, “Metallic evolution of small magnesium clusters”, *J. Eur. Phys. D-Atomic, Molecular, Optical and Plasma Physics*, **16(1)**, (2001), 21-24. <https://doi.org/10.1007/s100530170051>
- [39] F. Reuse, S.N. Khanna, V. de Coulon, and J. Buttet, “Pseudopotential local-spin-density studies of neutral and charged  $Mg_n$  ( $n=1-7$ ) clusters”, *Phys. Rev. B*, **41(17)**, (1990), 11743-11759. <https://doi.org/10.1103/physrevb.41.11743>
- [40] V. Kumar, and R. Car, “Structure, growth, and bonding nature of Mg clusters”, *Phys Rev B*, **44(15)**, (1991), 8243–8255. <https://doi.org/10.1103/PhysRevB.44.8243>
- [41] A. Köhn, F. Weigend, and R. Ahlrichs, “Theoretical study on clusters of magnesium”, *Physi. Chem. Chem. Phys.*, **3(5)**, (2001), 711-719. <https://doi.org/10.1039/B007869G>
- [42] P. Delaly, P. Ballone, and J. Buttet, “Metallic bonding in magnesium microclusters”, *Phys. Rev. B*, **45(7)**, (1992), 3838–3841. <https://doi.org/10.1103/PHYSREVB.45.3838>

- [43] S.N. Belyaev, S.V. Panteleev, S.K. Ignatov, and A.G. Razuvaev, “Structural, electronic, thermodynamic and spectral properties of  $Mg_n$  ( $n=2-31$ ) clusters: A DFT Study”, *Comp. Th. Chem.*, **1079**, (2016), 34–46. <https://doi.org/10.1016/j.comptc.2016.01.011>
- [44] A. Lyalin, I.A. Solovyov, A.V. Solovyov, and W. Greiner, “Evolution of the electronic and ionic structure of Mg clusters with increase in cluster size”, *Physical Rev. A*, **67(6)**, (2003), 063203. <https://doi.org/10.1103/PhysRevA.67.063203>.
- [45] P.H. Acioli, and J. Jellinek, “Electron binding energies of anionic magnesium clusters and the nonmetal-to-metal transition”, *Phys. Rev. Lett.*, **89(21)**, (2002), 213402. <https://doi.org/10.1103/PhysRevLett.89.213402>
- [46] O.C. Thomas, W. Zhen, S. Xu, and Jr. K.H. Bowen, “Onset of metallic behavior in magnesium clusters”. *Phys. rev. lett.*, **89(21)**, (2002), 213403. <https://doi.org/10.1103/PhysRevLett.89.213403>
- [47] I. Heidari, S. De, S.M. Ghazi, S. Goedecker, and D.G. Kanhere, “Growth and Structural Properties of  $Mg_n$  ( $N= 10-56$ ) Clusters: Density Functional Theory Study”, *J Phys. Chem. A*, **115(44)**, (2011), 12307-12314. <https://doi.org/10.1021/jp204442e>
- [48] T. Diedrich, T. Döppner, Th. Fennel, J. Tiggesbäumker, and K.H. Meiwes-Broer, “Shell structure of magnesium and other divalent metal clusters”, *Phys. Rev. A*. **72(2)**, (2005), 3203-3214. <https://doi.org/10.1103/PhysRevA.72.023203>
- [49] T. Diedrich, T. Döppner, J. Braune, J. Tiggesbaumker, and K.H.M. Broer “Electron Delocalization in Magnesium Clusters Grown in Supercold Helium Droplets”, *Phys. Rev. Lett.*, **86(21)**, (2001), 4807. <https://doi.org/10.1103/PhysRevLett.86.4807>
- [50] X. Xia, X. Kuang, C. Lu, Y. Jin, X. Xing, G. Marino, and A. Hermann, “Deciphering the structural evolution and electronic properties of magnesium clusters: An aromatic homonuclear metal  $Mg_{17}$  cluster”, *J. Phys. Chem. A*, **120(40)**, (2016), 7947–7954. <https://doi.org/10.1021/acs.jpca.6b07322>

- [51] D. Shen, C.P. Kong, R. Jia, P. Fu, and H.X. Zhang, “Investigation of Properties of  $Mg_n$  clusters and their hydrogen storage mechanism: a study based on DFT and a global minimum optimization method”, *The J. Phys. Chem. A*, **119(15)**, (2015), 3636-3643. <https://doi.org/10.1021/acs.jpca.5b01474>
- [52] S. Janecek, E. Krotscheck, M. Liebrecht, and R. Wahl, “Structure of  $Mg_n$  and  $Mg_n^+$  clusters up to  $n=30$ ”, *Eur. Phys. J. D*, **63**, (2011), 377–390. [10.1140/epjd/e2011-10694-2](https://doi.org/10.1140/epjd/e2011-10694-2)
- [53] F. Zhang, H. Zhang, W. Xin, P. Chen, Y. Hu, X. Zhang, and Y. Zhao, “Probing the structural evolution and electronic properties of divalent metal  $Be_3Mg_n$  clusters from small to medium size”, *Sci. Rep.*, **10**, (2020), 6052. <https://doi.org/10.1038/s41598-020-63237-8>
- [54] B.J. Kooi, G. Palasantzas, and J.T.M. De Hasson, “Gas-phase Synthesis of Magnesium Nanoparticles: A High-Resolution Transmission Electron Microscopy Study”, *Appl. Phys. Lett.*, **89(16)**, (2006), 161914-1–161914-3. <https://doi.org/10.1063/1.2358860>
- [55] A. Kaufmann, A. Kornath, A. Zoermer, and R. Ludwig, “Small magnesium clusters: between van der Waals and valence bonds”, *Inorg. Chem.*, **49(8)**, (2010), 3851–3856. <https://doi.org/10.1021/ic902485z>
- [56] F. Daniel, “Hydrogen Storage in Mg based alloys”, Budapest, (2010).
- [57] J.C. Crivello, B. Dam, R.V. Denys, M. Dornheim, D.M. Grant, J. Hout, T.R. Jenson, P. de Jongh, M. Latroche, C. Milanese, D. Milcius, G.S. Walker, C.J. Webb, C. Zlotes, and V.A. Yartys, “Review of magnesium hydride-based materials: development and optimisation”, *Appl. Phys. A*, **122(97)**, (2016), (1–20). <https://doi.org/10.1007/s00339-016-9602-0>
- [58] H. Haberland (Ed.), “Clusters of Atoms and Molecules: Theory, Experiment, and Clusters of Atoms”, first ed., Springer-Verlag, Berlin, 1994.

- [59] B.C. Zhu, P.J. Deng, L. Zeng, and J. Guo, “Computational exploration of gallium-doped neutral and anionic magnesium nanocluster materials:  $\text{Ga}_2\text{Mg}_n$  ( $n = 1-11$ ;  $q = 0, -1$ ) nanoclusters properties based on DFT”, *Mater. Today Com.*, **29**, (2021), 103004. <https://doi.org/10.1016/j.mtcomm.2021.103004>
- [60] S.G. Xi, Q.Y. Li, Y.F. Hu, Y.Q. Yuan, Y.R. Zhao, J.J. Yuan, M.C. Li, and Y.J. Yang, “Probing the structural and electronic properties of divalent metal  $\text{Mg}_{n+1}$  and  $\text{SrMg}_n$  ( $n = 2-12$ ) clusters and their anions”, *Chin. Phys. B*, **31(1)**, (2022), 1056. <https://doi.org/10.1088/1674-1056/ac04aa>
- [61] X.F. Chen, Y. Zhang, K.T. Qi, B. Li, Z.H. Zhu, and Y. Sheng, “Density functional theory study on Ni-doped  $\text{Mg}_n\text{Ni}$  ( $n = 1-7$ ) clusters”, *Chin. Phys. B*, **19(3)**, (2010), 1-5. <https://doi.org/10.1088/1674-1056/19/3/033601>
- [62] C.M. Li, D. Wu, T. Xiao, Y. Dan, Y. Li, and W. Chen, “Probing the effect of carbon doping on structures, properties, and stability of magnesium clusters”, *Theo. Chem. Acc.*, **140(111)**, (2021), 1-15. <https://link.springer.com/article/10.1007/s00214-021-02810-4>
- [63] C. Li, Y. Cui, H. Tian, Q. Shao, J. Zhang, B. Ren, and Y. Yuan, “Systematic investigation of geometric structures and electronic properties of lithium doped magnesium clusters”, *Comput. Mater. Sci.*, **200**, (2021), 110800. <https://doi.org/10.1016/j.commatsci.2021.110800>
- [64] Z. Li, Z. Zhao, Z. Zhou, H. Wang, and S. Li, “First-principles calculations on small  $\text{Mg}_n\text{Zn}$  and  $\text{Mg}_{n-1}\text{Zn}_2$  clusters: structures, stability, electronic properties”, *Mater. Chem. Phys.*, **199**, (2017), 585-590. <https://doi.org/10.1016/j.matchemphys.2017.07.049>
- [65] B.C. Zhu, P. Deng, J. Guo, L. Zeng, and J. Zhao, “A single palladium atom immerses in magnesium clusters:  $\text{PdMg}_n$  ( $n = 2-20$ ) clusters DFT study”, *New J. Phys.*, **23** (2021), 103002. <https://doi.org/10.1088/1367-2630/ac2853>

- [66] L. Zeng, M.K. Liang, X.F. Wei, J. Guo, W. Dai, and B.C. Zhu, “New potential stable structures of  $\text{XMg}_n$  ( $X = \text{Ge, C, Sn; } n = 2\text{--}12$ ) clusters:  $\text{XMg}_8$  with high stability”, *J. Phys.: Cond. Matter*, **33(6)**, (2021), 065302. <https://doi.org/10.1088/1361-648X/abc401>
- [67] A. Droghetti, N. Baadji, and S. Sanvito, “MgN: A possible material for spintronics applications”, *Phys. Rev. B.*, **80(23)**, (2009), 1–6. <https://doi.org/10.1103/PhysRevB.80.235310>
- [68] B. Boruah, and B. Kalita, “Role of transition metal doping in determining the electronic structures and properties of small magnesium clusters: a DFT-based comparison of neutral and cationic states”, *J. Nanopart. Res.*, **22(370)**, (2020), 370–378. <https://doi.org/10.1007/s11051-020-05083-3>
- [69] T. Husain, T.A. Mark, B. Pathak, and R. Ahuja, “Improvement in the hydrogen desorption from  $\text{MgH}_2$  upon transition metals doping: a hybrid density functional calculation”, *AIP Adv.* **3(10)**, (2013), 102117-1–102117-8. <https://doi.org/10.1063/1.4826521>
- [70] F. Kong, and Y. Hu, “Density functional study of small X doped  $\text{Mg}_n$  ( $X = \text{Fe, Co, Ni, } n = 1\text{--}9$ ) bimetallic clusters: equilibrium structures, stabilities, electronic and magnetic properties”, *J. Mol. Model.*, **20(2087)**, (2014), 1–10. <https://doi.org/10.1007/s00894-014-2087-x>
- [71] M. Pozzo, and D. Alfe, “Hydrogen dissociation and diffusion on transition metal (Ti, Zr, V, Fe, Ru, Co, Rh, Ni, Pd, Cu, Ag) - Doped Mg (0001) surfaces”, *Int. J Hydrogen Energy*, **34(4)**, (2009), 1922-30. <https://doi.org/10.1016/j.ijhydene.2008.11.109>
- [72] A.B. Philips, B.S. Shivaram, and G.R. Myneni, “Hydrogen absorption at room temperature in nanoscale titanium benzene complexes”, *Int. J Hydrogen Energy*, **37(2)**, (2012), 1546-1550. <https://doi.org/10.1016/j.ijhydene.2011.09.136>



- [73] H. Lee, M.C. Nguyen, and J. Ihm, “Titanium functional group complexes for high-capacity hydrogen storage materials”, *Solid State Commun.*, **146(9-10)**, (2008), 431-434. <https://doi.org/10.1016/j.ssc.2008.03.018>
- [74] S. Banerjee, C.G.S. Pillai, and C. Majumder, “Adsorption and desorption of hydrogen in Mg nanoclusters: Combined effect of size and Ti doping”, *Int. J Hydrogen Energy*, **35(6)**, (2010), 2344-2350. <https://doi.org/10.1016/j.ijhydene.2009.12.176>
- [75] Y. Liu, L. Ren, Y. He, and H.P. Cheng, “Titanium decorated graphene for high-capacity hydrogen storage studied by density functional simulations”, *J Phys Cond. mater*, **22(44)**, (2010), 445301. <https://doi.org/10.1088/0953-8984/22/44/445301>
- [76] F. Zuliani, L. Bernasconi, and E.J. Bacrends, “Titanium as a potential addition for High-Capacity Hydrogen storage medium”, *J Nanotech.*, **2012**, (2012), 831872. <https://doi.org/10.1155/2012/831872>
- [77] C. Zhou, Z.Z. Fang, C. Ren, J. Li, and J. Lu, “Effect of Ti Intermetallic Catalysts on Hydrogen Storage Properties of Magnesium Hydride”, *J. Phys. Chem. C*, **117(25)**, (2013), 12973-12980. <https://doi.org/10.1021/jp402770p>
- [78] M. Calizzi, F. Venturi, M. Ponthieu, F. Cuevas, V. Morandi, T. Perkisas, S. Bals, and L. Pasquini, “Gas-phase synthesis of Mg–Ti nanoparticles for solid-state hydrogen storage”, *Phys. Chem. Chem. Phys.*, **18(1)**, (2016), 141-148. <https://doi.org/10.1039/C5CP03092G>
- [79] K. Asano, H. Kim, K. Sakaki, K. Jimura, S. Hayashi, Y. Nakamura, K. Ikeda, T. Otomo, A. Machida, and T. Watanuki, “Structural variation of self-organized Mg hydride nanoclusters in immiscible Ti matrix by hydrogenation”, *Inorg. Chem.*, **57(18)**, (2018), 11831-11838. <https://doi.org/10.1021/acs.inorgchem.8b02015>
- [80] A. Baldi, R. Gremaud, D.M. Borsa, C.P. Balde, A.M.J. van der Eerden, G.L. Kruijtzter, P.E. de Jongh, B. Dam, and R. Griessen, “Nanoscale composition modulations in  $Mg_yTi_{1-y}H_x$  thin film alloys for hydrogen storage”, *Int. J Hydrogen Energy*, **34(3)**, (2009), 1450-1457. <https://doi.org/10.1016/j.ijhydene.2008.11.090>

- [81] B. Bogdanovic, and M. Schwickardi, “Ti-doped alkali metal aluminum hydrides as potential novel reversible hydrogen storage materials”, *J. Alloys Compd.*, **253-254** (1997), pages 1-9. [https://doi.org/10.1016/S0925-8388\(96\)03049-6](https://doi.org/10.1016/S0925-8388(96)03049-6)
- [82] T.J. Fraukcombe, “Proposed mechanism for the catalytic activity of Ti in NaAlH<sub>4</sub>”, *Chem. Rev.*, **112(4)**, (2012), 2164-2178. <https://doi.org/10.1021/cr2001838>
- [83] D. Pukazhselvan, M.S.L. Hudson, B.K. Gupta, M.A. Shaz, and O.N. Srivastava, “Investigations on the desorption kinetics of Mm-doped NaAlH<sub>4</sub>”, *J. Alloy Compd.*, **439(1-2)**, (2007), 243-248. <https://doi.org/10.1016/j.jallcom.2006.08.060>
- [84] G.L. Xia, H.Y. Leng, N.X. Xu, Z.L. Li, Z. Wu, J.L. Du, and X.B. Yu, “Enhanced hydrogen storage properties of LiBH<sub>4</sub> MgH<sub>2</sub> composite by the catalytic effect of MoCl<sub>3</sub>”, *Int. J. Hydrogen Energy*, **36(12)**, (2011), 7128-7135. <https://doi.org/10.1016/j.ijhydene.2011.03.060>
- [85] C. Paduani, and P. Jena, “Role of Ti-based catalysts in the dehydrogenation mechanism of magnesium borohydride: A cluster approach”, *Int. J. hydrogen energy*, **38(5)**, (2013), 2357-2362. <https://doi.org/10.1016/j.ijhydene.2012.11.060>
- [86] J. Wang, A.D. Ebner, R. Zidane, and J.A. Ritter, “Synergistic effects of co-dopants on the dehydrogenation kinetics of sodium aluminum hydride”, *J. Alloys Compd.*, **391(1-2)**, (2005), 245-255. <https://doi.org/10.1016/j.jallcom.2004.08.069>
- [87] D. Kyoï, T. Sato, E. Rönnebro, N. Kitamura, A. Uedac, M. Ito, S. Katsuyama, S. Hara, D. Noréus, and T. Sakai, “A new ternary magnesium–titanium hydride Mg<sub>7</sub>TiH<sub>n</sub> with hydrogen desorption properties better than both binary magnesium and titanium hydrides”, *J. Alloys Compd.*, **372(1-2)**, (2004), 213–217. <https://doi.org/10.1016/j.jallcom.2003.08.098>
- [88] D.J. Durbin, N.L. Allan, and C. Malardier-Jugroot, “Physisorption of molecular hydrogen in curved carbon nanomaterials: a computational study”, *WIT Trans. Eng. Sci.*, **77**, (2013), WIT Press. <https://doi.org/10.2495/MC130131>

- [89] J. Engel, S. Francis, and A. Roldan, “The influence of support materials on the structural and electronic properties of gold nanoparticles – A DFT study”, *Phys. Chem. Chem. Phys.*, **21(35)**, (2019), 19011-19025. <https://doi.org/10.1039/C9CP03066B>
- [90] H.Y Wu, X. Fan, J.L. Kuo, and W.Q. Deng, “DFT Study of Hydrogen Storage by Spillover on Graphene with Boron Substitution”, *J. Phys. Chem. C*, **115(18)**, (2011), 9241-9249. <https://doi.org/10.1021/jp200038b>.
- [91] L.M. Molina, and B. Hammer “Theoretical study of CO oxidation on Au nanoparticles supported by MgO (100)”, *Phys. Rev. B.*, **69(15)**, (2004), 155424. <https://doi.org/10.1103/PhysRevB.69.155424>
- [92] C.R.C. Rego, P. Tereshchuk, L.N. Oliveira, and J.L.F. Da Silva, “Graphene-supported small transition-metal clusters: A density functional theory investigation within van der Waals corrections”, *Phys. Rev. B*, **95(23)**, (2017), 235422-235433. <https://link.aps.org/doi/10.1103/PhysRevB.95.235422>
- [93] K. Takahashi, S. Isobe, K. Omori, T. Mashoff, D. Convertino, V. Miseikis, C. Coletti, V. Tozzini, and S. Heun, “Revealing the Multibonding State between Hydrogen and Graphene-Supported Ti Clusters”, *J. Phys. Chem. C*, **120(24)**, (2016), 12974–12979. <https://doi.org/10.1021/acs.jpcc.6b05207>
- [94] S. Sahoo, M.E. Gruner, S.N. Khanna, and P. Entel, “First-principles studies on graphene-supported transition metal clusters”, *J. Chem. Phys.*, **141(7)**, (2014), 074707. <https://doi.org/10.1063/1.4893328>
- [95] H. Johll, J. Wu, S.W. Ong, H.C. Kang, and E.S. Tok, “Graphene-adsorbed Fe, Co, and Ni trimers and tetramers: Structure, stability, and magnetic moment”, *Phys. Rev. B*, **83(20)**, (2011), 205408. <https://link.aps.org/doi/10.1103/PhysRevB.83.205408>
- [96] R.C. Longo, J. Carrete, J. Ferrer, and L.J. Gallego, "Structural, magnetic, and electronic properties of Ni<sub>n</sub> and Fe<sub>n</sub> nanostructures (n= 1–4) adsorbed on zigzag graphene nanoribbons," *Phys. Rev. B*, **81(11)**, (2010), 115418. <https://doi.org/10.1103/PhysRevB.81.115418>

- [97] A. Pulido, M. Boronat, and A. Corma, "Theoretical investigation of gold clusters supported on Graphene sheets", *New J. Chem.*, **35(10)**, (2011), 2153-2161. <https://doi.org/10.1039/c1nj20215d>
- [98] L. Wang, K. Lee, Y.Y. Sun, M. Lucking, Z. Chen, J.J. Zhao, and S.B. Zhang, "Graphene oxide as an ideal substrate for hydrogen storage." *ACS Nano.*, **3(10)**, (2009), 2995-3000. <https://doi.org/10.1021/mn900667s>.
- [99] Bo. Han, Bo. Yu, J. Wang, M. Liu, G. Gao, K. Xia, Q. Gao, and C. Zhou, "Understanding the electronic metal-support interactions of the supported Ni cluster for the catalytic hydrogenation of ethylene", *Molecular Catalysis*, **511**, (2021), 111731. <https://doi.org/10.1016/j.mcat.2021.111731>.
- [100] A. Kulkarni, R.J.L. Lapidus, and B.C. Gates, "Metal clusters on supports: synthesis, structure, reactivity, and catalytic properties", *Chem. Commun.*, **46(33)**, (2010), 5997-6015. <http://dx.doi.org/10.1039/C002707N>
- [101] Y. Wang, and H. Gao, "Influence of a ZrO<sub>2</sub> Support and Its Surface Structures on the Stability and Nucleation of Pt<sub>n</sub> (n = 1–5) Clusters: A Density Functional Theory Study", *J. Phys. Chem. B*, **121(9)**, (2017), 2132–2141. <https://doi.org/10.1021/acs.jpcc.7b00017>
- [102] J. Xiao, A. Vaida, and J.E. McGrady, "Quantum chemical models for the absorption of endohedral clusters on Si(111)-(7 × 7): a subtle balance between W–Si and Si–Si bonding", *Phys. Chem. Chem. Phys.*, **21(25)**, (2019), 13686-13695. <http://dx.doi.org/10.1039/C9CP01841G>.
- [103] J. Li, E. Croiset, and R.S. Luis, "Carbon clusters on the Ni (111) surface: A density functional theory study", *Phys. chem. chem. phys.*, **16(7)**, (2014). 2954-2961. <https://doi.org/10.1039/c3cp54376e>.
- [104] B.T. Teng, F.M. Wu, W.X. Huang, X.D. Wen, L.H. Zhao, and M.F. Luo, "A DFT Study of the Structures of Au<sub>x</sub> Clusters on a CeO<sub>2</sub> (111) Surface", *Chem. Phys. Chem.*, **13(5)**, (2012), 1261-1271. <https://doi.org/10.1002/cphc.201101007>

- [105] Z. Li, C.V. Ciobanu, J. Hu, J.P. Palomares-Báez, J.L. Rodríguez-López, and R. Richards, “Experimental and DFT studies of gold nanoparticles supported on MgO (111) nano-sheets and their catalytic activity”, *Phys. Chem. Chem. Phys.*, **13(7)**, (2011), 2582-2589. <https://doi.org/10.1039/c0cp01820a>.
- [106] D. Pillay, and G.S. Hwang, “Structure of small Au<sub>n</sub>, Ag<sub>n</sub>, and Cu<sub>n</sub> clusters (n=2–4) on rutile TiO<sub>2</sub>(110): A density functional theory study.” *J.Mol. Struct. theo-chem.*, **771(1-3)**, (2006), 129-133. <https://doi.org/10.1016/j.theochem.2006.03.040>
- [107] L. Núria, I. Francesc, and P. Gianfranco, “Electronic Effects in the Activation of Supported Metal Clusters: Density Functional Theory Study of H<sub>2</sub> Dissociation on Cu/SiO<sub>2</sub>”, *J. Phys. Chem. B*, **103(40)**, (1999), 8552-8557. <https://doi.org/10.1021/jp991655t>.
- [108] A.A. Garcia, J.C. Luque-Ceballos, L.O. Paz-Borbón, and I.L. Garzón, “Theoretical study on the cluster–surface interaction: The case of subnanometer Pt–Re clusters supported on MgO(100)”, *Comp. Mat. Sci.*, **214**, (2022), 111697. <https://doi.org/10.1016/j.commatsci.2022.111697>
- [109] L.N. Kantorovich, A.L. Shluger, P.V. Sushko, J. Günster, P. Stracke, D.W. Goodman, and V. Kempter, “Mg clusters on MgO surfaces: study of the nucleation mechanism with MIES and abinitio calculations”, *Faraday Discuss*, **114**, (1999), 173-194. <http://dx.doi.org/10.1039/A903241J>
- [110] Y.G. Zhang, H.Y. He, and B.C. Pan, “Structural features and electronic properties of MgO nanosheets and nanobelts”, *J. Phys. Chem. C*, **116(43)**, (2012), 23130-23135. <https://doi.org/10.1021/jp3077062>
- [111] M.J. Frisch, G.W. Trucks, H.B. Schlegel, G.E. Scuseria, M.A. Robb, J.R. Cheeseman, G. Scalmani, V. Barone, B. Mennucci, G.A. Petersson, H. Nakatsuji, M. Caricat, X. Li, H.P. Hratchian, A.F. Izmaylov, J. Bloino, G. Zheng, J.L. Sonnenberg, M. Hada, M. Ehara, K. Toyota, R. Fukuda, J. Hasegawa, M. Ishida, T. Nakajima, Y. Honda, O. Kitao, H. Nakai, T. Vreven, Jr J.A. Montgomery, J.E. Peralta, F. Ogliaro, M. Bearpark, J.J. Heyd, E. Brothers, K.N. Kudin, V.N. Staroverov, T. Keith, R. Kobayashi, J.

Normand, K. Raghavachari, A. Rendell, J. C. Burant, S.S. Iyengar, J. Tomasi, M. Cossi, N. Rega, J.M. Millam, M. Klene, J. E. Knox, J.B. Cross, V. Bakken, C. Adamo, J. Jaramillo, R. Gomperts, R.E. Stratmann, O. Yazyev, A.J. Austin, R. Cammi, C. Pomelli, J.W. Ochterski, R.L. Martin , K. Morokuma, V.G. Zakrzewski, G.A. Voth, P. Salvador, J.J. Dannenberg, S. Dapprich, A.D. Daniels, O. Farkas, J.B. Foresman, J.V. Ortiz, J. Cioslowski, D.J. Fox (2013) Gaussian'09, Revision D.01, Gaussian, Inc., Wallingford C.

# CHAPTER-2

---

## METHODOLOGY

### 2.1 Introduction

This part discusses the theoretical methods used for calculating electronic structures and the computational methods. This part can be categorized into two sections. The 1<sup>st</sup> section contains the concept of theories and the theoretical methods. In the 2<sup>nd</sup> section, a discussion on the computational approach, GAUSSIAN'09, Gauss-View, and Multiwfn software used for the simulations are briefly discussed.

### 2.2 Theoretical Approach of Quantum Chemistry Calculations

#### 2.2.1 Quantum Theories and Ideas of Multielectron System

To simulate a chemical composite or many-bodies atomic system consisting of an 'N' number of interacting electrons, the multibody wavefunction is defined as  $\Psi(r, R)$  which is used to describe the quantum state of the system. The wavefunction  $\Psi$  is dependent on 'r' known as the electronic coordinate, which also can be denoted as  $\vec{r}$  representing the position vector for electrons, and 'R' is the coordinate of nuclei or can be denoted as  $\vec{R}$ , the position vector for nuclei, respectively. The non-relativistic time-independent Schrodinger equation [1] can be written as

$$\hat{H}\Psi = E\Psi \quad (2.1)$$

The time-dependent Schrödinger equation for wavefunction  $\Psi$  can be written as

$$\left( -\frac{\hbar^2}{2m} \nabla^2 + V \right) \Psi(\vec{r}, t) = i\hbar \frac{\partial \Psi(\vec{r}, t)}{\partial t} \quad (2.2)$$

Where  $\Psi$  is the wavefunction,  $\vec{r}$  is the position vector, t is the time. Here,

$$\left( -\frac{\hbar^2}{2m} \nabla^2 + V \right) = \hat{H} \quad (2.3)$$

$\hat{H}$  is known as the Hamiltonian operator, which is basically the sum of kinetic energy and the potential energy operator. For multielectron or many-body atomic systems, the Hamiltonian operator  $\hat{H}$  takes the form like

$$\hat{H} = \hat{T}_e + \hat{T}_A + \hat{V}_{Ae} + \hat{V}_{ee} + \hat{V}_{AA} \quad (2.4)$$

Where,  $\hat{T}_e$  is the kinetic energy term of electrons which can be mathematically expressed as,

$$\hat{T}_e = -\sum_{i=1}^N \frac{\hbar^2 \nabla_i^2}{2e} \quad (2.5)$$

Where ‘N’ is the number of interacting electrons.

The second term of equation (2.4) of Hamiltonian is  $\hat{T}_A$ . It represents the kinetic energy of ions and it can be expressed as,

$$\hat{T}_A = -\sum_{A=1}^M \frac{\hbar^2 \nabla_A^2}{2M_A} \quad (2.6)$$

Here, M is the number of ions and  $M_A$  is mass of nucleus A. The third term of equation (2.4) is  $\hat{V}_{Ae}$  denotes the attractive interaction energy between electrons and ions. It can be mathematically expressed as,

$$\hat{V}_{Ae} = \sum_{i=1}^N \sum_{A=1}^M \frac{e^2 Z_A}{|r_i - R_A|} \quad (2.7)$$

Where  $r_i$  is electronic coordinate,  $R_A$  is the nuclear coordinate and  $Z_A$  is the atomic number of the nucleus A. The fourth term of the equation (2.4) is  $\hat{V}_{ee}$ , which represents repulsive interaction energy between the electrons and can be mathematically expressed as,

$$\hat{V}_{ee} = \sum_{i=1}^N \sum_{j>1}^N \frac{e^2}{|r_i - r_j|} \quad (2.8)$$

The fifth and the last term of equation (2.4) is  $\hat{V}_{AA}$ , which defines the repulsive interaction energy between the ions and it can be defined as,

$$\hat{V}_{AA} = \sum_{A=1}^M \sum_{B>1}^M \frac{e^2 Z_A Z_B}{|R_A - R_B|} \quad (2.9)$$

Thus, finally, we may express the Hamiltonian of the multi-body system for  $i^{\text{th}}$  electron and  $A^{\text{th}}$  nucleus as,



$$\hat{H} = \left( -\sum_{i=1}^N \frac{\hbar^2 \nabla_i^2}{2e} - \sum_{n=1}^M \frac{\hbar^2 \nabla_A^2}{2M_A} - \sum_{i=1}^N \sum_{A=1}^M \frac{e^2 Z_A}{|r_i - R_A|} + \sum_{i=1}^N \sum_{j>1}^N \frac{e^2}{|r_i - r_j|} + \sum_{A=1}^M \sum_{B>1}^M \frac{e^2 Z_A Z_B}{|R_A - R_B|} \right) \quad (2.10)$$

The above Hamiltonian also can be expressed in a simple form as,

$$\hat{H} = \left( -\sum_{i=1}^N \frac{\nabla_i^2}{2} - \sum_{n=1}^M \frac{\nabla_A^2}{2M_A} - \sum_{i=1}^N \sum_{A=1}^M \frac{Z_A}{|r_{iA}|} + \sum_{i=1}^N \sum_{j>1}^N \frac{1}{|r_{ij}|} + \sum_{A=1}^M \sum_{B>1}^M \frac{Z_A Z_B}{|R_{AB}|} \right) \quad (2.10b)$$

So, finally the Schrödinger equation takes the form like

$$\hat{H}\Psi = E\Psi$$

$$\left( -\sum_{i=1}^N \frac{\nabla_i^2}{2} - \sum_{n=1}^M \frac{\nabla_A^2}{2M_A} - \sum_{i=1}^N \sum_{A=1}^M \frac{Z_A}{|r_{iA}|} + \sum_{i=1}^N \sum_{j>1}^N \frac{1}{|r_{ij}|} + \sum_{A=1}^M \sum_{B>1}^M \frac{Z_A Z_B}{|R_{AB}|} \right) \Psi = E\Psi \quad (2.11)$$

Here,  $\nabla_i^2$  and  $\nabla_A^2$  are the Laplacian Operators and  $Z_A$  is atomic number of nucleus A as mentioned earlier. The third term also represents coulomb attraction between the electrons. Thus, as we can see the Hamiltonian of multibody system is very complicated and as a result, solving the Schrödinger equation of a more extensive system will be more difficult, complicated and time as well as energy consuming. So, there is a need to introduce some approximation to show a better and easier way to deal with such a complicated problem.

### 2.2.2 Born-Oppenheimer Approximation

This approximation is based on the mass difference between nuclei and electrons, that nuclei are much heavier and almost 1800 times more massive than that of electrons. As a result, the electron's kinetic energy is much higher than that of nuclei. Thus, while solving the electronic problem, one can easily ignore the nuclear kinetic energy as electron's kinetic energy is much higher than kinetic energy of nuclei. In this way, this approximation allows us to deal with such kind of complicated many-body problems more efficiently. It reduces the complexities of the modified multi-body Schrödinger equation, especially in a "frozen" nuclei configuration.

We had the Hamiltonian as,

$$\hat{H} = -\sum_{i=1}^N \frac{\nabla_i^2}{2} - \frac{1}{2M_A} \sum_{A=1}^M \nabla_A^2 - \sum_{i=1}^N \sum_{A=1}^M \frac{Z_A}{r_{iA}} + \sum_{i=1}^N \sum_{j>1}^N \frac{1}{r_{ij}} + \sum_{A=1}^M \sum_{B>A}^M \frac{Z_A Z_B}{R_{AB}} \quad (2.10b)$$

By recalling the equation (2.10b), the above equation is basically the total Hamiltonian of the system. The Born-Oppenheimer approximation [2] plays a significant role in reducing the above complicated Hamiltonian. As discussed before, the nuclei are much heavier in mass than the electrons and electrons move much faster than the nuclei, hence nuclei can be considered as fixed and not moving anywhere. Thus, the second term of the Hamiltonian, which is nothing but the kinetic energy of nuclei, can be ignored or neglected. Similarly, the fifth or the final term of the above Hamiltonian which is the term coming due to the repulsion between the nuclei, can be considered as constant for nuclei. Thus, the reduced and simplified Hamiltonian takes the mathematical form like

$$\hat{H}_{ele} = -\sum_{i=1}^N \frac{\nabla_i^2}{2} - \sum_{i=1}^N \sum_{A=1}^M \frac{Z_A}{r_{iA}} + \sum_{i=1}^N \sum_{j>1}^N \frac{1}{r_{ij}} \quad (2.12)$$

The above Hamiltonian equation (2.12) is known as electronic Hamiltonian or the electronic part of the total Hamiltonian of the system. Similarly, the total wavefunction of the whole multibody system can have two parts: the electronic part  $\Psi_e$  and the nuclear part  $\Psi_A$ . Thus, the electron wavefunction with Schrödinger equation can be expressed as,

$$\left( \hat{H}_e + \hat{V}_{AA} \right) \Psi(r, R) = E_e(R) \Psi(r, R) \quad (2.13)$$

Here, the electrons are considered as they are moving under the influence of potential field due to nuclei. For the practical use, the electronic wavefunction is appropriate, where

$$\hat{H}_e = \hat{T}_e + \hat{V}_{ee} + \hat{V}_{Ae}$$

Thus, as we all know, that the simplest form of Schrödinger equation can be written as,

$$\begin{aligned} \hat{H}\Psi &= E\Psi \\ \therefore \int \Psi^* \hat{H}\Psi d\tau &= \int \Psi^* E\Psi d\tau \end{aligned}$$

So, we can calculate the energy E as

$$E = \frac{\int \Psi^* \hat{H}\Psi d\tau}{\int \Psi^* \Psi d\tau} \quad (2.14)$$

### 2.2.3 Hartree-Fock (H-F) Theory

It has been observed that the approximation of non-interacting electrons also should be introduced to calculate the Schrödinger equation for a multi-electron system. The Hamiltonian of all electrons present in the system can be represented as,

$$\hat{H}_{ei} = \hat{T}_{ei} + \sum_A V_{Ai} \quad (2.15)$$

Where  $\hat{T}_{ei}$  is the kinetic energy of electrons and  $V_{Ai}$  is the potential energy developed due to the electron-nucleus interaction. So, for single electron system, the Schrödinger equation can be solved as  $\hat{H}_{ei}\Psi_i = \varepsilon_i\Psi_i$ , where  $\Psi_i$  is the wavefunction of the single-electron (say:  $i^{\text{th}}$  electron presents in the system) and  $\varepsilon_i$  the energy value.

As we are discussing about the electrons, one thing we must have in our mind, that electrons are fermions and possess anti-symmetry of the multi-electron wavefunction [3]. The wavefunction  $\Psi$  is not a physically observable quantity. For a system that consist of N number of electrons, Slater proposed his theory and said that a linear combination of single electrons spin functions can be represented as an anti-symmetrized determinant in which each row of the determinant represents an electron and each column present a spin-orbital. Such determinants can be expressed as,

$$\Psi = \frac{1}{N!} \begin{vmatrix} \chi_1(1) & \chi_2(1) \cdots \cdots \cdots & \chi_N(1) \\ \chi_1(2) & \chi_2(2) \cdots \cdots \cdots & \chi_N(2) \\ \vdots & \ddots & \vdots \\ \vdots & & \vdots \\ \chi_1(N) & \chi_2(N) \cdots \cdots \cdots & \chi_N(N) \end{vmatrix} \quad (2.16)$$

where,  $\chi$  is a set of electronic wavefunction including spin orbitals and  $1, 2, 3, \dots, N$  are the electrons or the coordinate of electrons or the position of the electrons. This above determinant is known as ‘‘Slater Determinant’’ [4]. According to the restricted Hartree-Fock method [5, 6], for all paired electrons, the Hartree-Fock equation can be expressed as,

$$f_i\Psi_i = \varepsilon_i\Psi_i \quad (2.17)$$

where,  $\Psi_i$  = Single-electron wavefunction,  $\varepsilon_i$  = eigenvalues,  $f_i$  represents the Fock operator and can be mathematically expressed as,

$$f_i = \hat{H}_{ei} + \sum_{j=1}^N (J_i(1) - K(1)) \quad (2.18)$$

In the above equation, J represents the coulomb integral, which describes the electrostatic repulsion between fermions, whereas K represents the exchange integral. “1” means the operator operates only on coordinates of number “1” electron. As the system is consist of the “N” number of electrons, so we have used summation starting from j=1 to N. In the system of N electrons, the electrons can be found nearer to each other than they have to be if the energy of each and every individual electron can be minimized. Thus, HF approximation [5, 6] may overestimate energy.

$$E_{corr} = E_{exact} - E_{HF} \quad (2.19)$$

It means the correlation energy can be estimated by the difference between the exact energy and the HF energy, which means the summation of single-electron energy values does not give the exact total energy of the consist of ‘N’ electrons. The reason behind this is, the electron-electron interaction energy will be calculated twice if we consider the equation (2.12) and (2.18). It can be rectified by dividing the entire interaction into two.

Thus, the HF energy will become

$$E_{HF} = \sum \varepsilon_i - \frac{1}{2} \sum_i \sum_j (J_{ij} - K_{ij}) \quad (2.20)$$

By solving the HF equation, one may get so many energy levels which are basically molecular orbitals in which each and every orbital represents certain energy levels. For a system consist of ‘N’ electrons, N orbitals can be found with lowest possible energy values, which leads to the lowest possible energy of the whole system, which can be considered as the most stable ground state energy of the system. As one can calculate the orbitals with certain energy, the MO (molecular orbital) can be found, including highest occupied molecular orbitals (HOMO) and lowest unoccupied molecular orbitals (LUMO). The linear combination of atomic orbitals (LCAO) can describe the molecular orbital (MO) as follows

$$\Psi_i = \sum C_{\sigma i} \phi_{\sigma} \quad (2.21)$$

Here,  $C_{\sigma_i}$  is the coefficient and  $\phi_{\sigma}$  denotes an atomic orbital. This means, with the help of the LCAO method one can calculate molecular orbitals using known functions with one unknown coefficient. By integrating over the volume, we can get Roothan equation [7]

$$FC = SC_{\epsilon} \quad (2.22)$$

Where F represents the Fock matrix, C denotes the coefficients  $C_{\sigma_v}$  and S is nothing but the matrices with overlap integrals  $S_{\sigma_v}$ . F and S can be expressed as,

$$\left. \begin{aligned} F_{\sigma_v} &= \int \Phi_{\sigma}^* f \Phi_{\sigma} d\tau \\ S_{\sigma_v} &= \int \Phi_{\sigma}^* \Phi_{\sigma} d\tau \end{aligned} \right\} \quad (2.23)$$

As discussed before, the lowest energy state represents the ground state of the energy, which is the most stable state of the system. The equation (2.22) and (2.23) involves a method in order to minimize the energy. To find out the most stable state of the system (ground state), it is very important to minimize the energy of the system. An iterative process can do this with a  $C_{\sigma_v}$  coefficient calculated by the energy minimization. This iterative process to minimize the system's energy to get the ground state is known as self-consistent field (SCF) method.

## 2.2.4 Density Functional Theory

### 2.2.4.1 Hohenberg-Kohn (H-K) Theorem

In the year of 1964, Pierre Hohenberg and Walter Kohn invented that the molecular wavefunction, the ground state energy, molecular properties like molecular orbitals of the system consist on 'N' number of electrons and system with non-degenerate ground state can be calculated as functionals of ground state electron density [8]. This means, the ground state energy of a system consist of 'N' electrons can be determined as a functional of ground state electron density of the system.

Let us consider the system is under the influence of an external potential  $V(r)$ . We can consider Hamiltonian as  $H = T + V + U$ . Where, Hamiltonian can be expressed as,

$$H = \sum_i \left\{ \left( -\frac{\hbar^2}{2m} \nabla_i^2 + \mathcal{G}(\vec{r}) \right) \right\} + \frac{1}{2} \sum_{i \neq j} \frac{e^2}{|r_i - r_j|} \quad (2.24)$$

where  $T$  is the kinetic energy of the electrons,  $\mathcal{G}(\vec{r})$  is the potential energy and the third term represents repulsive interaction energy between the electrons. If we consider  $\mathcal{G}_a$  and  $\mathcal{G}_b$  are the external potential,  $H_a$  and  $H_b$  are the correspondingly Hamiltonian of the system, similarly, if we consider  $\Psi_{0,a}$  and  $\Psi_{0,b}$  are the ground state energies of the system. According to Hohenberg and Kohn, the expectation value of Hamiltonian  $H_a$  over wavefunction  $\Psi_{0,b}$  will be higher than the ground state energy  $E_{0,a}$ .

$$\begin{aligned} \text{Thus, } E_{0,a} &< \langle \Psi_{0,b} | \hat{H}_a | \Psi_{0,b} \rangle < \langle \Psi_{0,b} | \hat{H}_a + \hat{H}_b - \hat{H}_b | \Psi_{0,b} \rangle \\ &< \langle \Psi_{0,b} | \hat{H}_a - \hat{H}_b | \Psi_{0,b} \rangle + \langle \Psi_{0,b} | \hat{H}_b | \Psi_{0,b} \rangle \end{aligned} \quad (2.25)$$

As discussed before, there are two different potentials  $\mathcal{G}_a$  and  $\mathcal{G}_b$ , so we have two different corresponding Hamiltonian  $H_a$  and  $H_b$ . Thus, we can write

$$E_{0,a} < \left\langle \Psi_{0,b} \left| \sum_{i=1}^n [\mathcal{G}_a(\vec{r}_i) - \mathcal{G}_b(\vec{r}_j)] \right| \Psi_{0,b} \right\rangle + E_{0,b} \quad (2.26)$$

where,  $\mathcal{G}_a(\vec{r}_i)$  and  $\mathcal{G}_b(\vec{r}_j)$  are one electron potential energy operators. So, we can write

$$E_{0,a} < \int n_{0,b}(\vec{r}) \{ \mathcal{G}_a(\vec{r}) - \mathcal{G}_b(\vec{r}) \} d\vec{r} + E_{0,b} \quad (2.27)$$

$$\text{Similarly, } E_{0,b} < \int n_{0,a}(\vec{r}) \{ \mathcal{G}_b(\vec{r}) - \mathcal{G}_a(\vec{r}) \} d\vec{r} + E_{0,a} \quad (2.28)$$

From Eq.no. (2.27) and (2.28), we can get

$$E_{0,a} + E_{0,b} < E_{0,b} + E_{0,a} \quad (2.29)$$

The above equation cannot exist and it is a valueless result as our initial assumption was to deal with non-degenerate ground state. Two different Potential will have two different Hamiltonian; thus, they have two different Schrödinger equations with different wavefunction. As a result, two different potentials cannot possess same ground state energy as well as they cannot have same ground state electron density for a non-degenerate ground state. As discussed before, the electronic Hamiltonian can be considered as,

$$H_{ele} = \hat{T}_e + V_{Ae} + V_{ee}$$

We have considered, that all the terms are as functional of ground state electrons density, so the above expression can be written as,

$$E = E(n_0) = T_e(n_0) + V_{Ae}(n_0) + V_{ee}(n_0) \quad (2.30)$$

$$\text{where } V_{Ae} = \left\langle \Psi_0 \left| \sum_{i=1}^n \mathcal{G}(\vec{r}_i) \right| \Psi_0 \right\rangle = \int \mathcal{G}(\vec{r}) n_0(\vec{r}) d\vec{r} \quad (2.31)$$

This can lead to

$$\begin{aligned} E = E(n_0) &= \int n_0(\vec{r}) \mathcal{G}(\vec{r}) d\vec{r} + T_e(n_0) + V_{ee}(n_0) \\ &= \int n_0(\vec{r}) \mathcal{G}(\vec{r}) d\vec{r} + F(n_0) \end{aligned} \quad (2.32)$$

The term,  $F(n_0) = T_e(n_0) + V_{ee}(n_0)$  does not depend on the external potential. As  $F(n_0)$  unknown we cannot compute the ground state energy of the 'N' number of electron system from  $n_0$ .

So, from the above equation, the ground state energy  $E_0$  cannot be calculated as the above equation failed to provide a proper way out. Thus, we need some other theory to calculate the system's ground state energy.

#### 2.2.4.2 The Second Hohenberg and Kohn (H-K) Theorem

Later, Hohenberg and Kohn gave another theory, where they considered a trial density function as  $n_\sigma(r)$  satisfying  $\int n_\sigma(\vec{r}) d\vec{r} = n$  and  $n_\sigma(\vec{r}) \geq 0$  for all r. For this density, the inequality stands  $E_0 \leq E_\nu[n_\sigma]$  [8]. According to the second theory of Hohenberg and Kohn, the trial density function  $n_\sigma(\vec{r})$  determines the external potential  $\mathcal{G}_\sigma(r)$  from the potential  $\mathcal{G}_\sigma(r)$ , wavefunction  $\Psi_\sigma(\vec{r})$  can be determined from the  $\Psi_\sigma(\vec{r})$  and from the equations (2.30), (2.31), and (2.32), we can write

$$\left\langle \Psi_\sigma \left| \hat{H} \right| \Psi_\sigma \right\rangle = \left\langle \Psi_\sigma \left| \hat{T}_e + \hat{V}_{ee} + \sum_{i=1}^n \mathcal{G}(\vec{r}_i) \right| \Psi_\sigma \right\rangle \geq E_0 = E_\nu[n_0] \quad (2.33)$$

As discussed before, kinetic and potential energies are the functional of the electron density, we can write

$$T_e(n_\sigma) + V_{ee}(n_\sigma) + \int n_\sigma \mathcal{G}_\sigma(\vec{r}) d\vec{r} \geq E_\nu \quad (2.34)$$

Now, if we look at the right-hand side of equation (2.34) and the left-hand side of equation (2.32), they look pretty same with the only difference is that,  $n_0$  in equation (2.32) is just

replaced by  $n_\sigma$  in equation (2.34). Only the actual electron ground state density can provide the authentic ground state energy. Actual ground state energy cannot be obtained from a trial electron density. Thus, the H-K theorem provides somehow an incomplete result.

### 2.2.4.3 Kohn-Sham Equations

In 1965, scientists W. Kohn and L. Sham placed their theory [9]. According to Kohn and Sham, if  $\Psi_i(\vec{r})$  denotes KS wavefunction and Kohn-Sham potential is denoted  $V_{KS}[n(\vec{r})]$  depending on  $n(\vec{r})$  the electron density, then

$$\left[ -\frac{1}{2}\nabla^2 + V_{KS}[n(\vec{r})] \right] \Psi_K(\vec{r}) = \varepsilon_K \Psi_K \quad (2.35)$$

$$\text{Thus, } \hat{H}_{KS} \Psi_K(\vec{r}) = \varepsilon_K \Psi_K(\vec{r}) \quad (2.36)$$

The ground state electron density depends on KS wavefunction

$$n(\vec{r}) = \sum_i^N |\Psi_K(\vec{r})|^2 \quad (2.37)$$

Now,  $V_{KS}[n(\vec{r})]$  consist of  $\mathcal{G}_{XC}[n(\vec{r})]$  the exchange and correlation potential due to nuclei.

Let us consider the Hartree potential as  $\mathcal{G}_{Hartree}(\vec{r})$ . Thus, the Kohn-Sham potential can be expressed as,

$$V_{KS}[n(\vec{r})] = \mathcal{G}_{ext}(\vec{r}) + \mathcal{G}_{Hartree}(\vec{r}) + \mathcal{G}_{XC}[n(\vec{r})] \quad (2.38)$$

$\mathcal{G}_{ext}(\vec{r})$  is the sum of all nuclear potentials.

$n_0(\vec{r})$ , the ground state electron density can be obtained from atomic densities for a solid-state system.

$$n_0(\vec{r}) = \sum_\beta n_\beta(\vec{r} - R_\beta) \quad (2.39)$$

Here, we are expressing the ground state electron as  $R_\beta$  is the position of  $\beta$  nucleus and  $n_\beta$  is atomic density. Now, the external potential  $\mathcal{G}_{ext}(\vec{r})$ , which is basically the sum of all nuclear potential (discussed before) can be represented as,

$$\mathcal{G}_{ext}(\vec{r}) = \sum_\beta \mathcal{G}_\beta(\vec{r} - R_\beta) \quad (2.40)$$

If  $Z_\beta$  be the nuclear charge, then the  $\mathcal{G}_\beta$  can be expressed as,



$$\mathcal{G}_\beta = -\frac{Z_\beta e^2}{r} \quad (2.41)$$

By the definition, the Hartree potential can be expressed as,

$$\mathcal{G}_{Hartree}(\vec{r}) = \int \frac{n(\vec{r}')}{|\vec{r} - \vec{r}'|} d^3\vec{r}' \quad (2.42)$$

By using Poisson equation, we can get

$$\nabla^2 \mathcal{G}_{Hartree}(\vec{r}) = -4\pi n(\vec{r}) \quad (2.43)$$

The exchange-correlation potential  $\mathcal{G}_{XC}[n(\vec{r})]$ , the third term of equation (2.38), can be expressed as,

$$\mathcal{G}_{XC}[n(\vec{r})] = \frac{\partial E_{XC}}{\partial n(\vec{r})} \quad (2.44)$$

Thus, the total energy of the system can be expressed as,

$$E_{Tot}(n) = T_s(n) + E_{ext}(n) + E_H(n) + E_{XC}(n) (+E_{ion}) \quad (2.45)$$

where KS kinetic energy is

$$T_s(n) = -\frac{1}{2m} \sum_K \theta_K \int d^3r \Psi_K^*(r) \nabla^2 \Psi_K(r) \quad (2.46)$$

The external potential energy is

$$E_{ext}[n] = \int d^3r \mathcal{G}_{ext}(\vec{r}) n(\vec{r}) \quad (2.47)$$

Where,  $\theta_K$  is the occupation function [10],  $\theta_K = \begin{cases} 1 & \text{for } \varepsilon_K \leq \varepsilon_F \\ 0 & \text{for } \varepsilon_F < \varepsilon_K \end{cases}$

The third term, Hartree energy, can be expressed as,

$$E_H[n] = \frac{e^2}{2} \int d^3\vec{r} \int d^3\vec{r}' \frac{n(\vec{r})n(\vec{r}')}{|\vec{r} - \vec{r}'|} \quad (2.48)$$

The exchange-correlation energy can be calculated using local density approximation (LDA)

$$E_{XC}^{LDA} = \int \xi^{XCE}(n) \Big|_{n=n(r)} d^3\vec{r} \quad (2.49)$$

$$\text{And, } \mathcal{G}_{XC}^{LDA}(r) = \frac{\partial}{\partial n(r)} \xi^{XCE}(n) \Big|_{n=n(\vec{r})} \quad (2.50)$$

The term  $\xi^{XCE}$  in the above two equations (2.49) and (2.50) represents the exchange-correlation energy per unit volume of the electron-gas with constant electron density  $n$ . Now,

from this derivation, we can calculate the system's total energy. Thus, from the Kohn-Sham theory and by using the above equation we can express the energy as,

$$E_{Tot}[n] = T_s(n) + E_{ext}(n) + E_H(n) + E_{XC}(n) + E_{ion}$$

$$E_{Tot}[n] = -\frac{1}{2m} \sum_K \theta_K \int d^3r \Psi_K^*(r) \nabla^2 \Psi_K(r) + \int \mathcal{G}_{ext}(\vec{r}) n(\vec{r}) d^3r + \frac{e^2}{2} \int d^3\vec{r} \int d^3\vec{r}' \frac{n(\vec{r})n(\vec{r}')}{|\vec{r}-\vec{r}'|} + E_{XC}(n) \quad (2.51)$$

The first term represents the Kohn-Sham kinetic energy, the second term of the above equation (2.51) indicates the external potential energy term, third term is the Hartree energy and the last and the final energy term  $E_{XC}[n]$  represents the exchange -correlation energy term.

The electrostatic repulsion of the nuclei in a pseudopotential frame work can be expressed as,

$$E_{ion} = \sum_{A < B=1}^{N_{ion}} \frac{Z_A Z_B e^2}{|R_A - R_B|}$$

$$\mathcal{G}_{ext}(r) = -\sum_{A=1}^{N_{ion}} \frac{Z_A e^2}{|r - R_A|}$$

To optimize a molecular geometry or an atomic cluster, it is very important to add this above term to the total energy term.

## 2.2.5 Exchange Correlation Functional

### 2.2.5.1 Local Density Approximation (LDA)

We already know that the exact form of exchange-correlation energy functional is unknown. Thus, the solution obtained from DFT calculation is directly dependent on the functional which has been chosen i.e.,  $E_{XC}$  [11]. Local density approximation (LDA) can be considered as the simplest approximation, which considers the concept of a uniform electron gas, where the electrons are placed in an infinite region of space, hypothetically with a uniform positive external potential. Thus,  $E_{XC}^{LDA}$  can be mathematically expressed as,

$$E_{XC}^{LDA} = \int \rho(\vec{r}) \varepsilon_{XC} \rho(\vec{r}) d\vec{r} \quad (2.52).$$

The exchange-correlation energy functional can be categorized into two parts as  $E_X$  and  $E_C$ . where  $E_X$  and  $E_C$  are the exchange functionals and correlation functionals respectively. Thus,

we can write  $E_{XC} = E_X + E_C$ . In the above equation (2.52), the term  $\varepsilon_{XC}$  is a functional which depends explicitly on the local density at each point  $\vec{r}$ . The  $E_X$  (exchange part) for the homogenous electron gas is known and it was derived by Bloch [12] and Dirac [13], but there is no such expression is known for  $E_C$  (the correlation part) [14-16]. The correlation part has been developed by few authors. The most widely used one has been invented by Perdew and Wang [17].

### 2.2.5.2 Local Spin Density Approximation (LSDA)

We have already discussed the local density approximation [18] previously. For the spin-polarized system, it is very essential to consider the spin during the calculation. Here, the exchange-correlation energy in LSDA can be mathematically expressed as,

$$E_{XC}^{LSDA}[\rho_\alpha, \rho_\beta] = \int dr \rho(r) \varepsilon_{XC}(\rho_\alpha, \rho_\beta) = \int \rho_\alpha(r) \varepsilon_{XC} \rho_\beta(r) d\vec{r} \quad (2.53)$$

Where,  $\rho_\alpha$  and  $\rho_\beta$  are the spin electronic densities. It provides much better results, especially during the optimization of structure geometries, Charge calculations, electrostatic potential, and vibrational frequencies for the system containing spin. Thus, LSDA is just an extension of LDA method, which contains spin-polarization as well.

### 2.2.5.3 Generalized -Gradient Approximation (GGA)

After LDA, another very well-known and widely used method come into the picture and that method is known as generalized gradient approximation (GGA) [19, 20]. Here, to evaluate  $E_{XC}$ , the information about the density  $\rho(\vec{r})$  at a particular point  $\vec{r}$  along with the information on the charge density gradient,  $\nabla\rho(\vec{r})$  is used for the non-homogeneity of the proper electron density. GGA exchange-correlation functional can be explained as,

$$E_{XC}^{GGA} = \int f(\rho, \nabla\rho) d\vec{r} \quad (2.54)$$

This kind of functional is suitable for a molecular system with non-uniform electron density. There are so-many GGA functionals available [19-22]. The most commonly used is the PBE functional by Perdew, Burk, and Ernzerhof (PBE) [22]. In this kind of method, spin-polarized versions of these functions are developed. It has been proved several times that the DFT-GGA approach is very reliable for a wide range of applications. However, GGAs still have some

disadvantages of yielding only approximate exchange continuous contributions, which result in certain problems expressing the exchange part of the energy. These difficulties can be overcome by including a component of the exact exchange energy calculated from the Hartree-Fock theory. Functional of such type is known as hybrid functional [23] and can be expressed as,

$$E_{XC}^{Hybrid} = cE_X^{HF} + (1-c)E_X^{DFT} + E_C^{DFT} \quad (2.55)$$

the coefficient  $c$  indicates the HF exchange contribution.

### 2.2.6 Basis Set

Basis set can be defined as a set of unknown basis functions with the help of which, the wavefunction can be expanded. A single electron wavefunction can be written as,

$$\Psi_i(r) = \sum_j C_j \xi_j(r) \quad (2.56)$$

where  $\xi_j(r)$  is a complete set of functions. Such kind of set of functions can be used as basis functions. In general, any basis function should exhibit similar kind of limiting behaviors as the real wavefunction holds and for any isolated atom or molecules they should decay to zero as they should not be very complicated or computationally expensive.

### 2.2.7 Plane Wave Basis Set

The expression of potential of a periodic system can be presented as,

$$V(r + na) = V(r) \quad (2.57)$$

Where 'n' is an integer and 'a' is lattice vector.

The wavefunction of a system can be written as

$$\Psi_i(r) = e^{ikr} \xi_i(r) \quad (2.58)$$

As discussed before, that the system has a periodicity, here  $\xi_i(r)$  can be expanded as set of plane wave as,

$$\xi_i(r) = \sum_G C_i G e^{iGr} \quad (2.59)$$

In the above equation,  $G$  represents the reciprocal lattice vector.

If we substitute the equation (2.59) in equation (2.58), we can get

$$\Psi_i(r) = \sum_G C_i G e^{i(K+G).r} \quad (2.60)$$

From the above equation, the largest wave vector can control the number of wavefunctions used for a particular simulation for a particular system. Here, K represents the wave vector.

The kinetic energy of an electron of such a system can be written as,

$$E_K = \frac{\hbar^2 |K|^2}{2m} \quad (2.61)$$

Thus, the Kohn-Sham equations can be written as [24]

$$\left[ \sum_{G'} \frac{\hbar^2}{2m} |K + G|^2 \delta_{GG'} + V_{en}(G - G') + V_{ee}(G - G') + V_{xc}(G - G') \right] C_i . K + G' = C_i . K + G'^{ei} \quad (2.62)$$

Here,  $V_{en}(G - G')$  is the Fourier transforms of electron-nuclei potential.

$V_{ee}(G - G')$  = Fourier transforms of electron-electron interaction potential

$V_{xc}(G - G')$  = Fourier transforms of exchange-correlation potentials.

### 2.2.8 Self-Consistent Field (SCF)

The solution for the molecular orbitals and the total energy of the 'N' body or multi-body system should be carried out by an iterative process starting from the initial guess. Each molecular orbital is dependent on the repulsive interaction of each electron in the orbitals with all other electrons in the system. Thus, it is next to impossible to optimize the molecular orbitals and simulate the energy of the system until or unless the field experienced by the electron is known. To deal with such cases, optimizing the molecular orbitals and simulating the system's energy using the iterative method is the only way out. This method is referred to as the self-consistent field method. The density functional energy of a multi-body system can be calculated by this iterative method named as self-consistent field method (SCF) [25]. For example, if we consider the H-F method, we can understand that in the case of the Hartree-Fock equation [5, 6], the Fock operator  $f_i$  is dependent on the HF potential on the spin orbitals. So, the eigenvalue problem has to be solved, which will be solved with the help of an iterative process. This procedure is known as a self-consistent field procedure. In this technique, the orbitals are derived from their own effective potential. The iterative method starts with an initial guess. In our work, this initial guess will be, a guessed set of orbitals, for which the HF

equations are solved. The resulting new set of orbitals is then used in the next iteration and so on until or unless we don't get the optimized lowest ground state energy.

### **2.2.9 B3LYP**

In our work, we have mainly considered B3LYP functional to calculate or simulate our system. It is a hybrid functional that is developed or invented in the late 80's. B3 is Becke 3-parameter exchange-correlation functional [26-28]. These functional utilize 3-parameters to mix the exact HF exchange-correlation and Lee, Yang, and Parr [29] correlation functional. The hybrid functional, which is a mixing of DFT and HF, include the exchange and correlation parts of both methods will give much better and more reliable results than the others. That is why B3LYP [26-29] is the most famous and widely used hybrid functional.

$$E_{XC}^{B3LYP} = E_X^{LDA} + a_0 (E_X^{HF} - E_X^{LDA}) + a_x (E_X^{GGA} - E_X^{LDA}) + E_C^{LDA} + a_c (E_C^{GGA} - E_C^{LDA}) \quad (2.63)$$

Where,  $E_X^{GGA}$  and  $E_C^{GGA}$  are the generalized gradient approximation exchange and correlation functionals respectively.  $E_C^{LDA}$  is the local density approximation correlation term. Here,  $a_0 = 0.20$ ,  $a_x = 0.72$ ,  $a_c = 0.81$ . Here,  $a_0$ ,  $a_x$  and  $a_c$  are 3 empirical parameters. These parameters determine the relative weight of each compared to this hybrid functional. Proper choice of Functional as well as the basis set is very important to get a reliable result in such kind of simulation process.

## **2.3 Computational Methodology**

### **2.3.0 Gaussian'09, GaussView & MultiWaveFunction**

In our work, all the simulation and calculations are performed using GaussView and Gaussian'09 program [30]. GaussView is a graphical user interface (GUI) program by which one can prepare the input file and submit the simulation job under a certain potential environment.

#### **2.3.1 Gaussian'09**

Gaussian' 09 [30] program is one of the most widely used simulation programs all over the world. After preparing the input file using the GaussView program that input file needs to be submitted for the calculation. When that input file gets submitted, the Gaussian

program starts the simulation process. After simulation, it produces the output file. The output file of Gaussian '09 contains the SCF energy of the system. Generally, the output file of Gaussian' 09 depends on the input file submitted using GaussView. Gaussian provides us with a wide range of calculation facilities such as one can perform geometry optimization, single point energy calculation, frequency, NBO analysis, Transition state, IRC (Intrinsic reaction coordinate) and many more. Thus, whatever information required in the output file strongly depends on the input file, the type of coding, and the type of calculation, the type of system, the potential environment and the degree of accuracy. In Gaussian, once the convergence criterion is met, the optimized geometry of the system is obtained.

### ***2.3.2 GaussView***

The Gauss view program allows us to prepare atomic systems of any chemical composition, atomic clusters, supercell geometries, nano-tube, etc. With the help of "GaussView" one can set the potential environment, a particular method of calculation such as a semi-empirical method, Hartree-Fock method, DFT method, MP2 (Moller-Plesset), MP4, CCSD, BD, etc. In "GaussView" we can also choose the basis set such as 3-21G, 6-31G, 6-311G, Lan12DZ, 6-311G(d), 6-311G (d, p), and many more. The functionals included in "GaussView" program are B3PW91, LSDA, B3LYP, PBE, TPSS, and many more. Spin and charge of a particular system also can be assigned here. Gaussian and "GaussView" provide us with a wide range of calculation types such as one can perform geometry optimization, single point energy calculation, frequency, NBO analysis, Transition state, IRC (Intrinsic reaction coordinate), and many more. After calculation, the output of the simulations can be visualized using "GaussView".

### ***2.3.3 MultiWaveFunction***

Multiwfn [31] is an open-source program that provides a wide range of calculations such as orbital calculations, topology analysis, IR, Raman, UV-Vis, NMR, electron density calculation, Electron localization function (ELF), basin analysis. Critical point (CP) determination, DOS, total DOS, partial DOS, photoelectron spectrum, and many more. In our work, the Multiwfn program is used for calculating the ELF and Critical point of the clusters.

## *References*

- [1] E. Schrödinger, “An Undulatory Theory of the Mechanics of Atoms and Molecules”, *Physical Review*, **28(6)**, (1926), 1049. <https://doi.org/10.1103/PhysRev.28.1049>
- [2] M. Born, and R. Oppenheimer, “On the quantum theory of molecules”, *Annals of Physics*, **389(20)**, (1927), 457-484. <http://dx.doi.org/10.1002/andp.19273892002>
- [3] A. Szabo, and N.S. Ostlund, “Modern quantum chemistry: Intro to advanced electronic structure theory” Dover Pub. New York (1996).
- [4] J.C. Slater, “The Theory of Complex Spectra”, *Physical Review*, **34(10)**, (1929), 1293. <https://link.aps.org/doi/10.1103/PhysRev.34.1293>
- [5] D.R. Hartree, “The Wave Mechanics of an Atom with a Non-Coulomb Central Field. Part I. Theory and Methods“, Cambridge Univ. Press, **24**, (1928)111-132. <http://dx.doi.org/10.1017/S0305004100011919>
- [6] V. Fock, “Approximation method for the solution for the quantum and mechanical multibody system”, *J. Physics*, **61**, (1930), 126-148. <http://dx.doi.org/10.1007/BF01340294>
- [7] C.C.J. Roothaan, “New Developments in Molecular Orbital Theory”, *Reviews of modern physics*, **23(2)**, (1951), 69. <http://dx.doi.org/10.1103/RevModPhys.23.69>
- [8] P. Hohenberg, and W. Kohn, “Inhomogeneous Electron Gas”, *Physical review*, **136(3B)**, (1964), B864. <https://doi.org/10.1103/PhysRev.136.B864>
- [9] W. Kohn, and L.J. Sham, “Self-Consistent Equations Including Exchange and Correlation Effects”, *Physical review*, **140(4A)**, (1965), A1133. <https://link.aps.org/doi/10.1103/PhysRev.140.A1133>
- [10] C. Fiolhais, F. Nogueira, and M. Marques, “A Primer in Density Functional Theory”, Springer, 2003.
- [11] G.E. Scuseria, and V.N. Staroverov, “Progress in the development of exchange-correlation functionals”, *Theory and Applications of Computational Chemistry*, (2005), 1-53. <https://doi.org/10.1016/B978-044451719-7/50067-6>.



- [12] F. Bloch, “Über die Quantenmechanik der Elektronen in Kristallgittern”, *Z. Physik*, **52**, (1929), 555–600. <https://doi.org/10.1007/BF01339455>.
- [13] P.A. Dirac, “Note on Exchange Phenomena in the Thomas Atom. Mathematical Proceedings of the Camb. Philo. Society”, **26(99)**, (1930) 376-385. <http://dx.doi.org/10.1017/S0305004100016108>
- [14] S.H. Vosko, L. Wilk, and M. Nusair, “Accurate Spin-Dependent Electron Liquid Correlation Energies for Local Spin Density Calculations: A Critical Analysis”, *Can. J. Phys*, **58**, (1980), 1200. <https://doi.org/10.1139/p80-159>
- [15] J.P. Perdew, and A. Zunger, “Self-Interaction Correction to Density-Functional Approximations for Many-Electron Systems”, *Physical Review B*, **23(10)**, (1981), 5048. <https://doi.org/10.1103/PhysRevB.23.5048>
- [16] L.A. Cole, and J. Perdew, “Calculated electron affinities of the elements”, *Physical Review A*, **25(3)**, (1982), 1265. <https://link.aps.org/doi/10.1103/PhysRevA.25.1265>
- [17] J.P. Perdew, and Y. Wang, “Accurate and simple analytic representation of the electron-gas correlation energy”, *Physical Review B*, **45(23)**, (1992), 13244. <https://link.aps.org/doi/10.1103/PhysRevB.45.13244>
- [18] J.P. Dahl, and J. Avery, “Local density approximations in quantum chemistry and solid-state physics”, Springer Science & Business Media, (2013).
- [19] J.P. Perdew, J.A. Chevary, S.H. Vosko, K.A. Jackson, M.R. Pederson, D.J. Singh, and C. Fiolhais, “Atoms, molecules, solids, and surfaces: Applications of the generalized gradient approximation for exchange and correlation”, *Physical Review B*, **48(7)**, (1993), 4978. <https://doi.org/10.1103/PhysRevB.48.4978.2>
- [20] G.J. Laming, V. Termath, and N.C. Handy, “A general purpose exchange-correlation energy functional”, *The J. Chem. Phys*, **99(11)**, (1993), 8765-8773. <https://doi.org/10.1063/1.465598>
- [21] M. Filatov, and W. Thiel, “A new gradient-corrected exchange-correlation density functional”, *Mol. Physics*, **91(5)**, (1997), 847-860. <https://doi.org/10.1080/002689797170950>.

- [22] J.P. Perdew, K. Burke, and M. Ernzerhof, “Generalized Gradient Approximation Made Simple”, *Phys. Rev. Lett.*, **78(7)**, (1997), 1396. <https://doi.org/10.1103/PhysRevLett.78.1396>
- [23] A.D. Becke, “A New Mixing of Hartree-Fock and Local Density-Functional Theories”, *J. Chem. Phys.*, **98(2)**, (1993), 1372-1377. <http://dx.doi.org/10.1063/1.464304>.
- [24] M.C. Payne, M.P. Teter, D.C. Allan, T. Arias, and J. Joannopoulos, “Iterative minimization techniques for ab initio total-energy calculations: molecular dynamics and conjugate gradients”, *Reviews of Modern Physics*, **64(4)**, (1992), 1045. <https://doi.org/10.1103/RevModPhys.64.1045>
- [25] S.M. Blinder, “Basic Concepts of Self-Consistent-Field Theory”, *American Journal of Physics*, **33(6)**, (1965), 431. <https://doi.org/10.1119/1.1971665>.
- [26] A.D. Becke, “Density-functional exchange-energy approximation with correct asymptotic behaviour”, *Phys. Rev. A*, **38(6)**, (1988), 3098–3100. <https://doi.org/10.1103/PhysRevA.38.3098>
- [27] K. Kim, and K.D. Jordan, “Comparison of Density Functional and MP2 Calculations on the Water Monomer and Dimer”, *J. Phys. Chem.*, 1994, **98(40)**, 10089–10094. <https://doi.org/10.1021/j100091a024>.
- [28] P.J. Stephens, F.J. Devlin, C.F. Chabalowski, and M.J. Frisch, “Ab Initio Calculation of Vibrational Absorption and Circular Dichroism Spectra Using Density Functional Force Fields”, *J. Phys. Chem.*, **98(45)**, (1994), 11623–11627. <https://doi.org/10.1021/j100096a001>
- [29] C. Lee, W. Yang, and R.G. Parr, “Development of the Colle-Salvetti correlation-energy formula into a functional of the electron density”, *Phys. Rev. B.*, **37(2)**, 1988, 785–789. <https://doi.org/10.1103/PhysRevB.37.785>
- [30] M.J. Frisch, G.W. Trucks, H.B. Schlegel, G.E. Scuseria, M.A. Robb, J.R. Cheeseman, G. Scalmani, V. Barone, B. Mennucci, G.A. Petersson, H. Nakatsuji, M. Caricat, X. Li, H.P. Hratchian, A.F. Izmaylov, J. Bloino, G. Zheng, J.L. Sonnenberg, M. Hada, M.

Ehara, K. Toyota, R. Fukuda, J. Hasegawa, M. Ishida, T. Nakajima, Y. Honda, O. Kitao, H. Nakai, T. Vreven, Jr. J.A. Montgomery, J.E. Peralta, F. Ogliaro, M. Bearpark, J.J. Heyd, E. Brothers, K.N. Kudin, V.N. Staroverov, T. Keith, R. Kobayashi, J. Normand, K. Raghavachari, A. Rendell, J.C. Burant, S.S. Iyengar, J. Tomasi, M. Cossi, N. Rega, J.M. Millam, M. Klene, J.E. Knox, J.B. Cross, V. Bakken, C. Adamo, J. Jaramillo, R. Gomperts, R.E. Stratmann, O. Yazyev, A.J. Austin, R. Cammi, C. Pomelli, J.W. Ochterski, R.L. Martin, K. Morokuma, V.G. Zakrzewski, G. A. Voth, P. Salvador, J.J. Dannenberg, S. Dapprich, A.D. Daniels, O. Farkas, J.B. Foresman, J.V. Ortiz, J. Cioslowski, D.J. Fox, Gaussian'09, Revision D.01, Gaussian, Inc., Wallingford C, 2013.

- [31] T. Lu, and F. Chen, "Multiwfn: A multifunctional wave function analyzer", *J Comp Chem.*, **33(5)**, (2011), 580-592. <https://doi.org/10.1002/jcc.22885>.

## CHAPTER-3

---

### THE ELECTRONIC STRUCTURES AND PROPERTIES OF $Mg_n$ ( $n=2-20$ ) NANOCCLUSERS: A DENSITY FUNCTIONAL INVESTIGATION

#### 3.1 Introduction

Nanoclusters containing a minimal number of atoms to hundreds of atoms became a center of importance because of their wide range of applications in nanoscience and nanotechnology. The physical properties of macroscopic materials are very much independent of their shape and size due to their very negligible surface to volume ratios, still, stable nanomaterials formed due to molecular or atomic simulation, a drastic change in surface to volume ratio occur and the system shows some exciting properties that depend very much on their size and shapes. Nanoclusters are essential not only due to their size-dependent physical and chemical properties but its wide range of applications as hydrogen storage, catalyst, biomedicines, electronic devices and mechanical appliances. The properties like chemical reactivity, stability, diffusion length, electron-free path, coherent domain size etcetera change with the size of the cluster because a significant fraction of the atoms lie on the surface of the cluster with different bond lengths, bond angles, and thus acquiring a discrete electronic structure. The phenomenon is very complex and the change of different parameters manifests differently due to changes in the orientation and size of clusters. With the experimental confirmation of electronic shell structures from mass spectra [1] and the theoretically established Jellium model in analogy with the nuclear shell model [2-5], atomic clusters may be considered as separate entities with their physical and chemical properties.

Magnesium is a promising candidate for mass sensitive applications, and it can store up to 7.6 wt.% of hydrogen. The metallic Mg has hexagonal (space group: P63/mmc) crystal structure with lattice parameters  $a=b=3.2094 \text{ \AA}$  and  $c=5.2108 \text{ \AA}$ . It is one of the alkaline earth metals and the eighth most abundant material in the Earth crust. It can be considered as a cheap material. Divalent Magnesium,  $[Ne] 3s^2$  has a closed-shell electronic configuration and medium reactivity with the environment. A considerable energy gap exists between the ground state  $3s^2$  and vacant  $3p$  state. Two Mg atoms interact very weakly with binding energy

0.0025eV compared to bulk material 1.51 eV/atom [6]. These small-sized diatomic Mg clusters are weakly bonded by Van der Waals forces, while in larger clusters, 3p electron involvement in sp hybridization increases. In pure clusters, with the increase in cluster size, the interaction between Mg atoms increases and the gap between highest occupied molecular orbital (HOMO, here 3s) and lowest un-occupied molecular orbital (LUMO, 3p) decreases. For higher size clusters, the gap becomes negligibly small, reaching the metal work function, and shows metallic characteristics [7, 8]. Many researchers have investigated evolution of structural growth of  $Mg_n$  clusters in the past [7-18, 22, and 23]. Reuse et al. studied the geometry, stability and electronic properties of small sized ( $n=1-8$ ) clusters using LDA approximation and concluded that  $Mg_n$  clusters tend to form compact structures [9]. Kumar et al. [10] reported for ( $n=2-13$ ), the base structure of  $Mg_n$  clusters are trigonal and tetrahedral. Energetics and structural properties of  $Mg_n$  ( $n=2-22$ ) has been reported by Kohn et al. [11] using DFT and reported  $n=4, 10$  and  $20$  are most stable clusters according to the shell model. With the increase of the number of atoms in the cluster, metallic characteristics appear with an ionization potential of 3.64 eV, and the band gap becomes very narrow for clusters above  $n=18$  are reported by Thomas et al. ( $n=3-35$ ) and Lyalin et al. [7, 14]. Using LDA approximation, a growth pattern has been reported by Delaly et al. in early 1992 [12] for ( $n=8-13$ ). Belyaev et al. reported a DFT study of  $Mg_n$  ( $n=2-31$ ) for singlet and triplet states [13]. The Mg-Mg bond length approaches that of Mg metal for  $n>20$  concluded from simulation using B3LYP with Hartree-Fock many body perturbations [14]. Jellinek et al. reported ( $n=2-22$ ) size induced insulator to metal transition [15, 16]; a study of electron affinity of alkali-earth materials has been reported by Torrejon et al. [17]. Heidari et al. [18] reported for ( $n=10-56$ ) as a theoretical counterpart of the experimental work of Diedrich [19, 20], for ( $n=2-17$ ) Shen et al. [22] using kick's method of global minimum structures reported optimized stable structures. Detailed structure and bond length has been reported by Xia et al. [21], Janecek et al. using Langevin molecular dynamics, reported nature and properties of  $Mg_n$  and  $Na_n$  for ( $n=2-30$ ) [23] and Zhang et al. reported structure and electronic properties for ( $n=2-20$ ) [24]. Boruah et al. reported influence of 3d metal doping for ( $n=2-10$ ) [25]. Experimental investigation of the stability of  $Mg_n$  clusters up to 80 atoms using mass spectroscopy has been reported by Diederich et al. [19, 20] found the deviation of magic numbers in case of clusters and established them using spherical shell model. The conclusions arrived from these results

for (n=2-20) agree well with the experimental results of mass and photoelectron spectroscopy [19, 20, 26-28].

A considerable number of theoretical investigations are done using Kohn-Sham Density Functional theory [29] with different exchange correlation functional [9-23], Hartree-Fock Theory [30], Moller-Plesset (MP) perturbation theory [31], Moller-Plesset of fourth order MP4 [32] etc. and their differences of results depending upon the method and basis set chosen, and also has been studied. Thus, before proceeding further towards applications of Mg nanoclusters it is worthy to perform a complete systematic study of pure Mg clusters using a proper method with a proper set of basis functions.

In this work, the structural growth of pure  $Mg_n$  clusters (n=2-20), interatomic distances, average binding energy per atom, second order change in energy, Fragmentation energy, HOMO-LUMO energy gap, Vertical ionization potential (VIP), Vertical electron affinity (VEA), Chemical potential ( $\mu$ ), Chemical hardness ( $\eta$ ), and Fermi energy are presented. HOMO-LUMO surface structures, Molecular electrostatic potential contours, and total electron density has been also studied. All the simulations are done within the framework of Kohn-Sham Density Functional Theory (DFT) using GAUSSIAN'09 [33]. A comparison of calculation of Vertical ionization potential (VIP) and Vertical electron affinity (VEA) has been made between the two methods viz. one is the anionic-cationic method, and the other one is Koopmans method [34]. The conclusions arrived from these results for (n=2-20) correlate well with experimental results of photoelectron spectroscopy and mass spectroscopy of Diedrich et al. and others [19, 20, 26-28].

### ***3.2 Computational Methodology***

In the current work, the geometry of all the clusters has been optimized within the Kohn-Sham Density Functional Theory (DFT) framework using GAUSSIAN'09 [33]. To optimize the pure  $Mg_n$  (n=2-20) clusters, B3LYP [35, 36] (Becke, 3-parameter, Lee-Yang-Parr) functional with 6-311G (d) basis set is used. While calculating potential energy surface, it is considered that all electrons of the cluster are available for interaction. With the growth of the clusters, as the size of clusters increases, calculations or optimizations of the clusters become more and more time demanding and high configuration computational system

demanding. Therefore, in the present work, we limit our investigation by the cluster size  $n=20$ . One of the essential characteristics of the Density Functional Theory is that here many-electron correlation with exchange-correlation potential is considered. This basis set consists of 6 contracted Gaussian primitive functional for the core, a triply split valance basis set using three, one and one Gaussian primitives. Total 18 basis functions for each atom of the first row are taken. The basis function produces one s one p and one d diffuse function for the third row of atoms. For all the clusters, geometries were optimized with unconstraint symmetry starting from the different initial configurations to avoid the minima of surface potential energy lock. Comparing these results with reported experimental, and theoretical studies it is confirmed that the computational methods adopted here and the results obtained agree with the reported works.

### ***3.3 Results and Discussions***

#### ***3.3.1 Growth Pattern of Pure Magnesium Nanoclusters $Mg_n$ ( $n=2-20$ )***

Pure  $Mg_n$  clusters ( $n=2-20$ ) with all possible isomers have been optimized. Among all optimized clusters, only ground-state clusters with minimum energy are chosen. The growth of clusters with point group symmetries has been discussed in this section. The first member of the pure  $Mg_n$  series is  $Mg_2$ .  $Mg_2$  is a dimer of two magnesium atoms whose bond length is 3.927 Å which is in good agreement with the experimental result of [19, 20, 26-28] and also in agreement with the computational chemistry benchmark database, a standard reference database [37]. The  $Mg_3$  cluster forms by giving one upper cap with  $Mg_2$  which is an Mg-Mg dimer.  $Mg_3$  cluster forms an equilateral triangle with point group symmetry  $D_{3h}$  and bond length 3.47 Å and binding energy per atom is increasing rapidly at this stage. The ground state configurations of  $Mg_4$ - $Mg_6$  are mostly tetrahedron-based clusters. Here,  $Mg_4$  has  $T_d$  point group symmetry and the other orientation of  $Mg_4$  has  $D_{2d}$  point group symmetry, whereas  $Mg_5$  possesses  $D_{3h}$  point group symmetry. The other orientation of the  $Mg_5$  cluster is cyclopentene, where all the carbon atoms are replaced with Mg atoms and hydrogen atoms are removed. This cluster possesses  $D_{5h}$  point group symmetry.

Mg <sub>2</sub> : D <sub>∞h</sub>	Mg <sub>3</sub> : D <sub>3h</sub>	Mg <sub>4</sub> : T <sub>d</sub>	Mg <sub>4</sub> B: D <sub>2d</sub> ΔE=2.23E-5	Mg <sub>5</sub> : D <sub>3h</sub>
Mg <sub>5</sub> B: D <sub>3h</sub> : ΔE = 0.42eV	Mg <sub>6</sub> : D <sub>3h</sub>	Mg <sub>6</sub> B: D <sub>3h</sub> : ΔE=0.22eV	Mg <sub>6</sub> : C <sub>1</sub>	Mg <sub>6</sub> B: C <sub>1</sub> : ΔE=0.014eV
Mg <sub>7</sub> C: C <sub>1</sub> : ΔE=0.073eV	Mg <sub>7</sub> : C <sub>1</sub>	Mg <sub>7</sub> B: C <sub>1</sub> : ΔE=0.006eV	Mg <sub>7</sub> C: C <sub>1</sub> : ΔE=0.218eV	Mg <sub>7</sub> : C <sub>1</sub>
Mg <sub>8</sub> B: C <sub>1</sub> : ΔE=0.08eV	Mg <sub>8</sub> C: C <sub>1</sub> : ΔE=1.00eV	Mg <sub>8</sub> : C <sub>1</sub>	Mg <sub>8</sub> B: C <sub>1</sub> : ΔE=0.099eV	Mg <sub>8</sub> C: C <sub>1</sub> : ΔE=0.064eV
Mg <sub>9</sub> : D <sub>3h</sub>	Mg <sub>9</sub> B: C <sub>1</sub> : ΔE=6.4E-5eV	Mg <sub>9</sub> : C <sub>1</sub>	Mg <sub>9</sub> B: C <sub>1</sub> : ΔE=0.18eV	Mg <sub>9</sub> C: C <sub>1</sub> : ΔE=0.33eV
Mg <sub>10</sub> D: D <sub>2d</sub> : ΔE=1.08eV	Mg <sub>10</sub> E: D <sub>2d</sub> : ΔE=2.59eV	Mg <sub>10</sub> : C <sub>1</sub>	Mg <sub>10</sub> B: C <sub>1</sub> : ΔE=0.033eV	Mg <sub>10</sub> C: C <sub>1</sub> : ΔE=0.039eV
Mg <sub>11</sub> D: C <sub>v</sub> : ΔE=0.48eV	Mg <sub>11</sub> : C <sub>1</sub>	Mg <sub>11</sub> B: C <sub>v</sub> : ΔE=0.26eV	Mg <sub>11</sub> C: C <sub>1</sub> : ΔE=0.01eV	Mg <sub>11</sub> : D <sub>3h</sub>
Mg <sub>12</sub> B: C <sub>s</sub> : ΔE=0.08eV	Mg <sub>12</sub> C: C <sub>1</sub> : ΔE=0.498eV	Mg <sub>12</sub> : C <sub>1</sub>	Mg <sub>12</sub> B: C <sub>1</sub> : ΔE=0.03eV	Mg <sub>12</sub> C: S <sub>8</sub> : ΔE=0.36eV
Mg <sub>13</sub> : C <sub>1</sub>	Mg <sub>13</sub> B: C <sub>1</sub>	Mg <sub>13</sub> C: C <sub>1</sub> : ΔE=0.006eV	Mg <sub>13</sub> D: C <sub>s</sub> : ΔE=0.8eV	Mg <sub>13</sub> : C <sub>1</sub>
Mg <sub>14</sub> B: C <sub>1</sub> : ΔE=0.072eV	Mg <sub>14</sub> C: C <sub>v</sub> : ΔE=0.14eV	Mg <sub>14</sub> : C <sub>s</sub>	Mg <sub>14</sub> B: C <sub>s</sub> : ΔE=1.08 eV	Mg <sub>14</sub> : C <sub>s</sub>

Fig. 3.1 Optimized ground state structures of pure Mg<sub>n</sub> (n=2-20) clusters with point group symmetry. All the pink balls are Magnesium atoms.



The Mg<sub>6</sub> has D<sub>2h</sub>, and Mg<sub>6\_B</sub> also has D<sub>2h</sub> point group symmetry. Mg<sub>6</sub> is nothing but a side cap with an Mg<sub>5</sub> cluster, and Mg<sub>6\_B</sub> can be achieved by giving an upper cap with an Mg<sub>5\_B</sub> cluster. The lowest energy state configuration of Mg<sub>7</sub> is a pentagonal-bipyramid-based cluster with C<sub>s</sub> point group symmetry. The Mg<sub>7\_B</sub> cluster can be made by giving one upper cap and one down cap on the Mg<sub>5\_B</sub> cluster. Mg<sub>7\_B</sub> cluster is with C<sub>s</sub> point group symmetry and Mg<sub>7\_C</sub> is also with C<sub>s</sub> point group symmetry. Mg<sub>8</sub> cluster has C<sub>s</sub> point group symmetry, and Mg<sub>8\_B</sub> is C<sub>1</sub> point group symmetry and Mg<sub>8\_C</sub> holds C<sub>s</sub> point group symmetry. Here, Mg<sub>8\_B</sub> can be formed by giving a side upper cap to the Mg<sub>7\_B</sub> cluster where Mg<sub>8\_C</sub> possesses a ring-type construction. The ground state cluster of Mg<sub>9</sub> can be achieved by giving an upper hat to the Mg<sub>8\_B</sub> cluster. The Mg<sub>9</sub> cluster holds C<sub>1</sub> point group symmetry. The other orientations, like Mg<sub>9\_B</sub>, also hold C<sub>1</sub> point group symmetry which can be achieved by giving an upper hat to the Mg<sub>8\_C</sub> cluster. Mg<sub>9\_C</sub> cluster possesses C<sub>1</sub> point group symmetry. The ground state orientation of the Mg<sub>10</sub> cluster is achieved by having a side cap to the Mg<sub>9</sub> cluster, which also holds C<sub>1</sub> point group symmetry. The other orientation structure Mg<sub>10\_B</sub> has C<sub>1</sub> point group symmetry where Mg<sub>10\_C</sub> can be achieved by giving two hats to the Mg<sub>8\_C</sub> cluster, one on one side and another one on the opposite side. This cluster holds point group C<sub>2</sub>. The lowest energy state of the Mg<sub>11</sub> cluster holds D<sub>3h</sub> point group symmetry which is nothing but an upper or a lower hat with the Mg<sub>10\_B</sub> cluster. Mg<sub>11\_B</sub> holds C<sub>2</sub> point group symmetry. The lower state of the Mg<sub>12</sub> cluster holds C<sub>1</sub> point group symmetry where Mg<sub>12\_B</sub> has C<sub>s</sub> point group symmetry, and Mg<sub>12\_C</sub> has C<sub>1</sub> point group symmetry. Here, Mg<sub>12</sub> is the most stable cluster, which comes under a new cluster category. Mg<sub>12\_D</sub> has D<sub>2d</sub> point group symmetry which can be achieved by adding two hexagons with each other. Mg<sub>12\_E</sub> is a very unstable cluster; we are not interested in it. The ground state Mg<sub>13</sub> cluster holds C<sub>1</sub> point group symmetry which can be formed by giving just a side hat to the Mg<sub>12</sub> cluster. Mg<sub>13\_B</sub> has C<sub>1</sub> and Mg<sub>13\_C</sub> also possess C<sub>1</sub> point group symmetry. Mg<sub>13\_D</sub> cluster holds C<sub>2v</sub> point group symmetry which can be made by adding a side cap to the Mg<sub>12\_B</sub> cluster. The ground state Mg<sub>14</sub> holds C<sub>1</sub> point group symmetry. A new category of cage-type clusters comes from the Mg<sub>14</sub> cluster. Mg<sub>14\_B</sub> holds a unique construction that possesses C<sub>2v</sub> point group symmetry where Mg<sub>14\_C</sub> can be made by adding an upper or a lower hat to the Mg<sub>13\_D</sub> cluster.

The ground state orientation of the Mg<sub>15</sub> cluster holds D<sub>3h</sub> point group symmetry. The construction of the Mg<sub>15</sub> cluster is very unique, it results in the high symmetry structures of

two connected Mg<sub>9</sub> clusters. Mg<sub>15\_B</sub> comes under C<sub>s</sub> point group symmetry, and Mg<sub>15\_C</sub> holds C<sub>1</sub> point group symmetry. Mg<sub>15</sub> clusters can be considered as a new starting point for forming an hcp lattice for Magnesium. The lowest energy state of Mg<sub>16</sub> holds C<sub>1</sub> point group symmetry, where Mg<sub>16\_B</sub> also has C<sub>1</sub> point group symmetry and Mg<sub>16\_C</sub> has S<sub>8</sub> point group symmetry. The lowest energy state and the most stable configuration of the Mg<sub>17</sub> cluster can be achieved by adding a central Mg atom to the center of Mg<sub>16\_C</sub> cluster. This configuration holds C<sub>1</sub> point group symmetry Mg<sub>17\_B</sub> and Mg<sub>17\_C</sub> also possess C<sub>1</sub> point group symmetry where Mg<sub>17\_D</sub> has C<sub>s</sub> point group symmetry and, from which Mg<sub>17</sub> is the most stable cluster. The ground state cluster of Mg<sub>18</sub> has C<sub>1</sub> point group symmetry and Mg<sub>18\_B</sub> holds C<sub>1</sub> and Mg<sub>18\_C</sub> has C<sub>2v</sub> point group symmetry, among which Mg<sub>18</sub> is the most stable cluster. These all cluster are 3 layer clusters; if we look at their construction, we can understand that there are three layers inside. The ground state configuration of Mg<sub>19</sub> cluster holds C<sub>s</sub> point group symmetry where the other orientation also holds C<sub>s</sub> point group symmetry.

Similarly, Mg<sub>20</sub> also holds C<sub>s</sub> point group symmetry, achieved by adding a single Mg atom with Mg<sub>19\_B</sub> cluster. It is seen that all pure clusters are singlet spin states with multiplicity 1. Magic numbers may be assigned with different polyhedral geometry viz. n=7 for decahedral geometry, n=4, 10, 20 as tetrahedral geometry etc. [11] Fig. 3.1 shows the growth of pure Mg<sub>n</sub> clusters.

The average bond lengths of all optimized clusters are given in Table 3.1. The values are compared with available bond length of previous work [37-39] and available experimental data [37]. Not all values of average bond length available from the literature, however, data available from Trivedi and Bandyopadhyay calculated using Gaussian'03, B3LYP for (n=2-10) and Duanmu et al. [39] presented bond lengths of only a few clusters (n=2-4) calculated using coupled cluster method CCSD (T) are compared. However, the bond length is available only for (n=2-10) from the literature [39]. It is seen that with an increase of cluster size, average bond length decreases nonlinearly from 3.927 Å to 3.14 Å. The minimum interatomic distance is 3.14 Å.

Cluster	Avg. Bond Length(Å) This work	Prev. work/ Expt. Value (Å)	Cluster	Average Bond Length(Å) This work	Prev work /Expt. Value (Å)
Mg <sub>2</sub>	3.927	3.96 <sup>a</sup> /3.891 <sup>b</sup> /3.929 <sup>c</sup> /3.93 <sup>d</sup>	Mg <sub>12</sub>	3.23	-
Mg <sub>3</sub>	3.47	3.45 <sup>b</sup> /3.33 <sup>c</sup> /3.43 <sup>d</sup>	Mg <sub>13</sub>	3.18	-
Mg <sub>4</sub>	3.17	3.13 <sup>b</sup> /3.06 <sup>c</sup> /3.18 <sup>d</sup>	Mg <sub>14</sub>	3.18	-
Mg <sub>5</sub>	3.32	3.24 <sup>b</sup> /3.33 <sup>d</sup>	Mg <sub>15</sub>	3.16	-
Mg <sub>6</sub>	3.56	3.16 <sup>b</sup> /3.3 <sup>d</sup>	Mg <sub>16</sub>	3.23	-
Mg <sub>7</sub>	3.24	3.82 <sup>b</sup> /3.32 <sup>d</sup>	Mg <sub>17</sub>	3.23	-
Mg <sub>8</sub>	3.44	3.91 <sup>b</sup> /3.25 <sup>d</sup>	Mg <sub>18</sub>	3.30	-
Mg <sub>9</sub>	3.16	3.19 <sup>b</sup> /3.09 <sup>d</sup>	Mg <sub>19</sub>	3.20	-
Mg <sub>10</sub>	3.23	3.89 <sup>b</sup> /3.06	Mg <sub>20</sub>	3.19	-
Mg <sub>11</sub>	3.14	-			-

<sup>a</sup>[36], <sup>b</sup>[37], <sup>c</sup>[25], <sup>d</sup>[39]

### 3.3.2 Relative Stability of Clusters

#### 3.3.2.1 Average Binding Energy and Stability of the Pure Mg<sub>n</sub> (n=2-20) Clusters

The binding energy per atom can be defined as

$$BE(Mg_n) = \frac{nE(Mg) - E(Mg_n)}{n} \quad (3.1)$$

E(Mg) represents the optimized energy of single Mg atom, E(Mg<sub>n</sub>) is the optimized energy of n<sup>th</sup> cluster and n represents the number of atoms in the cluster.

The pure Mg<sub>n</sub> (n=2-20) clusters are optimized using the B3LYP method with 6-311G (d) basis set.

Let us discuss the behavior of the binding energy of pure clusters as a function of cluster size. In Fig.3.2 the number of Mg atoms in the clusters has been plotted along x-axis, and the average binding energy per atom in eV/atom has been plotted along y-axis. Here, the variation of binding energy with the increase of cluster size is compared with that reported earlier [11, 14, 22, and 23]. It is found that the nature of the graphs is almost same as each other except

$n=16$ . The binding energy per atom of reference [15, 16] differs due to functional and the basis set chosen. This indicates our process of calculation is in right direction.

According to the electronic shell model, electronic shell such as 1S, 1P, 1D, 2S, 1F, 2P ... are fully occupied by 2, 8, 18, 20, 34, 40... number of electrons, respectively. It gives  $n=4$ , 10, and 20 are closed shell clusters. Again, the deformed jellium clusters that have closed electronic sub-shells hold higher stability. According to the theory of superatom, all these shells correspond to superatomic orbitals. For that reason, the clusters with valence electrons 6, 10, 14, 18, 22, 26, 30, 34 etc. are relatively more stable than the other clusters. These give rise to some more magic numbers such as 3, 5, 7, 9, 11, 13, 15, and 17 as closed shell systems. According to the photoelectron, mass spectroscopy [19, 20] and high-resolution transmission electron microscopy [26] it is reported that clusters with  $n=5$ , 10, 15, 18, 20, 25, 28, 30, 35, 40, 47, 56, 59, 62 and 69 are most stable clusters.

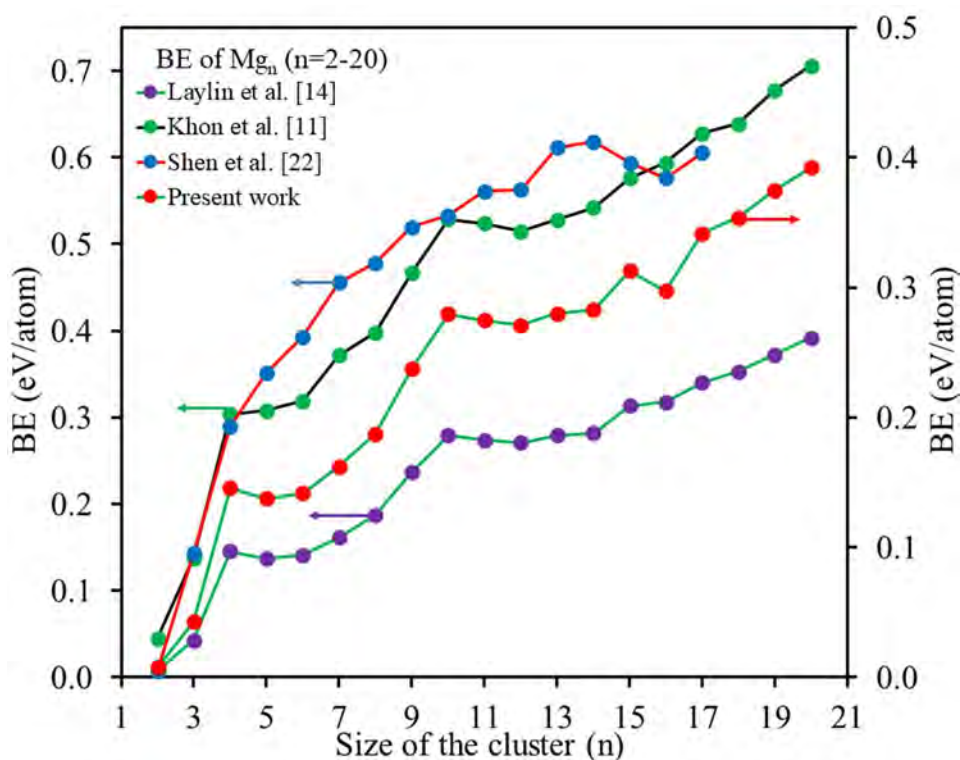


Fig. 3.2 Variation of average binding energy per atom with cluster size.

In this study, from Fig. 3.2 and Table-3.2 it is seen that the binding energy per atom rises with the increase of cluster size. A higher the rate of change in binding energy leads to higher stability of the clusters. The behavior of binding energy indicates the local maxima at  $n=4$ , 10,

20, which corresponds to the most stable geometry of the magic magnesium cluster respectively. In our study also, Mg<sub>4</sub>, which has eight valence electrons and possesses 1S<sup>2</sup>1P<sup>6</sup> electronic configuration, the Mg<sub>10</sub> cluster has 20 numbers of valence electrons and holds 1S<sup>2</sup>1P<sup>6</sup>1D<sup>10</sup>2S<sup>2</sup> electronic configuration, Mg<sub>17</sub> cluster has 34 numbers of electrons and has 1S<sup>2</sup>1P<sup>6</sup>1D<sup>10</sup>2S<sup>2</sup>1F<sup>14</sup> electronic configuration and Mg<sub>20</sub> cluster possesses 40 numbers of electrons and its electronic configuration is 1S<sup>2</sup>1P<sup>6</sup>1D<sup>10</sup>2S<sup>2</sup>1F<sup>14</sup>2P<sup>6</sup>. Thus, these behaviors of binding energy in our calculations agree with the spherical jellium model.

The second order change in cluster energy is considered as a parameter for stability. Large positive values of Δ<sub>2</sub>E are an indication of gain in energy during the growth process from the just lower size cluster and lower gain in energy for the next higher size.

Thus, higher is the value of Δ<sub>2</sub>E the higher the stability of the cluster. Δ<sub>2</sub>E is calculated with the relation

$$\Delta_2 E(Mg_n) = [E(Mg_{n+1}) + E(Mg_{n-1}) - 2E(Mg_n)] \quad (3.2)$$

This graph also supports the previous BE graph. As we can see, according to the stability graph (Fig.3.3) 4, 7, 10, 13, 15, 17, and 20 are showing local peaks and positive stability values. We have already discussed the spherical Jellium model.

The analysis of stability graph also confirms the binding energy graph and its conclusion and also gives an indication about relative stability of the Mg<sub>13</sub>, Mg<sub>15</sub>, and Mg<sub>17</sub> along with the stable clusters Mg<sub>4</sub>, Mg<sub>10</sub> and Mg<sub>20</sub>.

The spheroidal Jellium model confirms that the orbital angular momentum is not an appropriate or proper quantum number to characterize the valance electron energy levels. We have already discussed the electronic configurations of some stable cluster like Mg<sub>4</sub>, Mg<sub>10</sub>, Mg<sub>17</sub> and Mg<sub>20</sub>, confirming that these clusters are shell filled clusters.

Fragmentation energy of clusters is also an indicator of relative stability of clusters compared to neighboring clusters. The higher the value of FE stronger is the interaction means a higher energy requirement to detach an atom from the cluster. The fragmentation energy is calculated as

$$\Delta(n, n - 1)Mg_n = (E(Mg_{n-1}) + E(Mg) - E(Mg_n)) \quad (3.3)$$

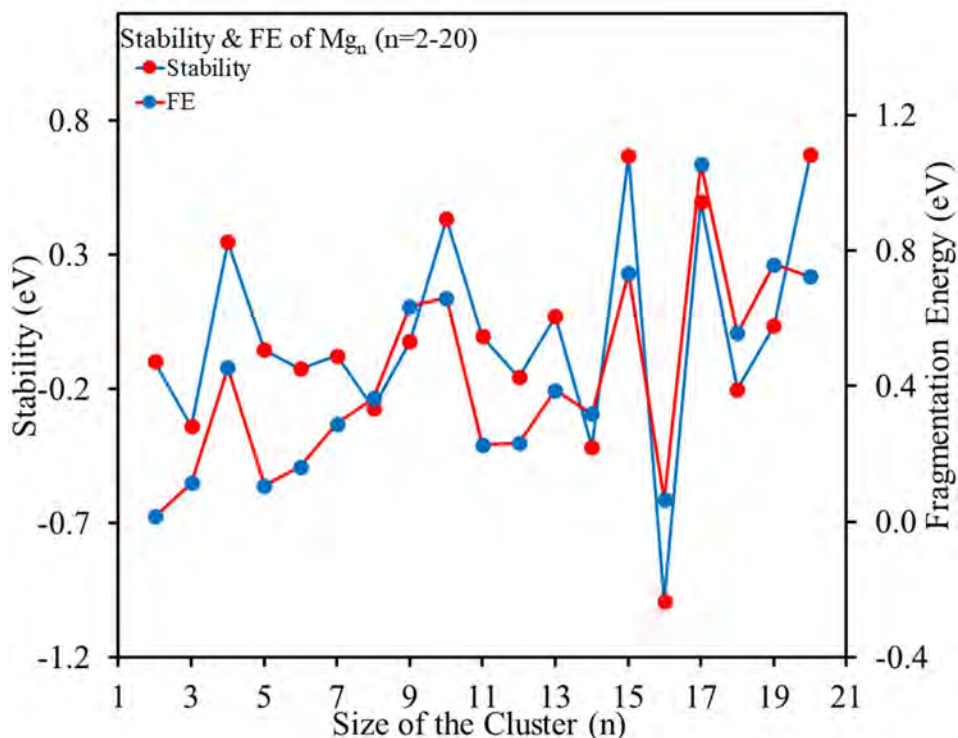


Fig. 3.3 Variation of stability and fragmentation energy with cluster size.

This implies larger stability of the cluster. From graph Fig. 3.3 it is seen that the local peaks of fragmentation energy are for  $n = 4, 10, 13, 15, 17, 19$ . The results for pure  $Mg_n$  clusters agree well with previous works [11-18]. The trend in stability is possibly due to size effect and it implies that the stability depends upon the compactness of a cluster.

### 3.3.3 HOMO-LUMO gap

HOMO is the highest occupied molecular orbital, the orbital may or may not be completely filled (singlet or triplet cases), whereas the valance band concept is the band up to which all states are filled. Similarly, LUMO is the lowest unoccupied molecular orbital, which implies the orbital is empty, but the conduction band is the band from which states are empty or partially empty so HOMO-LUMO gap in clusters cannot be considered the same as band gap in metal, semiconductors and insulators. However, a cluster with a larger HOMO-LUMO gap possesses higher chemical stability and higher inertness. It also reflects the kinetic stability and electrical conductivity of the cluster. If the HOMO-LUMO energy gap is high,

high energy is required for electrons to jump from highest occupied orbit to lowest unoccupied orbit of a cluster.

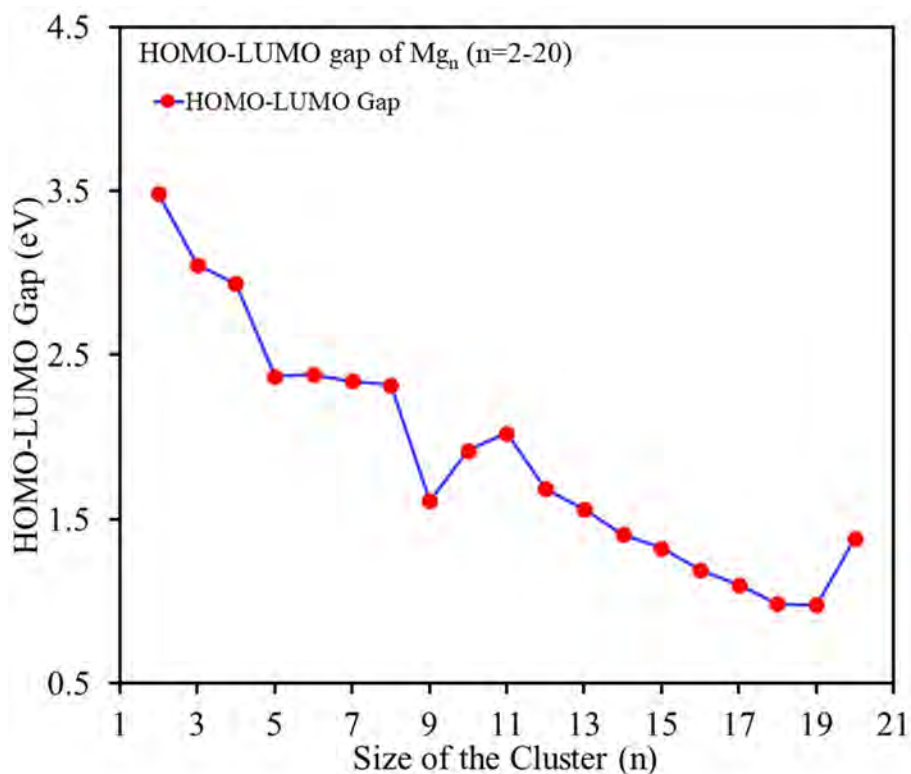


Fig. 3.4 Variation of HOMO-LUMO gap with size of clusters.

On the other hand, when the HOMO-LUMO energy gap is low, it represents the higher chemical reactivity, mean that much low energy is required for an electron to jump from HOMO to LUMO. Fig.3.4 shows the variation of energy gap between the highest occupied molecular orbital and lowest unoccupied molecular orbital (HOMO-LUMO gap) for pure Mg<sub>n</sub> clusters as a function of cluster size. In the study of HOMO-LUMO gap for pure Mg<sub>n</sub> (n=2-20) cluster, it is found that maxima at n= 4, 10, 20, which indicates these cluster are more stable than others (Fig. 3.4), these clusters follow the jellium model. The gap gradually decreases with increase of the number of atoms in cluster 3.485 eV for Mg<sub>2</sub> to 0.977 eV for Mg<sub>19</sub>, which indicates the metallic behavior of pure Mg<sub>n</sub> clusters starts from Mg<sub>18</sub>. This is due to overlapping of more and more atomic orbitals, with increase of atom number, energy levels come closer and closer.

### 3.3.4 Vertical Ionization Potential (VIP), Vertical Electron Affinity (VEA), Chemical Potential ( $\mu$ ) and Chemical Hardness ( $\eta$ )

To study the chemical reactivity of the pure  $Mg_n$  cluster, the study of the reactivity indicators, such as vertical ionization potential (VIP), vertical electron affinity (VEA), chemical hardness ( $\eta$ ), chemical potential ( $\mu$ ) etc. are performed.

Vertical Ionization Potential (VIP) expresses the tendency of a cluster to release or gain an electron. The vertical ionization potential is the amount of energy absorbed when an electron is detached from the neutral atom considering particle relaxation is not allowed. The decrease in VIP may occur due to increase of energy of the occupied orbital due to a donor electron. A higher value of VIP means more energy is required to detach an electron from an atom. So, they are more stable. The optimized energy difference between the cationic and neutral cluster can estimate it. Mathematically one can express it as,

$$VIP(Mg_n) = E(Mg_n^+) - E(Mg_n) \quad (3.4)$$

Again, according to Koopmans's theorem, VIP can be calculated from HOMO-LUMO energies of clusters as

$$VIP = -E_{HOMO} \quad (3.5)$$

The ground state of pure  $Mg_4$  with  $T_d$  point group symmetry,  $Mg_8$  with  $C_s$  point group symmetry, and  $Mg_{10}$  with  $C_1$  point group symmetry, all of them have higher value of VIP. There is a drop of VIP occurs at  $n=7, 10, 13, 15, 17, 19$ .

Electron affinity describes the tendency of a cluster to absorb an electron from neighbor. VEA may predict the stability of a cluster since it is the amount of energy liberated when an extra atom is added to a cluster.

It may be calculated as the difference of optimized energy of pure cluster and anionic cluster as,

$$VEA(Mg_n) = E(Mg_n) - E(Mg_n^-) \quad (3.6)$$

According to Koopmans theorem VEA can be defined in terms of HOMO and LUMO as

$$VEA = -E_{LUMO} \quad (3.7)$$



Estimation of VIP and VEA using both cationic and anionic method and Koopmans method is presented here (Fig. 3.5(a)). It is seen that the nature of variation is same in the two methods but there is an average difference of 0.97 eV between the two processes. Here, since B3LYP functional, a hybrid functional, and Gaussian'09 uses extended Koopmans theorem one may rely on the values obtained from Koopmans theorem. The values obtained from cationic and anionic method gives poorer values with respect to experimental values.

Chemical Potential can be evaluated as

$$\mu = -\frac{E_{HOMO} + E_{LUMO}}{2} \quad (3.8)$$

And Chemical hardness can be defined as

$$\eta = \frac{(E_{HOMO} - E_{LUMO})}{2} \quad (3.9)$$

Chemical hardness also can be defined as

$$\eta = \frac{(VIP - VEA)}{2} \quad (3.10)$$

Where VIP is the vertical ionization potential and VEA is the electron affinity.

Global softness (S) is defined as the inverse of hardness and Fermi energy can be represented by

$$E_F = -\mu \quad (3.11)$$

Based on all calculated energetics parameters, we can consider Mg<sub>4</sub> as one of the most stable clusters.

If we apply the concept of Jellium model, one can conclude that for Mg<sub>n</sub> clusters, n= 4, 8, 10, 20 etc. are most stable clusters.

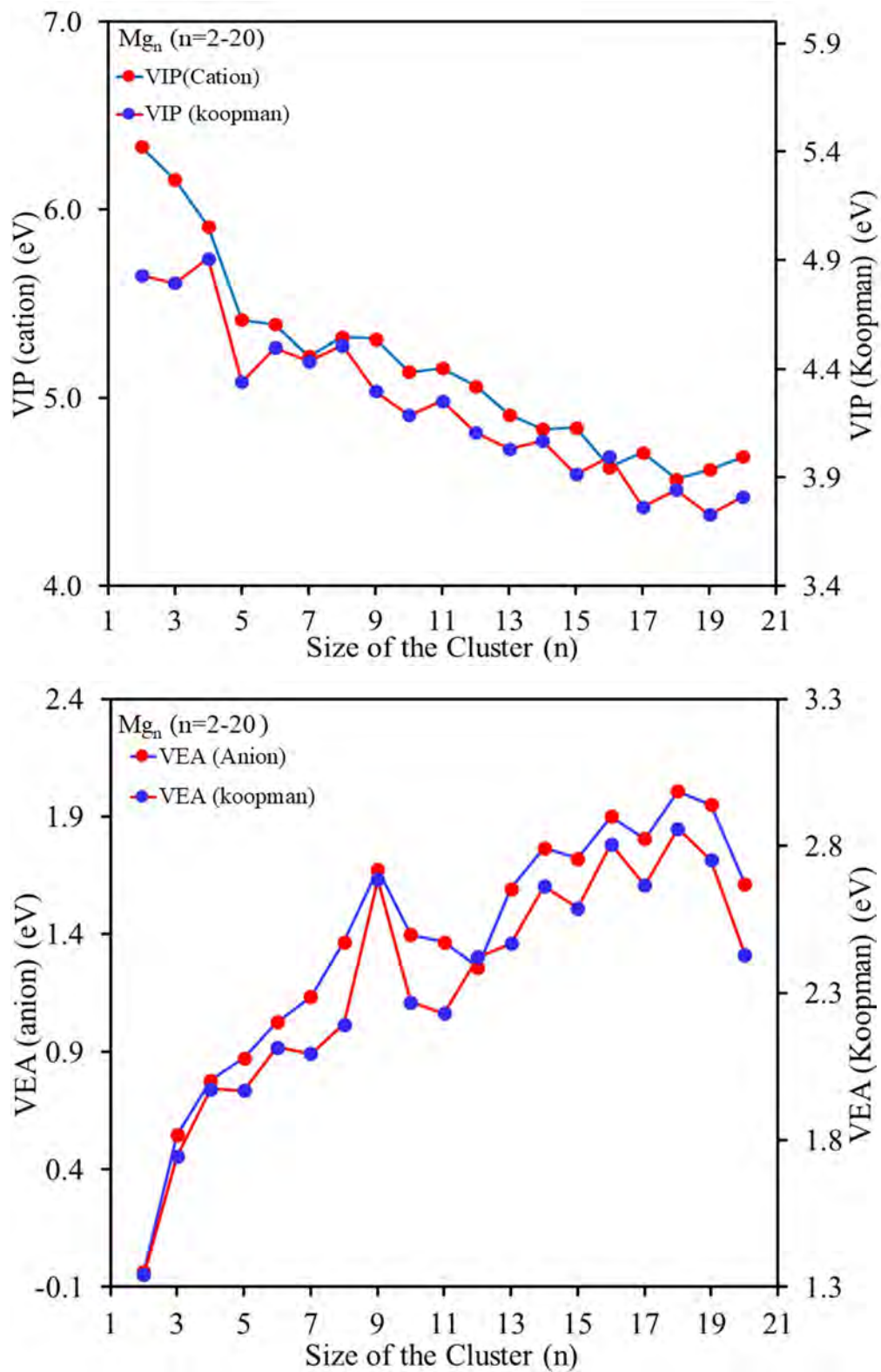


Fig. 3.5(a) Variation of VIP and VEA with cluster size for both anionic-cationic methods and Koopmans method.

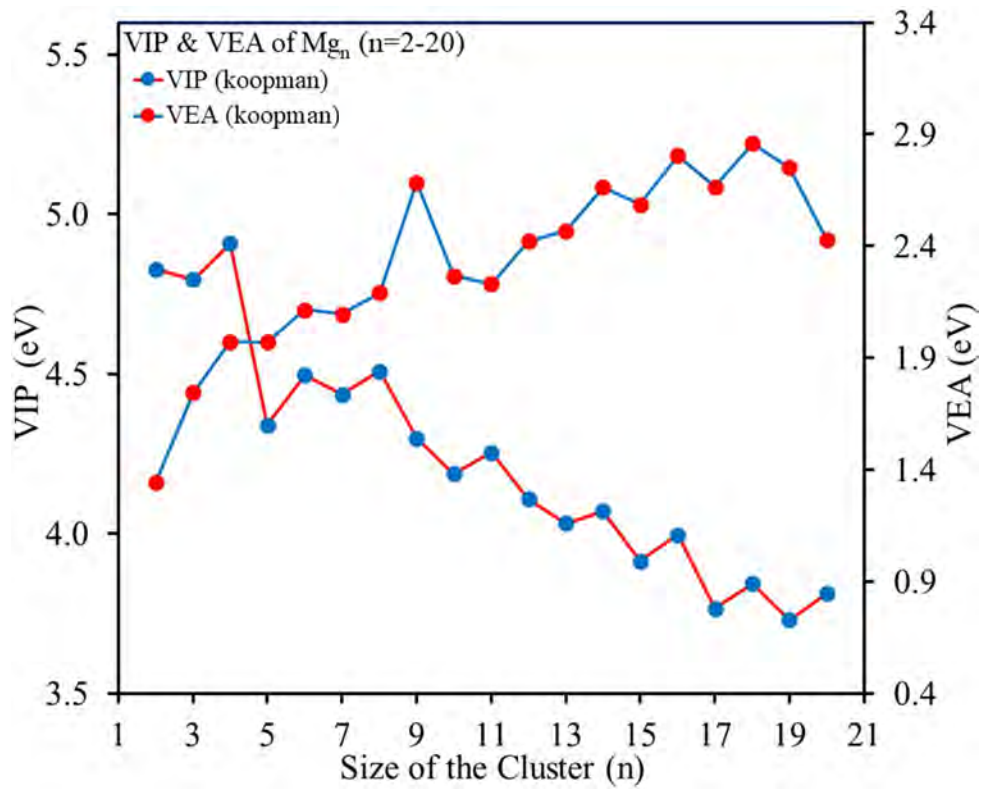


Fig. 3.5(b) Variation of VIP and VEA with cluster size (Koopmans method).

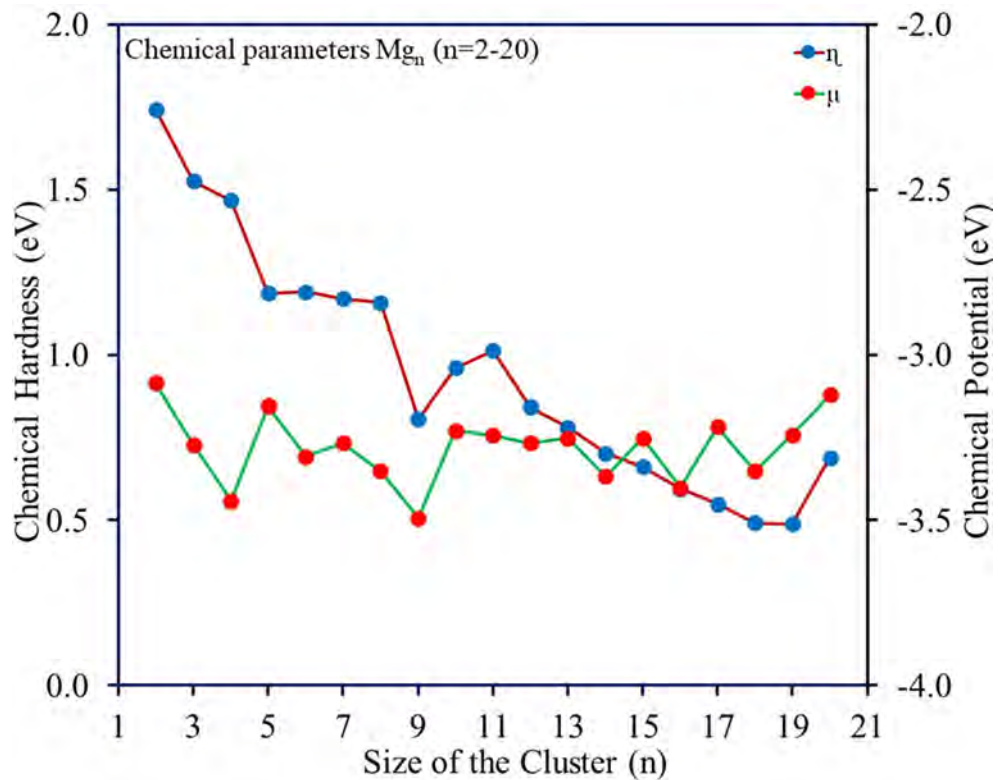


Fig. 3.6 Variation of chemical hardness and chemical potential with the size of cluster.

**Table 3.2 Thermodynamic, Electronic and Chemical properties of Mg<sub>n</sub> (n=2-20) in eV.**

Cluster	Avg. BE (eV/atom)	$\Delta_2E$ Stability	FE	H-L Gap	VIP	VEA	Chem. Pot. $\mu$	Chem. Hard. $\eta$
Mg <sub>2</sub>	0.01	-0.10	0.02	3.49	4.83	1.34	-3.09	1.74
Mg <sub>3</sub>	0.04	-0.34	0.11	3.05	4.80	1.74	-3.27	1.53
Mg <sub>4</sub>	0.15	0.35	0.45	2.93	4.91	1.97	-3.44	1.47
Mg <sub>5</sub>	0.14	-0.06	0.11	2.37	4.34	1.97	-3.15	1.19
Mg <sub>6</sub>	0.14	-0.13	0.16	2.38	4.50	2.12	-3.31	1.19
Mg <sub>7</sub>	0.16	-0.08	0.29	2.34	4.44	2.10	-3.27	1.17
Mg <sub>8</sub>	0.19	-0.27	0.36	2.31	4.51	2.19	-3.35	1.16
Mg <sub>9</sub>	0.24	-0.02	0.64	1.61	4.30	2.69	-3.49	0.81
Mg <sub>10</sub>	0.28	0.43	0.66	1.92	4.19	2.27	-3.23	0.96
Mg <sub>11</sub>	0.27	-0.01	0.23	2.02	4.25	2.23	-3.24	1.01
Mg <sub>12</sub>	0.27	-0.16	0.23	1.69	4.11	2.42	-3.26	0.84
Mg <sub>13</sub>	0.28	0.07	0.39	1.56	4.03	2.47	-3.25	0.78
Mg <sub>14</sub>	0.28	-0.42	0.32	1.41	4.07	2.66	-3.37	0.70
Mg <sub>15</sub>	0.31	0.67	0.73	1.33	3.91	2.59	-3.25	0.66
Mg <sub>16</sub>	0.30	-0.99	0.06	1.19	4.00	2.81	-3.40	0.60
Mg <sub>17</sub>	0.34	0.50	1.05	1.10	3.77	2.67	-3.22	0.55
Mg <sub>18</sub>	0.35	-0.20	0.56	0.99	3.84	2.86	-3.35	0.49
Mg <sub>19</sub>	0.38	0.03	0.76	0.98	3.73	2.75	-3.24	0.49
Mg <sub>20</sub>	0.39	0.67	0.72	1.38	3.81	2.43	-3.12	0.69

In the present work of calculation of VEA, the electron affinity is lower for 7, 10, 15, 17, 19 and 20. It increases almost monotonically with the increase in the cluster size (Fig.3.5 (b) and Table 3.2).

Chemical hardness can be expressed as resistance to change in the number of electrons. A minimum value of hardness means maximum tendency to exchange electrons or maximum reactivity i.e., lower stability. So, the greater the value of hardness, the larger will be the stability of clusters. It is seen from the Fig.3.6 that the magnitudes of chemical hardness for pure clusters decreases with the growth of pure Mg<sub>n</sub> clusters. For more clear understanding of chemical stability and reactivity of pure Mg<sub>n</sub> clusters we have studied chemical potential also. Fig 3.6 shows the variation of chemical potential as function of cluster size. Chemical potential is high for 7, 10, 13, 17, and 19.





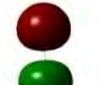
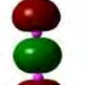


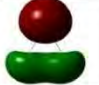
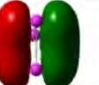
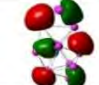
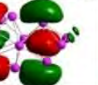
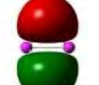

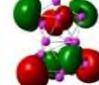
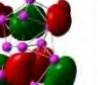
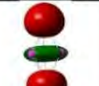



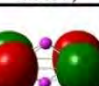
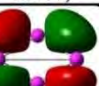
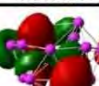

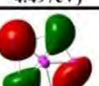

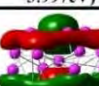

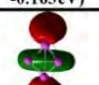
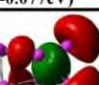
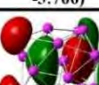


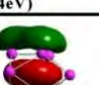
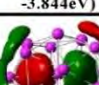
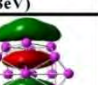
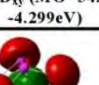
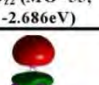
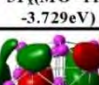
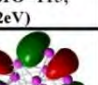
Cluster	HOMO	LUMO	Cluster	HOMO	LUMO
Mg <sub>1</sub>			Mg <sub>11</sub>		
	1S(MO=6, -0.19431eV)	2Pz (MO=7, -0.03233eV)		4D <sub>yz</sub> (MO=66, -0.15634eV)	5G <sub>z4</sub> (MO=67, -0.08196eV)
Mg <sub>2</sub>			Mg <sub>12</sub>		
	2P <sub>y</sub> (MO=12, -4.828eV)	3D <sub>z2</sub> (MO=13, -1.343 eV)		4F <sub>xx<sup>2</sup></sub> (MO=72, -4.108eV)	4F <sub>z(x<sup>2</sup>-y<sup>2</sup>)</sub> (MO=73, -2.422eV)
Mg <sub>3</sub>			Mg <sub>13</sub>		
	2P <sub>y</sub> (MO=18, -4.795eV)	2P <sub>x</sub> (MO=19, -1.745 eV)		4F <sub>yz</sub> (MO=78, -4.033eV)	4F <sub>yz</sub> (MO=79, -2.468eV)
Mg <sub>4</sub>			Mg <sub>14</sub>		
	2P <sub>y</sub> (MO=24 -4.908eV)	4D <sub>xz</sub> (MO=25, -1.974eV)		4F <sub>yz</sub> (MO=84, -0.14955eV)	4F <sub>z(x<sup>2</sup>-y<sup>2</sup>)</sub> (MO=85, -0.09785eV)
Mg <sub>5</sub>			Mg <sub>15</sub>		
	3D <sub>z2</sub> (MO=30, -4.34eV)	3D <sub>z<sup>2</sup>-y<sup>2</sup></sub> (MO=31, -1.97eV)		4F <sub>z(x<sup>2</sup>-y<sup>2</sup>)</sub> (MO=90, -0.14386eV)	5F <sub>yz</sub> MO=91, -0.0951eV)
Mg <sub>6</sub>			Mg <sub>16</sub>		
	1F:3D <sub>xz</sub> (MO=36, -4.497eV)	1F:3D <sub>xz</sub> (MO=37, -2.117eV)		4F <sub>yz</sub> (MO=96, -3.997eV)	4F <sub>z(x<sup>2</sup>-y<sup>2</sup>)</sub> (MO=97, -2.806eV)
Mg <sub>7</sub>			Mg <sub>17</sub>		
	3D <sub>xz</sub> (MO=42, -0.163eV)	3D <sub>z<sup>2</sup>-y<sup>2</sup></sub> (MO=43, -0.077eV)		4F <sub>z<sup>3</sup></sub> (MO=102, -3.766)	4F <sub>yz</sub> (MO=103, -2.666)
Mg <sub>8</sub>			Mg <sub>18</sub>		
	3D <sub>z2</sub> (MO=48, -4.511eV)	4D <sub>xz</sub> (MO=49, -2.194eV)		4D <sub>yz</sub> (MO=108, -3.844eV)	4F <sub>yz</sub> (MO=109, -2.858eV)
Mg <sub>9</sub>			Mg <sub>19</sub>		
	3D <sub>xy</sub> (MO=54, -4.299eV)	3D <sub>z2</sub> (MO=55, -2.686eV)		3P <sub>x</sub> (MO=114, -3.729eV)	4F <sub>z3</sub> (MO=115, -2.752eV)
Mg <sub>10</sub>			Mg <sub>20</sub>		
	4D <sub>xz</sub> (MO=60, -4.187eV)	4F <sub>z3</sub> (MO=61, -2.268eV)		5F <sub>yz</sub> (MO=120, -3.812eV)	5G <sub>z3</sub> MO=121, -2.43eV)

Fig. 3.7 HOMO and LUMO surface of pure Mg<sub>n</sub> cluster.

### 3.3.5 HOMO-LUMO Orbital Study of Nanoclusters

Highest occupied molecular orbital (HOMO) and lowest unoccupied molecular orbital (LUMO) are the most important parameters in quantum condensed matter physics or quantum chemistry. HOMOs are the most outer orbital containing electrons; thereby free electrons are available from them. As per Koopmans theorem, ionization potential can be directly obtained from the HOMO energy value and on the other side, electron affinity can be obtained from LUMO energy of the system. The study of HOMO-LUMO provides information regarding the charge transfer among the atoms within the cluster. The HOMO-LUMO energy gap can be obtained by subtracting the LUMO and HOMO orbital energy.

We can study the stability of the molecule from the HOMO-LUMO energy gap. The more is the HOMO-LUMO gap, the higher is the stability. On the other hand, the lower is the gap, the higher is the reactivity of the cluster and lower is the stability. The approximate HOMO-LUMO surfaces of the clusters of pure Magnesium from our previous experiences of HOMO-LUMO surfaces of compounds available in the standard texts are presented in Fig. 3.7. The HOMO and LUMO energies of each cluster obtained from the study are given in the Fig. 3.7. Here, the red coloured surface indicates positive diffuse where green coloured surface refers to negative phase. It is seen that the HOMO and LUMO surfaces of some clusters fits well with our known surfaces, whereas some surfaces obtained are nearly approximated surfaces.

### 3.3.6 Molecular Electrostatic Potential and Total Electron Density Mapping

Molecular electrostatic potential can be studied either by plotting the top surface or by plotting the contour. If one plots the MEP surface, then that particular one can only see the top surface. Instead of doing that if we can plot each MEP surfaces as a contour around each molecule to see all the MEP.

To study molecular reactivity, it is crucial to study electrostatic potential,  $V(r)$ , produced in a molecule due to the electrons and nuclei.  $V(r)$  can be addressed by

$$V(r) = \sum \frac{Z_0}{|R_0 - r|} - \int \frac{\rho(r') dr'}{|r' - r|} \quad (3.12)$$

Cluster	Electrostatic Potential	Total Electron Density	Cluster	Electrostatic Potential	Total Electron Density
Mg <sub>1</sub>			Mg <sub>11</sub>		
Mg <sub>2</sub>			Mg <sub>12</sub>		
Mg <sub>3</sub>			Mg <sub>13</sub>		
Mg <sub>4</sub>			Mg <sub>14</sub>		
Mg <sub>5</sub>			Mg <sub>15</sub>		
Mg <sub>6</sub>			Mg <sub>16</sub>		
Mg <sub>7</sub>			Mg <sub>17</sub>		
Mg <sub>8</sub>			Mg <sub>18</sub>		
Mg <sub>9</sub>			Mg <sub>19</sub>		
Mg <sub>10</sub>			Mg <sub>20</sub>		

Fig. 3.8 MEP and total electron density of pure Mg<sub>n</sub> (n =2-20) clusters.

where  $Z_0$  represents the nuclear charge at  $R_0$  and  $\rho(r)$  the electron density of the molecule. Electrostatic potential can be referred as a sum of positive and negative contribution from electrons nuclei. The sign of electrostatic potential of the system depends on major and minor contribution. If electrostatic potential is positive, it indicates that the major contribution is from nuclei, and if the sign is negative, it means significant contribution is coming from electrons [40, 41].

Molecular electrostatic potential is very much informative; especially in order to study the nuclear and electronic charge distribution of the molecules. It is also very useful to study the chemical reactivity of the system. MEP effectively represents the reactivity map of an atomic cluster from which we can get some useful information regarding the most probable region for nucleophilic and electrophilic. In Fig. 3.8 Red colours in MEP map indicates the negative region, which means electron-rich region, blue region is the positive region where the electron density is poor. The green region represents zero electrostatic potential. The negative region is the region where electrophilic attacks occur and the nucleophilic attack region is indicated by the positive region. The electron density flows in the following order Blue < Green < Yellow < Orange < Red. In our study of MEP, each contour curve around each atom is the MEP surface. There is a colour scale that indicates the positive and negative values. Here, we have basically yellow and red colours. The red-colour region defines the negative electrostatic potential whereas the positive potential is indicated by yellow in our study.

### ***3.4 Summary and Conclusions***

The chapter is aimed at a systematic complete study of pure  $Mg_n$  ( $n=2-20$ ) clusters. The structural growth of pure  $Mg_n$  clusters ( $n=2-20$ ), interatomic distances, the average binding energy per atom (BE), second-order change in energy (Stability), Fragmentation energy (FE); HOMO-LUMO energy gap, Vertical ionization potential (VIP), Vertical electron affinity (VEA), Chemical potential ( $\mu$ ), Chemical hardness ( $\eta$ ), Fermi energy ( $E_F$ ), HOMO-LUMO orbital surface structures, Molecular electrostatic potential contours (MEP), total electron density (TED) has been studied within the framework of Kohn-Sham Density Functional Theory (DFT) using GAUSSIAN'09. Since the vertical ionization potential (VIP) and vertical electron affinity (VEA) can be calculated using either the anionic-cationic method



or using Koopmans method, the parameters are calculated here by both methods and compared.

The conclusions arrived from these results ( $n=2-20$ ) have a good correlation with the experimental results of photoelectron spectroscopy and mass spectroscopy of Diedrich et al. and others [19, 20, 39]. In the study of the growth pattern of the clusters, it is found that the most stable structures of  $Mg_{4-6}$  are tetrahedron based and  $Mg_7$  and  $Mg_8$  are pentagonal bipyramid based. The ground state clusters of  $Mg_9-Mg_{15}$  are trigonal prism based.  $Mg_{17}-Mg_{20}$  is derivatives of  $Mg_{16}$ . These structures agree well with earlier works [7-14]. The interatomic distances of the clusters have been studied for  $Mg_n$  ( $n=2-20$ ) the values are compared with available experimental and theoretical data of other authors [25, 36-38]. Only a few interatomic distance data available, and that at most up to  $n=10$ . Here, inter atomic distance up to  $n=20$  are presented. It is seen that the average separation varies with increase of cluster size and it decreases nonlinearly from 3.927 Å to 3.14 Å. The minimum interatomic distance is 3.14 Å. The binding energy graph (Fig.3.2) shows  $Mg_4$ ,  $Mg_{10}$ ,  $Mg_{15}$ ,  $Mg_{20}$  have local peaks from which  $Mg_4$ ,  $Mg_{10}$  and  $Mg_{20}$  are very stable as they are spherical closed shell clusters possess 8, 20, 40 valence electrons respectively. Again,  $Mg_{13, 15, 17}$  are also stable clusters. The BE per atom assumes values 0.01 eV for  $Mg_2$  which rises to 0.39 eV for  $Mg_{20}$ . The behaviors of the stability and fragmentation energy (Fig.3.3) with the growth of the cluster supports the results of BE graph. Stability is positive for  $n=4, 10, 13, 15, 19$  and 20 whereas fragmentation energy possesses local peaks for  $n=4, 10, 13, 15$  and 20. The HOMO-LUMO gap has a maximum value of 3.485 eV for  $Mg_2$  which gradually decreases to 0.986 eV at  $Mg_{18}$  which signifies that the metallic behavior of the pure clusters starts from  $Mg_{18}$ . Here, chemical parameters are calculated using both the methods. It is seen that the nature of variation is identical in the two methods. In respect of values, an average scaling of 0.97 eV is required for VIP equivalence of the two methods. In Fig. 3.7 the HOMO-LUMO orbitals and the MO number energy values in eV are presented. The molecular electrostatic potential contours and total electron density contours (Fig. 3.8) explains the electron delocalization in the clusters. This wide variation of HOMO-LUMO gap makes these clusters suitable for fabrication of electronic devices. It can be seen that, Mg atoms are basically with s and p atomic orbital's whereas the TM has s, p and d orbitals. So, if we dope pure  $Mg_n$  clusters by 3d TM atoms (TM= Co, Cu, Sc, Fe, Ti, V, Zn etc.) then there will be a significant interaction between s and

p orbitals of Mg and s, p, d orbitals of TM. Where, s orbital will be marked at Mg site and 3d orbitals will be marked at TM site. This may lead to highly stable clusters, some of which can behave like an elemental atoms and may give rise to 'superatom' [42, 43] and some of them can be used as a great hydrogen storage system because of the catalytic effect of doped TM atoms and higher reactivity. In order to find the suitable hydrogen storage system, it needs more study in different environment.

## References

- [1] W.D. Knight, K. Clemenger, W.A. de Heer, W.A. Saunders, M.Y. Chou, and M.L. Cohen, “Electronic Shell Structure and Abundances of Sodium Clusters”, *Phys. Rev. Lett.* **52(24)**, (1984), 2141. <https://doi.org/10.1103/PhysRevLett.52.2141>
- [2] Haberland Hellmut (Ed), “Clusters of Atoms and Molecules: Theory, Experiment, and Clusters of Atoms”, Editors. 1<sup>st</sup> Ed. Berlin: Springer-Verlag, (1994).
- [3] V.A. Yartys, M.V. Lototsky, E. Akiba, R. Albert, V.E. Antonov, J.R. Ares, M. Baricco, N. Bourgeois, C.E. Buckley, J.M. Bellosta von Colbe, J.C. Crivello, F. Cuevas, R.V.R. Denys, M. Dornheim, M. Felderhoff, D.M. Grant, B.C. Hauback, T. D. Humphries, I. Jacob, T.R. Jensen, P.E. de Jongh, J.M. Joubert, M.A. Kuzovnikov, M. Latroche, M. Paskevicius, L. Pasquini, L. Popilevsky, V.M. Skripnyuk, E. Rabkin, M.V. Sofianos, A. Stuart, G. Walker, H. Wang, C.J. Webb, and Min Zhu, “Magnesium based materials for hydrogen based energy storage: Past, present and future”, *Int. J Hydrogen Energy* **44(15)**, (2019), 7809-7859. <https://doi.org/10.1016/j.ijhydene.2018.12.212>.
- [4] J. Zhang, Z. Li, Y. Wu, X. Guo, J. Ye, B. Yuan, and L. Jiang, “Recent advances on the thermal destabilization of Mg-based hydrogen storage materials”, *RSC adv.*, **9(1)**, (2019), 408-428. <https://doi.org/10.1039/C8RA05596C>
- [5] E. Roduner, “Size matters: why nanomaterials are different”, *Chem. Soc. Rev.* **35(7)**, (2006), 583–592. <https://doi.org/10.1039/B502142C>.
- [6] C. Kittel, “Introduction to solid state physics”, 7<sup>th</sup>Edn. New York: Wiley; (1996).
- [7] O.C. Thomas, W. Zhen, S. Xu, and Jr K.H. Bowen, “Onset of metallic behavior in magnesium clusters”. *Phys. rev. lett.*, **89(21)**, (2002), 213403. <https://doi.org/10.1103/PhysRevLett.89.213403>
- [8] J. Akola, K. Rytönen, and M. Manninen, “Metallic evolution of small magnesium clusters”, *J Eur. Phys, D-Atomic, Molecular, Optical and Plasma Physics*, **16(1)**, (2001), 21-24. <https://doi.org/10.1007/s100530170051>

- [9] F. Reuse, S.N. Khanna, V. de Coulon, and J. Buttet, “Pseudopotential local-spin-density Studies of neutral and charged  $Mg_n$  ( $n=1-7$ ) clusters”, *Phys. Rev. B*, **41(17)**, (1990), 11743-11759. <https://doi.org/10.1103/physrevb.41.11743>
- [10] V. Kumar, and R. Car, “Structure, growth, and bonding nature of Mg clusters”, *Phys. Rev. B*, **44(15)**, (1991), 8243–8255. <https://doi.org/10.1103/PhysRevB.44.8243>
- [11] A. Köhn, F. Weigend, and R. Ahlrichs, “Theoretical study on clusters of magnesium”, *Phys. Chem. Chem. Phys.*, **3(5)**, (2001), 711-719. <https://doi.org/10.1039/B007869G>
- [12] P. Delaly, P. Ballone, and J. Buttet, “Metallic bonding in magnesium microclusters”, *Phys. Rev. B*, **45(7)**, (1992), 3838–3841. <https://doi.org/10.1103/PHYSREVB.45.3838>
- [13] S.N. Belyaev, S.V. Panteleev, S.K. Ignatov, and A.G. Razuvaev, “Structural, electronic, thermodynamic and spectral properties of  $Mg_n$  ( $n=2-32$ ) clusters: A DFT Study”, *Comp. Th. Chem.*, **1079**, (2016), 34–46. <https://doi.org/10.1016/j.comptc.2016.01.011>
- [14] A. Lyalin, I.A. Solovyov, A.V. Solovyov, and W. Greiner, “Evolution of the electronic and ionic structure of Mg clusters with increase in cluster size”, *Physical Rev. A*, **67(6)**, (2003), 063203. <https://doi.org/10.1103/PhysRevA.67.063203>.
- [15] J. Jellinek, and P.H. Acioli, “Magnesium clusters: structural and electronic properties and the size-induced nonmetal-to-metal transition”, *The J. Phys. Chem. A*, **106(45)**, (2002), 10919-10925. <https://doi.org/10.1021/jp020887g>
- [16] P.H. Acioli, and J. Jellinek, “Electron binding energies of anionic magnesium clusters and the nonmetal-to-metal transition”, *Phys. Rev. Lett.*, **89(21)**, (2002), 213402. <https://doi.org/10.1103/PhysRevLett.89.213402>
- [17] C.C.D. Torrejon, F.E. Magana, and I.G. Kaplan, “Comparative theoretical study of the electron affinities of the alkaline-earth clusters:  $Be_n$ ,  $Mg_n$ , and  $Ca_n$  ( $n = 2, 3$ )”, *Int. J. of Quantum Chem.*, **111(1)**, (2011), 103-110. <https://doi.org/10.1002/qua.22387>

- [18] I. Heidari, S. De, S.M. Ghazi, S. Goedecker, and D.G. Kanhere, “Growth and Structural Properties of  $Mg_n$  ( $N= 10-56$ ) Clusters: Density Functional Theory Study”, *J Phys. Chem. A*, **115(44)**, (2011), 12307-12314. <https://doi.org/10.1021/jp204442e>
- [19] T. Diedrich, T. Döppner, Th. Fennel, J. Tiggesbäumker, and K.H. Meiwes-Broer, “Shell structure of magnesium and other divalent metal clusters”, *Phys. Rev. A.*, **72(2)**, (2005), 3203-3214. <https://doi.org/10.1103/PhysRevA.72.023203>
- [20] T. Diedrich, T. Döppner, J. Braune, J. Tiggesbaumker, and K.H.M. Broer, “Electron Delocalization in Magnesium Clusters Grown in Supercold Helium Droplets”, *Phys. Rev. Lett.*, **86(21)**, (2001), 4807. <https://doi.org/10.1103/PhysRevLett.86.4807>
- [21] X. Xia, X. Kuang, C. Lu, Y. Jin, X. Xing, G. Merino, and A. Hermann, “Deciphering the structural evolution and electronic properties of magnesium clusters: An aromatic homonuclear metal  $Mg_{17}$  cluster”, *J. Phys. Chem. A*, **120(40)**, (2016), 7947–7954. <https://doi.org/10.1021/acs.jpca.6b07322>
- [22] D. Shen, C.P. Kong, R. Jia, P. Fu, and H.X. Zhang, “Investigation of Properties of  $Mg_n$  clusters and their hydrogen storage mechanism: a study based on DFT and a global minimum optimization method”, *J. Phys. Chem. A*, **119(15)**, (2015), 3636-3643. <https://doi.org/10.1021/acs.jpca.5b01474>
- [23] S. Janecek, E. Krotscheck, M. Liebrecht, and R. Wahl, “Structure of  $Mg_n$  and  $Mg_n^+$  clusters up to  $n=30$ ”, *Eur. Phys. J. D.*, **63**, (2011), 377–390. <https://doi.org/10.1140/epjd/e2011-10694-2>
- [24] F. Zhang, H. Zhang, W. Xin, P. Chen, Y. Hu, X. Zhang, and Y. Zhao, “Probing the structural evolution and electronic properties of divalent metal  $Be_2Mg_n$  clusters from small to medium size”, *Sci. Rep.*, **10(6052)**, (2020), 1–10. <https://doi.org/10.1038/s41598-020-63237-8>
- [25] B. Boruah, and B. Kalita, “Role of transition metal doping in determining the electronic structures and properties of small magnesium clusters: a DFT-based

- comparison of neutral and cationic states”, *J. Nanopart. Res.*, **22(370)**, (2020), 370–378. <https://doi.org/10.1007/s11051-020-05083-3>
- [26] B.J. Kooi, G. Palasantzas, and J.Th.M. De Hasson, “Gas-phase Synthesis of Magnesium Nanoparticles: A High-Resolution Transmission Electron Microscopy Study”, *Appl. Phys. Lett.*, **89(16)**, (2006), 161914-1–161914-3. <https://doi.org/10.1063/1.2358860>
- [27] A. Kaufmann, A. Kornath, A. Zoermer, and R. Ludwig, “Small magnesium clusters: between van der Waals and valence bonds”, *Inorg. Chem*, **49(8)**, (2010), 3851–3856. <https://doi.org/10.1021/ic902485z>
- [28] F. Daniel, “Hydrogen Storage in Mg based alloys”. Budapest. (2010).
- [29] W. Kohn, and L.J. Sham, “Self-Consistent Equations Including Exchange and Correlation Effects”, *Phys. Rev.*, **140(4A)**, (1965), A1133–A1138. <https://link.aps.org/doi/10.1103/PhysRev.140.A1133>
- [30] D.R. Hartree, “The Wave Mechanics of an Atom with a Non-Coulomb Central Field. Part I. Theory and Methods”, *Mathematical Proc. Cam. Philo. Soc.*, **24(1)**, (1928), 89–110. <http://dx.doi.org/10.1017/S0305004100011919>
- [31] V. Fock, “Approximation method for the solution of the quantum mechanical multi-body problem”, *Z. Physik*, **61**, (1930), 126–148. <http://dx.doi.org/10.1007/BF01340294>
- [32] C. Møller, and M.S. Plesset, “Note on an Approximation Treatment for Many-Electron Systems”, *Phys. Rev.*, **46(7)**, (1934), 618–622. <https://doi.org/10.1103/PhysRev.46.618>
- [33] M.J. Frisch, G.W. Trucks, H.B. Schlegel, G.E. Scuseria, M.A. Robb, J.R. Cheeseman, G. Scalmani, V. Barone, B. Mennucci, G.A. Petersson, H. Nakatsuji, M. Caricato, X. Li, H.P. Hratchian, A. F. Izmaylov, J. Bloino, G. Zheng, J.L. Sonnenberg, M. Hada, M. Ehara, K. Toyota, R. Fukuda, J. Hasegawa, M. Ishida, T. Nakajima, Y. Honda, O. Kitao, H. Nakai, T. Vreven, Jr J. A. Montgomery, J.E. Peralta, F. Ogliaro, M. Bearpark,

J.J. Heyd, E. Brothers, K.N. Kudin, V.N. Staroverov, T. Keith, R. Kobayashi, J. Normand, K. Raghavachari, A. Rendell, J.C. Burant, S.S. Iyengar, J. Tomasi, M. Cossi, N. Rega, J.M. Millam, M. Klene, J.E. Knox, J.B. Cross, V. Bakken, C. Adamo, J. Jaramillo, R. Gomperts, R.E. Stratmann, O. Yazyev, A.J. Austin, R. Cammi, C. Pomelli, J.W. Ochterski, R.L. Martin, K. Morokuma, V.G. Zakrzewski, G.A. Voth, P. Salvador, J.J. Dannenberg, S. Dapprich, A.D. Daniels, O. Farkas, J.B. Foresman, J.V. Ortiz, J. Cioslowski, D.J. Fox (2013) Gaussian'09, Revision D.01, Gaussian, Inc., Wallingford C.

- [34] T. Koopmans, "On the assignment of wave functions and eigenvalues to the individual electrons of an atom", *Physica*, **1(1-6)**, (1934), 104-113. [https://doi.org/10.1016/S0031-8914\(34\)90011-2](https://doi.org/10.1016/S0031-8914(34)90011-2)
- [35] A.D. Becke, "Density-functional exchange-energy approximation with correct asymptotic behavior", *Phys. Rev. A*, **38(6)**, (1988), 3098-3100. <https://doi.org/10.1103/physreva.38.3098>
- [36] C. Lee, W. Yang, and R.G. Parr, "Development of the Colle-Salvetti correlation energy formula into a functional of the electron density", *Phys Rev B.*, **37(2)**, (1998), 785. <https://doi.org/10.1103/PhysRevB.37.785>.
- [37] Computational Chemistry Comparison and Benchmark Data Base Std. Ref database 101; National Institute of Standards and Technology (NIST) USA (2020). <https://cccbdb.nist.gov>.
- [38] R. Trivedi, and D. Bandyopadhyay, "Hydrogen storage in small size  $Mg_nCo$  clusters: A density functional study", *Int. J. Hydrogen Energy*, **40(37)**, (2015), 12727-12735. <https://doi.org/10.1016/j.ijhydene.2015.07.122>
- [39] K. Duanmu, O. Roberto-Neto, F.B.C. Machado, J.A. Hansen, J. Shen, P. Piecuch, and D.G. Truhlar, "Geometries, Binding Energies, Ionization Potentials, and Electron Affinities of Metal Clusters:  $Mg_n^{0,\pm 1}$ ,  $n = 1-7$ ", *Journal of Phys. Chem. C.*, **120(24)**, (2016), 13275-13286. <https://doi.org/10.1021/acs.jpcc.6b03080>

- [40] C.F. Matta, and R.J. Gillespie, “Understanding and Interpreting Molecular Electron Density Distributions”, *J. Chem. Ed.*, **79(9)**, (2002), 1141-1152. <https://doi.org/10.1021/ed079p1141>.
- [41] J.S. Muray, and P. Politzer, “The Electrostatic Potential: an overview”, *Comp. Mol. Sci.* **1(2)**, (2011), 153-163, <https://doi.org/10.1002/wcms.19>
- [42] G.X. Ge, Y. Han, J.G. Wan, J.J. Zhao, and G.H. Wang, “First-principles prediction of magnetic superatoms in 4d-transition-metal-doped magnesium clusters”, *J. Chem. Phys.*, **139(17)**, (2013), 174309, <https://doi.org/10.1063/1.4827515>.
- [43] A.T. Flores, and A. Muñoz-Castro, “Bonding and properties of superatoms. Analogs to atoms and molecules and related concepts from superatomic clusters”, *Int. J. Quantum Chem.*, **119(2)**, (2018), 25756, 1-12. <https://doi.org/10.1002/qua.25756>



## **CHAPTER-4**

---

### **SYSTEMATIC STUDY OF Ti DOPED MAGNESIUM (TiMg<sub>n</sub>) (n=2-20) CLUSTERS: A DENSITY FUNCTIONAL APPROACH**

#### ***4.1 Introduction***

Divalent Magnesium clusters remain the fundamental topic of interest of the theoreticians and experimentalists for decades. It is because the group II metal clusters possess some unique features like; exciting physiochemical tuning properties, tunable electronic properties, ability of transition from weakly bonded (Van der Waal type) small cluster to metallic characteristic in large clusters due to successive addition of Mg atoms and many more. With the increase in the size of clusters, the s-p hybridization increases and non-additive many-body exchange interaction component becomes significant. Another essential feature of Mg clusters is the rapid increase of binding energy per atom with an increase of cluster size in the case of small clusters [1-4].

Many theoretical and experimental studies on pure clusters have been reported in the past [5-20]. Theoretical studies using Kohn Sham density functional theory (DFT) [5] with exchange correlation functional on Mg clusters have been reported [7-18] after reporting the existence of electronic shell structures by Knight et al. [6] with an experimental study. Ab initio calculation using Hartree Fock theory [21, 22], Moller-Plesset theory (MP) [23] has also been reported. Experimental studies of Mg clusters using gas phase spectroscopy, Photoelectron spectroscopy [24, 25], and Raman spectroscopy [26] has been reported for very few to hundreds of magnesium atomic clusters. The experimental finding supports the theoretical predictions to a larger extent.

Here a systematic study of Ti doped magnesium clusters is presented. The clusters are made to use as a material for hydrogen storage. One of the notable findings in earlier studies of pure Mg clusters is the high thermodynamic stability with high hydrogen storage capacity of Magnesium hydrides (MgH<sub>2</sub>) [27-29]. But higher stability imposes constraints in practical

applications as it requires high desorption temperature  $\sim 350^\circ\text{C}$  at normal atmospheric pressure. Low rate of absorption and desorption results in slow diffusion through hydrides which ultimately reduces hydrogen kinetics. High surface to volume ratio and- high enthalpy of formation are the main barrier for industrial use.

Doping a cluster by a foreign atom tunes the structural, physical, chemical and electronic properties of the cluster to a great extent. Doping with a foreign atom into a pure cluster forms a mixture that prevents production of single crystals. Depending upon the number and nature of atoms used for doping and place of dopant on the surface (exohedrally) or inside (endohedrally) the cluster, the change of nature of property occurs. Doping can change the charge state of the cluster. For different practical applications, clusters must be doped with suitable dopant. As a result, suitably doped clusters may find various fields of applications viz. hydrogen storage material, catalysts, Photo-voltaic applications, portable power module, sensors; biomedicines and nano electronic applications.

Doping a pure  $\text{Mg}_n$  with selective transition metal atoms can improve the stability, physiochemical properties, and absorption-desorption kinetics of magnesium clusters [30-50]. Zhang et al. [30] reported structural growth and electronic properties of  $\text{Be}_3\text{Mg}_n$  ( $n=1-20$ ) is which from  $n=10$  cage clusters were studied and found  $\text{Be}_3\text{Mg}_n$  as most stable cluster. Xi et al. [31] reported electronic properties of strontium doped  $\text{Mg}_n$  ( $n=2-12$ ) clusters. Ni doped  $\text{Mg}_n$  ( $n=1-7$ ) clusters has been reported by Chen et al. [32] and reported that Ni atom starts trapped in cage clusters from  $n=5$ . Li et al. [33] reported carbon doped  $\text{Mg}_n$  ( $n=1-12$ ) and found  $\text{Mg}_8\text{C}$  and  $\text{Mg}_{11}\text{C}$  are most stable structures in endohedral doping. C. Li et al. [34] reported Li doped  $\text{Mg}_n$  ( $n=2-11$ ) clusters and found  $\text{LiMg}_9$  with  $C_{4v}$  symmetry possesses high stability and a strong Li-Mg interaction. Zn doped  $\text{Mg}_n$  ( $n=1-5$ ) has been reported by Zhi Li et al. [35], who claimed  $\text{Mg}_3\text{Zn}$  and  $\text{Mg}_3\text{Zn}_2$  are the most stable clusters. Zhu et al. [36] reported Pd doped  $\text{Mg}_n$  ( $n=2-20$ ) clusters. Ge, Sn and C doped  $\text{Mg}_n$  ( $n=2-12$ ) has been studied by Zeng et al. [37] and found  $\text{XMg}_8$  ( $X= \text{Ge, Sn, C}$ ) is the most stable one. A. Droghetti et al. [38] investigated the N-doped Mg system as a promising material for the spintronics application. They reported that if  $\text{MgN}$  is possible to make then  $\text{MgO/MgN}$  system will be a suitable system platform for tunnel junctions. 3d, transition metal (TM) doped  $\text{Mg}_n$  ( $n=2-10$ ) has been studied by Boruah et al. for natural and cationic clusters and reported  $\text{Mg}_3\text{TM}$  as the

most stable cluster [39]. Hussain et al. [40] reported TM (Sc, V, Fe, Co, Ni, Cu, Y, Zn, Nb) doping on  $Mg_5H_2$ . Fe, Co, Ni, doped  $Mg_n$  ( $n=1-9$ ) clusters has been studied by Kong et al. [41], who reported that  $Mg_4$  doped with (Fe, Co, Ni) is the highest stable cluster.  $Mg_{17}$  doped with Ti and Ni is reported by Charkin et al. [42]. Studies on Co doped  $Mg_n$  ( $n=1-10$ ) have been reported by Trivedi et al. [43], who reported  $Mg_5Co$  as best suitable for a hydrogen storage. Again, Rh doped  $Mg_n$  ( $n=1-10$ ) has been reported by Trivedi et al. [44], who reported  $Mg_9Rh$  is the best suitable material for hydrogen storage. Ma et al. on 2017 reported a study of Ti and Nb doped  $Mg_{55}$  clusters [45]. Kumar and Tarakeshwar [46] compared the variation of chemisorption energy with number of hydrogen absorption in  $M_{13}H_{2n}$  ( $M=Sc, Ti, Zr$ ) transition metal clusters. Experimental studies on TM doped  $Mg_n$  clusters reported by Bobet et al. [47, 48], who reported  $Mg_7Ti$  is the most suitable material for hydrogen storage. The catalytic effect of TM on Mg clusters reported by Shelyapins et al. [49]. Studies on  $MgH_2$ -TM (TM= Ti, V, Mn, Fe, Ni) has been experimentally studied by Liang et al. [50] and reported that  $MgH_2$ -Ti shows best desorption Kinetics over V, Mn, Fe, Ni doped clusters. Liang et al. [50] first reported the catalytic effect of 3d transition metal doping (like Fe, Co, Ni) the time taken to reach maximum desorption rate reduces by almost 50% and ball milled  $Mg_nTi$  exhibits most rapid adsorption and desorption rate over all first row of transition metal elements. Doping Mg with rare earth fcc atoms shows fast adsorption kinetics but does not adsorb hydrogen appreciably [51]. It is understood from the study that fast kinetics is due to the fcc structure of the dopant. The first row of transition metals (Ti, V, and Cr) is exceptionally suitable materials for hydrogen storage material as they possess high gravimetric density and also produce an fcc structure of hydrides [52-58]. Silva et al. [57] reported electronic characteristics and reactivity of Ti doped  $Mg_n$  ( $n=1-6$ ) using MP2 (Moller-Plesset second order) optimization using 6-311G (d) basis set. Kyoji et al. [59] experimentally studied TiMg hydrides and reported  $Mg_7TiH_n$  as the most stable cluster.

Complete systematic studies on Ti doped  $Mg_n$  clusters with both exohedral and endohedral doping have yet to be reported. This work presents thermodynamic, chemical and electronic studies of  $Mg_n$  clusters ( $n=2-20$ ) with exohedral doping of small sized clusters ( $n=1-6$ ) and both exohedral & endohedral doping of  $n=6-20$ . The global ground state energies are taken from the both types of doping for study the variation of average binding energy per atom,

second order change in energy commonly known as stability, fragmentation energy, and embedding energy. The difference between highest occupied molecular orbital (HOMO) energy and lowest occupied molecular energy (LUMO) with vertical ionization potential (VIP), vertical electron affinity (VEA), chemical potential ( $\mu$ ) and chemical hardness ( $\eta$ ) for the global GS structures are presented. The variation of interatomic distances with cluster size, nearest neighbor distance of dopant, variation of dipole moment, charge transfer between Ti atom and Mg atoms, shapes of HOMO, LUMO orbitals, molecular electrostatic potential contour, total electron density contours are also studied. Later, the electron localization function (ELF), Critical points (Cps), nucleus independent chemical shift (NICS), of the most stable cluster have been studied to understand its stability.

## ***4.2 Computational Methodology***

Computational involved in the presented work is self-consistent-field (SCF) electronic structure calculations on all clusters within the density functional theory (DFT) framework. During the calculations, molecular orbitals (MO) are expressed as a linear combination of atom-centered basis functions for which the 6-311G(d) inbuilt in the Gaussian'09 program package [60] is used. Spin-polarized calculations are carried out using the Becke three-parameter exchange and the Lee, Yang, and Parr generalized gradient approximation (GGA), popularly known as B3LYP functional [61, 62] with 6-311G(d) basis set for pure as well as for Ti-doped  $Mg_n$  clusters. As a preliminary step, geometry optimization was performed, and harmonic vibrational frequency calculations were computed to ensure that the clusters were global minima in each size range. All geometries were optimized with unconstrained symmetry starting from the different initial configurations to avoid the minimum surface potential energy lock. Further, the Electron Localization Function (ELF) and the Critical Point (CP) of the most stable and suited cluster are studied using MultiWfn open-source program.

To verify the accuracy of the method adopted in this work some test calculations (viz. Bond length and Vibrational frequencies) with methods and basis sets are available in the Gaussian'09 package. The calculated results are compared with the experimental data [63] presented in Table 4.1. Comparing these results with reported experimental and the present

works confirmed that the B3LYP method under the 6-311G (d) basis set is appropriate for the present system under study.

<b>Table 4.1 Comparison between the present work with experimental bond lengths and lowest frequency in different dimmers</b>							
Method	Dimer	Bond length (Å)			Lowest frequency (cm <sup>-1</sup> )		
		6-311G(d)	6-311++G(d)	Expt. [48]	6-311G(d)	6-311++G(d)	Expt.
B3LYP	Mg-Mg	3.93	3.99	3.89	45	44	48 [48]
	Ti-Ti	1.932	1.912	1.943	618	594	408
	Mg-Ti	3.044	2.42		242	242	
B3PW91	Mg-Mg	3.60	3.61	3.89	1563	1564	48 [48]
	Ti-Ti	1.826	1.904	1.943	566	259	408
	Mg-Ti	2.974	2.428		242	322	

From the above table, one may conclude the B3LYP/6-311G (d) is the best compared to the other methods and basis sets combination when the calculated results are compared with the available experimental data of dimers. Therefore, we have used the B3LYP method with a 6-311G(d) basis set in the present study. Variations of the minimum value of the Mg-Mg and Mg-Ti bond lengths in pure Mg<sub>n</sub> and TiMg<sub>n</sub> are shown in Fig 4.2.

### ***4.3 Results and Discussion***

#### ***4.3.1 Growth Pattern of Magnesium Nanoclusters in Pure and Doped Form***

Most stable structures of Mg<sub>4-6</sub> are tetrahedron based and Mg<sub>7</sub> and Mg<sub>8</sub> are pentagonal bipyramid based. The ground state clusters of Mg<sub>9-15</sub> are trigonal prism based. Mg<sub>17-18</sub> are derivatives of Mg<sub>16</sub>. They are obtained by adding magnesium, atom to Mg<sub>16</sub>. These structures agree well with earlier works [6, 7, 9, 12, and 15]. All optimized doped clusters are displayed in Fig.4.1. TiMg has C<sub>∞v</sub> point group symmetry. Pure Mg<sub>2</sub> is nothing but a Mg-Mg dimer with C<sub>2v</sub> point group symmetry. TiMg<sub>2</sub> is formed by adding a Ti atom as upper cap

to pure  $\text{Mg}_2$  to forms an equilateral triangle in shape with  $C_s$  point group symmetry i.e., it has a mirror plane in addition to identity.

The ground state configuration of  $\text{TiMg}_3$  holds  $C_{2v}$  point group symmetry where the Ti atom is added perpendicularly on  $\text{Mg}_3$  cluster. The global minimum state of the cluster is a triplet. The ground state configuration of  $\text{TiMg}_4$  is tetrahedron based cluster with  $C_{2v}$  point group symmetry which can be obtained by a side cap with Mg to  $\text{TiMg}_3$  cluster. The global minimum state of  $\text{TiMg}_4$  is also a triplet state. The ground state of  $\text{TiMg}_5$  is also a triplet state. The most stable configuration of  $\text{TiMg}_5$  comes under  $C_s$  point group symmetry. It is formed with a lower cap of Mg on  $\text{TiMg}_4$  cluster. Next global minimum structure is  $\text{TiMg}_5\_B$  with  $C_1$  point group symmetry has energy 0.26 eV higher than  $\text{TiMg}_5$ . The global ground state of  $\text{TiMg}_6$  is a triplet state. The most stable structure  $\text{TiMg}_6$  holds  $C_1$  point group symmetry, which can be achieved with a diagonal capping of Mg atom to  $\text{TiMg}_5$  cluster. The next global minimum structure is  $\text{TiMg}_6\_B$  with 0.5 eV higher energy. The lowest energy state configuration of pure  $\text{Mg}_7$  is pentagonal bipyramid-based cluster with  $C_1$  point group symmetry in which Ti atom is doped endohedrally. The global ground state of  $\text{TiMg}_7$  is a singlet state. The next higher energy structures are with 0.17 eV and 0.26 eV  $\text{TiMg}_7$  structures. The ground state of  $\text{TiMg}_8$  cluster is with  $C_2$  point group symmetry which has a ring type construction in which Ti atom has been doped at the centre of the cluster. The other endohedrally and exohedrally doped structures are with  $C_1$  point group symmetry with 0.01 eV and 1.35 eV higher energy respectively. The lowest energy state of  $\text{TiMg}_9$  cluster holds  $C_1$  point group symmetry which can be made by giving an upper or a lower cap of Mg atom to  $\text{TiMg}_8$  cluster. The exohedrally doped  $\text{TiMg}_9$  cluster with  $C_s$  point group symmetry has 0.81 eV higher energy. The ground state of  $\text{TiMg}_{10}$  cluster holds  $C_1$  point group symmetry which can be obtained by giving a side cap of Mg atom to  $\text{TiMg}_9$  cluster. The other optimized clusters of  $\text{TiMg}_{10}$  are 0.79 eV and 2.83 eV higher energy. The next member in our series of clusters is  $\text{TiMg}_{11}$  whose ground state orientation possess  $C_{2v}$  point group symmetry and it can be made by giving a side cap of Mg atom to  $\text{TiMg}_{10}$  cluster. Exohedrally and endohedrally doped other  $\text{TiMg}_{11}$  clusters are of  $C_1$  point group symmetry with 0.89 eV and 1.53 eV higher energy respectively. The lowest energy state of  $\text{TiMg}_{12}$  is singlet with  $C_1$  point group symmetry. It has a unique type of construction. Other optimized clusters of

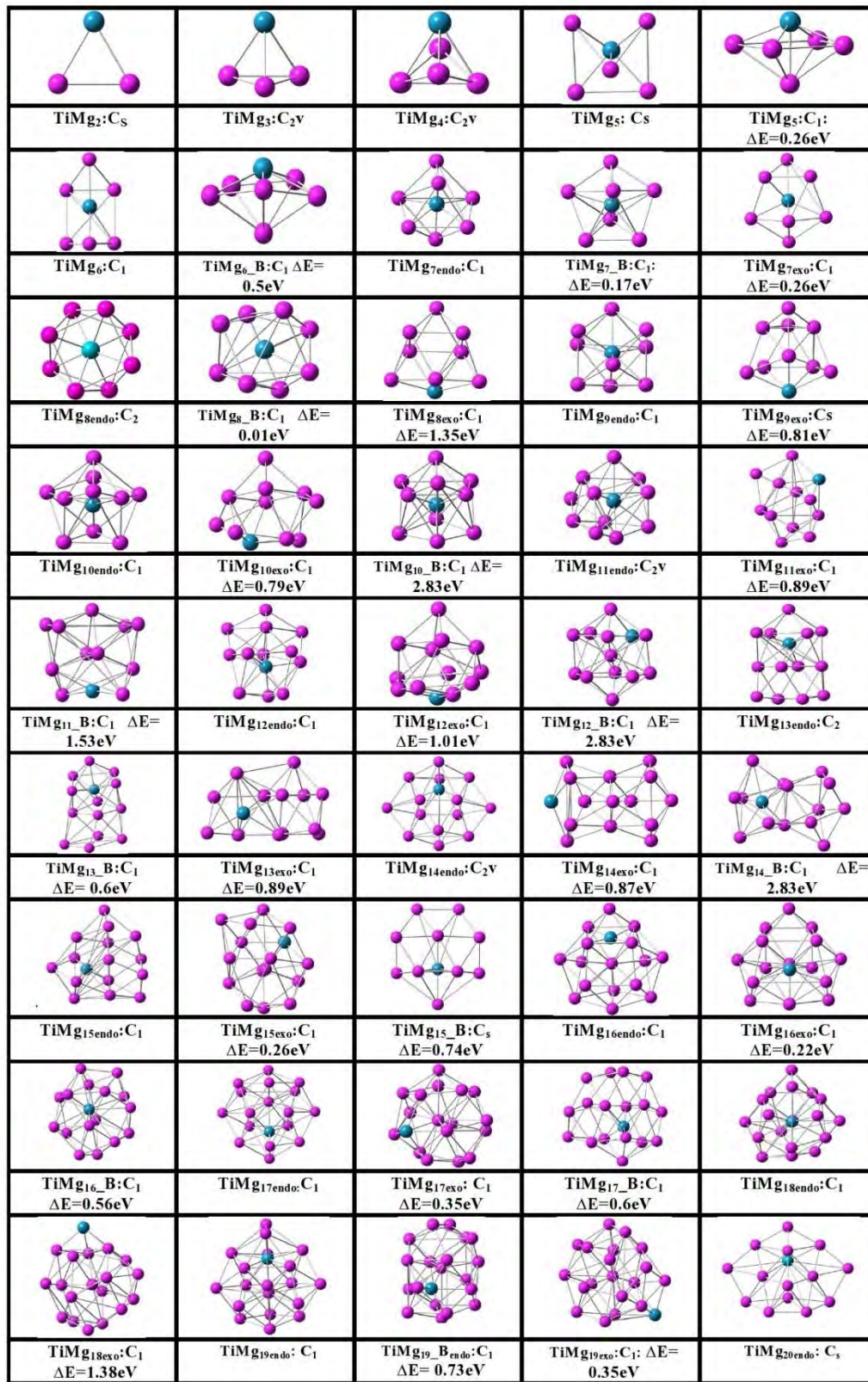


Fig. 4.1 Optimized global GS TiMg<sub>n</sub> (n=2-20) clusters.

TiMg<sub>12</sub> are of 1.01 eV and 2.83 eV higher energy. The exohedrally doped TiMg<sub>12</sub> is just the global minimum structure with an upper cap with Ti atom. The ground state orientation of TiMg<sub>13</sub> is with C<sub>2</sub> point group symmetry which can be made by giving a cap of Mg atom to TiMg<sub>12</sub> cluster. Other TiMg<sub>13</sub> structures are of C<sub>1</sub> point group symmetry having 0.6 eV and 0.89 eV higher energy. The lowest energy state of TiMg<sub>14</sub> holds C<sub>2v</sub> point group symmetry and it has a unique construction, with 3 layers atomic planes. From TiMg<sub>14</sub> a new trend of construction of clusters which is made of three layers of atom is starting. Other structures are TiMg<sub>14</sub><sub>exo</sub> and TiMg<sub>14</sub>\_B are of C<sub>1</sub> point group symmetry with 0.87 eV and 2.83 eV higher energy respectively. The next member is very stable TiMg<sub>15</sub> cluster which possess C<sub>1</sub> point group symmetry and it also has unique 3-layer construction. The exohedrally doped cluster has 0.26 eV higher energy. Another endohedrally doped TiMg<sub>15</sub>\_B has C<sub>s</sub> point group symmetry with 0.74 eV higher energy. The lowest energy state of TiMg<sub>16</sub> is with C<sub>1</sub> point group symmetry. Exohedrally doped TiMg<sub>16</sub> and endohedrally doped TiMg<sub>16</sub>\_B clusters are of C<sub>1</sub> point group symmetry. They are 0.22 eV and 0.56 eV higher energy than the global minimum cluster. The ground state of TiMg<sub>17</sub> which holds C<sub>1</sub> point group symmetry and it can be achieved by giving a side cap with Mg to TiMg<sub>16</sub> cluster. Other clusters of TiMg<sub>17</sub> are at 0.35 eV and 0.6 eV higher energy. From TiMg<sub>18</sub> to TiMg<sub>20</sub>, all the clusters hold C<sub>1</sub> point group symmetry and all of them can be achieved by giving either an upper hat or side hat with Mg atom to its just previous cluster, viz. TiMg<sub>18</sub> cluster can be achieved by giving an upper cap with Mg atom to TiMg<sub>17</sub> cluster. The exohedrally doped cluster of TiMg<sub>18</sub> has 1.38 eV higher energy. The ground state of TiMg<sub>19</sub> can be made by having side cap with Mg atom to TiMg<sub>18</sub> cluster and TiMg<sub>20</sub> is nothing but a side cap to TiMg<sub>19</sub> cluster. The exohedrally doped TiMg<sub>19</sub> cluster has 0.35 eV higher energy and another endohedrally doped TiMg<sub>19</sub> cluster (TiMg<sub>19</sub>\_B<sub>endo</sub>) holds C<sub>1</sub> point group symmetry has 0.73 eV higher energy than the global minimum cluster. From TiMg<sub>7</sub> all the clusters are cage type clusters in which Ti atom has been doped endohedrally and exohedrally to the clusters.

In the current work, global minimum GS structures are considered for further analysis from all exohedrally and endohedrally doped clusters.

The average bond length and nearest neighbor distance between Ti-Mg atom and Mg-Mg atoms of the global minimum GS structures are presented in Table 4.2 and Fig. 4.2 The



stability of a cluster depends on the size of the cluster. The minimum bond length measures the compactness of the cluster.

The average bond length of  $\text{TiMg}_7$  (Ti-Mg=2.75Å, Mg-Mg=3.59Å),  $\text{TiMg}_8$  (Ti-Mg=2.7Å, Mg-Mg=3.3Å),  $\text{TiMg}_{13}$  (Ti-Mg=2.79Å, Mg-Mg= 3.42Å) and  $\text{TiMg}_{18}$  (Ti-Mg=2.88Å, Mg-Mg=3.3Å) showing local minima and thus from the structural point of view they are relatively stable clusters.

Size of Cluster (n)	Average Bond Length for $\text{TiMg}_n$		Nearest neighbor for s p hybridization	
	Ti-Mg	Mg-Mg	Min Ti-Mg	Min Mg-Mg
2	3.16	3.21	3.16	3.21
3	3.09	3.14	3.09	3.14
4	3.05	3.21	2.97	3.09
5	3.00	3.21	2.90	3.34
6	2.96	3.65	2.93	3.09
7	2.75	3.59	2.65	3.24
8	2.70	3.30	2.70	3.21
9	2.81	3.35	2.78	3.11
10	2.81	3.41	2.75	3.15
11	2.79	3.35	2.72	3.17
12	2.80	3.45	2.68	3.03
13	2.79	3.42	2.67	2.94
14	2.82	3.33	2.65	2.74
15	2.80	3.25	2.68	2.90
16	2.77	3.44	2.77	2.95
17	2.81	3.32	2.71	3.03
18	2.88	3.39	2.70	2.91
19	2.91	3.34	2.76	2.96
20	3.10	3.19	2.96	2.74

Among the nearest neighbor distances of Ti, TiMg<sub>7</sub> (2.65Å), TiMg<sub>8</sub> (2.7Å), TiMg<sub>13</sub> (2.67Å) and TiMg<sub>18</sub> (2.67Å) are the lowest. So, s-p hybridization is expected to be more pronounced in these clusters.

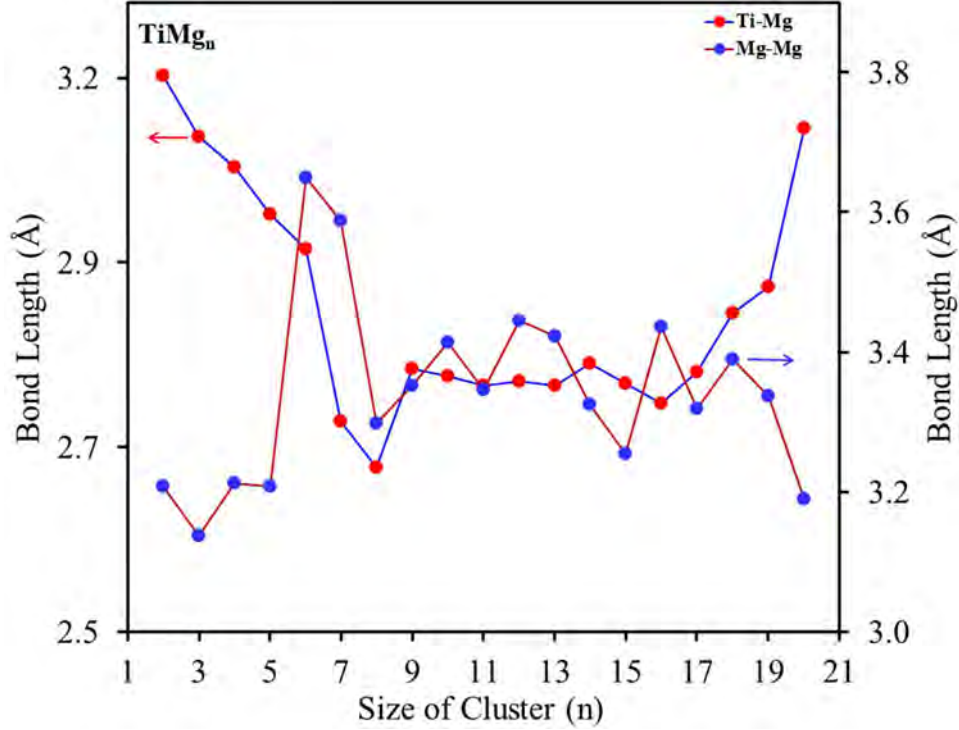


Fig. 4.2 Variation of bond length (Ti-Mg and Mg-Mg) of TiMg<sub>n</sub> (n=2-20) clusters with cluster size (n).

#### 4.3.2 Relative Stability

The relative stability of optimized clusters for pure, Ti-doped Mg<sub>n</sub> clusters (n=2-20) is estimated from the variation of thermodynamic, chemical and electronic parameters such as average binding energy per atom (BE), second-order change in binding energy, Fragmentation energy (FE) of GS structures. Since the binding energy per atom is the average gain in energy per atom during the formation of a cluster, it may be calculated for pure BE (Mg<sub>n</sub>) and doped BE (TiMg<sub>n</sub>) clusters as,

$$BE(Mg_n) = \frac{[nE(Mg) - E(Mg_n)]}{n} \quad (4.1)$$

$$BE(TiMg_n) = \frac{[nE(Mg) + E(^M Ti) - E(^M TiMg_n)]}{(n+1)} \quad (4.2)$$

Where,  $E(Mg)$ ,  $E(^M Ti)$ ,  $E(Mg_n)$  and  $E(^M TiMg_n)$  are the optimized global minimum energies of Mg, Ti,  $Mg_n$  and  $TiMg_n$  respectively, M and n represents the multiplicity and number of atoms in the cluster respectively. The variation of average BE per atom with cluster size is depicted in Fig. 4.3. Binding energy increases with increasing cluster size according to the liquid drop model in both pure and doped clusters as reported in the literature [7-19]. The rate of change of BE is more significant for  $TiMg_8$ ,  $TiMg_{13}$ ,  $TiMg_{15}$  and  $TiMg_{18}$  for global minimum clusters, indicating higher stability of these clusters. The trend is due to an increased number of nearest neighbors with cluster size as it enhances the number of interactions per atom. In doped clusters, the binding energy of clusters enhances due to doping, showing more stability due to doping .

Another thermodynamic parameter which gives information about stability of a cluster is the embedding energy(EE). Obeying Wigner-Witmer spin conservation rule, the embedding energy(EE) can be calculated as

$$EE^{WW} = E(Mg_n) + E(^M Ti) - E(^M TiMg_n) \quad (4.3)$$

All global minimum energy pure magnesium clusters are singlets (M=1), global minimum energy Ti cluster is triplets (M=3) whereas, for doped clusters, clusters with n=2-6 are triplets, other clusters are singlets. All values of embedding energy are positive, which means addition of Ti atom to the  $Mg_n$  cluster is favourable. M denotes multiplicity. Since all pure clusters are singlets, Ti is a triplet, and clusters from n=2-6 are triplets while other clusters are singlets.

Fig. 4.3 presents the variation of average binding energy per atom and embedding energy with the size of clusters. The BE per atom increases initially and reaches saturation at n=8. It shows local maxima for n= 8, 13, 15 and 18. Embedding energy shows the local maxima for n=8, 13, 15 and 18. The second-order change in cluster energy is considered as a parameter for stability. Large positive values of  $\Delta_2E$  indicate a gain in energy during the growth process from the just lower size cluster and a lower gain in energy for the next higher size. Thus higher the value of  $\Delta_2E$ , the higher the stability of the cluster.

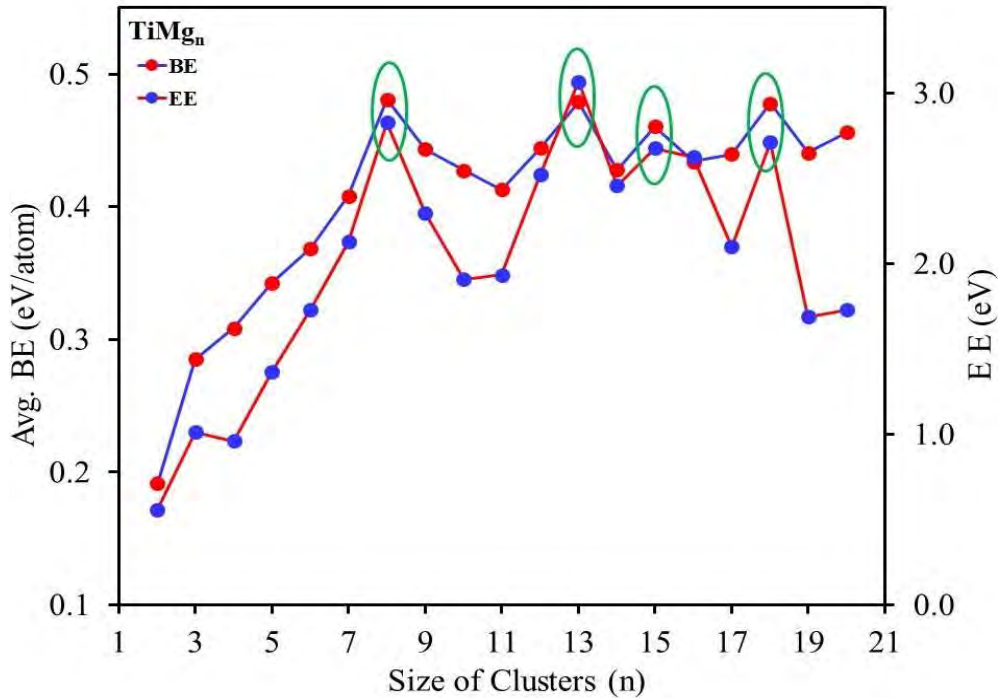


Fig. 4.3 Average binding energy and embedding energy of global GS  $\text{TiMg}_n$  ( $n=2-20$ ) clusters. The encircled points are showing local peaks present in the variation of the BE and EE.

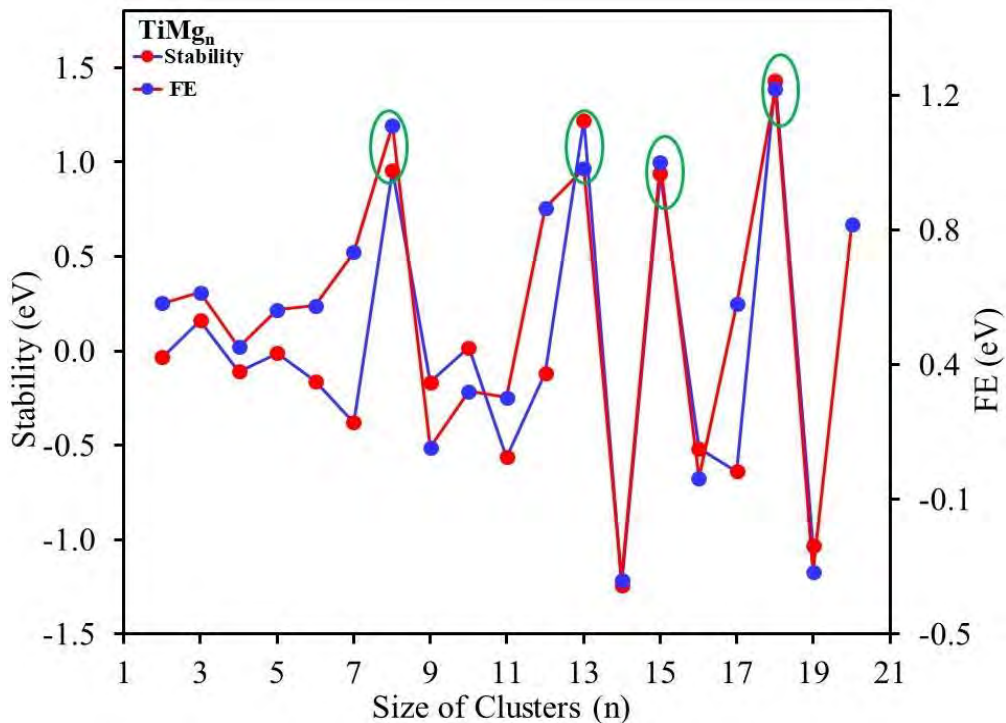


Fig. 4.4 Second order changes in energy and fragmentation energy of  $\text{TiMg}_n$  ( $n=2-20$ ) clusters with cluster size ( $n$ ). The encircled points are showing local peaks present in the variation of the stability and FE.

The second order change in energy  $\Delta_2E$  is calculated with the relation

$$\Delta_2(TiMg_n) = [E(TiMg_{n-1}) + E(TiMg_{n+1}) - 2E(TiMg_n)] \quad (4.4)$$

The fragmentation energy of clusters indicates the relative stability of clusters compared to neighboring clusters. The higher the value of FE, the stronger is the interaction means a higher energy requirement to detach an atom from the cluster. The fragmentation energy is calculated as

$$\Delta(n, n-1)_{TiMg_n} = (E(TiMg_{n-1}) + E(Mg) - E(TiMg_n)) \quad (4.5)$$

The variation of  $\Delta_2E$  and FE are shown in Fig. 4.4. It shows doped GS clusters n=8, 13, 15 and 18 have local peaks for both second order change in energy and fragmentation energy. Thus clusters with n=8, 13, 15 and 18 have local maxima for average BE per atom, Embedding energy, second order change in energy, and fragmentation energy. In the case of  $TiMg_8$ , if we assume each Mg atom donate two electrons to the valance manifold and the Ti atom possesses valancy four, the cluster bocomes a 20-electron cluster. The closed shell configuration is  $1S^21P^61D^{10}2S^2$  according to shell model. The situation is similar to  $Ge_{10}Ni$  or  $Si_{12}Fe$  cluster. On the other hand, the electronic shell configuration of  $TiMg_8$  is  $1s^22s^22p^63s^23p^64s^2$ , which shows a closed shell configuration.

Again,  $TiMg_{18}$  is also a stable cluster having closed shell configuration  $1S^21P^61D^{10}2S^21F^{14}2P^6$  with 40 electrons. Due to ellipsoidal shell closure, in the case of n=13 with number of electrons, 30 assumes configuration  $1S^21P^61D^{10}2S^21F^{10}$ . Again, due to spheroidal deformation of the cluster core with number of electrons 34 for  $TiMg_{15}$  got closed shell configuration  $1S^21P^61D^{10}2S^21F^{14}$ . The average binding energy per atom, Fragmentation energy, HOMO-LUMO energy gap are presented in Table 4.3 with cluster size (n=2-20). The trend in stability is possibly due to the size effect and it implies that the stability depends upon the compactness of a cluster.

**Table 4.3 Average Binding energy per atom in eV, Fragmentation energy (FE) in eV and HOMO-LUMO gap in eV for  $Mg_n$  and  $TiMg_n$  ( $n=2-20$ ) clusters.**

n	$Mg_n$			$TiMg_n$		
	BE	FE	Gap	BE	FE	Gap
2	0.01	0.02	3.49	0.19	0.53	2.06
3	0.04	0.11	3.05	0.28	0.56	1.93
4	0.15	0.45	2.93	0.31	0.40	1.79
5	0.14	0.11	2.37	0.34	0.51	1.93
6	0.14	0.16	2.38	0.37	0.52	1.71
7	0.16	0.29	2.34	0.41	0.68	1.45
8	0.19	0.36	2.31	0.48	1.06	1.47
9	0.24	0.64	1.61	0.44	0.10	1.32
10	0.28	0.66	1.92	0.43	0.27	1.40
11	0.27	0.23	2.02	0.41	0.25	1.27
12	0.27	0.23	1.69	0.44	0.82	1.15
13	0.28	0.39	1.56	0.48	0.93	1.34
14	0.28	0.32	1.41	0.43	-0.29	1.25
15	0.31	0.73	1.33	0.46	0.95	1.17
16	0.30	0.06	1.19	0.43	0.01	1.08
17	0.34	1.05	1.10	0.44	0.53	0.98
18	0.35	0.56	0.99	0.48	0.92	1.14
19	0.38	0.76	0.98	0.44	-0.02	1.15
20	0.39	0.72	1.38	0.46	0.77	1.02

### 4.3.3 Electronic Properties

#### 4.3.3.1 HOMO-LUMO

Highest occupied molecular orbital (HOMO) and lowest unoccupied molecular orbital (LUMO) are considered as the most valuable parameters in quantum condensed matter physics or quantum chemistry. HOMOs can be defined as outer orbital that contains electrons; thereby it acts as electron donor. Ionization potential is directly proportional to the HOMO. On the other side, LUMO acts as electron acceptor where LUMO energy is related to electron affinity of the system. The study of HOMO-LUMO provides information regarding the charge transfer among the molecule. Higher HOMO-LUMO gap implies higher kinetic energy and higher stability [59]. We can study the stability of the molecule from the HOMO-LUMO energy gap where the hard molecular system exhibits much higher HOMO-LUMO energy gap. One can get an idea of chemical reactivity of the system by studying HOMO-LUMO energies. HOMO- LUMO energy gap is a measure of the energy of electron jump from an occupied to an unoccupied energy orbital and it reflects the electronic stability of the cluster. The HOMO-LUMO energy gap is calculated as

$$E_{Gap} = E(LUMO) - E(HOMO) \quad (4.6)$$

The plot (Fig. 4.6) shows a gradual decrease of the energy gap with cluster size. This is due to the fact as molecular orbitals are formed from the overlap of more and more atomic orbital, the energy levels come closer. This indicates that the clusters showing metallic characteristics. In the case of pure clusters, the gap reduces to less than 1 eV from n=18. The HOMO-LUMO gap is higher for magic numbers than for shell closing in small metal clusters. HOMO-LUMO gap of  $TiMg_n$  (n=2-20) varies from 2.06 eV to 0.98 eV for global minimum doped clusters (Table-4.3). This establishes that the energy gap decreases from small clusters to large clusters and becoming metal like clusters. As the HOMO-LUMO gap increases, the possibility of electron transfer from HOMO to LUMO decreases. Higher values of the gap correspond to the higher kinetic stability of the cluster [13]. Here HOMO-LUMO gap has local peaks for n= 5, 10, 13, and 19.

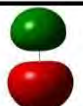

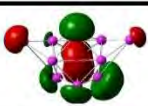

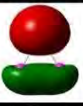
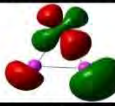
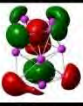



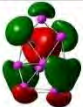
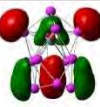
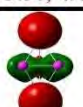
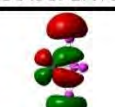

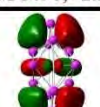
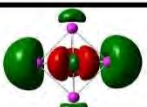
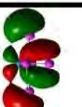
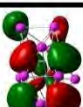

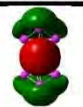
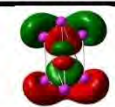


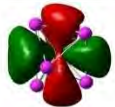

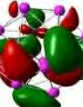

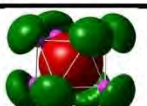
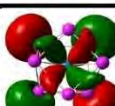
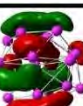
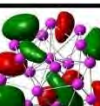
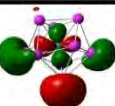



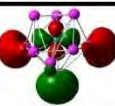
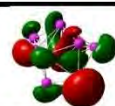


Cluster	HOMO	LUMO	Cluster	HOMO	LUMO
TiMg <sub>1</sub>			TiMg <sub>11</sub>		
	1P <sub>y</sub> ,MO:18,-4.39eV	1D <sub>xz</sub> ,MO:19,-2.62eV		3d <sub>x<sup>2</sup>-y<sup>2</sup></sub> ,MO:77, 3.47eV	3D <sub>yz</sub> ,MO:78,-2.2eV
TiMg <sub>2</sub>			TiMg <sub>12</sub>		
	1P <sub>y</sub> ,MO:24,-4.25eV	1D <sub>yz</sub> ,MO:25, -2.19eV		F <sub>z(x<sup>2</sup>-y<sup>2</sup>)</sub> MO:83,-3.45eV	MO:84, -2.3eV
TiMg <sub>3</sub>			TiMg <sub>13</sub>		
	1P <sub>y</sub> ,MO:30,-4.40eV	1D <sub>z</sub> ,MO:31,-2.47eV		D <sub>xz</sub> MO: 89,-3.58eV	F <sub>xz<sup>2</sup></sub> , MO:90, -2.24eV
TiMg <sub>4</sub>			TiMg <sub>14</sub>		
	1D <sub>z<sup>2</sup></sub> , MO:36,-3.88eV	1D <sub>yz</sub> ,MO:37,-2.35eV		F <sub>z(x<sup>2</sup>-y<sup>2</sup>)</sub> MO:95, -3.74eV	F <sub>xz<sup>2</sup></sub> MO:96,-2.54eV
TiMg <sub>5</sub>			TiMg <sub>15</sub>		
	1D <sub>x</sub> , MO:43,-3.58eV	1D <sub>yz</sub> ,MO:44,-2.19eV		F <sub>xz<sup>2</sup></sub> , MO:101,-3.54eV	G MO:102, -2.36eV
TiMg <sub>6</sub>			TiMg <sub>16</sub>		
	1D <sub>z<sup>2</sup></sub> , MO:48,-3.63eV	1D <sub>xz</sub> , MO:49,-2.29eV		D <sub>xz</sub> , MO:107, -3.58eV	F <sub>xz<sup>2</sup></sub> MO:108, -2.5eV
TiMg <sub>7</sub>			TiMg <sub>17</sub>		
	1D <sub>xz</sub> , MO:53, -3.8eV	1 D <sub>z<sup>2</sup></sub> MO:54, -2.29eV		F <sub>xz<sup>2</sup></sub> , MO:113, -3.53eV	F <sub>xz<sup>2</sup></sub> MO:114,-2.55eV
TiMg <sub>8</sub>			TiMg <sub>18</sub>		
	D <sub>z<sup>2</sup></sub> MO:59, -3.42eV	D <sub>xz</sub> MO:60, -2.04eV		F <sub>xz<sup>2</sup></sub> MO:119,-3.6eV	F <sub>xz<sup>2</sup></sub> MO:120, -2.46eV
TiMg <sub>9</sub>			TiMg <sub>19</sub>		
	D <sub>x<sup>2</sup>-y<sup>2</sup></sub> MO:65,-3.41eV	1 G MO:66,-2.09eV		P <sub>x</sub> , MO:125,-3.74eV	G <sub>z<sup>3</sup></sub> , MO=126,-2.59eV
TiMg <sub>10</sub>			TiMg <sub>20</sub>		
	F <sub>xz</sub> ; MO:72,-3.55eV	F <sub>x(x<sup>2</sup>-3y<sup>2</sup>)</sub> MO:73,-2.19eV		D <sub>x<sup>2</sup>-y<sup>2</sup></sub> MO:131,-3.32eV	D <sub>xy</sub> MO:132, -2.36eV

Fig. 4.5 Representation of HOMO-LUMO surfaces of TiMg<sub>n</sub>.



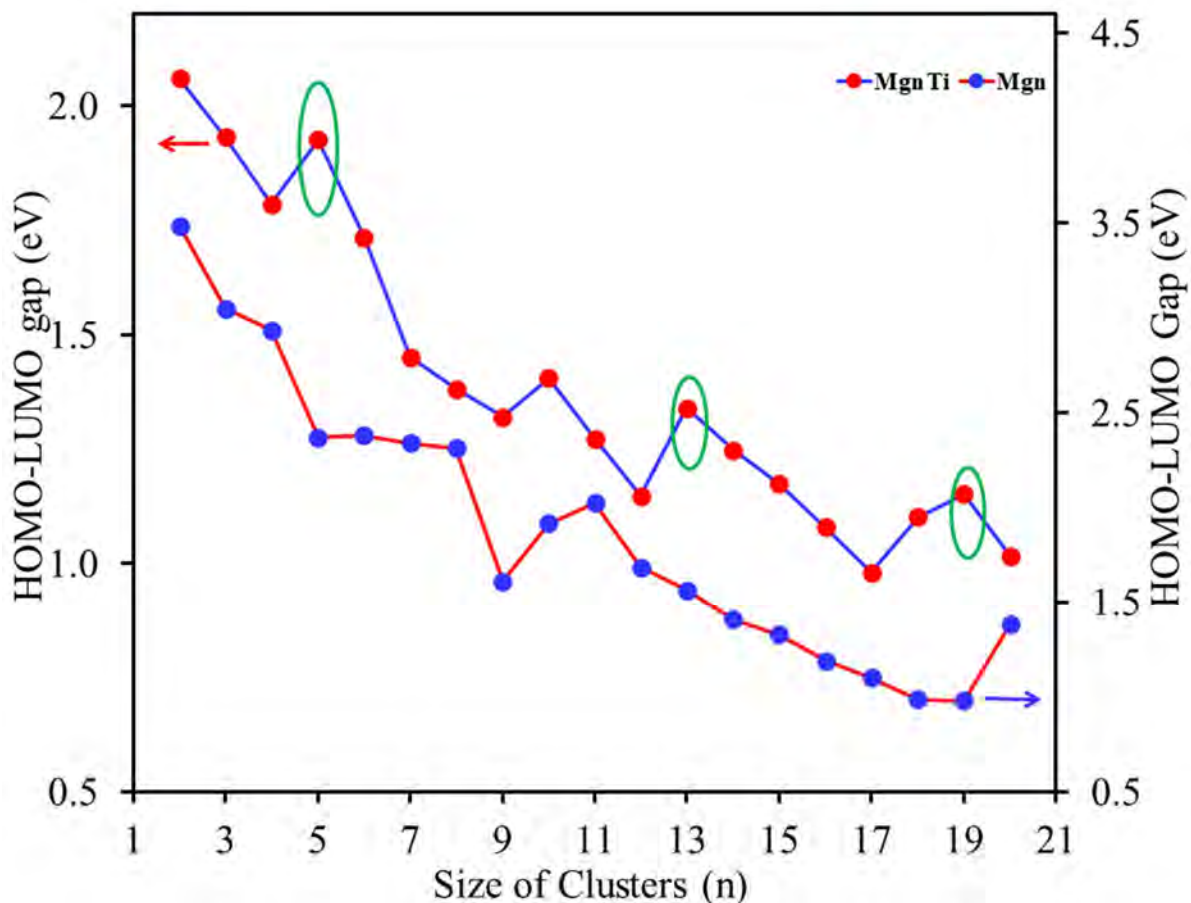


Fig. 4.6 Variation of HOMO-LUMO energy gap of Mg<sub>n</sub> & TiMg<sub>n</sub> (n=2-20) clusters with cluster size (n). The encircled points are showing local peaks present in the variation of the HOMO-LUMO gap.

The shape of HOMO and LUMO orbitals of each cluster along with number of molecular orbitals and energies in electron volts are presented in Fig. 4.5. Here, the red colored surface indicates positive diffusion, where green colored surface refers to negative phase means the red colored surface denotes the negative charge. In contrast, the green colored surface denotes the positive charge for the addressed molecule. Since clusters follow neither atomic orbitals nor molecular orbitals, here it is tried to assign orbitals as a composition of the two.

#### 4.3.3.2 Reactivity Indicators

With the help of reactivity, indicators viz. Vertical ionization potential (VIP) Vertical electron affinity (VEA), Chemical Hardness ( $\eta$ ) and Chemical Potential ( $\mu$ ) the change in electronic properties of clusters with cluster size are studied.

According to Koopmans theorem [64], the VIP and VEA can be calculated from HOMO LUMO energies of clusters as [26, 39]

$$VIP = -E_{HOMO}; \quad VEA = -E_{LUMO} \quad (4.7)$$

Chemical Potential

$$\mu = -\frac{E_{HOMO} + E_{LUMO}}{2} \quad (4.8)$$

The global Hardness can be expressed as [39]

$$\eta = \frac{E_{LUMO} - E_{HOMO}}{2} \quad (4.9)$$

The vertical ionization potential is the amount of energy absorbed when an electron is detached from the neutral atom considering particle relaxation is not allowed. The decrease in VIP may occur due to increase of energy of occupied orbitals due to a donor electron. A higher value of VIP means more energy is required to detach an electron from an atom. So, they are more stable. VEA may predict the stability of a cluster since it is the amount of energy liberated when an extra atom is added to a cluster.

$$VIP(TiMg_n) = E(TiMg_n^+) - E(TiMg_n) \quad (4.10)$$

In Fig. 4.7(b), TiMg<sub>5</sub>, TiMg<sub>8</sub>, TiMg<sub>10</sub>, TiMg<sub>13</sub>, TiMg<sub>15</sub> and TiMg<sub>18</sub> cluster showing local peaks in VIP and also TiMg<sub>5</sub>, TiMg<sub>8</sub>, TiMg<sub>13</sub>, TiMg<sub>15</sub>, TiMg<sub>18</sub> possesses lower value of electron affinity. The values of VIP, VEA,  $\mu$ ,  $\eta$  are calculated using anion-cation method. The variation of VIP, VEA and Chemical hardness & chemical potential are presented in Fig. 4.7(a, b) and Fig. 4.8(a, b).

Koopmans gave a concept which indicates the energy required to detach an electron from a closed-shell system is basically approximated as minus the orbital energy of the molecular orbital from which the electron has been removed.

As this is an approximation by Koopman's, it is inaccurate because

1. It neglects the changes in the forms of the molecular orbitals which takes place during ionization.
2. It also neglects the change in correlation energy terms that happens between the neutral molecule and ion.

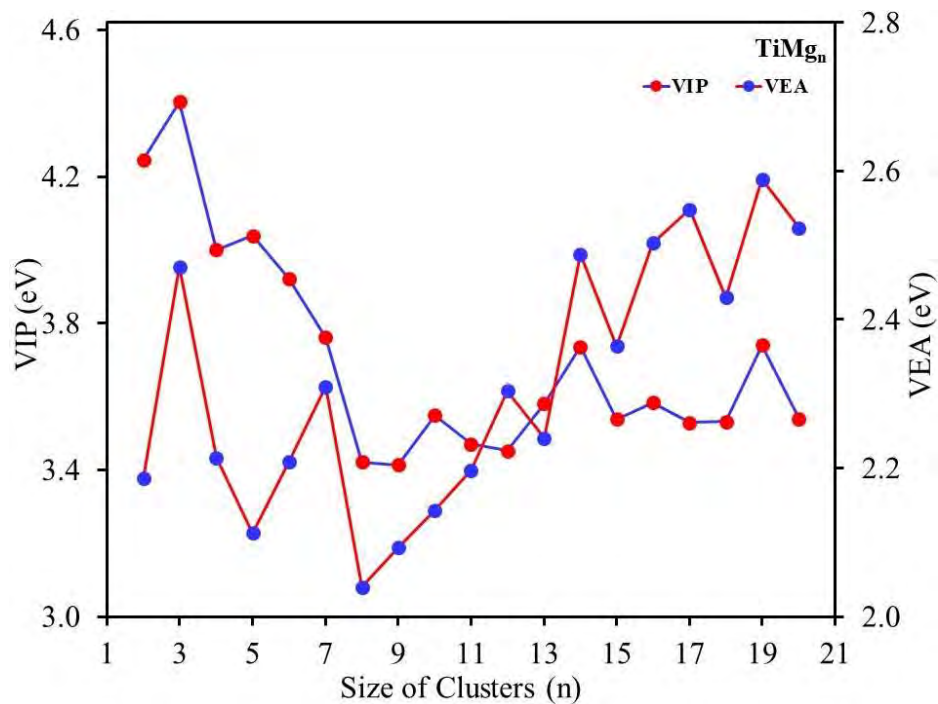


Fig. 4.7(a) Variation of VIP and VEA of  $TiMg_n$  ( $n=2-20$ ) clusters with cluster size( $n$ ) (Koopman).

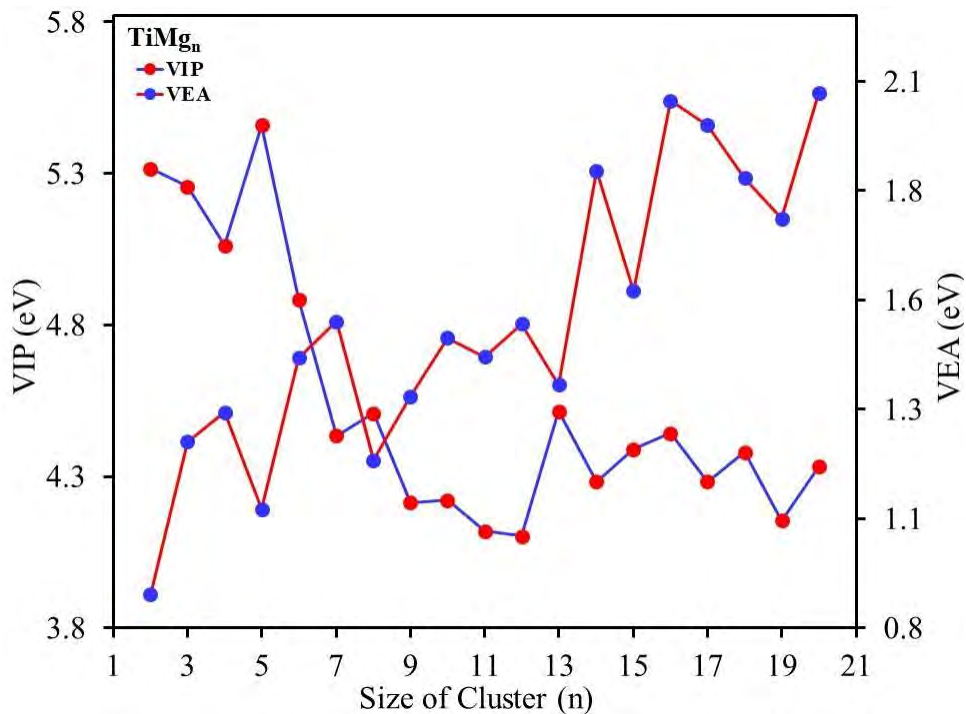
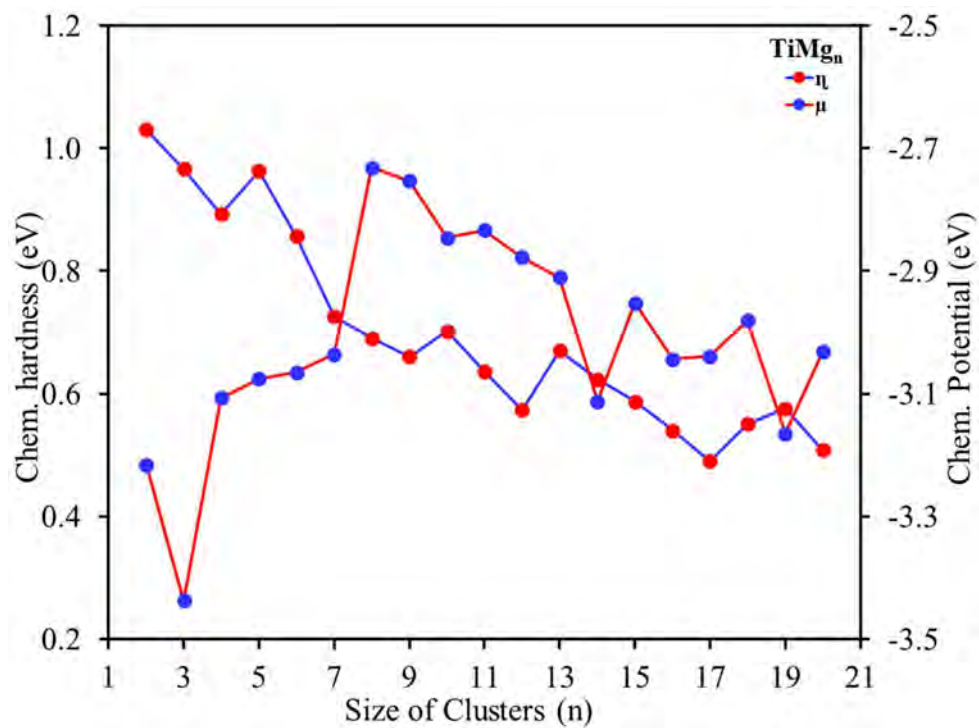
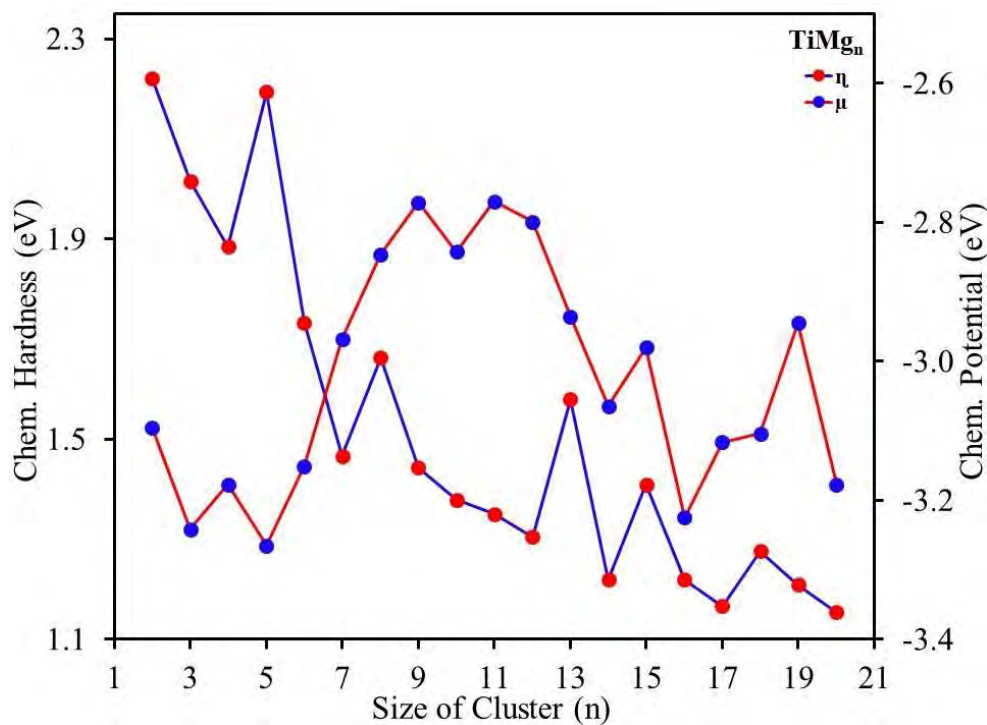


Fig. 4.7(b) Variation of VIP and VEA of  $TiMg_n$  ( $n=2-20$ ) clusters with cluster size( $n$ ) (Anion-cation method).



**Fig. 4.8(a) Variation of chemical hardness and chemical potential of  $TiMg_n$  ( $n=2-20$ ) clusters with cluster size( $n$ ) (Koopman).**



**Fig. 4.8(b) Variation of chemical hardness and chemical potential of  $TiMg_n$  ( $n=2-20$ ) clusters with cluster size( $n$ ) (Anion Cation Method)**

That is why we may not get a good results or accurate results if we calculate VIP, VEA, chemical hardness and chemical potential only by using HOMO-LUMO energies. There are so many good journals in which physicists and scientists have reported the calculation of VIP, VEA, chemical hardness and chemical potential by using cation and anion method which is more accurate than the Koopman's method. This is because this anion and cation method involves the change in energy that happens between the neutral molecule and ion during the ionization.

n	VIP	VEA	$\mu$	$\eta$	n	VIP	VEA	$\mu$	$\eta$
1	5.67	0.57	-3.12	2.55	11	4.12	1.42	-2.77	1.35
2	5.32	0.88	-3.10	2.22	12	4.10	1.50	-2.80	1.30
3	5.26	1.23	-3.24	2.02	13	4.51	1.36	-2.94	1.58
4	5.06	1.29	-3.18	1.88	14	4.28	1.85	-3.06	1.22
5	5.46	1.07	-3.27	2.19	15	4.39	1.57	-2.98	1.41
6	4.88	1.42	-3.15	1.73	16	4.44	2.01	-3.22	1.22
7	4.43	1.50	-2.97	1.47	17	4.28	1.95	-3.12	1.17
8	4.51	1.18	-2.85	1.66	18	4.38	1.83	-3.10	1.28
9	4.21	1.33	-2.77	1.44	19	4.15	1.74	-2.95	1.21
10	4.22	1.46	-2.84	1.38	20	4.33	2.02	-3.18	1.15

Chemical hardness is the second energy derivative with several electrons at constant external potential

$$\eta = \frac{1}{2} \left( \frac{\delta\mu}{\delta N} \right)_{ext.Pot} = \frac{1}{2} \left( \frac{\partial^2 E}{\partial N^2} \right)$$

Also, it can be defined as  $\eta = \frac{VIP - VEA}{2}$  where, VIP is the ionization potential and VEA is the electron affinity. Chemical hardness can be expressed as resistance to exchange

the number of electrons. A minimum value of hardness means maximum tendency to exchange electrons or maximum reactivity i.e. lower stability. Chemical hardness shows local peaks for n= 5, 8, 13, 15, 18, showing enhanced stability. The expression of VEA can be written as,

$$VEA(TiMg_n) = E(TiMg_n) - E(TiMg_n^-) \quad (4.11)$$

Calculated values of VIP, VEA chemical Hardness and chemical potential of TiMg<sub>n</sub> clusters for n=2-20 are presented in Table 4.4.

#### 4.3.4 Molecular Electrostatic Potential (MEP) and Total Electron Density Contours

Molecular electrostatic potential can be studied either by plotting the top surface or by plotting the contour. If one plots the MEP surface, then in that particular case one can only see the top surface. Instead of doing that we can plot each MEP surfaces as a contour around each molecule to see all the MEP.

It is really important to study electrostatic potential, V(r) produced in a molecule due to the electrons and nuclei to study the molecular reactivity [65]. V(r) can be written as

$$V(r) = \sum \frac{Z_0}{|R_0 - r|} - \int \frac{\rho(r') dr'}{|r' - r|} \quad (4.12)$$

Where,  $Z_0$  is the charge of the nucleus at  $R_0$  and  $\rho(r')$  is the electron density of the molecule. Electrostatic potential can be referred as a sum of positive and negative contribution from electrons nuclei. The sign of the electrostatic potential of the system depends on the major and minor contributions.

If electrostatic potential is positive, it indicates that the major contribution is from nuclei and if the sign is negative, the significant contribution is coming from electrons. In the study of MEP, each contour curves around each atom are the MEP surface. There is a color scale that indicates the positive and negative value. Here, we have basically yellow and red color. The red colored region defines the negative electrostatic potential, where the positive potential is indicated by yellow is our study. The contour plot of total electron density of TiMg<sub>n</sub> (n=2-20) is shown if Fig. 4.9.

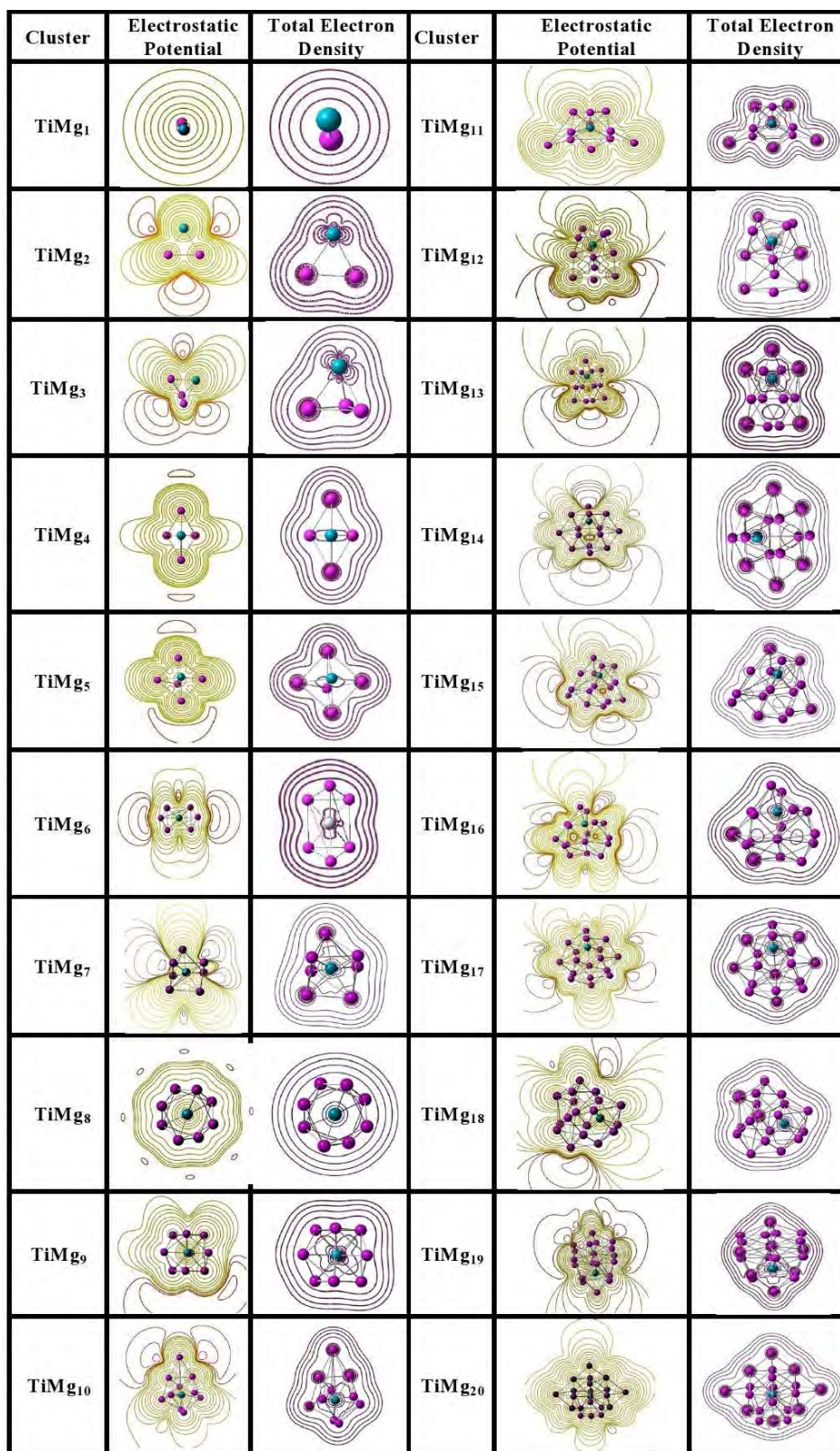


Fig. 4.9 Contour of electrostatic potential and electron density of TiMg<sub>n</sub>.

The contours are obtained from DFT calculation using B3LYP functional and 6311G (d) basis set. The iso value is 0.001, resolution 0.1Å in a 2D grid of -10Å to +10Å. Here the positive charge contour centers around Ti atom whereas the negative charge contours on the Mg cluster. The electron density distribution depends on the electrostatic interaction of the core and the electrons. The electron density is high in spherical regions and diffused in the outer cluster region.

#### 4.3.5 Mulliken Charge Distribution Between Ti Atom and Mg Atoms

The transfer of charge between the dopant atom (Ti) and the atoms of the cluster (Mg) is a crucial parameter to discuss about the possibility of hydrogenation-dehydrogenation using clusters and the possibility of being used as a hydrogen storage material [66]. It is very much interesting to see that in all the Ti doped Mg clusters, Ti atom donates charge to nearest neighbor acceptor Mg atoms. Here, Ti atom acts as donor and Mg atoms act as acceptor. As a result, Ti atom gets positively charged and nearest Mg atoms becomes negatively charged and becomes reactive site for hydrogen adsorption.

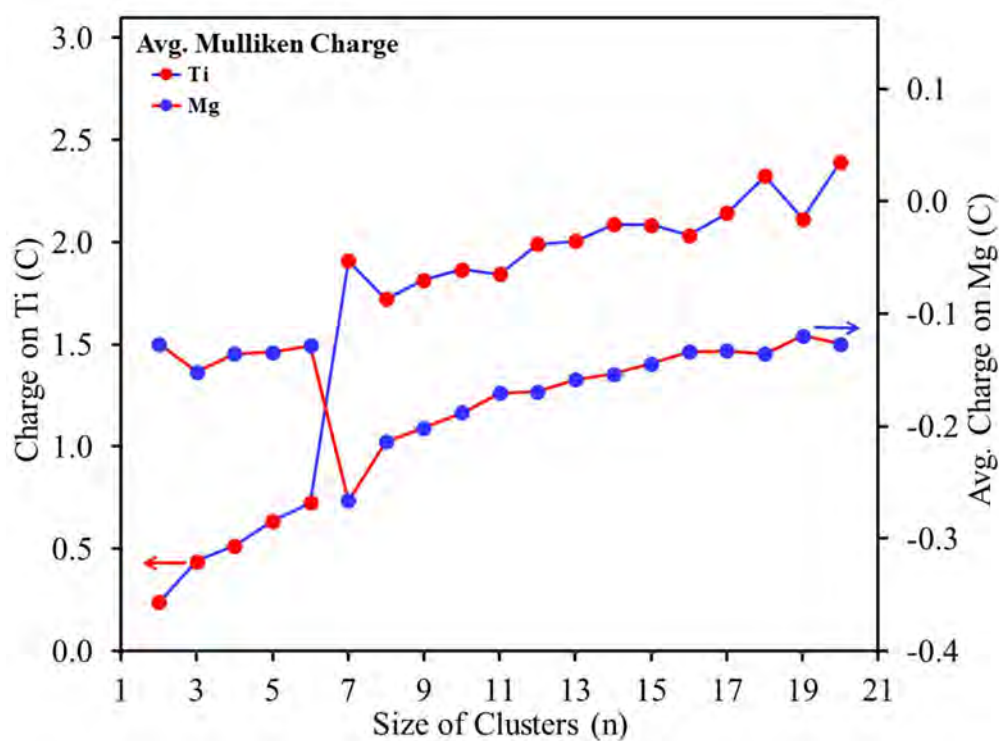


Fig. 4.10 Variation of average charge on Ti and on Mg atom in coulombs with cluster size (n).



The charge transfer mechanism may be considered as interaction between the orbitals of the donor and the acceptor atoms. The interaction occurs between HOMO of donor and LUMO of acceptor. The physical process of charge transfer is responsible for cluster formation. There is a redistribution of charge density in the orbitals. The electronic charge transfer between 4s, 3d, 4p orbitals of Ti and 3s, 3d orbitals of Mg occurs to make the clusters stable. Due to the charge transfer mechanism the average bond length also changes to form a stable cluster. In case of  $\text{TiMg}_7$ , there is an abrupt transfer of charge (Fig. 4.10).

#### 4.3.6 Electrostatic Dipole-moment and Polarizability of $\text{TiMg}_n$ Clusters

Polarizability is a measure of asymmetry of the structures and their orbital distributions. It also measures the change of the cluster properties under an electrostatic field [67, 68].

The variation of polarizability and dipole moment of the clusters are shown in Fig. 4.11. The polarizability increases with cluster size with a dip in  $n=7, 13$ . The dipole moment holds local minima at  $n=5, 8, 11$  and  $14$ . Also it is seen that the chemical hardness is higher for  $n=5, 8, 13, 15, 18$  which implies that the clusters are less polarizable.

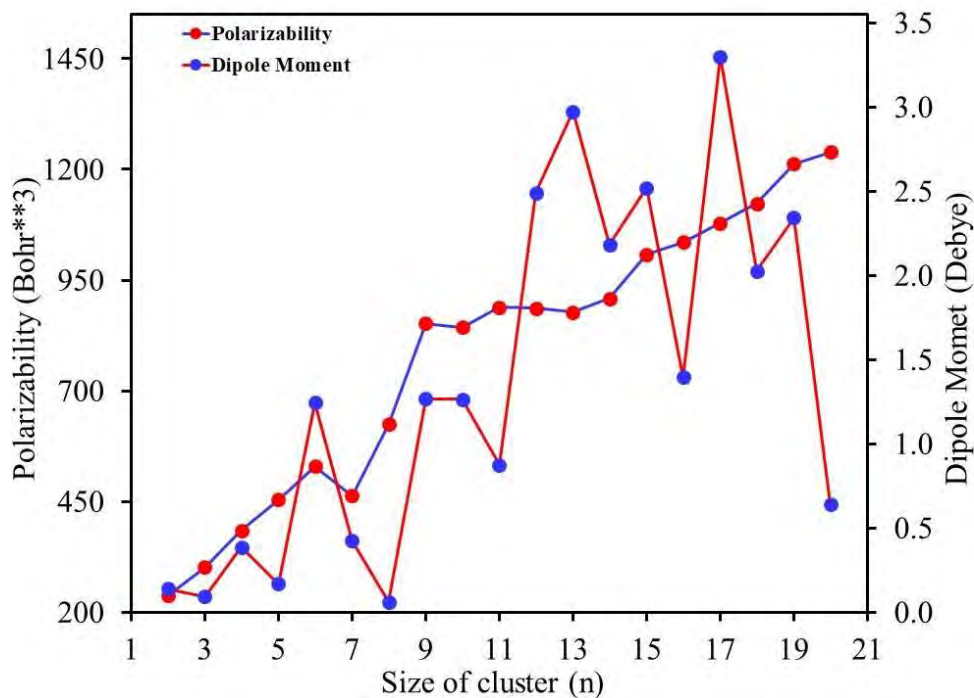


Fig. 4.11 Variation of electrostatic dipole moment and polarizability with cluster size (n).

The calculated data are given in Table 4.5.

<b>Table 4.5 Variation of Charge transfer, Dipole moment, Polarizability and vibrational frequency of TiMg<sub>n</sub> with cluster size (n).</b>					
n	Charge Q in Coulombs		Dipole Moment	Polarizability	Vibr.
	Q <sub>Ti</sub>	Q <sub>Mg</sub> (Avg.)	Debye	in Bohr <sup>3</sup>	Frequency(cm <sup>-1</sup> )
2	0.24	-0.12	0.14	237.51	123.71
3	0.44	-0.15	0.09	302.19	130.88
4	0.52	-0.13	0.39	385.08	78.00
5	0.64	-0.13	0.17	454.37	47.99
6	0.73	-0.12	1.24	529.73	17.58
7	1.91	-0.27	0.42	463.21	19.38
8	1.72	-0.22	0.6	624.24	18.52
9	1.82	-0.20	1.27	852.06	32.91
10	1.87	-0.19	1.26	843.12	11.78
11	1.85	-0.17	0.88	888.63	31.34
12	1.99	-0.17	2.49	886.56	15.40
13	2.01	-0.15	2.97	878.29	49.17
14	2.09	-0.13	2.18	908.28	35.11
15	2.09	-0.14	2.52	1007.69	36.22
16	2.04	-0.13	1.40	1035.56	34.56
17	2.14	-0.13	3.30	1078.57	103.14
18	2.33	-0.13	2.03	1123.31	38.29
19	2.12	-0.11	2.34	1212.13	19.56
20	2.39	-0.12	0.64	1239.46	38.12

#### **4.3.7 Population Analysis**

From natural population analysis one can have explanation of charge transfer within the cluster [69]. The NBO calculation of lowest energy clusters of TiMg<sub>n</sub> are shown in the

Table 4.6. The redistribution of charge among the nearest neighbours taken place. The most reactive site in the cluster having most negative charge is seen to be the closest Mg element from Ti, the calculated distance is shown in the table. The elements that gains electrons becomes negatively charged. Almost in all cases, Ti atom shows positive charge means Mg atoms gains electrons from Ti atoms and Mg atoms becomes negative. To have a closer look into the fact, the electronic configuration of Ti atoms and electronic configuration of Mg atoms are presented in Table 4.6. It is seen that in case of Ti doped clusters in Ti atoms 4s and 3d orbitals forms the core and 4p has very little contribution. Similarly, in Mg atoms 3s and 3p orbitals forms the core showing strong sp hybridization while 3d, 4s, 4p orbitals contribute very weakly. The results of NBO analysis of the clusters viz charge of most reactive site, electronic configuration of Ti and average electronic configuration of Mg atoms for global minimum GS clusters are shown in Table 4.6. It is interesting to note that the charge distribution with Mulliken and NBO are largely different. In Mulliken distribution all Ti atoms are donors and Mg atoms are acceptors whereas in NBO TiMg<sub>7</sub>, TiMg<sub>8</sub>, TiMg<sub>11</sub> and TiMg<sub>12</sub>, Ti atoms are acceptors and as such number of reactive sites differ in the two processes.

After studying all the TiMg<sub>n</sub> clusters ranges from n=1-20, it has been found from their thermodynamic and chemical properties, TiMg<sub>8</sub> cluster is showing enhanced stability. From the study it is seen that TiMg<sub>8</sub> possesses local peak in BE/atom, EE, FE, Stability, VIP, Chemical hardness and Local dip in VEA. The exceptional stability of TiMg<sub>8</sub> can be explained using electron counting rule as: one Mg atom has two valence electron and one Ti atom has four valence electron so, TiMg<sub>8</sub> has Mg<sub>8</sub> (16) + Ti (4) =20 valence electrons and it has shell model configuration like 1S<sup>2</sup>1P<sup>6</sup>1D<sup>10</sup>2S<sup>2</sup> which is a closed shell configuration. On the other hand, like atoms the electronic configuration of TiMg<sub>8</sub> is 1s<sup>2</sup>2s<sup>2</sup>2p<sup>6</sup>3s<sup>2</sup>3p<sup>6</sup>4s<sup>2</sup> It is found that the cluster having 20 valence electrons is relatively more stable than other

**Table 4.6 Natural electronic configuration of Ti and Mg atoms in TiMg<sub>n</sub> (n=2-20).**

n	Multiplicity	Mulliken Charge		Highest -ve charge on Mg atom and No. of reactive sites from NBO	Electronic configuration Ti atoms	Electronic configuration of Mg atoms
		Charge on Ti	Av. Charge on Mg			
2	3	0.24	-0.12	-0.101 (2)	4s <sup>1.64</sup> 3d <sup>2.14</sup> 4p <sup>0.01</sup> 5s <sup>0.01</sup>	3s <sup>1.75</sup> 3p <sup>0.33</sup> 3d <sup>0.01</sup> 4p <sup>0.01</sup>
3	3	0.44	-0.15	-0.147 (3)	4s <sup>1.35</sup> 3d <sup>2.19</sup> 4p <sup>0.01</sup> 5s <sup>0.01</sup>	3s <sup>1.55</sup> 3p <sup>0.57</sup> 4s <sup>0.01</sup> 3d <sup>0.01</sup> 4p <sup>0.01</sup>
4	3	0.52	-0.13	-0.198 (4)	4s <sup>1.17</sup> 3d <sup>2.33</sup> 4p <sup>0.02</sup> 5s <sup>0.01</sup>	3s <sup>1.49-1.59</sup> 3p <sup>0.44-0.69</sup> 3d <sup>0.01</sup> 4p <sup>0.01-0.02</sup>
5	3	0.64	-0.13	-0.235 (5)	4s <sup>1.04</sup> 3d <sup>2.46</sup> 4p <sup>0.03</sup>	3s <sup>1.41-1.53</sup> 3p <sup>0.46-0.79</sup> 3d <sup>0.01</sup> 4p <sup>0.02-0.03</sup>
6	3	0.73	-0.12	-0.110 (4)	4s <sup>1.02</sup> 3d <sup>2.54</sup> 4p <sup>0.03</sup> 4d <sup>0.01</sup>	3s <sup>1.46-1.52</sup> 3p <sup>0.43-0.63</sup> 3d <sup>0.01</sup> 4p <sup>0.01-0.02</sup>
7	1	1.91	-0.27	-0.181 (2)	4s <sup>0.64</sup> 3d <sup>3.51</sup> 4p <sup>0.05</sup>	3s <sup>1.26-1.29</sup> 3p <sup>0.64-0.75</sup> 3d <sup>0.01</sup> 4p <sup>0.02-0.03</sup>
8	1	1.72	-0.22	0.00 (0)	4s <sup>0.80</sup> 3d <sup>3.24</sup> 4p <sup>0.05</sup>	3s <sup>1.27</sup> 3p <sup>0.67</sup> 3d <sup>0.01</sup> 4p <sup>0.02</sup>
9	1	1.82	-0.20	-0.055 (6)	4s <sup>0.76</sup> 3d <sup>3.23</sup> 4p <sup>0.04</sup>	3s <sup>1.25-1.29</sup> 3p <sup>0.63-0.77</sup> 3d <sup>0.01</sup> 4p <sup>0.02-0.04</sup>
10	1	1.87	-0.19	-0.301 (4)	4s <sup>0.74</sup> 3d <sup>3.19</sup> 4p <sup>0.05</sup>	3s <sup>1.21-1.48</sup> 3p <sup>0.20-1.05</sup> 3d <sup>0.01</sup> 4p <sup>0.01-0.03</sup>
11	1	1.85	-0.17	-0.282 (5)	4s <sup>0.73</sup> 3d <sup>3.23</sup> 4p <sup>0.06</sup>	3s <sup>1.19-1.49</sup> 3p <sup>0.19-1.04</sup> 3d <sup>0.0-0.01</sup> 4p <sup>0.01-0.03</sup>
12	1	1.99	-0.17	-0.587 (7)	4s <sup>0.73</sup> 3d <sup>3.24</sup> 4p <sup>0.05</sup>	3s <sup>1.05-1.33</sup> 3p <sup>0.36-1.39</sup> 3d <sup>0.01</sup> 4p <sup>0.01-0.04</sup>
13	1	2.01	-0.15	-0.3945(5)	4s <sup>0.69</sup> 3d <sup>3.24</sup> 4p <sup>0.04</sup>	3s <sup>1.05-1.21</sup> 3p <sup>0.56-1.32</sup> 3d <sup>0.01</sup> 4p <sup>0.02-0.03</sup>
14	1	2.09	-0.15	-0.1724 (9)	4s <sup>0.55</sup> 3d <sup>2.89</sup> 4p <sup>0.02</sup> 5s <sup>0.04</sup>	3s <sup>1.11-1.23</sup> 3p <sup>0.71-1.18</sup> 3d <sup>0.01-0.02</sup> 4p <sup>0.02-0.04</sup>
15	1	2.09	-0.14	-0.7831 (7)	4s <sup>0.66</sup> 3d <sup>2.23</sup> 4p <sup>0.034</sup>	3s <sup>1.01-1.35</sup> 3p <sup>0.29-1.75</sup> 3d <sup>0.01</sup> 4p <sup>0.01-0.03</sup>
16	1	2.04	-0.13	-0.1710 (8)	4s <sup>0.57</sup> 3d <sup>2.40</sup> 4p <sup>0.03</sup> 5s <sup>0.03</sup>	3s <sup>1.01-1.07</sup> 3p <sup>0.88-1.13</sup> 3d <sup>0.0-0.01</sup> 4p <sup>0.02-0.03</sup>
17	1	2.14	-0.13	-1.5481 (7)	4s <sup>0.57</sup> 3d <sup>3.18</sup> 4p <sup>0.04</sup>	3s <sup>0.86-1.15</sup> 3p <sup>0.49-2.67</sup> 3d <sup>0.01</sup> 4p <sup>0.01-0.03</sup>
18	1	2.33	-0.13	-1.220 (7)	4s <sup>0.57</sup> 3d <sup>3.03</sup> 4p <sup>0.04</sup> 5s <sup>0.01</sup>	3s <sup>0.91-1.13</sup> 3p <sup>0.56-1.58</sup> 3d <sup>0.01</sup> 4p <sup>0.01-0.03</sup>
19	1	2.12	-0.11	-1.3370 (5)	4s <sup>0.55</sup> 3d <sup>3.08</sup> 4p <sup>0.04</sup>	3s <sup>0.74-1.13</sup> 3p <sup>0.44-2.53</sup> 3d <sup>0.01</sup> 4p <sup>0.01-0.05</sup>
20	1	2.39	-0.12	-0.4420(10)	4s <sup>0.42</sup> 3d <sup>2.3</sup> 4p <sup>0.04</sup> 5s <sup>0.13</sup>	3s <sup>0.9-1.35</sup> 3p <sup>0.21-1.41</sup> 4s <sup>0.01</sup> 3d <sup>0.01</sup> 4p <sup>0.01-0.02</sup>

clusters in the series. There is a local peak in VIP at n=8 and a sharp drop in VIP as the valence electron count increase by 1, means when the electron count comes 20 to 21. So it can be understood that the magic cluster lies between n=2 to n=12.

Our main focus is to find out a promising cluster which can store hydrogen with higher efficiency. Smaller clusters are more efficient in hydrogen storage compared to the higher size endohedrally doped clusters. For these reasons, we limited our study from n=1 upto n=10. The hydrogen storing efficiency of these clusters has been discussed in the next chapter of my thesis. For now and from now we limit our study upto n=12 clusters only because of the above reasons.

#### 4.3.8 Electron Localization Function (ELF)

One can find a strongly localized electron-pair in a molecular system from the electron localization function. Thus, it gives the probability of finding two electrons of opposite spin in a particular region in an atomic or molecular system. These electron-pair can interact with other electrons outside the region. The ELF can be obtained from the expression [70]

$$D(r) = \text{Electron localization} = T(r) - \frac{1}{4} \frac{(\nabla \rho(r))^2}{\rho(r)} = \frac{1}{2} \sum_{i=1}^N |\nabla \psi_i(r)|^2 - \frac{1}{8} \frac{|\nabla \rho(r)|}{\rho(r)} \quad (4.13)$$

Where  $\rho$  denotes the electron spin density,  $T(r)$  represents the kinetic energy density. The second term represents the bosonic kinetic energy density. From the above relation one can get the expression for uniform electron gas like

$$D_h(r) = \text{uniform electron gas} = \frac{3}{5} (6\pi^2)^{2/3} \rho^{5/3}(r) = \frac{3}{10} (3\pi^2)^{2/3} \rho^{5/3}(r) \quad (4.14)$$

Thus, the ratio

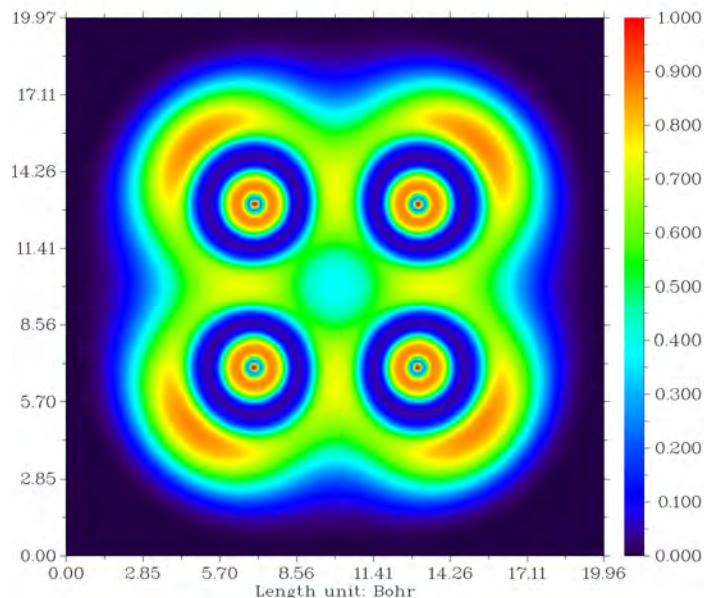
$$\chi(r) = \frac{D(r)}{D_h(r)}$$

where,  $\chi(r)$  can be defined as the ratio of electron localization  $D(r)$  w.r.t uniform electron gas  $D_h(r)$ .

The ELF function can be defined as,

$$ELF(r) = \frac{1}{1 + \chi^2(r)}; \chi(r) = \frac{D(r)}{D_h(r)}$$

ELF of the TiMg<sub>8</sub> cluster is shown in Fig. 4.12. ELF 2D map contains three regions, regions with ELF =0, represents the region with low electron-pair localization, and is represented by blue or deep blue color in the ELF -2D map. The portion with ELF=0.5 or around 0.5 is the zone with metallic bonding picturized with green color in the ELF map.



**Fig. 4.12 Representation of ELF-2D map of TiMg<sub>8</sub> cluster.**

Finally, the third portion, where ELF = 1.0 or nearly 1.0 represents the zone where a strongly localized electron pair is present, shaded by the red color in the ELF map.

ELF map of TiMg<sub>8</sub> indicates no such region where strong electron-pair localization, as ELF is less than 0.9 everywhere. Most of the region is shaded by green and contains only very few regions where the ELF value is around 0.85 means less than 0.9. This map indicates that this TiMg<sub>8</sub> cluster is the most stable with no reactive sites.

#### 4.3.9 Critical Points (CP's) of TiMg<sub>8</sub> Cluster

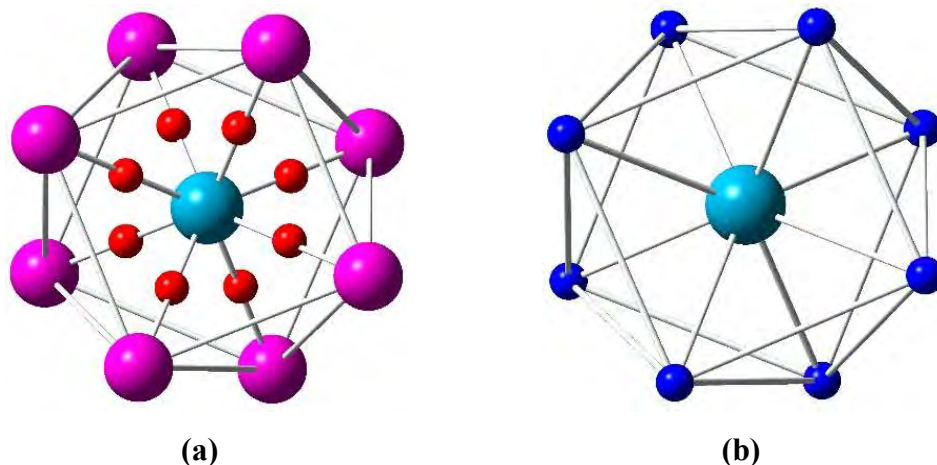
Here the critical points and NICS are studied for the most symmetric TiMg<sub>8</sub> cluster which is found to be the most stable cluster from the study of thermodynamic and electronic properties. The ring cluster TiMg<sub>8</sub> consist of Mg-Mg and Mg-Ti interactions. The Mg atoms that are bonded with Ti atoms can be examined by the study of critical points (CP). The bond length at which the electron density vanished is the so-called critical point. The indices at which the critical points occur can be evaluated by diagonalizing the Hessian matrices of the electron density. At a critical point, the eigenvalues of the Hessian matrix are real as well as non-zero values. There are two components of critical pint one is rank 'R' and another one is signature 'S'. The rank 'R' of a critical point can be referred to as the number of non-zero eigenvalues and the signature 'S' of critical point can be defined as the algebraic sum of signs of the eigenvalues. The topological features of CP's can be represented as (R, S) [71, 72].

In the present work, the bond-critical points (BCP) are (3, -1), which means the rank is 3 and the signature is -1. The bond-critical point (3, -1), here the electron density falls down in two perpendicular directions of space and rises in the thired direction. The bond critical point is a saddle point along the bond path at the inter atomic surface where the shared electron density reaches a minimum. The atomic critical point (3, -3) can be defined as the space where the electron density falls down in all three perpendicular direction of space. For all atoms except hydrogen it is also the position of nucleus. In our system TiMg<sub>8</sub> clusters, the number of bond-critical points is 8 in (3,-1). Another type of critical point is the atomic critical point (3,-3). Here, the number of atomic critical points is 9 (3, -3). Fig. 4.13(a) shows (3, -1) bond critical point and Fig. 4.13(b) shows (3, -3) atomic critical points of TiMg<sub>8</sub> cluster.

For, the completeness of study of the topological space Poincare-Hopf rule is to be verified. According to the Poincare-Hopf rule [72]

$$n - b + r - c = 1$$

Where, n is the number of (3, -3) CPs., b the number of (3, -1) CPs, r is the number of (3, +1) CPs, and c the number of (3, +3) CPs. Where (3, +1) and (3,+3) are ring CP and cage CP respectively. For the TiMg<sub>8</sub> cluster, there are 9 (3,-3) CPs and 8 (3,-1) CPs. So the rule is readily verified as, 9-8+0-0=1. Thus Poincare-Hopf rule is satisfied.



**Fig. 4.13 (a) represents (3, -1) bond critical point and (b) represents (3, -3) atomic critical points of  $\text{TiMg}_8$  cluster.**

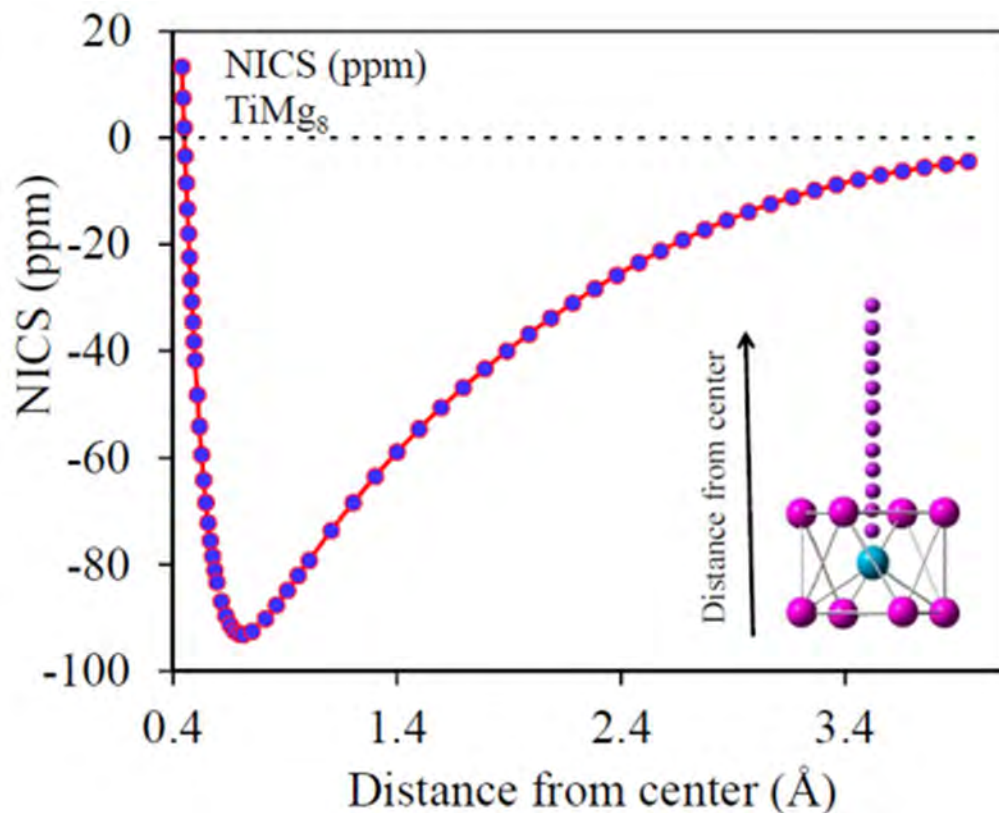
(3, -1) CPs show that there are 8 Mg-Ti bonds, In the  $\text{TiMg}_8$  cluster. It is clear from the (3, -1) CP that the Ti atom is bonded to all of the Mg atoms in  $\text{TiMg}_8$  and its valance electron count is 20 . Also, in all the stability parameters like BE, EE, FE, stability, etc  $\text{TiMg}_8$  holds local peaks and showing enhanced stability. (3, -3) is denoting atomic CPs. According to ELF and CP configuration, it can be inferred that there is no uniform electron-rich region inside the cluster.

#### ***4.3.10 Nucleus Independent Chemical Shift (NICS) of $\text{TiMg}_8$ Cluster***

Nucleus-independent chemical shift (NICS) and anisotropy of magnetic susceptibility are the important and widely used method for studying the aromaticity of a particular ring-type cluster. The NICS is represented as the negative value of absolute magnetic shielding evaluated at the ring center. To be an aromatic compound, the chemical species should obey the  $4n+2$  Huckel rule for monoclinic  $\pi$ -systems [73]. Although, electron counts do not provide in-depth evidence of aromaticity or anti-aromaticity, especially in the case of metal systems [74, 75].

An aromatic system can be defined as a conjugated cyclic  $\pi$ -electron compound that possesses a chemical shift. It shows the magnetic shielding at the center of the cluster. If a ring-type chemical species or a ring cluster exhibits negative values of NICS then it can be concluded that the cluster is showing aromaticity.





**Fig. 4.14** Variation of Nucleus-independent chemical shift (NICS) of  $\text{TiMg}_8$  cluster with the distance from the center of the cluster.

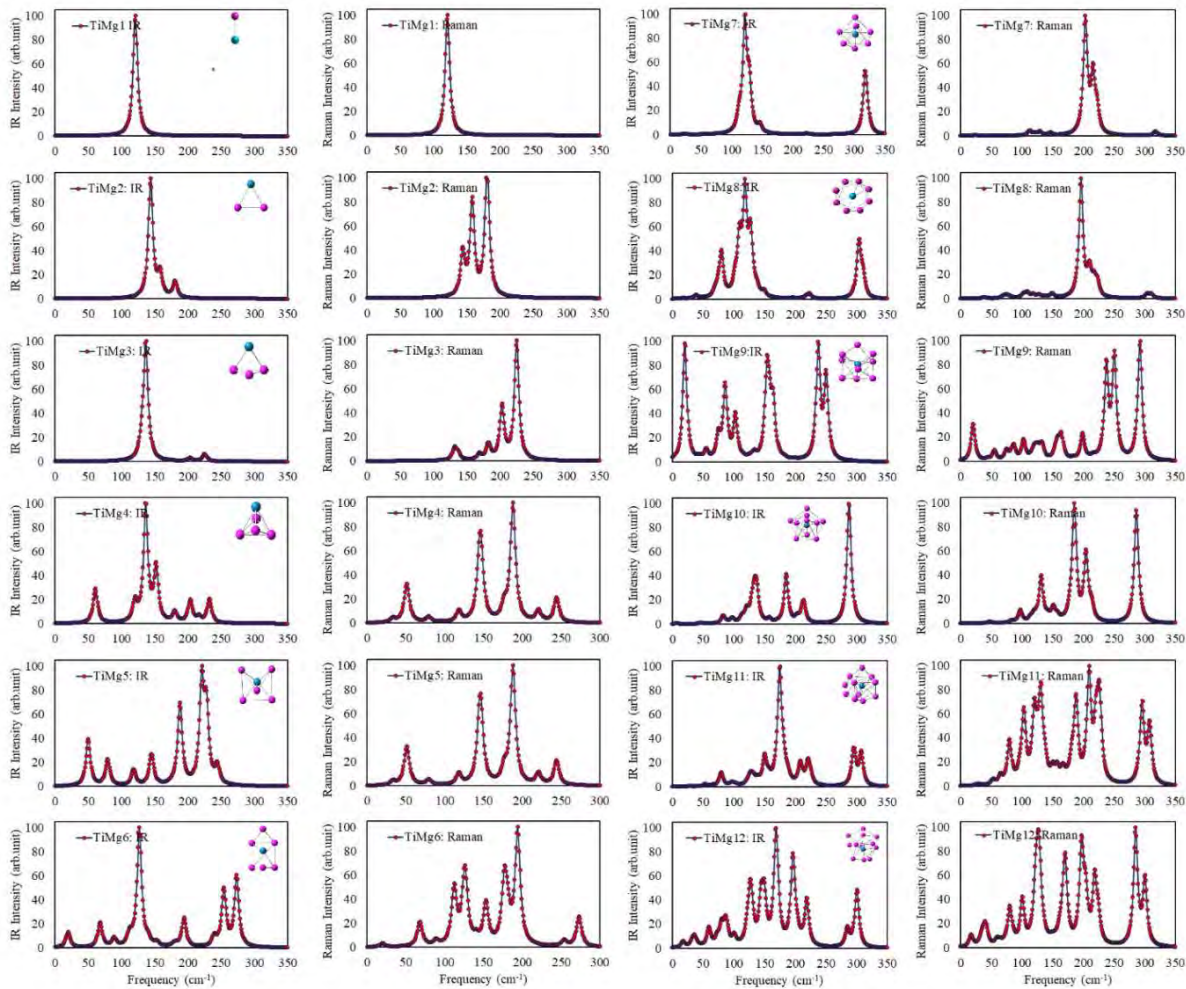
An aromatic cluster in nature shows enhanced stability. Although, positive or zero NICS magnitude indicates anti-aromaticity or non-aromaticity of that particular ring system. In the present computation, NICS of the ring-type atomic cluster ( $\text{TiMg}_8$ ) has been calculated under Kohn-Sham DFT using Gaussian' 09. B3LYP functional with 6-311G(d) basis set with effective core potential is used to calculate the NMR using the gauge-independent atomic orbital (GIAO) method for the  $\text{TiMg}_8$  ring cluster. The NICS graph (Fig. 4.14) shows the variation of NICS of the  $\text{TiMg}_8$  cluster with the distance from the central Ti atom. It is seen that NICS values near the surface or above the outer surface are relatively less than the NICS value inside the cage. It can be seen from the graph that, the minimum value of NICS is -93.17 ppm at a distance 0.7 Å above the Ti atom at the center of the cluster. The nature of the NICS of the  $\text{TiMg}_8$  cluster is pretty similar to the nature of the NICS of the benzene ring,  $\text{MoGe}_{12}$ ,  $\text{NbGe}_{12}$  clusters. [74, 75]. Which are very valuable confirmations of the aromaticity and higher stability of the  $\text{TiMg}_8$  cluster.

#### ***4.3.11 IR and Raman Spectra of the Doped Clusters***

The optical properties of the clusters are tested by calculating the vibrational (IR) and Raman spectra of the optimized geometries in order to predict the abundance of the nanoclusters experimentally and are presented in Fig. 4.15. As displayed in Fig. 4.15, the IR and Raman spectra of  $\text{TiMg}_n$  ( $n=1-10$ ) clusters are distributed in the frequency range (wave number) of  $0 \text{ cm}^{-1}$  to  $350 \text{ cm}^{-1}$ . In the study of MEP, each contour curves around each atom is MEP surface. Following the IR spectrum of  $\text{TiMg}_n$  cluster presented has many peaks. The dominating mode in IR and Raman are indicated by the bold letter in Table 4.7 in addition to all modes.

A Gaussian width  $4 \text{ cm}^{-1}$  is added to the frequencies to draw the IR and Raman spectrum. The absence of an imaginary frequency in the spectrum represents the real nature of the clusters with the absence of any geometry with a transition state. The low-frequency modes in the IR spectrum of the endohedrally doped Ti clusters ( $n=7-12$ ) are mainly due to the vibration of Mg atoms on the cage surface.

In such modes, hardly any movement of the Ti atoms occurs. On the other hand, at the dominating mode in IR, the displacement of the caged Ti atom is much higher compared to the caged Mg atoms. The vibrations of the Mg atoms in the cage are mainly of two types. In the low-frequency IR modes, the cage Mg atoms do not have any regularity in phase between them. In the most dominant mode in Raman, all the Mg atoms in the cage move in phase. This mode is known as breathing mode. The animations of such modes are presented in the SI. The intensity of the breathing mode in most of the cases is much higher than the other modes (but always highest) present in Raman spectrum. But the picture is different in the case of exohedral doping of Ti atom in Mg cluster ( $n=3-6$ ). In such clusters, the highest mode is the breathing mode where all the atoms in the clusters vibrate in the same phase. The low intensity in the spectrum of the vibrational modes of the doped atom indicates the weak binding between the doped atom and the cluster.



**Fig. 4.15** IR and Raman spectrum of different ground state isomer of  $TiMg_n$  ( $n=1-12$ ).

The high-frequency region indicates the higher bond energy between the elements. Comparing the intensity spectrum with the binding energy graph, it can be said that the increase in bond energies helps to increase the binding energy per atom in the clusters. Comparing the spectra of clusters of the same size with the frequency of the dope This indicates that the interaction between Mg and Ti increases in doped clusters due to the hybridization of Mg atoms in the clusters with the doped element of the clusters in the high-frequency region, the frequency is less in both the IR and Raman spectra.

**Table 4.7 Frequency (cm<sup>-1</sup>) of IR and Raman spectra of TiMg<sub>n</sub> (n=1-12). The bold frequency values are the dominating mode in IR and Raman respectively**

1	2	3	4	5	6	7	8	9	10	11	12
120.77	<b>143.84</b>	<b>131.42</b>	60.75	49.95	19.76	23.43	16.92	<b>20.34</b>	6.61	27.58	17.06
	<b>157.96</b>	<b>136.76</b>	102.84	51.52	68.13	24.56	38.68	43.95	46.14	50.81	32.39
	180.44	168.59	120.28	79.3	88.99	102.24	69.34	54.8	48.48	52.96	36.2
		182.36	<b>136.47</b>	118.22	112.21	111.91	75.04	74.86	55.64	64.94	40.83
		202.85	<b>151.94</b>	144.77	125.07	112.59	80.03	78.63	82.97	71.39	59.18
		224.85	180.12	176.59	<b>127.03</b>	112.78	101.71	85.99	94.97	79.63	64.93
			203.34	<b>187.9</b>	140.53	<b>121.33</b>	106.56	102.4	97	102.9	73.16
			216.44	<b>220.59</b>	153.04	<b>121.59</b>	109	114.44	113.25	116.5	80.32
			232.05	227.78	176.89	128.86	109.77	114.61	118.97	120.27	87.28
				244.02	181.19	145.14	<b>117.89</b>	119.87	121.09	125.27	100.39
					193.98	146.42	118.34	124.46	130.73	125.82	113.47
					239.22	203.06	<b>127.3</b>	126.25	133.48	127.94	122.12
					253.83	215.25	137.42	126.86	134.32	130.52	125.97
					<b>272.97</b>	215.45	149.05	130.99	137.26	136.48	129.54
						222.12	195.92	133.08	141.82	139.18	135.11
						316.61	203.39	153.73	150.94	150.19	144.08
						316.96	216.9	157.99	157.74	157.47	149.23
						319.58	222.61	164.15	173.41	166.39	153.87
							302.15	182.11	178.36	170.34	161.22
							304.1	198.62	<b>185.11</b>	<b>174.55</b>	164.96
							310.26	215.26	202.85	180.9	<b>168.12</b>
								<b>237.21</b>	204.14	187.86	170.58
								250.17	213.06	208	<b>195.27</b>
								291.99	213.11	208.93	197.31
									285.73	220.06	203.68
									287.16	224.59	217.12
									288.28	226.79	218.61
										<b>295.14</b>	224.27
										306.88	284.82
										308.8	299.36
											300.57

#### ***4.4 Summary and Conclusions***

Present study represents a systematic study of Ti doped Magnesium clusters for number of Magnesium atoms  $n=2-20$ .

The cluster containing more than seven Mg atoms can form a cage-type cluster, and these clusters are capable of absorbing the Ti atom endohedrally during the growth process. Always endohedrally Ti atom doped  $Mg_n$  cage clusters are more stable than exohedrally doped clusters due to hybridization between Ti -3d and Mg -3s and -3p orbitals. Also, due to the addition of the Ti atom with the  $Mg_n$  cluster, BE increases, and hence the addition of a Ti atom improves the thermodynamic stability of the cluster. From the variation of different thermodynamic parameters (BE, EE, FE,  $\Delta_2$ , etc.) and chemical parameters (VIP, VEA, etc.), it is found that  $TiMg_8$  is the most stable cluster under the present range of study. The electron localization function (ELF)-2D plot showing low index value of localized electron-pair confirming higher stability of the cluster. The NICS study shows negative values of NICS, confirming that the  $TiMg_8$  cluster is aromatic and of higher stability. Orbital analysis shows that the  $TiMg_8$  cluster has 20 valence electrons, and it follows the closed-shell configuration with a sequence  $1S^21P^61D^{10}2S^2$  which is in good agreement with the shell model. NBO analysis also supports the results obtained from thermodynamic and chemical properties. From the IR and Raman spectra analysis, it is found that in the low-frequency region, the contribution in the spectrum is primarily due to the vibration of the Mg atoms in the cage in a random phase. However, in the breathing mode in the Raman spectrum, the doped Ti atom is mostly static, and the Mg atoms in the cage oscillate in the same phase. Infrared intensities and Raman activities show distinct spectra for different optimized clusters. It also reflects the change in the nature of bonding with the size of the clusters. IR and Raman spectra do not show any imaginary frequency in the optimized geometries. The spectral analysis could help to understand the experimental abundance of different  $TiMg_n$  clusters and design more clusters of a bigger size. In the end, calculated CP's satisfied the Poincare-Hopf rule. According to ELF and CP configuration, it can be inferred that there is a lack of uniform electron-rich regions inside the cluster. Hence, it indicates the existence of localized electron clouds that helps to strengthen the bond strength to stabilize the  $TiMg_8$  cluster. The cluster fills octet as 2, 8, 8 with valancy

2 in 4s shell. It may be considered as an superatom [73-75] with 18 electron core and an electron gas of 4s electrons like  $4s^2$  group of elements of the periodic table.  $TiMg_8$  obeys 20 electron counting rule [67] it may be possible to form stable alkaline earth compound. This study thus indentifies a magnesium based superatom which can be used as building blocks of materials for tunable alkaline earth materials. Calcium is a s-block element with  $4s^2$  electronic configuration.  $TiMg_8$  is a diamagnetic cluster like s-block elements with lowest electron affinity and high stability. This superaton may mimic Calcium atom.

Again,  $TiMg_{18}$  is also a stable cluster having closed shell configuration  $1S^21P^61D^{10}2S^21F^{14}2P^6$  with 40 electrons. It also satisfies the essential characteristics of a stable cluster.  $TiMg_8$  having HOMO-LUMO gap 1.47 eV and  $TiMg_{18}$  with 1.14 eV and average bond length of Ti-Mg 2.7 Å and 2.87 Å may find applications as single junction PV cells.

On the other hand,  $TiMg_5$  having less second order change in energy but with higher rate of change of BE/atom, local peak in HOMO-LUMO gap, VIP, Chemical hardness, chemical potential, higher polarizability with lower VEA and a fall in electrostatic dipole moment, lower interatomic seperation may be suitable for hydrogen storage material.  $TiMg_7$  having high rate of change of BE/atom, lower bond length with dip in VIP, chemical hardness, high charge trasfer and peak in chemical potential, VEA and local dip in HOMO-LUMO becomes most reactive cluster with compact structure. However, further investigation is required to establish  $TiMg_5$  or  $TiMg_7$  as a high efficiency hydrogen storage material with low activation energy and at room temperature.

## References

- [1] V.A. Yartys, M.V. Lototsky, E. Akiba, R. Albert, V.E. Antonov, J. Ares Jr, M. Baricco, N. Bourgeois, C.E. Buckley, J.M.B. von Colbe, J.C. Crivello, F. Cuevas, R.V.R. Denys, M. Dornheim, M. Felderhoff, D.M. Grant, B.C. Hauback, T.D. Humphries, I. Jacob, T.R. Jensen, P.E. de Jongh, J.M. Joubert, M.A. Kuzovnikov, M. Latroche, M. Paskevicius, L. Pasquini, L. Popilevsky, V.M. Skripnyuk, E. Rabkin, M.V. Sofianos, A. Stuart, G. Walker, H. Wang, C.J. Webb, and M. Zhu, “Magnesium based materials for hydrogen based energy storage: Past, present and future”, *Int. J. Hydrogen Energy*, **44(15)**, (2019), 7809-7859. <https://doi.org/10.1016/j.ijhydene.2018.12.212>.
- [2] J.C. Crivello, B. Dam, R.V. Denys, M. Dornheim, D.M. Grant, J. Hout, T.R. Jensen, P.de Jongh, M. Latroche, C. Milanese, D. Milcius, G.S. Walker, C.J. Webb, C. Zlotos, and V.A. Yartys, “Review of magnesium hydride-based materials: development and optimization”, *Appl. Phys. A*, **122**, (2016), 97. <https://doi.org/10.1007/s00339-016-9602-0>
- [3] H. Haberland (Ed.), “Clusters of Atoms and Molecules: Theory, Experiment and Clusters of Atoms”, first ed., Springer-Verlag, Berlin, 1994.
- [4] E. Roduner, “Size matters: why nanomaterials are different”, *Chem. Soc. Rev.*, **35(7)**, (2006), 583–592. <https://doi.org/10.1039/B502142C>.
- [5] W. Kohn, and L.J. Sham, “Self-Consistent Equations Including Exchange and Correlation Effects”, *Phys. Rev.*, **140(4A)**, (1965), A1133–A1138. <https://doi.org/10.1103/PhysRev.140.A1133>
- [6] W.D. Knight, K. Clemenger, W.A. de Heer, W.A. Saunders, M.Y. Chou, and M.L. Cohen, “Electronic Shell Structure and Abundances of Sodium Clusters”, *Phys. Rev. Lett.*, **52(24)**, (1984), 2141-2143. <https://doi.org/10.1103/PhysRevLett.52.2141>
- [7] V. Kumar, and R. Car, “Structure growth and bonding nature of mg clusters”, *Phys. Rev. B*, **44(15)**, (1991), 8243–8255. <https://doi.org/10.1103/PhysRevB.44.8243>

- [8] O.C. Thomas, W. Zhen, S. Xu, and Jr K.H. Bowen, “Onset of metallic behavior in magnesium clusters”. *Phys. Rev. Lett.*, **89(21)**, (2002), 213403-213406. <https://doi.org/10.1103/PhysRevLett.89.213403>
- [9] J. Akola, K. Rytönen, and M. Manninen, “Metallic evolution of small magnesium clusters”, *Eur. Phys. J. D-Atomic, Molecular, Optical and Plasma Physics*, **16(1)**, (2001), 21-24. <https://doi.org/10.1007/s100530170051>
- [10] F. Reuse, S.N. Khanna, V. de Coulon, and J. Buttet, “Pseudopotential local-spin-density Studies of neutral and charged  $Mg_n$  ( $n \leq 7$ ) clusters”, *Phys. Rev. B*, **41(17)**, (1990), 11743-11759. <https://doi.org/10.1103/physrevb.41.11743>
- [11] A. Köhn, F. Weigend, and R. Ahlrichs, “Theoretical study on clusters of magnesium”, *Phys. Chem. Chem. Phys.*, **3(5)**, (2001), 711-719. <https://doi.org/10.1039/B007869G>
- [12] P. Delaly, P. Ballone, and J. Buttet, “Metallic bonding in magnesium microclusters”, *Phys. Rev. B*, **45(7)**, (1992), 3838–3841. <https://doi.org/10.1103/PHYSREVB.45.3838>
- [13] S.N. Belyaev, S.V. Panteleev, S.K. Ignatov, and A.G. Razuvaev, “Structural, electronic, thermodynamic and spectral properties of  $Mg_n$  ( $n=2-31$ ) clusters: A DFT Study”, *Comp. Th. Chem.*, **1079**, (2016), 34–46. <https://doi.org/10.1016/j.comptc.2016.01.011>
- [14] I.A. Lyalin, A. Solovyov, V. Solovyov, and W. Greiner, “Evolution of the electronic and ionic structure of Mg clusters with increase in cluster size”, *Phys. Rev. A*, **67(6)**, (2003), 063203. <https://doi.org/10.1103/PhysRevA.67.063203>.
- [15] J. Jellinek, and P.H. Acioli, “Magnesium clusters: structural and electronic properties and the size-induced nonmetal-to-metal transition”, *J. Phys. Chem. A*, **106(45)**, (2002), 10919-10925. <https://doi.org/10.1021/jp020887g>
- [16] P.H. Acioli, and J. Jellinek, “Electron binding energies of anionic magnesium clusters and the nonmetal-to-metal transition”, *Phys. Rev. Lett.*, **89(21)**, (2002), 213402. <https://doi.org/10.1103/PhysRevLett.89.213402>



- [17] C.C. Diaz-Torrejón, F.S. Magaña, and I.G. Kaplan, “Comparative theoretical study of the electron affinities of the alkaline-earth clusters:  $\text{Be}_n$ ,  $\text{Mg}_n$ , and  $\text{Ca}_n$  ( $n = 2, 3$ )”, *Int. J. Quantum Chem.*, **111(1)**, (2011), 103-110. <https://doi.org/10.1002/qua.22387>
- [18] S. Heidari, S. De, S.M. Ghazi, S. Goedecker, and D.G. Kanhere, “Growth and Structural Properties of  $\text{Mg}_n$  ( $N= 10\text{--}56$ ) Clusters: Density Functional Theory Study”, *J Phys. Chem. A*, **115(44)**, (2011), 12307-12314. <https://doi.org/10.1021/jp204442e>
- [19] T.P. Martin, T. Bergmann, H. Göhlich, and T. Lange, “Electronic shells and shells of atoms in metallic clusters”, *Chem. Phys. Lett.*, **19**, (1991), 25-29. <https://doi.org/10.1007/BF01448248>
- [20] E. Voloshina, and B. Paulus,” Correlation energies for small Mg-clusters in comparison to bulk magnesium”, *Mol. Phys.*, **105(19-22)**, (2007), 2849-2855. <https://doi.org/10.1080/00268970701704794>
- [21] D. Hartree, “The Wave Mechanics of an Atom with a Non-Coulomb Central Field. Part I. Theory and Methods”, *Mathematical Proc. Camb. Philo. Soc.*, **24(1)**, (1928), 89-110. <http://dx.doi.org/10.1017/S0305004100011919>
- [22] V. Fock, “Approximation method for the solution of the quantum mechanical multi-body problem”, *Z. Physik*, **61**, (1930), 126-148. <https://doi.org/10.1007/BF01340294>
- [23] C. Møller, and M.S. Plesset, “Note on an Approximation Treatment for Many-Electron Systems”, *Phys. Rev.*, **46(7)**, (1934), 618–622. <https://link.aps.org/doi/10.1103/PhysRev.46.618>
- [24] Th. Diedrich, T. Döppner, Th. Fennel, J. Tiggesbäumker, and K.H.M. Broer, “Shell structure of magnesium and other divalent metal clusters”, *Phys. Rev. A.*, **72(2)**, (2005), 023203-023214. <https://doi.org/10.1103/PhysRevA.72.023203>
- [25] Th. Diedrich, T. Döppner, J. Braune, J. Tiggesbaumker, and K.H.M. Broer, “Electron Delocalization in Magnesium Clusters Grown in Supercold Helium Droplets”, *Phys. Rev. Lett.*, **86(21)**, (2001), 4807-4810. <https://doi.org/10.1103/PhysRevLett.86.4807>

- [26] A. Kaufmann, A. Kornath, A. Zoermer, and R. Ludwig, “Small magnesium clusters: between van der Waals and valence bonds”, *Inorg. Chem*, **49(8)**, (2010), 3851–3856. <https://doi.org/10.1021/ic902485z>
- [27] D. Shen, C.P. Kong, R. Jia, P. Fu, and H.X. Zhang, “Investigation of Properties of  $Mg_n$  clusters and their hydrogen storage mechanism: a study based on DFT and a global minimum optimization method”, *The J. Phys. Chem. A*, **119(15)**, (2015), 3636–3643. <https://doi.org/10.1021/acs.jpca.5b01474>
- [28] S.A. Shevlin, and Z.X. Guo, “ $MgH_2$  Dehydrogenation thermodynamics: nanostructuring and transition metal doping”, *J Phys. Chem. C*, **117(21)**, (2013), 10883–10891. <https://doi.org/10.1021/jp3117648>.
- [29] P. Larsson, C.M. Araujo, J.A. Larsson, P. Jena, and R. Ahuja, “Role of catalysts in dehydrogenation of  $MgH_2$  nanoclusters”, *Proc. Nat. Acad. Sci.*, **105(24)**, (2008), 8227–8231. <https://doi.org/10.1073/pnas.0711743105>
- [30] F. Zhang, H. Zhang, W. Xin, P. Chen, Y. Hu, X. Zhang, and Y. Zhao, “Probing the structural evolution of electronic properties of divalent metal  $Be_3Mg_n$  clusters from small to medium size”, *Sci. Rep.*, **10(1)**, (2020), 6052(1–10). <https://doi.org/10.1038/s41598-020-63237-8>
- [31] S.G. Xi, Q.Y. Li, Y.F. Hu, Y.Q. Yuan, Y.R. Zhao, J.J. Yuan, M.C. Li, and Y.J. Yang, “Probing the structural and electronic properties of divalent metal  $Mg_n^{+1}$  and  $SrMg_n$  ( $n = 2–12$ ) clusters and their anions”, *Chin. Phys. B*, **31(1)**, (2021), 016106. <https://doi.org/10.1088/1674-1056/ac04aa>
- [32] X.F. Chen, Y. Zhang, K.T. Qi, B. Li, Z.H. Zhu, and Y. Sheng, “Density functional theory study on Ni-doped  $Mg_nNi$  ( $n = 1–7$ ) clusters”, *Chin. Phys. B*, **19(3)**, (2010), 033601. <https://dx.doi.org/10.1088/1674-1056/19/3/033601>
- [33] C.M. Li, D. Wu, T. Xiao, Y. Dan, Y. Li, and W. Chen, “Probing the effect of carbon doping on structures, properties, and stability of magnesium clusters”, *Theo. Chem. Acc.*, **140**, (2021), 111. <https://doi.org/10.1007/s00214-021-02810-4>

- [34] C. Li, Y. Cui, H. Tian, Q. Shao J. Zhang, B. Ren, and Y. Yuan, “Systematic investigation of geometric structures and electronic properties of lithium doped magnesium clusters”, *Comp. Mat. Sci.*, **200**, (2021), 110800. <https://doi.org/10.1016/j.commatsci.2021.110800>
- [35] Z. Li, Z. Zhao, Z. Zhou, H. Wang, and S. Li, “First-principles calculations on small  $Mg_nZn$  and  $Mg_{n-1}Zn_2$  clusters: structures, stability, electronic properties”, *Mat. Chem. Phys.* **199**, (2017), 585–590. <https://doi.org/10.1016/j.matchemphys.2017.07.049>
- [36] B.C. Zhu, P. Deng, J. Guo, Z. Lu, and J. Zhao, “A single palladium atom immerses in magnesium clusters:  $PdMg_n$  ( $n = 2-20$ ) clusters DFT study”, *New J. Phys.*, **23(10)**, (2021), 103002. <https://doi.org/10.1088/1367-2630/ac2853>
- [37] L. Zeng, M.K. Liang, X.F. Wei, J. Guo, W. Dai, and B.C. Zhu, “New potential stable structures of  $XMg_n$  ( $X = Ge, C, Sn; n = 2-12$ ) clusters:  $XMg_8$  with high stability”, *J. Phys. Cond. Matter*, **33**, (2021), 065302. <https://doi.org/10.1088/1361-648X/abc401>
- [38] A. Droghetti, N. Baadji, and S. Sanvito, “MgN: a possible material for spintronics applications”, *Phys. Rev. B.*, **80(23)**, (2009), 235310. <https://doi.org/10.1103/PhysRevB.80.235310>
- [39] B. Boruah, and B. Kalita, “Role of transition metal doping in determining the electronic structures and properties of small magnesium clusters: a DFT-based comparison of neutral and cationic states”, *J. Nanopart. Res.*, **22(12)**, (2020), 370–378. <https://doi.org/10.1007/s11051-020-05083-3>
- [40] T. Husain, T.A. Mark, B. Pathak, and R. Ahuja, “Improvement in the hydrogen desorption from  $MgH_2$  upon transition metals doping: a hybrid density functional calculation”, *AIP Adv.*, **3(10)**, (2013), 102117-1–102117-8. <https://doi.org/10.1063/1.4826521>
- [41] F. Kong, and Y. Hu, “Density functional study of small X doped  $Mg_n$  ( $X = Fe, Co, Ni, n = 1-9$ ) bimetallic clusters: equilibrium structures, stabilities, electronic and magnetic properties”, *J. Mol. Model.*, **20(3)**, (2014), 2087-1–2087-10. <https://doi.org/10.1007/s00894-014-2087-x>

- [42] O.P. Charkin, and A.P. Maltsev, "Density Functional Theory Modeling of Reactions of Addition of H<sub>2</sub> Molecules to Magnesium Clusters Mg<sub>17</sub>M Doped with Atoms M of Transition 3d Elements", *J. Phys. Chem. A.*, **125(11)**, (2021), 2308–2315. <https://doi.org/10.1021/acs.jpca.1c00211>
- [43] R. Trivedi, and D. Bandyopadhyay, "Hydrogen storage in small size Mg<sub>n</sub>Co clusters: A density functional study", *Int. J. Hydrogen Energy*, **40(37)**, (2015), 12727-12735. <https://doi.org/10.1016/j.ijhydene.2015.07.122>
- [44] R. Trivedi, and D. Bandyopadhyay, "Study of adsorption and dissociation pathway of H<sub>2</sub> molecule on Mg<sub>n</sub>Rh (n= 1–10) clusters: A first principle investigation", *Int. J. hydrogen energy*, **41(44)**, (2016), 20113-20121. <https://doi.org/10.1016/j.ijhydene.2016.09.007>.
- [45] X. Ma, S. Liu, and S. Huang, "Hydrogen adsorption on the TM doped (TM=Ti, Nb) Mg<sub>55</sub> nanoclusters: a DFT study", *Int. J. Hydrogen Energy*, **42(39)**, (2017), 24797-24810. <https://doi.org/10.1016/j.ijhydene.2017.08.086>.
- [46] T.J.D. Kumar, P. Tarakeshwar, and N. Balakrishnan, "Geometric & electronic structure of hydrogenated transition metal (Sc, Ti, Zr) Clusters", *Phys. Rev. B.*, **79(20)**, (2009), 205415. <https://link.aps.org/doi/10.1103/PhysRevB.79.205415>
- [47] J.L. Bobet, E. Akiba, Y. Nakamura, and B. Darriet, "Study of Mg-M (M = Co, Ni and Fe) mixture elaborated by reactive mechanical alloying-hydrogen sorption properties", *Int. J. Hydrogen Energy*, **25(10)**, (2000), 987-996. [https://doi.org/10.1016/S0360-3199\(00\)00002-1](https://doi.org/10.1016/S0360-3199(00)00002-1)
- [48] J.L. Bobet, C. Even, Y. Nakamura, E. Akiba, and B. Darriet, "Synthesis of magnesium and titanium hydride via reactive mechanical alloying: Influence of 3d-metal addition on MgH<sub>2</sub> synthesis", *J. Alloys and Compd.*, **298(1-2)**, (2000), 279-284. [https://doi.org/10.1016/S0925-8388\(99\)00628-3](https://doi.org/10.1016/S0925-8388(99)00628-3)
- [49] M.G. Shelyapina, and D. Fruchart, "Role of Transition elements in Stability of Magnesium Hydride: A review of theoretical studies", *Solid State Phenom.*, **170**, (2011), 227-231. <https://doi.org/10.4028/www.scientific.net/SSP.170.227>

- [50] G. Liang, J. Huot, S. Boily, A. Van Neste, and R. Schulz, "Catalytic effect of transition metals on hydrogen sorption in nanocrystalline ball milled MgH<sub>2</sub>-TM (TM= Ti, V, Mn, Fe and Ni) systems", *J. Alloys and Compd.*, **292(1-2)**, (1999), 247-252. [https://doi.org/10.1016/S0925-8388\(99\)00442-9](https://doi.org/10.1016/S0925-8388(99)00442-9)
- [51] A.B. Philips, B.S. Shivaram, and G.R. Mynenib, "Hydrogen absorption at room temperature in nanoscale titanium benzene complexes", *Int. J. Hydrogen Energy*, **57(2)**, 2012, 1546-1550. <https://doi.org/10.1016/j.ijhydene.2011.09.136>
- [52] H. Lee, M.C. Nguyen, and J. Ihm, "Titanium functional group complexes for high-capacity hydrogen storage materials", *Solid State Commun.*, **146(9-10)**, (2008), 431-434. <https://doi.org/10.1016/j.ssc.2008.03.018>
- [53] S. Banerjee, C.G.S. Pillai, and C. Majumder, "Adsorption and desorption of hydrogen in Mg nanoclusters: Combined effect of size and Ti doping", *Int. J Hydrogen Energy*, **35(6)**, (2010), 2344-2350. <https://doi.org/10.1016/j.ijhydene.2009.12.176>
- [54] M. Pozzo, and D. Alfe, "Hydrogen dissociation and diffusion on transition metal (Ti, Zr, V, Fe, Ru, Co, Rh, Ni, Pd, Cu, Ag) - Doped Mg (0001) surfaces", *Int. J. Hydrogen Energy*, **34(4)**, (2009), 1922-1930. <https://doi.org/10.1016/j.ijhydene.2008.11.109>
- [55] Y. Liu, L. Ren, Y. He, and H.P. Cheng, "Titanium decorated graphene for high-capacity hydrogen storage studied by density functional simulations", *J. Phys. Cond. mat.*, **22(44)**, (2010), 445301. <https://doi.org/10.1088/0953-8984/22/44/445301>
- [56] F. Zuliani, L. Bernasconi, and E.J. Bacrends, "Titanium as a potential addition for High-Capacity Hydrogen storage medium", *J. Nanotech.*, **2012**, (2012), 831872, 9p. <https://doi.org/10.1155/2012/831872>
- [57] W. Silva, T.N. Truong, and F. Mondragon, "Electronic characterization and reactivity of bimetallic clusters of the Ti(Mg<sub>n</sub>) type for hydrogen storage applications", *J. Alloys Compd.*, **509(34)**, (2011), 8501-8509. <https://doi.org/10.1016/j.jallcom.2011.06.022>
- [58] S. Yanagisawa, T. Tsuneda, and K. Hirao, "An Investigation of Density Functionals: The First-Row Transition Metal Dimer Calculations", *J. Chem. Phys.*, **112(2)**, (2000), 545-553. <https://doi.org/10.1063/1.480546>

- [59] D. Kyoji, T. Sato, E. Rönnebro, N. Kitamura, A. Ueda, M. Ito, S. Katsuyama, S. Hara, D. Noréus, and T. Sakai, “A new ternary magnesium–titanium hydride  $Mg_7TiH_n$  with hydrogen desorption properties better than both binary magnesium and titanium hydrides”, *J. Alloys Compd.*, **372(1-2)**, (2004), 213–217. <https://doi.org/10.1016/j.jallcom.2003.08.098>
- [60] M.J. Frisch, G.W. Trucks, H.B. Schlegel, G.E. Scuseria, M.A. Robb, J.R. Cheeseman, G. Scalmani, V. Barone, B. Mennucci, G.A. Petersson, H. Nakatsuji, M. Caricato, X. Li, H.P. Hratchian, A.F. Izmaylov, J. Bloino, G. Zheng, J.L. Sonnenberg, M. Hada, M. Ehara, K. Toyota, R. Fukuda, J. Hasegawa, M. Ishida, T. Nakajima, Y. Honda, O. Kitao, H. Nakai, T. Vreven, Jr J.A. Montgomery, J.E. Peralta, F. Ogliaro, M. Bearpark, J.J. Heyd, E. Brothers, K.N. Kudin, V.N. Staroverov, T. Keith, R. Kobayashi, J. Norm, K. Raghavachari, A. Rendell, J.C. Burant, S.S. Iyengar, J. Tomasi, M. Cossi, N. Rega, J.M. Millam, M. Klene, J.E. Knox, J.B. Cross, V. Bakken, C. Adamo, J. Jaramillo, R. Gomperts, R.E. Stratmann, O. Yazyev, A.J. Austin, R. Cammi, C. Pomelli, J.W. Ochterski, R.L. Martin, K. Morokuma, V.G. Zakrzewski, G.A. Voth, P. Salvador, J.J. Dannenberg, S. Dapprich, A.D. Daniels, O. Farkas, J.B. Foresman, J.V. Ortiz, J. Cioslowski, D.J. Fox (2013) Gaussian’09, Revision D.01, Gaussian, Inc., Wallingford C.
- [61] A.D. Becke, "Density-functional exchange-energy approximation with correct asymptotic behavior", *Phys. Rev. A*, **38(6)**, (1988), 3098–3100. <https://doi.org/10.1103/physreva.38.3098>
- [62] C. Lee, W. Yang, and R.G. Parr, “Development of the Colle-Salvetti correlation energy formula into a functional of the electron density”, *Phys. Rev. B.*, **37(2)**, (1998), 785-789. <https://doi.org/10.1103/PhysRevB.37.785>.
- [63] Computational Chemistry Comparison, and Benchmark Data Base Std. Release 22, Ref database 101; National Institute of Standards and Technology (NIST) USA (2020). <https://cccbdb.nist.gov>.

- [64] T. Koopmans, "About the assignment of wave functions and eigenvalues to the individual electrons of an atom", *Physica*, **1(1-6)**, (1934), 104-113. [https://doi.org/10.1016/S0031-8914\(34\)90011-2](https://doi.org/10.1016/S0031-8914(34)90011-2)
- [65] J.S. Muray, and P. Politzer, "The Electrostatic Potential: an overview", *Comp. Mol. Sci.* **1(2)**, (2011), 153-163. <https://doi.org/10.1002/wcms.19>
- [66] R.S. Mulliken, "Electronic Population Analysis on LCAO-MO Molecular Wave Functions", *J. Chem. Phys.*, **23**, (1955), 1833-1840. <https://doi.org/10.1063/1.1740588>
- [67] J. Lasse A. Per-Olof, A. Osted, J. Kongsted, and K.V. Mikkelsen, "Polarizability of molecular clusters as calculated by a dipole interaction model", *J. Chem. Phys.* **116(10)**, (2002), 4001-4010. <http://doi.org/10.1063/1.1433747>
- [68] A.L. Hickey, and C.N. Rowley, "Benchmarking Quantum Chemical Methods for the Calculation of Molecular Dipole Moments and Polarizabilities", *J. Phys. Chem. A*, **118(20)**, (2014), 3678–3687. <https://doi.org/10.1021/jp502475e>
- [69] F. Weinhold, C.R. Landis, and E.D. Glendening, "What is NBO analysis and how is it useful?", *Int. Rev. Phys. Chem.*, **35(3)**, (2016), 399-440. <https://doi.org/10.1080/0144235X.2016.1192262>
- [70] A. D. Becke and K. E. Edgecombe, A simple measure of electron localization in atomic and molecular systems, *J. Chem. Phys.* **92(9)**, (1990). 5397–5403. <http://doi.org/10.1063/1.458517>
- [71] M. Palusiak, and T.M. Krygowski, "Application of AIM Parameters at Ring Critical Points for estimation of  $\pi$ -Electron localization in six-membered Aromatic and quasi aromatic Rings", *Chem. Euro. J.* **13(28)**, (2007), 7996-8006. <https://doi.org/10.1002/chem.200700250>
- [72] A. Kumar, S.R. Gadre, X. Chenxia, T. Xu, and S.R. Krik, "Hybrid QTAIM and electrostatic potential-based quantum topology phase diagrams for water clusters", *Phys. Chem. Chem. Phys.*, **17**, (2015), 15258-15273. <http://dx.doi.org/10.1039/C5CP01039J>

- [73] P.V.R. Schleyer, C. Maerker, A. Dransfeld, H. Jiao, and N.J.R. van Eikema Hommes, “Nucleus-independent chemical shifts: a simple and efficient aromaticity probe”, *J. Am. Chem. Soc.*, **118(26)**, (1996), 6317-6318. <https://doi.org/10.1021/ja960582d>
- [74] R. Trivedi, and D. Bandyopadhyay, “Insights of the role of shell closing model and NICS in the stability of NbGe<sub>n</sub> (n = 7–18) clusters: a first-principles investigation”, *J. Mat. Sci.* **54**, (2019), 515-528. <https://doi.org/10.1007/s10853-018-2858-3>
- [75] D. Bandyopadhyay, P. Kaur, and P. Sen, “New insights into applicability of electron-counting rules in transition metal encapsulating Ge cage clusters”, *J. Phys. Chem. Soc. A*, **114(50)**, (2010), 12986-12991. <https://doi.org/10.1021/jp106354d>



## **CHAPTER-5**

---

### **CATALYTIC EFFECT OF Ti DOPING ON HYDROGENATION OF Mg<sub>n</sub> (n=2-8) NANOCCLUSERS: A DENSITY FUNCTIONAL STUDY**

#### ***5.1 Introduction***

To cope with the growing energy need of modern civilization and to address the problems of depleting fossil fuel, climate change owing to pollution, and temperature change due to the rise of CO<sub>2</sub> in the environment, the crying need of the day is to develop clean nontoxic, renewable, low cost and pollution-free energy sources. Throughout the past few decades, quite sizeable research has been conducted to develop a sustainable non-conventional energy source. Still, it could not meet the standards to replace fossil fuels. Only up-to-date 29% replacement has been done globally [1-7].

Hydrogen is the most abundant element in the universe; it can be estimated that about 90% of the visible universe contains hydrogen. But a tiny fraction of hydrogen is available in Earth's atmosphere. It contains a higher energy density per unit mass of ~120 MJ/kg. In contrast, Diesel/ Gasoline has an energy density of ~45.5 MJ/kg, reacts non-toxically, and produces only water as a by-product. In this sense, it is recyclable. In terms of power, it contains ~39kWh/kg. Hydrogen is not a fuel source but an energy carrier [3]. To develop a practically useable hydrogen fuel cell, at first, hydrogen must be produced from water, bio-sources, or fossil fuels for storage. Secondly, a proper hydrogen storage material is required to store hydrogen. It is not only a challenge, but the challenges that one has to face to make hydrogen fuel cell-driven vehicles include production, storage, transportation, and distribution. Considering these facts, the European Commission placed hydrogen as a potential material for energy sources for use in mobile and transport applications. The International Energy Agency (IEA) decided to lead the global policy on hydrogen [7]. Storing hydrogen in liquid or gas form is highly efficient, but it requires high pressure ~700 bar and low temperature (~20K), which enhances cost [5]. In the past decade, very efficient hydrogen storage materials have been proposed, including metal hydrides, amides, composite materials, metal-organic

frameworks, porous hydrates, etc. Hydrogen can bond with almost every material except some inert gases. Hydrogen can be stored in atomic or molecular form and extracted by thermal or electrochemical processes. The Mechanism of solid-state hydrogen storage systems consists of two steps:

- (a) Hydrogenation: It includes (i) adsorption of hydrogen atoms on the surface of the metal by weak Van der Waals interaction (Physisorption), (ii) dissociation of hydrogen molecule into atomic hydrogen, (iii) diffusion of the atomic hydrogen to the atoms of the cluster material (iv) chemical interaction of the hydrogen atom and the solid material by strong bonding (Chemisorption) (v) formation of metal hydride interface.
- (b) Dehydrogenation: The process includes (i) the release of hydrogen by metal hydride, (ii) diffusion of hydrogen atoms to the metal interface, (iii) recombination of hydrogen atoms to hydrogen molecules, and the release of hydrogen molecules.

During hydrogen intake by metal atoms, heat is evolved. As a result, the operating temperature enhances, reducing hydrogen intake and adsorption rate. Again, oxide or hydroxide formation on the metal surface reduces the diffusion rate during hydrogenation [8]. Since the hydrogen atoms are chemically bonded with Mg atoms, it requires higher detachment energy. So, releasing hydrogen atoms to form hydride requires heat (endothermic for Mg metal). The process becomes thermodynamically viable by considering hydrogenation (exothermic) and dehydrogenation (endothermic). During these processes and these steps, the step with a higher energy barrier is the rate-limiting step. Physisorption is a fast process and is not a rate-limiting step. The main rate-limiting steps are the diffusion steps in both adsorption and desorption. The dissociation of hydrogen from hydrides requires higher energy and may be considered a rate-limiting step. High pressure and high temperature increase the kinetics in the steps. Thus, during this process, some potential barrier exists that stop or decreases the speed or rate of the process of hydrogen migration in the cluster which can be realized as the hydrogen spillover effect.

In atomic chemisorption processes, the binding energy is  $>1.2$  eV/H<sub>2</sub>. In the molecular chemisorption processes, the binding energy lies between 0.3 eV/H<sub>2</sub> to 0.7 eV/H<sub>2</sub>, whereas in

the physisorption process, the binding energy is less than 0.3 eV/H<sub>2</sub>. In CH<sub>4</sub> (Covalent or ionic bond), the binding energy is higher ~4.5 eV/H<sub>2</sub>, whereas, in carbon and BN nanostructures, the binding energy becomes less than 0.2 eV/H<sub>2</sub>. A minimal quantity of hydrogen can be stored [9]. Porous materials have open pores, which make hydrogen kinetics faster, and they are highly reversible. Still, it has the disadvantage that their hydrogen uptake requires high pressure (~20 bar) proportional to the surface area, leading to low material density [10]. In carbon nanotubes and other carbon-related nanostructures, the binding energy is <0.2 eV/H<sub>2</sub>; in the structures, a minimal amount of hydrogen storage can be achieved [11]. Complex hydrides show enhanced hydrogen uptake with higher hydrogen kinetics, but the only difficulty lies in higher desorption temperatures (300-1000 K) [12-19]. However, attempts have been made to reduce desorption temperature below 100 K [20], but after three cycles, the gravimetric density falls from 6 wt.%/H to 3.2 wt.%/H. Studies on the hydrogenation properties of Mg-based systems have been reported in the past [21-30]. Magnesium hydrides (MgH<sub>2</sub>) have high thermodynamic stability and hydrogen storage capacity. It has also been reported that higher stability imposes constraints in practical applications as it requires high desorption temperature~350°C at normal atmospheric pressure. Lower rate of adsorption and desorption results in slow diffusion through hydrides which ultimately reduces hydrogen kinetics. High surface-to-volume ratio and high enthalpy of formation are the main barriers to industrial use [31, 32]. The low rate of adsorption and desorption of hydrogen may be due to other reasons, viz., surface oxidation of the magnesium-based system may be one of them. If it happens, the activation process can remove the oxide layer. The activation process can be performed under the hydrogen atmosphere. Even after activating and removing such an oxide layer, Mg-H<sub>2</sub> can be formed completely after several hours at around 350-400°C [33]. Adding a small impurity into the pure Mg cluster may dramatically improve the hydrogen kinetics. Especially, transition metal d-block elements show higher catalytic effects (TiMg>NiMg>VMg>CoMg>MoMg) [8]. The d-block elements exhibit vacant d-orbital, and so they can hold variable vacancies. These vacancies are very helpful in storing hydrogen in these vacancies. This stored hydrogen can be released when needed at an applied particular temperature and pressure. Generally, d-block TM elements form a complex compound that finds applications related to energy storage, transportation, PV cells, and energy harvesting. Doping can be made in two ways, a) Exohedral and b) Endohedral to the cluster. Doping a

pure  $Mg_n$  cluster by TM atoms can reduce the ignition temperature for hydrogen dissociation [32]. An extensive review of endohedrally doped clusters is presented by Zhao et al. [34]. Hussain et al. [35] reported TM (Sc, V, Fe, Co, Ni, Cu, Y, Zn, Nb) doping on  $Mg_5H_2$ . Fe, Co, Ni, doped  $Mg_n$  ( $n=1-9$ ) clusters have been studied by Kong et al. [36], and reported that  $Mg_4$  doped with (Fe, Co, Ni) is the highest stable cluster.  $Mg_{17}$  doped with Ti and Ni is reported by Charkin et al. [37]. Studies on Co-doped  $Mg_n$  ( $n=1-10$ ) have been reported by Trivedi et al. [38], and reported  $Mg_5Co$  as best suitable for hydrogen storages. Again, Rh-doped  $Mg_n$  ( $n=1-10$ ) has been reported by Trivedi et al. [39], and  $Mg_9Rh$  is the best suitable material for hydrogen storage. Bandyopadhyay et al. [40] reported hydrogenation properties of  $TiMg_n$  ( $n=2-12$ ) clusters and reported  $TiMg_5$  is the best cluster for hydrogen storage. Chatterjee and Bandyopadhyay [41] studied the catalytic behavior of Ti on  $Mg_n$  ( $n= 1-12$ ) clusters and reported that  $TiMg_8$  is the most stable structure in the series of  $Mg_n$ . Ma et al. 2017 report the study of Ti and Nb-doped  $Mg_{55}$  clusters [42]. Kumar and Tarakeshwar [43] compared the variation of chemisorption energy with the number of hydrogen adsorption in  $M_{13}H_{2n}$  ( $M=Sc, Ti, Zr$ ) transition metal clusters. Yanagisawa et al. [44] reported an investigation on the first row of transition metal dimmers using different Gaussian basis functions, and they have studied the performance of several DFT approaches, including Becke-3 Lee-Yang-Parr correlation functional, OP correlation (BOP), Perdew-Wang exchange-correlation, etc. Zeng et al. studied Ge, Sn, and C doped  $Mg_n$  ( $n=2-12$ ) [45] and found  $XMg_8$  ( $X= Ge, Sn, C$ ) is the most stable one. A study on  $MgH_2$ -TM (TM= Ti, V, Mn, Fe, Ni) has been experimentally studied by Liang et al. [46] and reported that  $MgH_2$ -Ti shows the best desorption kinetics over V, Mn, Fe, Ni-doped clusters. Liang et al. [46] first reported the catalytic effect of 3d transition metal doping (like Fe, Co, and Ni). The time taken to reach maximum desorption rate reduces by almost 50%, and ball-milled  $TiMg_n$  exhibits the most rapid adsorption and desorption rate overall first row of transition metal elements. The first row of transition metals (Ti, V, and Cr) is an exceptionally suitable material for hydrogen storage as they possess high gravimetric density and produce an fcc structure of hydrides [47-56]. Silva et al. [57] reported electronic characteristics and reactivity of Ti-doped  $Mg_n$  ( $n=1-6$ ) using MP2 (Moller-Plesset second order) optimization using a 6-311G (d) basis set. Wang et al. [58] report the catalytic effect of Ti in  $MgH_2$  hydrogenation studies, Kyoji et al. [59] experimentally studied  $Mg_nTi$  hydrides and reported  $Mg_7TiH_n$  as the most stable cluster and reported  $Mg_7Ti$  is the most suitable

material for hydrogen storage. A thorough study on hydrogen storage with pure and Ti-doped Mg clusters has not been reported.

This chapter contains a comprehensive study of pure  $Mg_n$ , Ti-doped  $Mg_n$  ( $n=2-8$ ) clusters, and their hydrogen adsorption/desorption properties using the global minimum method. The reason behind choosing  $n=2-8$  lies in the fact that the ground states of the higher clusters ( $n>7$ ) are endohedral doped clusters, as the endohedrally doped clusters are comparatively more stable than the exohedral clusters with low reactivity to that of exohedral clusters. Thus, for hydrogen storage, exohedral clusters are more suitable than endohedral clusters. Due to higher reactivity, hydrogen storage at reactive sites can take place.

In this chapter, the chemical and thermodynamic stabilities viz. average binding energy per atom (BE), relative stability, Vertical Ionization Potential (VIP), Vertical Electron Affinity (VEA), chemical hardness ( $\eta$ ), and chemical potential ( $\mu$ ) are studied. To have an idea about the localization of electrons around the reactive atoms 2D plot of the Electron Localization Function (ELF) of selected clusters is presented. Adsorption energy ( $E_{ad}$ ), Chemisorption energy (CE) for hydrogenated clusters are presented. Transition states (TS) and Intrinsic Reaction Coordinates (IRC) for the most promising clusters are given for confirmation. An attempt to estimate the catalytic effect of Ti doping on the  $TiMg_5$  cluster by adding extra hydrogen to the doped cluster and evaluating the number of extra hydrogen it can accommodate is presented. The enhancement of the gravimetric density also has been studied to have a clear understanding of the catalytic behavior of doped Ti atom in the  $Mg_n$  clusters.

## ***5.2 Computational Methodology***

To investigate the thermodynamic and electronic properties of the clusters during the growth process and hydrogenations, we did all calculations using the Gaussian'09 program package [60]. The present computational work performed the electronic structure calculations using density functional theory (DFT). We used Becke three-parameter hybrid functional with Lee, Yang, and Parr generalized Gradient approximation (GGA), famously known as B3LYP functional [61, 62]. Several initial guess geometries are chosen for each size. The redundant internal coordinates of the guess clusters are relaxed from each initial structure to achieve the

optimized energy state. The convergence criterion of the optimization is set as very tight. The convergence threshold in SCF is set as  $10^{-9}$  on RMS change in density matrix and  $10^{-7}$  on maximum change in density matrix as implemented in the Gaussian' 09 program package. During the optimization of pure, doped, and hydrogenated clusters, an all-electron basis set 6-311G (d, p) basis set has been used from the inbuilt Gaussian'09 program package. The relaxed structures were found to have zero imaginary frequency in all cases. So total bonding energies and geometries for each stable cluster and its stable isomers correspond to local minima. Further, natural bond orbitals (NBO) have been studied. The open-source Multiwfn program [63] is used to study the electron localization function on the surface of  $Mg_5$ ,  $Mg_5-2H$ ,  $TiMg_5$ , and  $TiMg_5-2H$  clusters. Finally, the most suitable clusters' intrinsic reaction coordinate (IRC) has been studied.

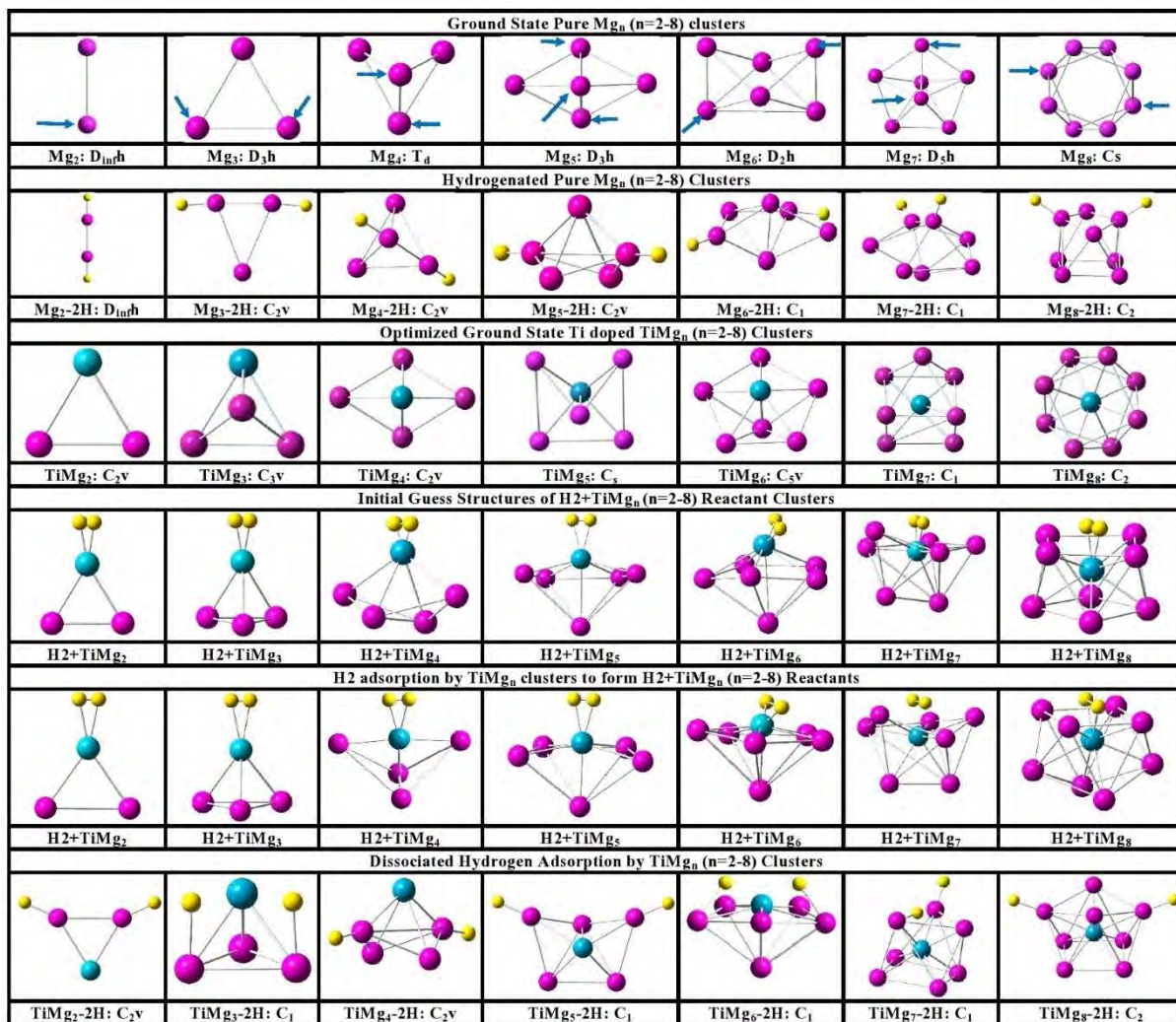
## ***5.3 Results and Discussion***

### ***5.3.1 The Structures***

#### ***5.3.1.1 Growth of Pure $Mg_n$ Clusters***

As a first step of the computation, several pure and doped  $Mg_n$  clusters ( $n=2-8$ ) and their isomers are modeled based on our previously reported systems [38-41] and optimized following the methodology explained in the previous section under no symmetry consideration. Only global ground state clusters in each size are considered for characterization among all optimized clusters. The growth of clusters is studied starting from Mg-Mg and Ti-Mg dimers.

In the present section, our primary focus is the hydrogenated  $Mg_n$  and  $TiMg_n$  ( $n=2-8$ ) clusters. The reactive sites of different clusters are shown in Fig. 5.1. At first, hydrogen molecules are released near the reactive sites of the clusters and optimized. After optimizing all the clusters and isomers, the global ground state clusters are selected for each size. Here the global ground state is not only in respect of spin-states but considering both exohedral and endohedral doping energies.



**Fig. 5.1** Optimized global minimum structures of pure, doped, Mg<sub>n</sub>-2H (n=2-8) and TiMg<sub>n</sub>-2H (n=2-8) clusters.

The pictorial growth process of doped and doped hydrogenated clusters is given in Fig. 5.2 and 5.3. The optimized pure Mg<sub>n</sub> (n=2-8) doubly hydrogenated pure clusters Mg<sub>n</sub>-2H, Ti-doped Mg<sub>n</sub> clusters i.e., TiMg<sub>n</sub>, and hydrogenated TiMg<sub>n</sub> i.e., TiMg<sub>n</sub>-2H clusters (n=2-8) with their point group symmetries are displayed in Fig. 5.1 The blue-colored arrowhead in the first row of pure clusters shows the reactive sites of pure clusters. The bond length and growth of clusters are studied starting from the pure (Mg-Mg and Ti-Ti) and hybrid dimer (Ti-Mg). Mg-Mg dimer has a bond length of 3.927Å which is in good agreement with the experimental result of Diedrich et al. [64, 65] and also in agreement with the Computational Chemistry Benchmark Database, a standard reference database [66]. Adding an Mg atom with the Mg-Mg dimer forms an equilateral triangle of the Mg<sub>3</sub> cluster with point group symmetry D<sub>3h</sub> and

bond length 3.47Å. The ground state configurations of Mg<sub>4</sub>, Mg<sub>5</sub>, and Mg<sub>6</sub> are mostly tetrahedron-based clusters. The ground state Mg<sub>4</sub> has T<sub>d</sub> point group symmetry, whereas Mg<sub>5</sub> possesses D<sub>3h</sub> point group symmetry. After the capping of Mg<sub>5</sub>, the ground state of n=6 size with D<sub>2h</sub> point group symmetry has formed. The lowest energy state configuration of Mg<sub>7</sub> is a pentagonal-bipyramid-based cluster with D<sub>5h</sub> point group symmetry. The ground state geometry of Mg<sub>8</sub> cluster has C<sub>s</sub> point group symmetry.

### **5.3.1.2 Growth of Mg<sub>n</sub>-2H (n=2-8)**

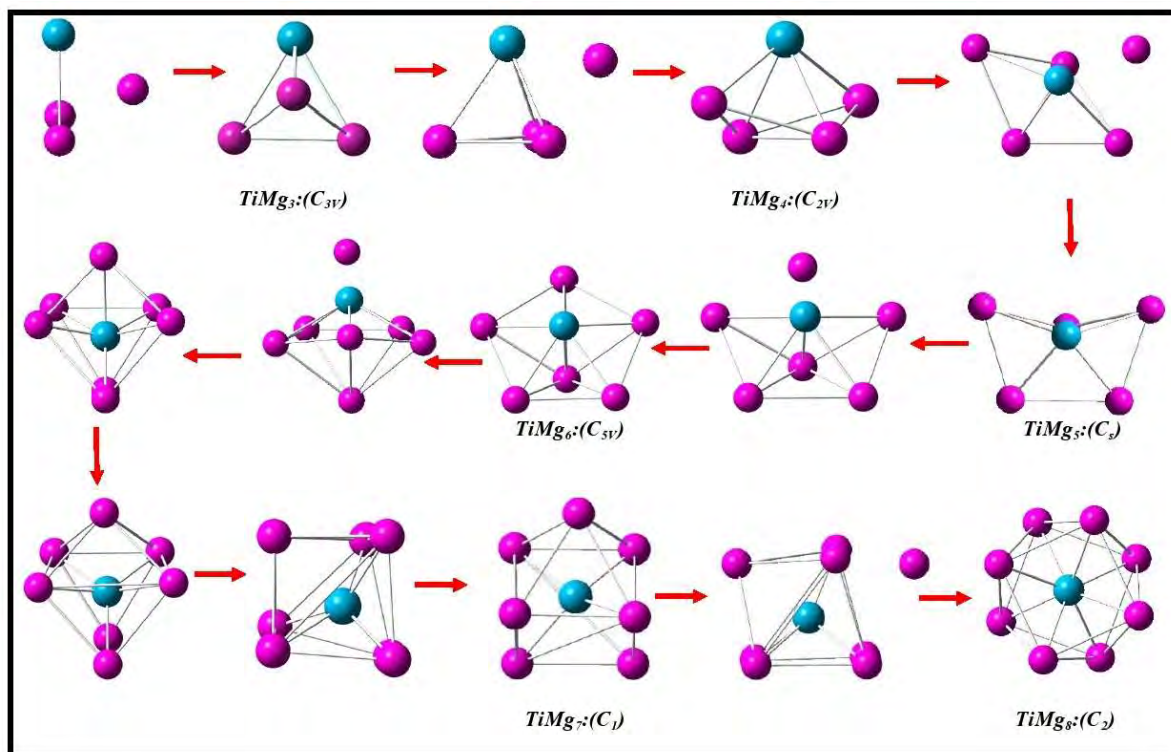
In this section, the growth of Mg<sub>n</sub>-2H clusters is discussed. The Mg<sub>1</sub>-2H cluster holds D<sub>∞h</sub> point group symmetry. The next member in the series is the Mg<sub>2</sub>-2H cluster which holds D<sub>∞h</sub> point group symmetry. The ground state of the Mg<sub>3</sub>-2H cluster is in a singlet state, and it holds C<sub>2v</sub> point group symmetry. This can be achieved by hydrogenating the pure ground state Mg<sub>3</sub> cluster. The ground state of Mg<sub>4</sub>-2H cluster also possesses C<sub>2v</sub> point group symmetry with a singlet state and can be obtained by hydrogenating the ground state pure Mg<sub>4</sub> cluster. The ground state of the Mg<sub>5</sub>-2H cluster has C<sub>2v</sub> point group symmetry, and the ground state of the Mg<sub>6</sub>-2H cluster also holds C<sub>1</sub> point group symmetry, both of which are singlet states. All the clusters can be obtained by adding hydrogen to the ground state of the particular pure Mg<sub>n</sub> clusters.

Similarly, Mg<sub>5</sub>-2H and Mg<sub>6</sub>-2H clusters are also achieved by doing the same. The next member, n=7, means the Mg<sub>7</sub>-2H cluster, which holds C<sub>s</sub> point group symmetry with a singlet state. The ground state of the Mg<sub>8</sub>-2H cluster possesses C<sub>2</sub> point group symmetry.

### **5.3.1.3 Growth Pattern of TiMg<sub>n</sub> (n=2-8) Clusters**

The growth pattern of all Ti-doped Mg<sub>n</sub> clusters is discussed thoroughly in the section. TiMg<sub>1</sub> has C<sub>∞v</sub> point group symmetry. The next cluster is TiMg<sub>2</sub> which can be formed by giving an upper cap of Ti atom with Mg<sub>2</sub> dimer, and it forms equilateral symmetry having C<sub>2v</sub> point group symmetry, and its ground state is a triplet state. The ground state configuration of TiMg<sub>3</sub> holds C<sub>3v</sub> point group symmetry where the Ti atom is added perpendicularly to the Mg<sub>3</sub> cluster. The minimum global state of the cluster is a triplet.





**Fig. 5.2 Pictorial view of the growth pattern of TiMg<sub>n</sub> (n=2-8) clusters.**

The next member is TiMg<sub>4</sub>, which can be achieved by giving a side cap of Mg atom to the TiMg<sub>3</sub> cluster forming a tetrahedron-based cluster, which holds C<sub>2v</sub> point group symmetry. Its ground state is also a triplet state. The lowest state of the TiMg<sub>5</sub> is also a triplet state. The most stable geometry of TiMg<sub>5</sub> holds C<sub>s</sub> point group symmetry. It can be obtained by giving a lower cap of Mg on the TiMg<sub>4</sub> cluster. The global ground state configuration of the TiMg<sub>6</sub> cluster is a triplet state which holds C<sub>5v</sub> point group symmetry and can be achieved with a diagonal capping of the Mg atom to the TiMg<sub>5</sub> cluster. The next cluster is the TiMg<sub>7</sub> cluster. It holds C<sub>1</sub> point group symmetry and is an endohedrally doped cluster, which means the Ti atom has been injected into the center of the cage-type cluster. The ground state of the TiMg<sub>8</sub> cluster is with C<sub>2</sub> point group symmetry, which has a ring-type construction in which the Ti atom has been doped at the cluster's center. Its ground state cluster is a singlet state. The other endohedrally and exohedrally doped structures are with C<sub>1</sub> point group symmetry with 0.01 eV and 1.35 eV higher energy, respectively, as the growth pattern of all exohedrally and endohedrally doped clusters of TiMg<sub>n</sub> (n=2-20) have been discussed in the last chapter (Chapter 4). In this chapter, the focus is on the hydrogenation of the clusters. For

hydrogenation, the smaller clusters are more important than the higher clusters. The pictorial view of the growth of  $\text{TiMg}_n$  clusters is shown in Fig. 5.2.

#### 5.3.1.4 Growth Pattern of Hydrogenated $\text{TiMg}_n$ ( $n=2-8$ ) Clusters

This section, the formation and structural properties of  $\text{TiMg}_n\text{-2H}$  clusters are discussed. Here, Fig. 5.3 shows the pictorial view of the hydrogenated  $\text{TiMg}_n$  ( $n=2-8$ ) growth pattern, i.e.,  $\text{TiMg}_n\text{-2H}$  clusters. The  $\text{TiMg}_1\text{-2H}$  holds a triplet state, and its point group symmetry is  $C_{2v}$ .

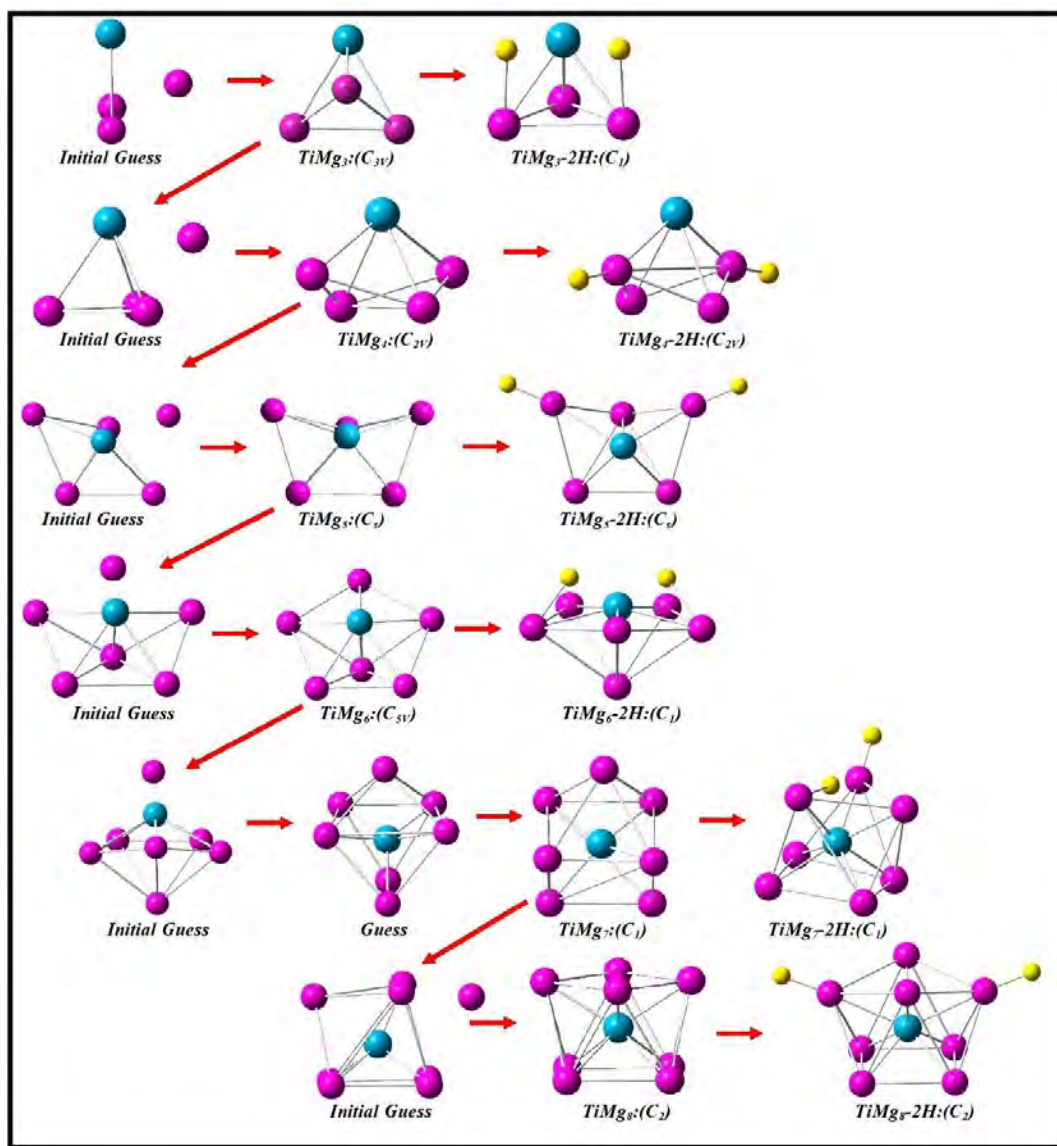


Fig. 5.3 Pictorial view of the growth pattern of hydrogenated  $\text{TiMg}_n$  ( $n=2-8$ ) clusters.

The next one is the TiMg<sub>2</sub>-2H cluster with C<sub>2v</sub> point group symmetry and a triplet state as its global ground state. After adding 2H molecules to the reactive sites of the TiMg<sub>3</sub> cluster, it got C<sub>1</sub> point group symmetry with a triplet state. The hydrogenated TiMg<sub>4</sub> cluster has C<sub>2v</sub> point group symmetry, and its ground state is a triplet. The next member in our cluster series is the TiMg<sub>5</sub> cluster with C<sub>s</sub> point group symmetry. After the hydrogenation, it retains C<sub>s</sub> point group symmetry. The global ground state of TiMg<sub>6</sub>-2H holds C<sub>1</sub> point group symmetry, and its ground state is also a triplet state. The lowest energy state of TiMg<sub>7</sub>-2H is its singlet state, and it retains C<sub>1</sub> point group symmetry. The next hydrogenated cluster TiMg<sub>8</sub>-2H also retains C<sub>2</sub> point group symmetry; its ground state is a singlet state. The steps of formation of the stable clusters and the hydrogenated stable structures for n=2-8 are presented in Fig. 5.3.

### 5.3.2 Thermodynamic and Electronic Properties of Mg<sub>n</sub>-2H and TiMg<sub>n</sub>-2H (n=2-8) Nanoclusters.

After optimization, different energetic parameters, such as binding energies (BE), stability (Δ<sub>2</sub>), vertical ionization potential (VIP), vertical electron affinity (VEA), etc., of the clusters are calculated. The variation of average binding energy per atom with cluster size with the cluster's growth is shown in Fig. 5.2. The binding energy of clusters can be defined as the average energy gain per unit atom during the growth of the clusters. The higher the rate of change in binding energy (atom to atom) higher is the stability. Similarly, if any clusters show local maxima in the BE graph, the cluster shows enhanced stability. The higher the binding energy higher is the stability. The average binding energy per atom of different clusters is defined [39-42] as,

$$BE_{Mg_n} (eV) = (nE_{Mg} - E_{Mg_n}) / n \quad (5.1)$$

$$BE_{TiMg_n} (eV) = (E_{Ti}^M + nE_{Mg}^M - E_{TiMg_n}^M) / (n + 1) \quad (5.2)$$

$$BE_{Mg_n-2H} (eV) = (nE_{Mg} + 2H - E_{Mg_n-2H}) / (n + 2) \quad (5.3)$$

$$BE_{TiMg_n-2H} (eV) = (E_{Ti}^M + nE_{Mg}^M + 2H - E_{TiMg_n-2H}^M) / (n + 3) \quad (5.4)$$

Variations of BE with the cluster size are shown in Fig. 5.4. In Fig. 5.4(a), the average BE per atom of pure (Mg<sub>n</sub>) and pure hydrogenated (Mg<sub>n</sub>-2H) clusters are presented.

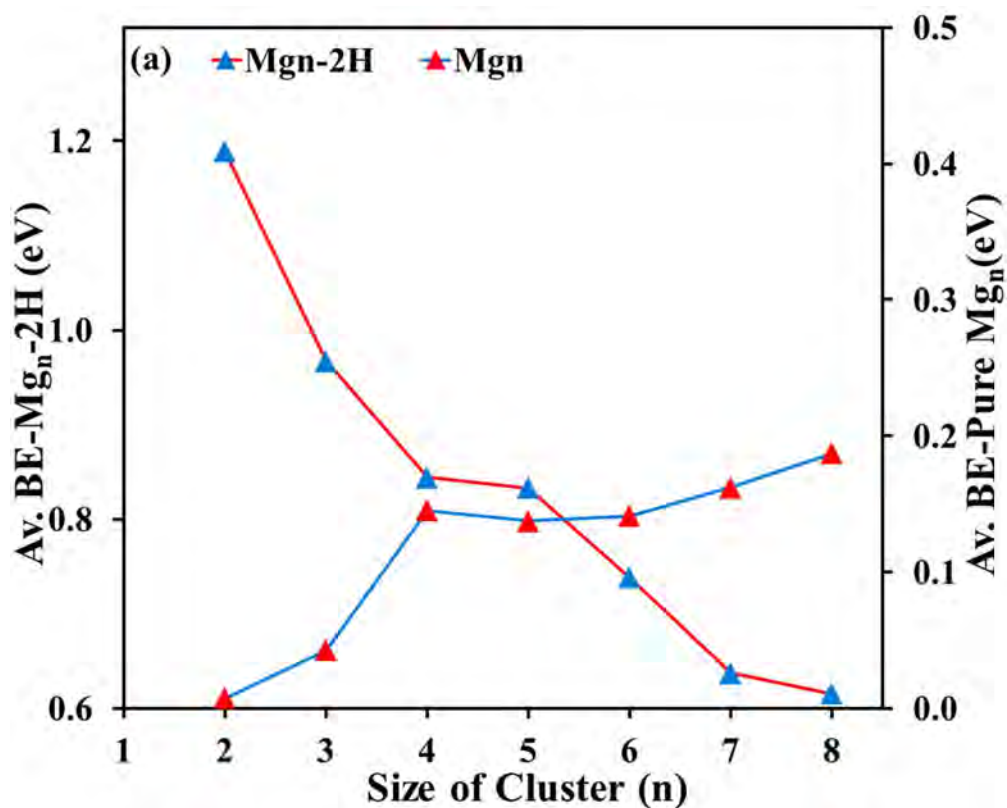


Fig. 5.4(a) Binding energy variation of Mg<sub>n</sub> and Mg<sub>n</sub>-2H clusters.

As reported earlier [42], the average BE of pure Mg<sub>n</sub> clusters rises with a peak at n=4. In the cases of pure hydrogenated clusters, the average binding energy continues an asymptotic fall from n=5 to 7 without any clear maxima or minima. After doping with Ti, the TiMg<sub>n</sub> cluster's average binding energy rises, with a sharp peak at n=8 in the present range of study. While in hydrogenated doped clusters (TiMg<sub>n</sub>-2H), a frequent fall of average BE for n=2-8, having a prominent dip at n=5, is observed.

From the study of average binding energy, it can be concluded that n=5 may show higher reactivity. Therefore, hydrogenation to Mg<sub>n</sub> and TiMg<sub>n</sub> clusters helps to decrease the average binding energy.

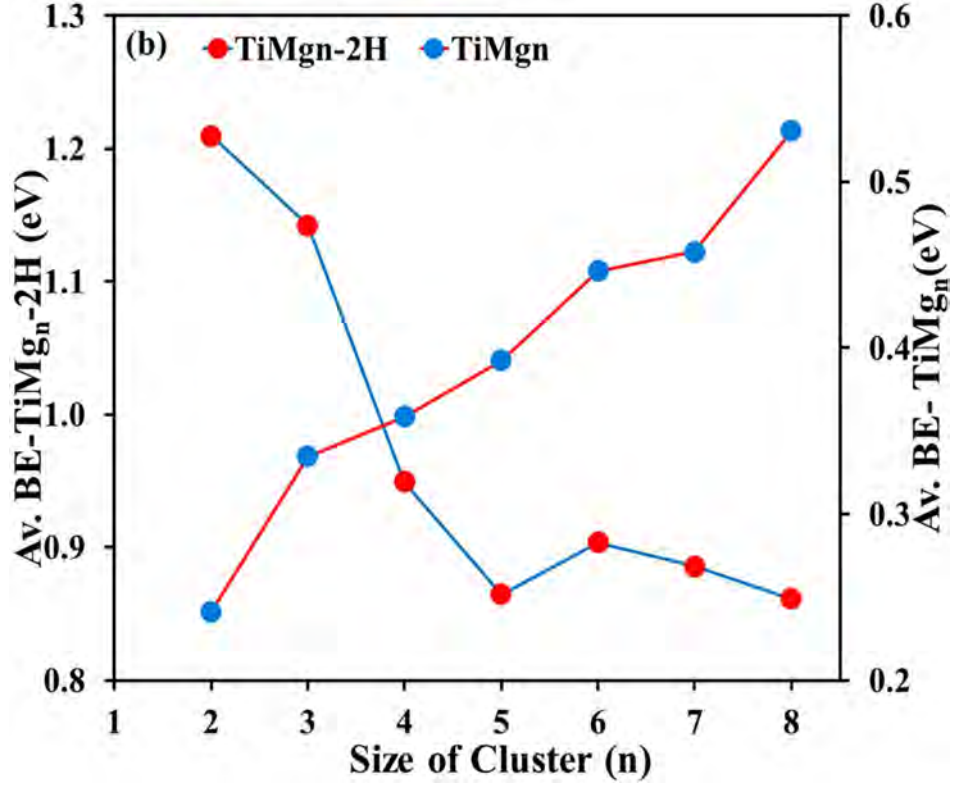


Fig. 5.4(b) Binding energy variations of  $TiMg_n$  and  $TiMg_n-2H$  clusters with cluster size.

The stability or 2<sup>nd</sup> order change in energy ( $\Delta_2$ ) can be obtained from the relations given below following our previous reports [39-42]

$$\Delta_{2Mg_n} (eV) = E_{Mg_{n+1}} + E_{Mg_{n-1}} - 2E_{Mg_n} \quad (5.5)$$

$$\Delta_{2TiMg_n} (eV) = E_{TiMg_{n+1}} + E_{TiMg_{n-1}} - 2E_{TiMg_n} \quad (5.6)$$

$$\Delta_{2Mg_n-2H} (eV) = E_{Mg_{n+1}-2H} + E_{Mg_{n-1}-2H} - 2E_{Mg_n-2H} \quad (5.7)$$

$$\Delta_{2TiMg_n-2H} (eV) = E_{TiMg_{n+1}-2H} + E_{TiMg_{n-1}-2H} - 2E_{TiMg_n-2H} \quad (5.8)$$

Fig. 5.5 presents the variation of stability parameters of  $Mg_n$ ,  $Mg_n-2H$ ,  $TiMg_n$ , and  $TiMg_n-2H$  clusters with the cluster size (n). The stability curve of pure clusters has local maxima for  $Mg_4$ . However, the maxima shifted to  $n=5$  after hydrogenation.  $TiMg_n-2H$  clusters possess local peaks at  $n = 3$  and  $6$ .

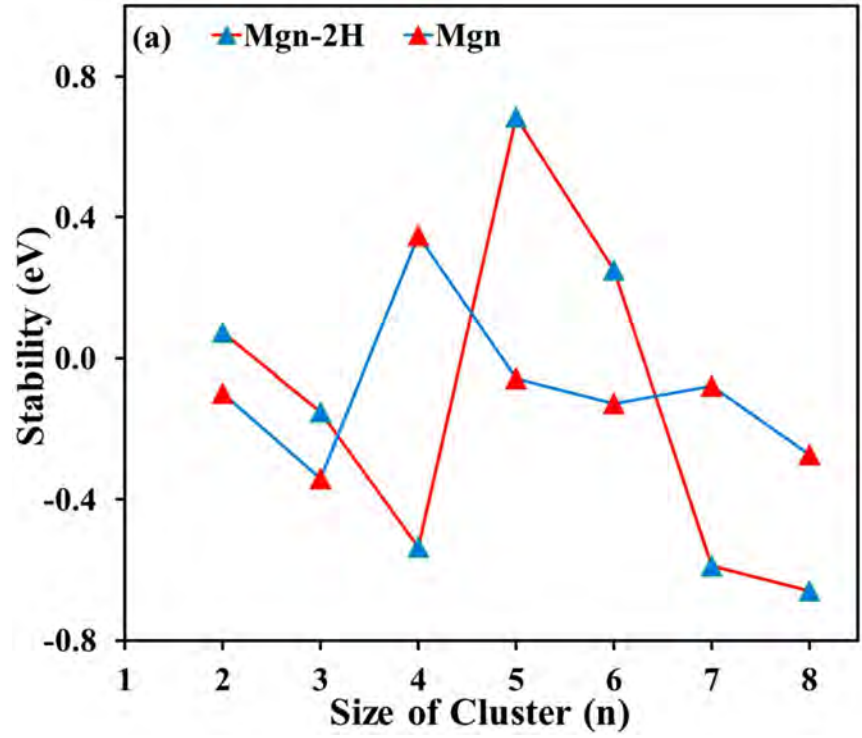


Fig. 5.5(a) The variation of stability of Mg<sub>n</sub>-2H and Mg<sub>n</sub> clusters.

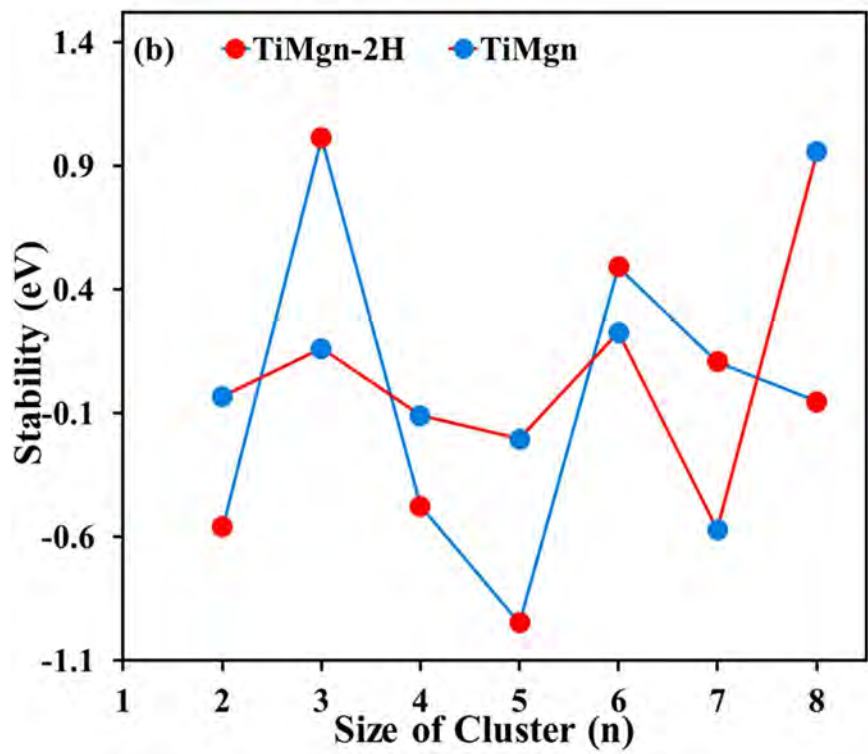


Fig. 5.5(b) The variation of stability of TiMg<sub>n</sub>-2H and TiMg<sub>n</sub> clusters with the growth of the clusters.

In all cases, the  $\text{TiMg}_8$  cluster shows very high stability as  $\text{TiMg}_8$  possesses a closed-shell configuration with  $1S^21P^61D^{10}2S^2$  [41]. Thus, it has a shell closure configuration according to the electron counting rule. Fig. 5.5 (a) represents the variation of the second-order change in energy which is famously known as the stability parameter of pure  $\text{Mg}_n$  and hydrogenated  $\text{Mg}_n\text{-2H}$  clusters, and Fig. 5.5 (b) shows the variation of the stability parameter of Ti-doped  $\text{Mg}_n$  cluster, i.e.,  $\text{TiMg}_n$  and hydrogenated  $\text{TiMg}_n$ , i.e.,  $\text{TiMg}_n\text{-2H}$  clusters with the increase of cluster size. Table 5.1 contains the calculated binding energy values per atom, relative stability, and HOMO-LUMO band gap energies for pure, pure hydrogenated, doped, and doped hydrogenated clusters for  $n=2\text{-}8$ .

To have a clearer picture of the effect of Ti doping, vertical ionization potential (VIP), vertical electron affinity (VEA), chemical hardness ( $\eta$ ), and chemical potential ( $\mu$ ) have been studied. Fig. 5.6 shows the behavior of vertical ionization potential (VIP) and vertical electron affinity (VEA) with the growth of the clusters.

n	BE (eV)				Stability				Band Gap (eV)			
	$\text{Mg}_n$	$\text{Mg}_n\text{-2H}$	$\text{TiMg}_n$	$\text{TiMg}_n\text{-2H}$	$\text{Mg}_n$	$\text{Mg}_n\text{-2H}$	$\text{TiMg}_n$	$\text{TiMg}_n\text{-2H}$	$\text{Mg}_n$	$\text{Mg}_n\text{-2H}$	$\text{TiMg}_n$	$\text{TiMg}_n\text{-2H}$
2	0.01	1.17	0.19	1.21	-0.10	0.074	-0.03	-0.56	3.49	3.78	2.06	2.21
3	0.04	0.95	0.28	1.14	-0.34	-0.151	0.16	1.13	3.05	3.16	1.93	2.08
4	0.15	0.82	0.31	0.93	0.35	-0.082	-0.11	-0.71	2.93	2.92	1.79	2.15
5	0.14	0.81	0.34	0.86	-0.06	-0.220	-0.20	-0.83	2.37	2.67	1.93	2.20
6	0.14	0.72	0.40	0.90	-0.13	0.704	0.23	0.49	2.38	1.96	1.77	1.46
7	0.16	0.62	0.41	0.89	-0.08	-0.590	-0.57	0.11	2.34	2.33	1.45	1.52
8	0.19	0.60	0.48	0.86	-0.27	-0.659	0.96	-0.05	2.32	2.33	1.38	1.68

By definition, the higher the value of VIP higher the stability, i.e., a cluster showing a local peak in VIP implies the cluster is showing higher stability. From Fig. 5.6(b), it can be easily seen that  $\text{TiMg}_5\text{-2H}$  and  $\text{TiMg}_7\text{-2H}$  possess local minima in VIP, which implies that these clusters are less stable and more reactive. This is a requirement for hydrogen storage material [40, 41]. It is noted that highly stable clusters are not appropriate for hydrogen storage.

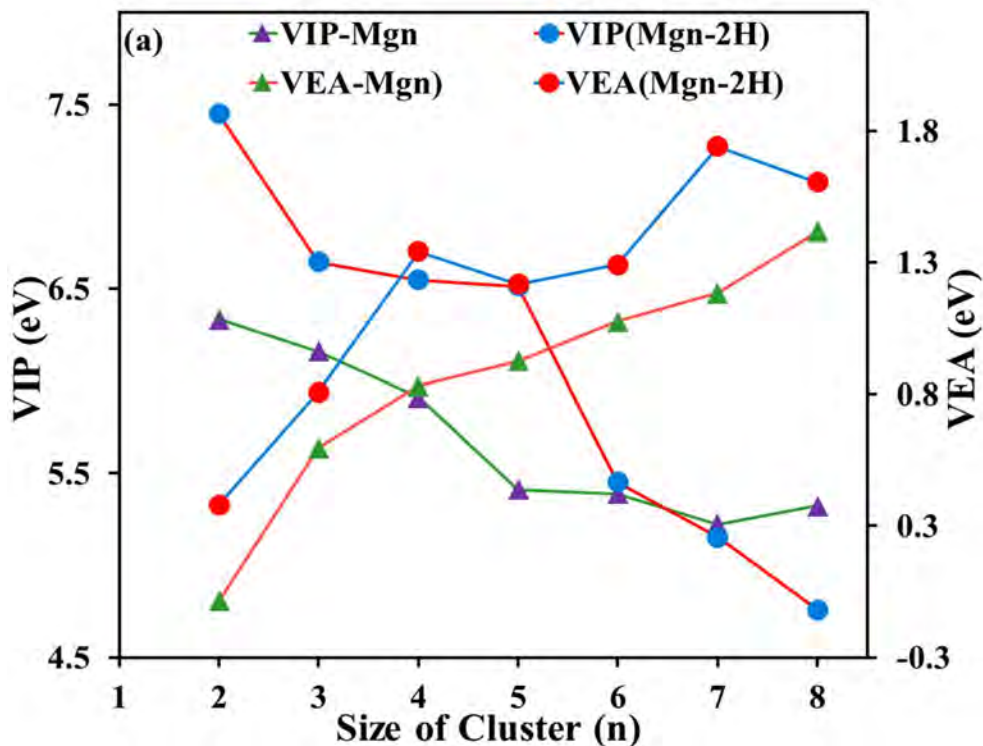


Fig. 5.6(a) The variation of VIP and VEA of  $Mg_n$ -2H and  $Mg_n$  clusters.

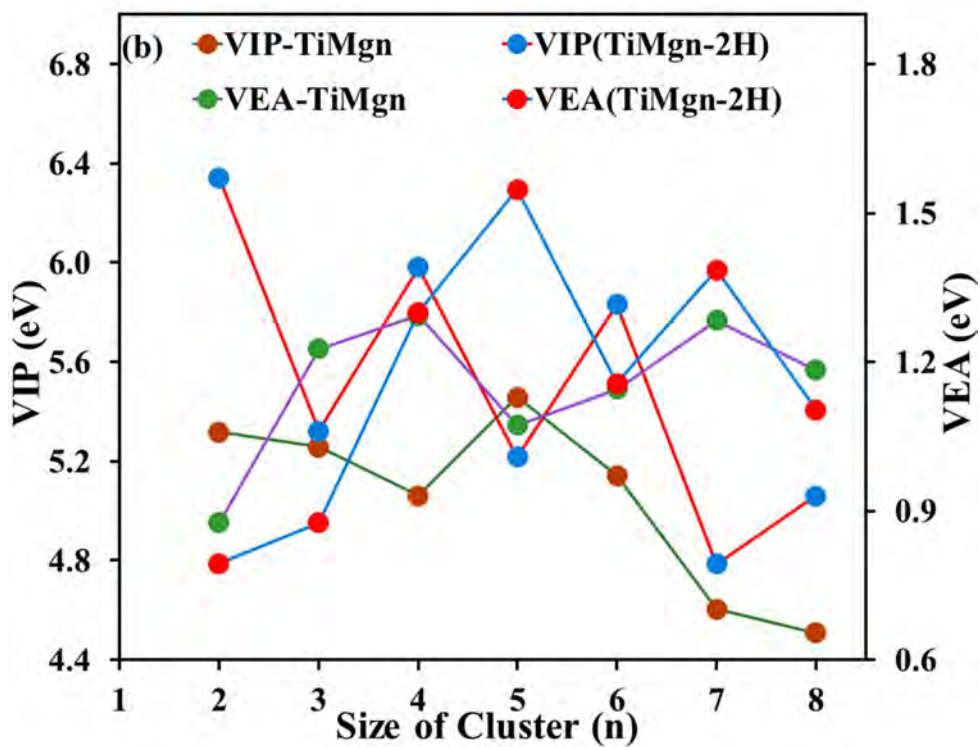


Fig. 5.6(b) The variation of VIP and VEA of  $TiMg_n$ -2H and  $TiMg_n$  clusters with the growth of the clusters.



On the other side, by definition, the higher the value of VEA, the higher its reactivity will be. From the variation of VEA with the growth of the clusters ( $n=2-8$ ), one can say that VEA has peaked for  $\text{TiMg}_5-2\text{H}$  and  $\text{TiMg}_7-2\text{H}$ ; these clusters have higher electron affinity and are less stable or more reactive. This is good for hydrogen storage. Similarly, in the variation of VIP for pure  $\text{Mg}_n-2\text{H}$  cluster (Fig. 5.6 a), one cannot see any sharp peak. Still, a fall after  $\text{Mg}_5-2\text{H}$  but local maxima and minima are present in doped hydrogenated clusters ( $\text{TiMg}_n-2\text{H}$ ).

Thus, it has been seen in several cases that Ti doping to pure  $\text{Mg}_n$  clusters improved magnesium clusters' hydrogen storage capacity.

Next, chemical hardness and potential have been studied to understand the chemical characteristics of  $\text{Mg}_n$ ,  $\text{TiMg}_n$ ,  $\text{Mg}_n-2\text{H}$ , and  $\text{TiMg}_n-2\text{H}$  clusters. The variation of chemical hardness and chemical potential has been presented in Fig. 5.7. Chemical hardness can be defined as the resistance to change to the electronic configuration of a chemical species, i.e., a measure of resistance to change in several electrons.

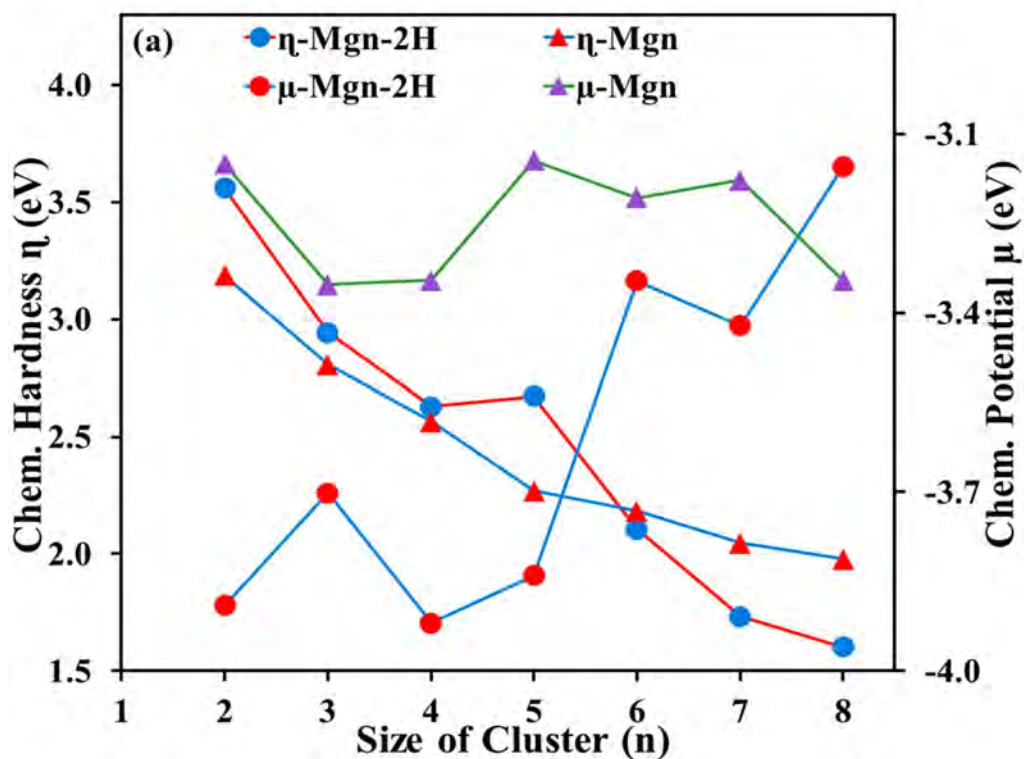


Fig. 5.7(a) The variation of Chem.Hard and Chem.Pot of  $\text{Mg}_n-2\text{H}$  and  $\text{Mg}_n$  clusters.

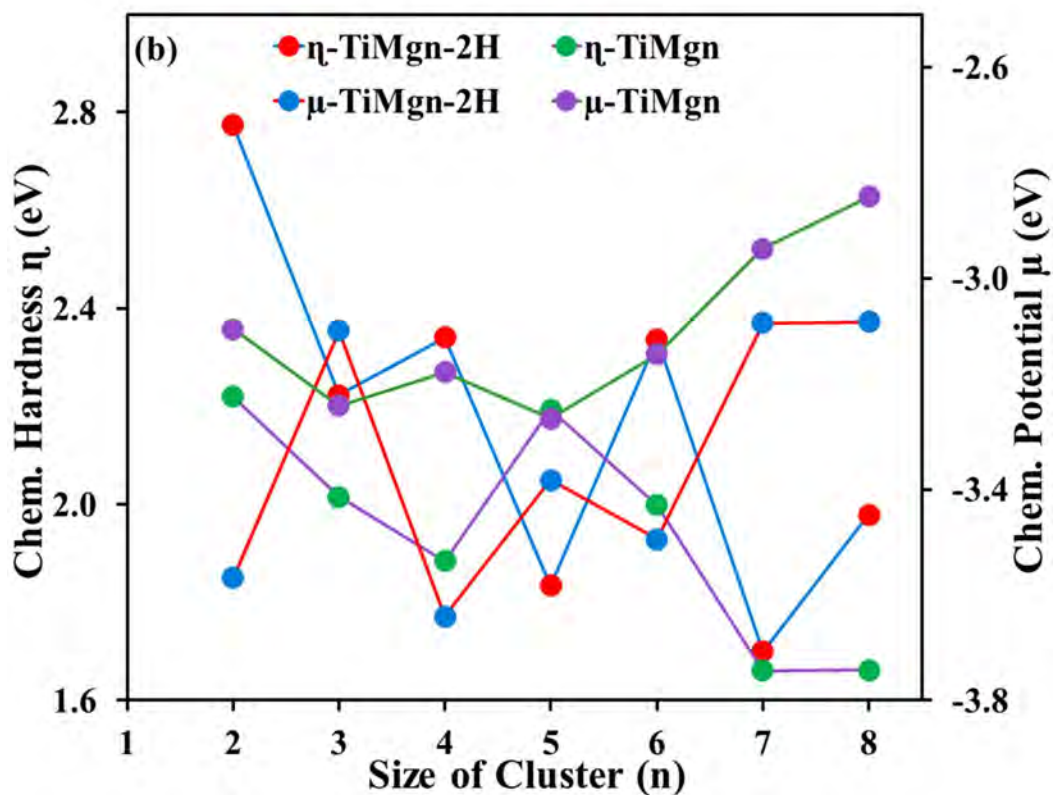


Fig. 5.7(b) The variation of Chem.Hard and Chem.Pot of  $TiMg_n-2H$  and  $TiMg_n$  clusters with the growth of the clusters.

**Table 5.2** Variation of VIP, VEA, Chem. Pot., Chem. Hardness in eV with the size of the cluster

n	VIP (eV)				VEA (eV)				$\mu$ (eV)				$\eta$ (eV)			
	Mg <sub>n</sub>	Mg <sub>n</sub> -2H	TiM <sub>g<sub>n</sub></sub>	TiM <sub>g<sub>n</sub></sub> -2H	Mg <sub>n</sub>	Mg <sub>n</sub> -2H	TiM <sub>g<sub>n</sub></sub>	TiM <sub>g<sub>n</sub></sub> -2H	Mg <sub>n</sub>	Mg <sub>n</sub> -2H	TiM <sub>g<sub>n</sub></sub>	TiM <sub>g<sub>n</sub></sub> -2H	Mg <sub>n</sub>	Mg <sub>n</sub> -2H	TiM <sub>g<sub>n</sub></sub>	TiM <sub>g<sub>n</sub></sub> -2H
2	6.33	7.45	5.32	6.34	0.04	0.33	0.88	0.79	-3.15	-3.89	-3.10	-3.57	3.19	3.56	2.22	2.77
3	6.16	6.64	5.26	5.32	0.55	0.76	1.23	0.88	-3.35	-3.70	-3.24	-3.10	2.81	2.94	2.02	2.22
4	5.91	6.55	5.06	5.98	0.78	1.29	1.29	1.30	-3.35	-3.92	-3.18	-3.64	2.56	2.63	1.88	2.34
5	5.41	6.51	5.46	5.22	0.88	1.17	1.07	1.55	-3.14	-3.84	-3.27	-3.38	2.27	2.67	2.19	1.83
6	5.39	5.45	5.14	5.83	1.03	1.24	1.15	1.16	-3.21	-3.35	-3.14	-3.49	2.18	2.10	2.00	2.34
7	5.22	5.15	4.60	4.78	1.13	1.69	1.28	1.38	-3.18	-3.42	-2.94	-3.08	2.05	1.73	1.66	1.70
8	5.32	4.76	4.51	5.06	1.37	1.55	1.18	1.10	-3.35	-3.16	-2.85	-3.08	1.98	1.60	1.66	1.98

Thus, the higher the chemical hardness, the higher the chemical inertness and stability. On the other hand, the higher the chemical potential, the higher the chemical reactivity and the lower the stability. The chemical hardness and chemical potential can be defined as,

$$\eta = \frac{VIP - VEA}{2} \quad (5.9)$$

$$\mu = -\frac{VIP + VEA}{2} \quad (5.10)$$

$\eta$  and  $\mu$  are the chemical hardness and chemical potential, respectively.

In the case of the pure hydrogenated  $Mg_5-2H$  cluster (Fig 5.7(a)), a small local peak in the chemical hardness and a rising chemical potential.

From Fig. 5.7(b), it is clear that the  $TiMg_5-2H$  cluster shows local minima in chemical hardness and local maxima for the chemical potential. This nature for both types of clusters supports that  $n=5$  could be the best choice for hydrogenation of pure and Ti-doped  $Mg_n$  clusters within the present range of study.

In Table 5.2, the evaluated values of VIP, VEA, chemical hardness, and chemical potential, all in electron volts, are given for pure, pure hydrogenated, doped, and doped hydrogenated clusters for the cluster size  $n=2-8$ .

### 5.3.3 Adsorption Energy ( $E_{ads}$ )

The adsorption energy may be expressed as

$$E_{ads}(Mg_n) = E(Mg_n H_2) - E(Mg_n) - E(H_2) \quad (5.11)$$

$$E_{ads}(TiMg_n) = E(TiMg_n H_2) - E(TiMg_n) - E(H_2) \quad (5.12)$$

The variation of  $H_2$  adsorption energy with cluster size is shown in Fig. 5.8.  $E_{ads}$  for pure  $Mg_5H_2$  shows local maxima, whereas the doped cluster  $TiMg_5H_2$  shows local minima. It indicates that the physisorption energy for the doped cluster is reduced from 0.22 eV to 0.09eV, a reduction of 59%.

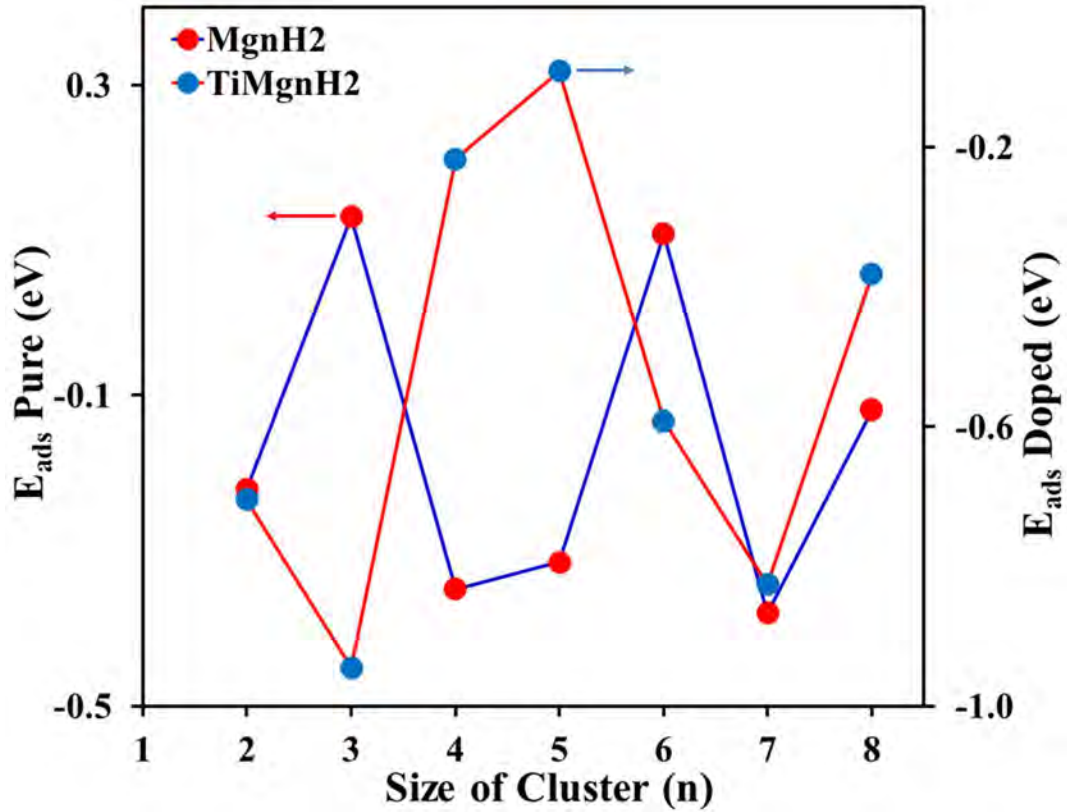


Fig. 5.8 Variation of H<sub>2</sub> adsorption energy with cluster size (n).

### 5.3.4 Chemisorption Energy

Chemisorption energy (CE) can be obtained by using the following relations:

$$CE_{Ti\ doped} = E(TiMg_n) - 2H - E(H_2) - E(TiMg_n) \quad (5.13)$$

$$CE_{pure} = E(Mg_n - 2H) - E(H_2) - E(Mg_n) \quad (5.14)$$

Fig. 5.9 shows the chemisorption energy of pure and doped Mg<sub>n</sub> clusters with cluster size. It is seen that a sharp fall in chemisorption energy for the Mg<sub>5</sub> cluster and a sharp peak of chemisorption energy occurs for the doped n=5 cluster.

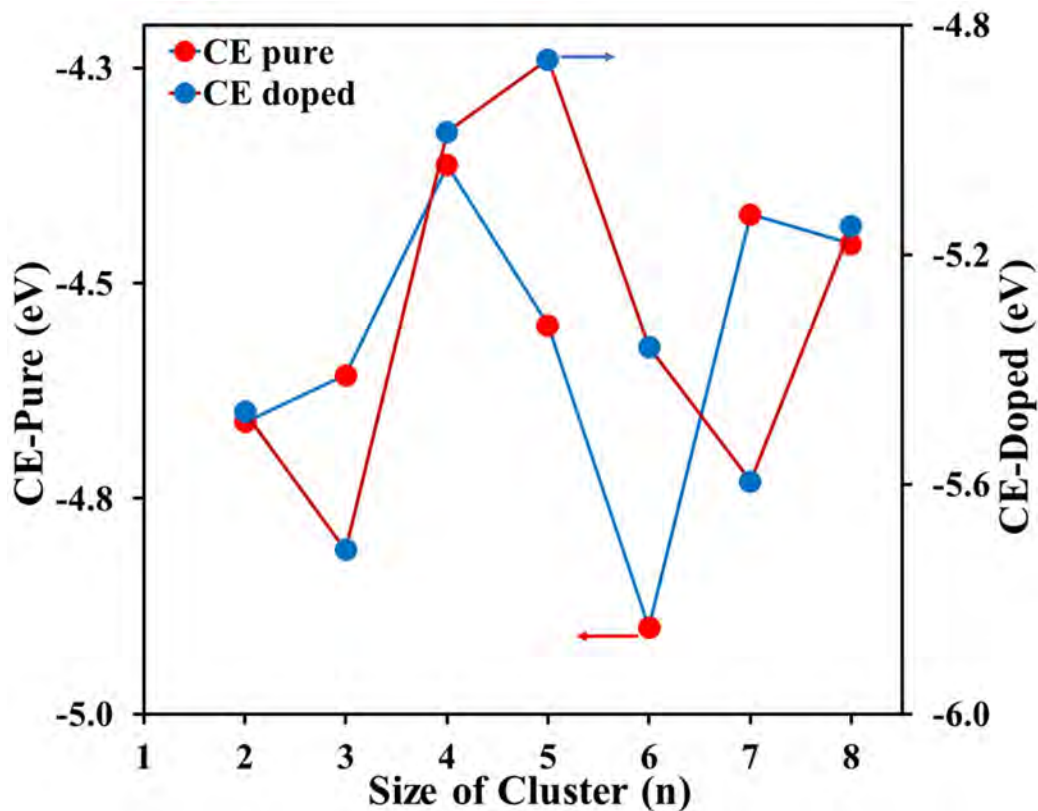


Fig. 5.9 The variation of chemisorption energy of  $Mg_n-2H$  and  $TiMg_n-2H$  with the growth of the clusters.

This result indicates that the  $TiMg_5$  cluster is capable of storing hydrogen. In Ti-doped  $Mg_n$  clusters, the Ti atom changes the cluster surface's properties. Due to the transfer of charge density from the Ti atom to the nearest neighbor Mg atoms, the Mg atoms become reactive sites and gain hydrogen intake capacity, evident from NBO analysis and ELF 2D-Map. The presence of the Ti atom changes the Fermi level of  $Mg_5-2H$  from 3.64 eV to 3.52 eV after Ti catalytic activity. This reduction, in turn, increases the diffusion rate of hydrogen atoms. In exohedrally doped  $Mg_n$  clusters, the hydrogenation/ dehydrogenation process starts with the adsorption of the  $H_2$  molecule by the Ti atom through weak Van der Waals forces by physisorption at a Ti-H distance of 1.8 Å. In the next step, the  $H_2$  molecule dissociates, forming two Ti-H bonds. The next step is the diffusion of H. The H atoms transfer to Mg atoms through partial bonds between Ti-H-Mg, clear from the electron localization near the Mg atom. The chemisorption of H atoms by the reactive Mg sites completes the step. The final product in the process is  $TiMg_n-2H$ . In the dehydrogenation process, the Mg atoms get spontaneously

released from Mg atoms. The H atoms then diffuse towards each other and recombine to form H<sub>2</sub> molecule to be used as an energy carrier.

### 5.3.5 Electron Localization Function (ELF)

The 2-D Electron Localization Function (ELF) has been studied to know about the reactivity of the clusters. It confirms the position of reactive atoms in the clusters Mg<sub>5</sub>-2H, TiMg<sub>5</sub>, and TiMg<sub>5</sub>-2H clusters. In the 2D-ELF plot of TiMg<sub>5</sub> (Fig. 5.10), the reddish region on the outer surface of the 2<sup>nd</sup>, 3<sup>rd</sup>, 4<sup>th</sup>, and 5<sup>th</sup> index of atoms indicates these atoms have electron-pair localization on the surface. The ELF can be defined as (5.15)

$$ELF(r) = \frac{1}{1 + \chi^2(r)}; \chi(r) = \frac{D(r)}{D_h(r)} \quad (5.15)$$

One can find the presence of a strongly localized electron pair in a molecular cluster from the electron localization function. It gives the probability of finding two electrons of opposite spin in a localized region of the molecular cluster under consideration. This electron pair can interact with other electrons outside the region. The ELF expression given above can be understood in detail in terms of  $D(r)$ ,  $D_h(r)$  and  $\chi(r)$  as follows:

$$D(r) = \text{Electron localization} = T(r) - \frac{1}{4} \frac{(\nabla \rho(r))^2}{\rho(r)} = \frac{1}{2} \sum_{i=1}^N |\nabla \psi_i(r)|^2 - \frac{1}{8} \frac{|\nabla \rho(r)|}{\rho(r)} \quad (5.16)$$

Where  $\rho$  denotes the electron spin density,  $T(r)$  is the kinetic energy density. The second term represents the bosonic kinetic energy density. From the above relation, one can get the expression for uniform electron gas:

$$D_h(r) = \text{uniform electron gas} = \frac{3}{5} (6\pi^2)^{2/3} \rho^{5/3}(r) = \frac{3}{10} (3\pi^2)^{2/3} \rho^{5/3}(r) \quad (5.17)$$

Based on the electron localization,  $D(r)$  uniform electron gas  $D_h(r)$   $\chi(r)$  is defined in terms of the ratio.

$$\chi(r) = \frac{D(r)}{D_h(r)} \quad (5.18)$$

In this study, ELF is calculated [38] for Mg<sub>5</sub>, Mg<sub>5</sub>-2H, TiMg<sub>5</sub>, and TiMg<sub>5</sub>-2H clusters with contour, as shown in Fig. 5.10. ELF can be categorized into three stages, viz. ELF= 0 indicates no electron density, electron pairs, or low electron localization zone with parallel electron signs (blue region). ELF= 0.5-0.6 represents the zone with metallic bonding (green region). The last and most crucial area is when ELF=0.9-1.0 represents the zone occupied by paired electrons means the location corresponds to perfect absolute electron pair localization (red region). To have a colored 2D-ELF map, Multiwfn software is used.

The ELF map (Fig. 5.10(a)) of the Mg<sub>5</sub> cluster shows that the pure Mg<sub>5</sub> cluster has three reddish regions indicating the three reactive sites at 1, 3, and 4 numbered Mg atoms. The ELF map presented in Fig. 5.10 (b) of the Mg<sub>5</sub>-2H cluster shows the electron localization profile of the cluster, where one can see that the hydrogen has been dissociated or adsorbed by the most reactive Mg atoms of Mg<sub>5</sub> clusters. The highly reactive Mg atoms are 1 and 3. Here, we can see the reddish regions shift towards the hydrogenated atoms, and after hydrogen adsorption, these Mg atoms (1 and 3) become positive. Similarly, the 2D ELF map of the TiMg<sub>5</sub> cluster (Fig. 5.10 (c)) shows reddish regions on the surface of the 1<sup>st</sup>, 2<sup>nd</sup>, 3<sup>rd</sup>, and 4<sup>th</sup> indexed Mg atoms. Therefore, the Ti atom acted as a charge donor after the Ti doping (partially endohedral) to the pure Mg<sub>5</sub> cluster.

In contrast, the Mg atoms in the Mg<sub>5</sub> clusters acted as charge acceptors. As a result, after doping Ti to the pure Mg<sub>5</sub> cluster, the Ti atom distributes the charges over the Mg atoms present in the cluster, producing more reactive sites.

From the ELF maps of the cluster, one can easily find that the Mg<sub>5</sub> cluster has three and TiMg<sub>5</sub> has four reactive sites. In addition, it also indicates robust electron pair localization on the surface of the 1<sup>st</sup>, 2<sup>nd</sup>, 3<sup>rd</sup>, 4<sup>th</sup>, and 5<sup>th</sup> index of Mg atoms of TiMg<sub>5</sub> clusters. After Ti doping in Mg<sub>5</sub>, the Ti atom becomes positive after sharing the charge among the Mg atoms. Here, the most reactive Mg atoms have adsorbed hydrogen. It indicates that the hydrogen molecule has dissociated successfully and gets adsorbed at the reactive sites of the cluster.

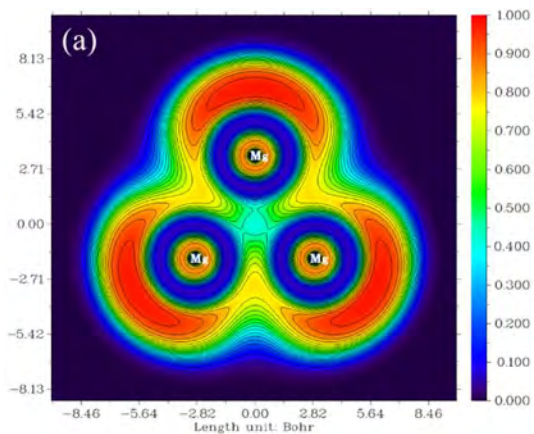


Fig. 5.10(a) 2D ELF map Mg<sub>5</sub>.

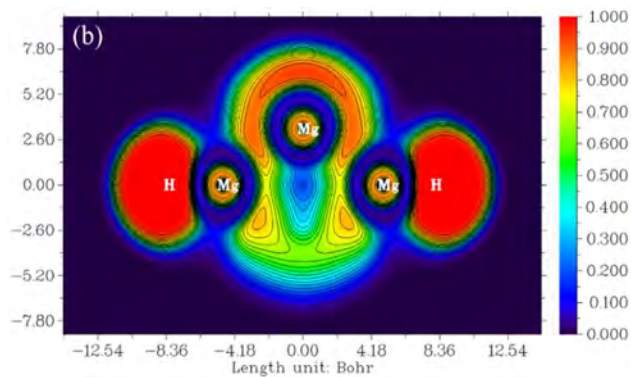


Fig. 5.10(b) 2D ELF map Mg<sub>5</sub>-2H.

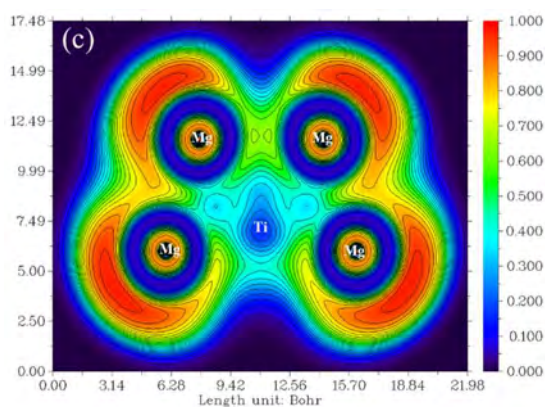


Fig. 5.10(c) 2D ELF map TiMg<sub>5</sub>.

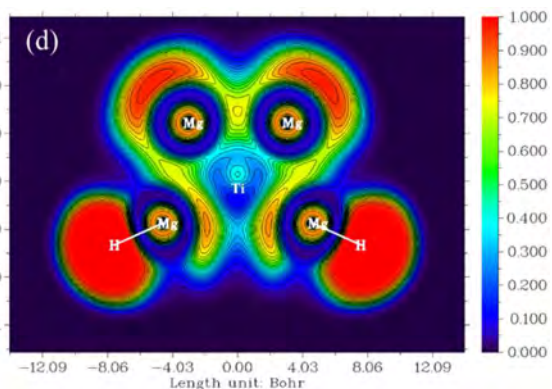


Fig. 5.10(d) 2D ELF map TiMg<sub>5</sub>-2H.

Fig. 5.10 Behavior of ELF (with contour) of Mg<sub>5</sub>, Mg<sub>5</sub>-2H, TiMg<sub>5</sub>, and TiMg<sub>5</sub>-2H.

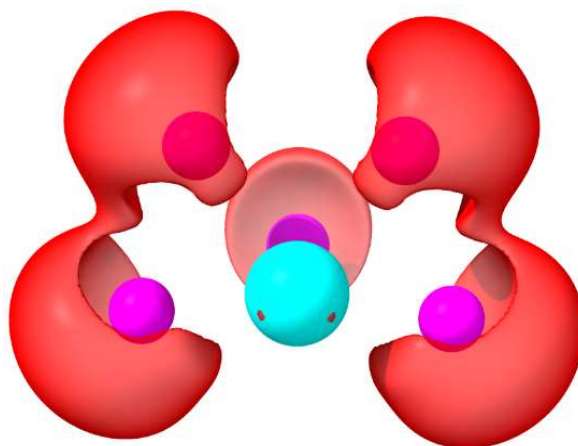


Fig. 5.11 3D representation of ELF of TiMg<sub>5</sub>-2H.



The ELF map indicates the position of the Ti atom by the blue region at the center of the map. There are other electron pair or electron density region in the TiMg<sub>5</sub>-2H cluster (Fig 5.10(d)). Here, again, the reddish region shifts towards the hydrogenated atoms after hydrogenation. Ti atom is positive and indicated by the blue shade in the ELF map. Hence the Ti atom plays an essential role in the cluster to make the cluster more promising for hydrogen storage. Ti doping in the Mg<sub>5</sub> cluster makes the cluster more reactive and with more affinity to adsorb hydrogen. From the stability parameter also, we can conclude that the TiMg<sub>5</sub> cluster is a more promising material for hydrogen storage than the pure Mg<sub>5</sub> cluster. After Ti doping, the electron pair localization on the outer surface of the cluster becomes stronger. It makes this TiMg<sub>5</sub> cluster more promising than Mg<sub>5</sub>. Exohedral Ti doping to the Mg<sub>5</sub> cluster also enhances the hydrogen intake of the cluster as TiMg<sub>5</sub> can adsorb two more H<sub>2</sub> molecule than the Mg<sub>5</sub> cluster (section 5.4). One can explain it from ELF as well. It is seen from the ELF of TiMg<sub>5</sub>-2H that hydrogenation occurred on the 1<sup>st</sup> and 4<sup>th</sup> indexed Mg atoms as they were more reactive. But there are still three reactive atoms, 2<sup>nd</sup>, 3<sup>rd</sup>, and 5<sup>th</sup> indexed Mg atoms, and additional hydrogen atoms may be adsorbed in the cluster.

### ***5.3.6 Mechanism of Catalytic Activity of Ti on Hydrogenation/ Dehydrogenation of TiMg<sub>5</sub> Cluster.***

In doped Mg<sub>5</sub> cluster with respect to pure clusters the BE rises from 0.14 eV to 0.34 eV, energy gap falls from 2.37 eV to 1.93 eV (~22.8%), VEA rises from 0.88 eV to 1.07 eV (~21.6%), chemical potential falls from -3.14 eV to -3.27 eV (~4%) and chemical hardness falls from 2.27 eV to 2.19 eV (~4%). In respect to pure hydrogenated Mg<sub>5</sub>-2H cluster, in the doped hydrogenated (TiMg<sub>5</sub>-2H) cluster, the BE rises from 0.81 eV to 0.86 eV (~ 6%), HOMO-LUMO gap falls from 2.67 eV to 2.2 eV (17.6%), VIP falls from 6.51 eV to 5.22 eV (19.8%), VEA rises from 1.17 eV to 1.55 eV (32.5%), chemical hardness falls from 2.67 eV to 1.83 eV (29.26%), and chemical potential rises from -3.84 eV to -3.38 eV (11.97%). As a result, the adsorption energy falls from 0.22 eV to 0.09 eV (59%), and chemisorption energy changes from -4.65 eV to -4.5 eV. In a nutshell, the change in the parameters mentioned above indicates that the catalytic activity of Ti prepares the Mg<sub>5</sub> cluster as an exceptionally suitable material for hydrogen storage.

### 5.3.7 Intrinsic Reaction Coordinate (IRC)

The so-called IRC path represents the process of hydrogenation and dehydrogenation graphically. The energy difference between reactants and products gives the reaction energy, or enthalpy, which can also be defined as the minimum energy required to start a chemical reaction. If it is negative, it is an exothermic process; if it is positive, the process is endothermic. The IRC nature of  $\text{TiMg}_3$ ,  $\text{TiMg}_4$ ,  $\text{TiMg}_5$ ,  $\text{TiMg}_6$ , and  $\text{TiMg}_7$  and their activation barriers are shown in Fig. 5.12. To show the catalytic effect of Ti, a comparison between activation barriers of pure and doped  $\text{Mg}_5$  clusters is presented in Fig. 5.12. Activation energy also has been obtained by calculating the energy difference between the reactants and the transition state (TS). It is clear that if the enthalpy of a reaction is negative, it is a good sign of hydrogenation dissociation.

The hydrogenated  $\text{TiMg}_3\text{-2H}$  cluster has an imaginary frequency of  $-137.84\text{ cm}^{-1}$ , the activation barrier has a value of  $1.845\text{ kcal/mole}$ ,  $\text{TiMg}_4\text{-2H}$  has a single imaginary frequency of  $-364.11\text{ cm}^{-1}$  and the activation barrier energy  $6.68\text{ kcal/mole}$ . For  $\text{TiMg}_6\text{-2H}$ , the imaginary frequency is  $-186.03\text{ cm}^{-1}$ . It has nearly Gaussian IRC with an activation barrier of  $1\text{ kcal/mole}$ . None of the clusters  $\text{TiMg}_3\text{-2H}$ ,  $\text{TiMg}_4\text{-2H}$ , or  $\text{TiMg}_6\text{-2H}$  have fair values of chemisorption energy, VIP, VEA, Chemical hardness, or chemical potential favorable for hydrogen storage. In the case of  $\text{TiMg}_7\text{-2H}$ , the single imaginary frequency is  $-392.31\text{ cm}^{-1}$ , and the activation barrier is relatively high at  $20.04\text{ kcal/mole}$ . Although  $\text{TiMg}_7\text{-2H}$  possesses higher VEA, lower VIP, lower chemical hardness, and higher chemical potential, it cannot be considered a suitable hydrogen storage cluster because of its lower chemisorption energy and high activation barrier energy.

For hydrogen adsorption on  $\text{TiMg}_5$  clusters, the reaction energy or enthalpy is  $-5.326\text{ kcal/mole}$ . Thus, according to enthalpy parameters,  $\text{TiMg}_5$  clusters are suitable for hydrogen storage.

The activation barrier energy of pure  $\text{Mg}_5$  and  $\text{TiMg}_5$  hydrogenated clusters is  $7.92\text{ kcal/mole}$  and  $5.326\text{ kcal/mole}$ , respectively. Due to the catalytic effect of Ti doping, the activation barrier energy falls about 32.75% to that of the pure cluster. The transition states of pure and doped  $\text{Mg}_5$  clusters contain only one imaginary frequency,  $-281.41\text{ cm}^{-1}$  and  $-454.56\text{ cm}^{-1}$ , respectively.

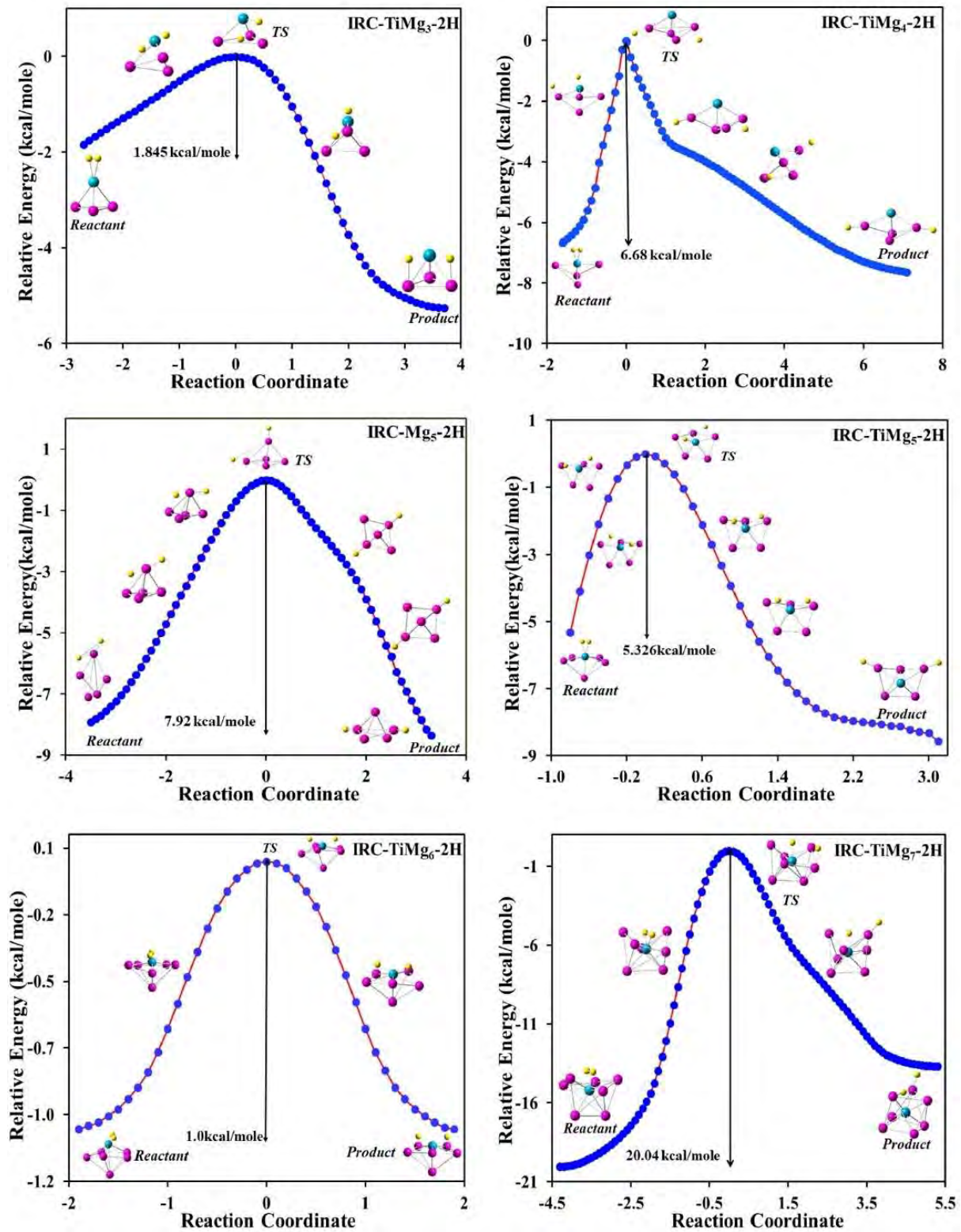


Fig. 5.12 IRC path for the transition from reactant to product via transition state (TS) of H<sub>2</sub>+TiMg<sub>5</sub> (reactant) to TiMg<sub>5</sub>-2H (product).

## 5.4 Gravimetric Density of Hydrogen Storage

The catalytic activity is manifested by (i) lowering the activation energy for forward and backward reactions and (ii) providing new avenues of reaction as discussed in the previous section. In the following section we have checked the maximum number of additional hydrogen molecule that can be adsorbed by TiMg<sub>5</sub> cluster.

The most important parameter for hydrogen storage system is its gravimetric density. It is calculated using the relation [67]

$$wt\% \text{ of } H_2 = \frac{N \times m_{H_2}}{(N \times m_{H_2} + m_{Ti} + n \times m_{Mg})} \times 100\% \quad (5.19)$$

where, N is the number of H<sub>2</sub> molecules adsorbed, n is the number of Mg atoms in the cluster, m<sub>H<sub>2</sub></sub>, m<sub>Ti</sub> and m<sub>Mg</sub> are the masses of H<sub>2</sub> molecule, Ti atom and Mg atoms.

It is seen from the study that bare Mg<sub>5</sub> atom can adsorb only one hydrogen molecule and after Ti doping due to catalytic effect of Ti three hydrogen molecules can be adsorbed by bare TiMg<sub>5</sub> cluster (Fig. 5.13). The binding energy per hydrogen atom falls from 0.95 eV to 0.71 eV. The reaction energy defined as the minimum energy required to start the adsorption reaction. It can be calculated from the difference of optimized energies of the reactants and products as

$$E_{Reaction} = E(TiMg_5) + E(nH_2) - E(TiMg_5nH_2) \quad (5.20)$$

The reaction energy of TiMg<sub>5</sub>-H<sub>2</sub> comes out to be 5.567 eV, which increases to 6.218 eV for 2H<sub>2</sub> molecules and 6.475 eV for 3H<sub>2</sub> molecules.

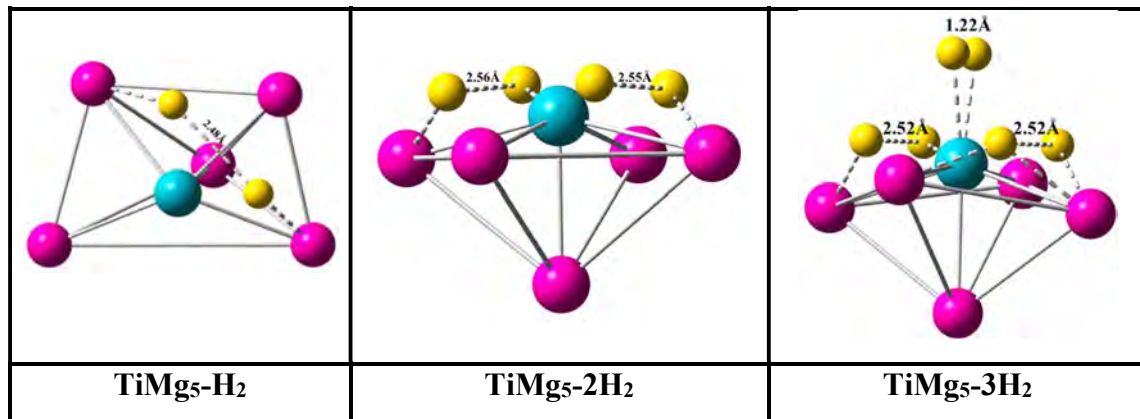
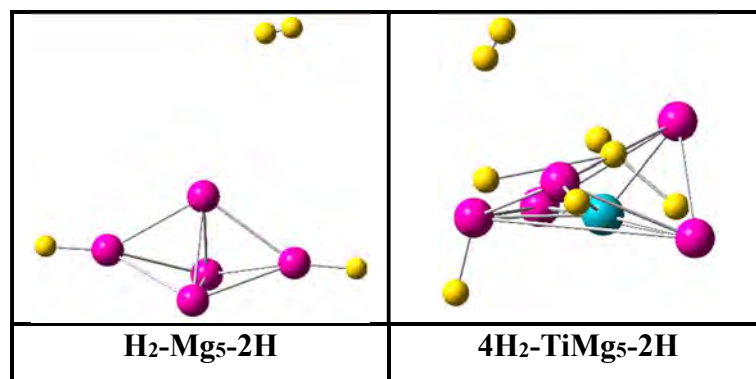


Fig. 5.13 Highest possible H<sub>2</sub> adsorption in TiMg<sub>5</sub> cluster systems.

The gravimetric density enhances from 1.18% ( $Mg_5$ ) to 3.45% ( $TiMg_5$ ) cluster. The optimized  $TiMg_5-2H$ ,  $H_2-TiMg_5-2H$  and  $2H_2-TiMg_5-2H$  cluster systems are shown in Fig 5.13. In case of adsorption of more than 2 atoms of hydrogen the pure  $Mg_5$  cluster throws the extra hydrogen away and it cannot split the hydrogen molecule at all. In case of  $TiMg_5$  cluster the cluster geometry breaks during 4 hydrogen molecule adsorptions.  $TiMg_5$  cluster can adsorb up to three hydrogen molecule and the splitting of hydrogen molecule can be observed. Fig. 5.14 is showing how pure  $Mg_5$  cluster throws the extra hydrogen away and it absolutely failed to split the hydrogen molecule. Fig. 5.14 also represents the way that the  $TiMg_5$  cluster breaks during four hydrogen molecule adsorption and it throws the extra hydrogen away.



**Fig. 5.14** The rejection of extra  $H_2$  molecules by the cluster.  $Mg_5-2H$  cannot adsorb one more  $H_2$  molecule where  $TiMg_5$  cluster is throwing the 4<sup>th</sup> hydrogen molecule away.

## 5.5 Summary and Conclusions

In the present report, a comparative study of hydrogen storage properties of  $Mg_n$  and  $TiMg_n$  ( $n=2-8$ ) clusters has been studied systematically before and after hydrogenation. Based on the comparative results drawn from the variations of different thermodynamic and chemical parameters with the increase of the size of the clusters, it is found that cluster  $Mg_5$  shows favorable properties to be a promising hydrogen storage material. Titanium doping changed the picture entirely. The doping improves the catalytic behavior of the cluster to split hydrogen. The complete study may be summarized as follows:

During the growth process of the clusters (Fig. 5.2), in the beginning, the binding energy increases rapidly both in  $TiMg_n$  and  $Mg_n$  clusters with the increase of the cluster size. After a

while, it tends to saturate in  $Mg_n$  clusters under the present range of study, whereas the binding energy in  $TiMg_n$  shows an increasing trend. The rapid increase in BE reflects the thermodynamic instability of the clusters. However, the average BE of the  $Mg_n$  and  $TiMg_n$  clusters rapidly drops after hydrogenation. However, the nature of stability shows a fluctuation about the zero value. The negative value of stability represents the unstable nature of the clusters. Sharp maxima at  $n=5$  in the pure cluster demand the stable nature of  $Mg_5$ . In doped clusters,  $TiMg_6$  and  $TiMg_8$  show relatively higher stability. But the rise in VIP, fall in VEA, and rise in chemical hardness makes them unsuitable for hydrogen storage—however, the stability of  $TiMg_5$  drops after hydrogenation, which is preferable for a hydrogenation reaction. The chemical potential and chemical hardness variation have supported it. In potential chemical variations,  $Mg_5-2H$  and  $TiMg_5-2H$  show relatively higher values, whereas chemical hardness indicates the opposite nature. The chemisorption energy drops from pure hydrogenated to doped hydrogenated case (-4.65 to -4.5 for  $n=5$ ) with the transition state (TS) frequency  $-454.56\text{ cm}^{-1}$ . From the intrinsic reaction coordinate (IRC), it is seen that the activation barrier for  $TiMg_5-2H$  falls to 5.326 kcal/mole from 7.92 kcal/mole (32.75%) of  $Mg_5-2H$  with a single imaginary frequency  $-281.41\text{ cm}^{-1}$  in the TS. Ti doping in the  $Mg_5$  cluster makes the cluster more reactive and with more affinity to adsorb hydrogen. From the stability parameter, the  $TiMg_5$  cluster is a more promising material for hydrogen storage than the pure  $Mg_5$  cluster. After Ti doping, the electron pair localization on the outer surface of the cluster becomes more robust, which supports our conclusion that the  $TiMg_5$  cluster is more promising than  $Mg_5$ .

Exohedral Ti doping to the  $Mg_5$  cluster also enhances the hydrogen intake of the cluster as  $TiMg_5$  can adsorb two more  $H_2$  molecule than the  $Mg_5$  cluster (section 5.3.7). One can explain it from ELF as well. It is seen from the ELF of  $TiMg_5-2H$  that hydrogenation occurred on the 1<sup>st</sup> and 4<sup>th</sup> indexed Mg atoms as they were more reactive. But there are still three reactive Mg atoms (2<sup>nd</sup>, 3<sup>rd</sup>, and 5<sup>th</sup> indexed) left, and they could be helpful for additional hydrogen atoms adsorption (Fig. 5.12). After one hydrogen atom absorption, the BE of  $TiMg_5-2H$  is still higher than the  $Mg_5-2H$  cluster. Absorption of one more additional hydrogen molecule at the Titanium site to have the nearly identical value of BE as a pure cluster without disturbing the cluster symmetry can be achieved. It also indicates the process remains repetitive after the

second cycle. The gravimetric density enhances from 1.62 wt.% to 3.54 wt.% due to Ti doping. In summary, the Titanium doped Mg<sub>5</sub> cluster is the most suitable material for hydrogen storage regarding hydrogen adsorption and desorption. In the process, the catalytic effect of Ti doping plays a vital role.

## References

- [1] V.A. Yartys, M.V. Lototsky, E. Akiba, R. Albert, V.E. Antonov, J.R. Ares, M. Baricco, N. Bourgeois, C.E. Buckley, J.M. Bellosta von Colbe, J.C. Crivello, F. Cuevas, R.V.R. Denys, M. Dornheim, M. Felderhoff, D.M. Grant, B.C. Hauback, T.D. Humphries, I. Jacob, T.R. Jensen, P.E. de Jongh, J.M. Joubert, M.A. Kuzovnikov, M. Latroche, M. Paskevicius, L. Pasquini, L. Popilevsky, V.M. Skripnyuk, E. Rabkin, M.V. Sofianos, A. Stuart, G. Walker, H. Wang, C.J. Webb and M. Zhu, “Magnesium based materials for hydrogen based energy storage: Past, present and future”, *Int. J Hydrogen Energy* **44(15)**, (2019), 7809-7859. <https://doi.org/10.1016/j.ijhydene.2018.12.212>.
- [2] N. Park, K. Choi, J. Hwang, D.W. Kim, D.O. Kim, and J. Ihm, “Progress on first-principles-based materials design for hydrogen storage”, *PNAS*, **109(49)**, (2012), 19893–19899. <https://doi.org/10.1073/pnas.1217137109>
- [3] P. Jena, “Materials for Hydrogen Storage: Past, Present, and Future”, *J. Phys. Chem. Lett.*, **2(3)**, (2011), 206–211, <https://doi.org/10.1021/jz1015372>.
- [4] Annemieke W.C. van den Berg, and C.O. Arean, “Materials for hydrogen storage: current research trends and perspectives”, *Chem. Commun.*, **6**, (2008), 668–681. <https://doi.org/10.1039/B712576N>
- [5] K.T. Moller, T.R. Jensen, E. Akiba, and H.W. Li, “Hydrogen - A sustainable energy carrier”, *Progress in Natural Science: Materials International* **27(1)**, (2017) 34–40. <https://doi.org/10.1016/j.pnsc.2016.12.014>
- [6] F. Schuth, “Challenges in hydrogen storage”, *Eur. Phys. J. Special Topics*, **176**, (2009), 155–166. <https://doi.org/10.1140/epjst/e2009-01155-x>. open access.
- [7] M. Hirscher, V.A. Yartys, M. Baricco, J.B. von Colbe, D. Blanchard, R.C. Bowman, D.P. Broom, C.E. Buckley, F. Chang, P. Chen, Y.W. Cho, J.C. Crivello, F. Cuevas, W.I.F. David, P.E. de Jongh, R.V. Denys, M. Dornheim, M. Felderhoff, Y. Filinchuk, G.E. Froudakis, D.M. Grant, E. Mac, A. Gray, B.C. Hauback, T. He, T.D. Humphries, T.R. Jensen, S.Kim, Y. Kohima, M Latroche, H.W. Li, M.V. Lototsky, J.W. Makepeace, K.T. Moller, L. Naheed, P. Ngene, D. Noreus, M.M. Nygard, S. Orimo, M. Paskevicius, L.



- Pasquini, D.B. Ravnsbaek, M.V. Sofianos, T.J. Udovic, T. Vegge, G.S. Walker, C.J. Webb, C. Weidenthaler, and C. Zlotea, "Materials for hydrogen-based energy storage – past, recent progress and future outlook", *Journal of Alloys and Compounds*, **827**, (2020),153548. <https://doi.org/10.1016/j.jallcom.2019.153548>
- [8] P. Pal, J.M. Ting, S. Agarwal, T. Ichikawa, and A. Jain, "The Catalytic role of d-block elements and their compounds for improving sorption kinetics of hydride materials: A Review", *Reaction*, **2(3)**, (2021), 333-364. <https://doi.org/10.3390/reactions2030022>.
- [9] H. Shao, "Hydrogen Storage: Preparation, Applications and Technology". (2018) NOVAPub. **ISAC: SCI024000**.
- [10] R.B. Xicohtencatl, M. Schlichtenmayer, and M. Hirscher, "Volumetric hydrogen storage capacity in metal-organic frameworks", *Energy Technol.*, **6(3)**, (2017), 578-582. <https://doi.org/10.1002/ente.201700636>
- [11] M. Becher, M. Haluska, M. Hirscher, A. Quintel, V. Skakalova, U. Dettlaff-Weglikovska, X. Chen, M. Hulman, Y. Choi, S. Roth, V. Meregalli, M. Parrinello, R. Strobel, L. Jorissen, M.M. Kappes, J. Fink, A. Zuttel, I. Stepanek, and P. Bernier, "Hydrogen storage in carbon nanotubes Stockage d'hydrogene dans les nanotubes de carbone", *Compt. Rendus Phys.*, **4(9)**, (2003) 1055-1062. [https://doi.org/10.1016/S1631-0705\(03\)00107-5](https://doi.org/10.1016/S1631-0705(03)00107-5)
- [12] G.G. Tibbetts, G.P. Meisner, and C.H. Olk, "Hydrogen storage capacity of carbon nanotubes, filaments, and vapor-grown fibers", *Carbon*, **39(15)**, (2001), 2291-2301. [https://doi.org/10.1016/S0008-6223\(01\)00051-3](https://doi.org/10.1016/S0008-6223(01)00051-3)
- [13] D.P. Broom, and M. Hirscher, "Irreproducibility in hydrogen storage material research", *Energy & Environ. Sci.*, **9(11)**, (2016), 3368-3380. <https://doi.org/10.1039/C6EE01435F>
- [14] A. El Kharbachi, E. Pinatel, I. Nuta, and M. Baricco, "A thermodynamic assessment of LiBH<sub>4</sub>", *Calphad*, **39**, (2012), 80-90. <https://doi.org/10.1016/j.calphad.2012.08.005>.
- [15] E.M. Dematteis, E.R. Pinatel, M. Corno, T.R. Jenson, and M. Baricco, "Phase diagrams of the LiBH<sub>4</sub>-NaBH<sub>4</sub>-KBH<sub>4</sub> system", *Phys. Chem. Chem. Phys.*, **19(36)**, (2017), 25071-25079. <https://doi.org/10.1039/C7CP03816J>

- [16] E.R. Pinatel, E. Albanese, B. Civalleri, and M. Baricco, “Thermodynamic modeling of  $\text{Mg}(\text{BH}_4)_2$ ”, *J. Alloy. Comp.*, **645(S1)**, (2015), S64-S68. <https://doi.org/10.1016/j.jallcom.2015.01.199>
- [17] M. Palumbo, F.J. Torres, J.R. Ares, C. Pisani, J.F. Fernandez, and M. Baricco, “Thermodynamic and ab initio investigation of the Al-H-Mg system”, *Calphad*, **31(4)**, (2007), 457-467. <https://doi.org/10.1016/j.calphad.2007.04.005>.
- [18] D. Pottmaier, E.R. Pinatel, J.G. Vitillo, S. Garroni, M. Oriova, M.D. Bravo, G.B.M. Vaughan, M. Fichtner, W. Lohstroh, and M. Baricco., “Structure and thermodynamic properties of the  $\text{NaMgH}_3$  perovskite: a comprehensive study”, *Chem. Mater.*, **23(9)**, (2011), 2317-2326. <https://doi.org/10.1021/cm103204p>
- [19] A. Wolczyk, E.R. Pinatel, M.R. Chierotti, C. Nervi, R. Gobetto, and M. Baricco, “Solidstate NMR and thermodynamic investigations on  $\text{LiBH}_4$ - $\text{LiNH}_2$  system”, *Int. J. Hydrogen Energy*, **41(32)**, (2016), 14475-14483. <https://dx.doi.org/10.1016/j.ijhydene.2016.03.040>.
- [20] M. Heere, S.H.P. GharibDoust, M. Brighi, C. Frommen, M.H. Sorby, R. Cerny, T.R. Jensen, and B.C. Houback, “Hydrogen sorption in erbium borohydride composite mixtures with  $\text{LiBH}_4$  and/or  $\text{LiH}$ ”, *Inorganics*, **5(2)**, (2017), 31. <https://doi.org/10.3390/inorganics5020031>
- [21] I.P. Jain, C. Lal, and A. Jain, “Hydrogen storage in Mg: A most promising material”, *Int. Journal of Hydrogen Energy*, **35(10)**, (2010), 5133-5144. <https://doi.org/10.1016/j.ijhydene.2009.08.088>
- [22] R.W.P. Wagemans, J.H. vaLenthe, P.E. de Jongh, A. jos van Dillen, and P. de jong Krijn, “Hydrogen Storage in Magnesium Clusters: Quantum Chemical Study”, *J. Am. Chem. Soc.*, **127(47)**, (2005), 16675-16680. <https://doi.org/10.1021/ja054569h>
- [23] D. Shen, C.P. Kong, R. Jia, P. Fu, and H.X. Zhang, “Investigation of Properties of  $\text{Mg}_n$  clusters and their hydrogen storage mechanism: a study based on DFT and a global minimum optimization method”, *J. Phys. Chem. A.*, **119(15)**, (2015), 3636-3643. <https://doi.org/10.1021/acs.jpca.5b01474>

- [24] J. Liu, J. Tyrrell, L. Cheng, and Q. Ge, "First-Principles Studies on Hydrogen Desorption Mechanism of  $Mg_nH_{2n}$  ( $n=3, 4$ )", *J. Phys. Chem. C*, **117(16)**, (2013), 8099-8104. <https://doi.org/10.1021/jp400969n>
- [25] H. Imamura, K. Masanari, M. Kusuhara, H. Katsumoto, T. Sumi, and Y. Sakata, "High hydrogen storage capacity of nanosized magnesium synthesized by high energy ball-milling", *J. Alloys Comp.*, **386(1-2)**, (2005), 211-216. <https://doi.org/10.1016/j.jallcom.2004.04.145>
- [26] Er. Suleyman, D. Tiwari, A. Gills de Wijs, and G. Brocks, "Tunable hydrogen storage in magnesium transition metal compounds: first principles calculations", *Phys. Rev. B.*, **79(2)**, (2009), 024105. <https://doi.org/10.1103/PhysRevB.79.024105>.
- [27] N. Wadnerkar, V. Kalamse, A.B. Phillips, B.S. Shivaram, and A. Chaudhari "Vibrational spectra of  $Ti:C_2H_4(nH_2)$  and  $Ti:C_2H_4(nD_2)$  ( $n=1-5$ ) complexes and the equilibrium isotope effect: Calculations and experiment", *Int. J. Hydrogen Energy*, **36(16)**, (2011), 9727-9732, <https://doi.org/10.1016/j.ijhydene.2011.05.034>
- [28] H. Chong, Y. Chen, and Y. Sheng. "First-principles study of molecular hydrogen adsorption on  $Mg_nZr$  ( $n=1-11$ ) clusters", *Eur. Phys. J. D*, **73(90)**, (2019), 1-8. <https://doi.org/10.1140/epjd/e2019-90521-6>
- [29] C. Milanese, A. Girella, G. Bruni, V. Berbenni, P. Cofrancesco, A. Marini, M. Villa, and P. Matteazzi, "Hydrogen storage in magnesium-metal mixtures: reversibility, kinetic aspects and phase analysis", *J. Alloys. Comp.*, **465(1-2)**, (2008), 396-405. <http://doi.org/10.1016/j.jallcom.2007.10.091>
- [30] J. Zhang, Z. Li, Y. Wu, X. Guo, J. Ye, B. Yuan, S. Wang, and L. Jiang, "Recent advances on the thermal destabilization of Mg-based hydrogen storage materials", *RSC Adv.*, **9(1)**, (2019), 408-428. <https://doi.org/10.1039/C8RA05596C>.
- [31] J.C. Crivello, B. Dam, R.V. Denys, M. Dornheim, D.M. Grant, J. Jout, T.R. Jenson, P. de Jongh, M. Latroche, C. Milanese, D. Milcius, G.S. Walker, C.J. Webb, C. Zlotea, and V.A. Yartys, "Review of magnesium hydride-based materials: development and

- optimisation”, *Appl. Phys. A*, **122(97)**, (2016), 9602. <https://doi.org/10.1007/s00339-016-9602-0>
- [32] M. Tian, and C. Shang, “Mg-based composites for enhanced hydrogen storage performance.” *Int. Journal of Hydrogen Energy*, **44(1)**, (2019), 338-344. <https://doi.org/10.1016/j.ijhydene.2018.02.119>
- [33] J. Zhang, L.Q. Sun, Y.C. Zhou, and P. Peng, “Dehydrogenation Thermodynamics of Magnesium Hydride Doped with Transition Metals: Experimental and Theoretical Studies”, *Comput. Mater. Sci.*, **98**, (2015), 211–219. [10.1016/j.commatsci.2014.11.016](https://doi.org/10.1016/j.commatsci.2014.11.016)
- [34] J. Zhao, Q. Du, S. Zhou, and V. Kumar, “Endohedrally Doped Cage Clusters”, *Chem. Rev.*, **120 (17)**, (2020), 9021-9163. <https://doi.org/10.1021/acs.chemrev.9b00651>.
- [35] T. Husain, T.A. Maark, B. Pathak, and R. Ahuja, “Improvement in the hydrogen desorption from MgH<sub>2</sub> upon transition metals doping: a hybrid density functional calculation”, *AIP Adv.*, **3(10)**, (2013), 102117-1–102117-8. <https://doi.org/https://doi.org/10.1063/1.4826521>.
- [36] F. Kong, and Y. Hu, “Density functional study of small X doped Mg<sub>n</sub> (X=Fe, Co, Ni, n=1-9) bimetallic clusters: equilibrium structures, stabilities, electronic and magnetic properties”, *J. Mol. Model.*, **20(3)**, (2014), 2087(1-10). <https://doi.org/10.1007/s00894-014-2087-x>.
- [37] O.P. Charkin, and A.P. Maltsev, “Density Functional Theory Modeling of Reactions of Addition of H<sub>2</sub> Molecules to Magnesium Clusters Mg<sub>17</sub>M Doped with Atoms M of Transition 3d Elements”, *J. Phys. Chem. A.*, **125(11)**, (2021), 2308–2315. <https://doi.org/10.1021/acs.jpca.1c00211>.
- [38] R. Trivedi, and D. Bandyopadhyay, “Hydrogen storage in small size Mg<sub>n</sub>Co clusters: A density functional study”, *Int. J. Hydrogen Energy*, **40(37)**, (2015), 12727-12735. <https://doi.org/10.1016/j.ijhydene.2015.07.122>
- [39] R. Trivedi, and D. Bandyopadhyay, “Study of adsorption and dissociation pathway of H<sub>2</sub> molecule on Mg<sub>n</sub>Rh (n= 1–10) clusters: A first principle investigation”, *Int. J. hydrogen energy*, **41(44)**, (2016), 20113-20121. <https://doi.org/10.1016/j.ijhydene.2016.09.007>.

- [40] D. Bandyopadhyay, S. Chatterjee, R. Trivedi, and K. Dhaka, “Insights into catalytic behavior of  $\text{TiMg}_n$  ( $n=1-12$ ) nanoclusters in hydrogen storage and dissociation process: A DFT investigation”, *Int. J. Hydrogen Energy*, **47(27)**, (2022), 13418-13429. <https://doi.org/10.1016/j.ijhydene.2022.02.091>
- [41] S. Chatterjee, and D. Bandyopadhyay, “Insights into the Electronic Structure and Stability of  $\text{TiMg}_n$  ( $n=1-12$ ) Clusters: Validation of Electron Counting Rule”, *Materials Today Communications*, **32**, (2022), 103860. <https://doi.org/10.1016/j.mtcomm.2022.103860>
- [42] X. Ma, S. Liu, and S. Huang, “Hydrogen adsorption and dissociation on the TM doped ( $\text{TM}=\text{Ti, Nb}$ )  $\text{Mg}_{55}$  nanoclusters: a DFT study”, *Int. J. Hydrogen Energy*, **42(39)**, (2017), 24797-24810. <https://doi.org/10.1016/j.ijhydene.2017.08.086>.
- [43] T.J.D. Kumar, P. Tarakeshwar, and N. Balakrishnan, “Geometric and electronic structures of hydrogenated transition metal (Sc, Ti, Zr) Clusters”, *Phys. Rev. B.*, **79(20)**, (2009), 205415. <https://link.aps.org/doi/10.1103/PhysRevB.79.205415>
- [44] S. Yanagisawa, T. Tsuneda, and K. Hirao, “An Investigation of Density Functionals: The First-Row Transition Metal Dimer Calculations”, *J. Chem. Phys.*, **112(2)**, (2000), 545-553. <https://doi.org/10.1063/1.480546>.
- [45] L. Zeng, M.K. Liang, X.F. Wei, J. Guo, W. Dai, and B.C. Zhu, “New potential stable structures of  $\text{XMg}_n$  ( $X = \text{Ge, C, Sn}$ ;  $n = 2-12$ ) clusters:  $\text{XMg}_8$  with high stability”, *J. Phys.: Condens. Matter.*, **33(6)**, (2021), 065302. <https://dx.doi.org/10.1088/1361-648X/abc401>
- [46] G. Liang, J. Huot, S. Boily, A. Van Neste, and R. Schulz, “Catalytic effect of transition metals on hydrogen sorption in nanocrystalline ball milled  $\text{MgH}_2$ -TM ( $\text{TM}=\text{Ti, V, Mn, Fe and Ni}$ ) systems”, *J. Alloys and Compounds*, **292(1-2)**, (1999), 247-252. [https://doi.org/10.1016/S0925-8388\(99\)00442-9](https://doi.org/10.1016/S0925-8388(99)00442-9)
- [47] M. Pozzo, and D. Alfe, “Hydrogen dissociation and diffusion on transition metal (Ti, Zr, V, Fe, Ru, Co, Rh, Ni, Pd, Cu, Ag)- Doped Mg (0001) surfaces”, *Int. J. Hydrogen Energy.*, **34(4)**, (2009), 1922-1930. <https://doi.org/10.1016/j.ijhydene.2008.11.109>.

- [48] A.B. Philips, B.S. Shivaram, and G.R. Mynenib, "Hydrogen absorption at room temperature in nanoscale titanium benzene complexes", *Int. J. Hydrogen Energy.*, **37(2)**, (2012), 1546-1550. <https://doi.org/10.1016/j.ijhydene.2011.09.136>.
- [49] H. Lee, M.C. Nguyen, and J. Ihm, "Titanium functional group complexes for high capacity hydrogen storage materials", *Solid State Commun.*, **146(9-10)**, (2008), 431-434. <https://doi.org/10.1016/j.ssc.2008.03.018>
- [50] S. Banerjee, C.G.S. Pillai, and C. Majumder, "Adsorption and desorption of hydrogen in Mg nanoclusters: Combined effect of size and Ti doping", *Int. J. Hydrogen Energy*, **35(6)**, (2010), 2344-2350. <https://doi.org/10.1016/j.ijhydene.2009.12.176>
- [51] Y. Liu, L. Ren, Y. He, and H.P. Cheng, "Titanium decorated grapheme for high-capacity hydrogen storage studied by density functional simulations", *J. Phys. Cond. matt.*, **22(44)**, (2010), 445301. <https://doi.org/10.1088/0953-8984/22/44/445301>.
- [52] F. Zuliani, L. Bernasconi, and E.J. Baerends, "Titanium as a Potential Addition for High Capacity Hydrogen Astorage Medium", *J. Nanotech.*, **2012**, (2012), 831872. <https://doi.org/10.1155/2012/831872>.
- [53] C. Zhou, Z. Zak F., C. Ren, J. Li, and J. Lu, "Effect of Ti Intermetallic Catalysts on Hydrogen Storage Properties of Magnesium Hydride", *J. Phys. Chem. C*, **117(25)**, (2013), 12973-12980. <https://doi.org/10.1021/jp402770p>.
- [54] M. Calizzi, F. Venturi, M. Ponthieu, F. Cuevas, V. Morandi, T. Perkisas, S. Bals, and L. Pasquini, "Gas-phase synthesis of Mg-Ti nanoparticles for solid-state hydrogen storage." *Phys. Chem. Chem. Phys.* **18(1)**, (2016), 141-148. <https://doi.org/10.1039/c5cp03092g>
- [55] K. Asano, H. Kim, K. Sakaki, K. Jimura, S. Hayashi, Y. Nakamura, K. Ikeda, T. Otomo, A. Machida, and T. Watanuki, "Structural variation of self-organized Mg hydride nanoclusters in immiscible Ti matrix by hydrogenation", *Inorg. Chem.*, **57(18)**, (2018), 11831-11838. <https://doi.org/10.1021/acs.inorgchem.8b02015>
- [56] A. Baldi, R. Gremaud, D.M. Borsa, C.P. Balde, A.M.J. van der Eerden, G.L. Kruijtzter, P.E. de Jongh, B. Dam, and R. Griessen, "Nanoscale composition modulations in Mg<sub>y</sub>Ti<sub>1-y</sub>

- $y\text{H}_x$  thin film alloys for hydrogen storage”, *Int. J. Hydrogen Energy*, **34(3)**, (2009), 1450-1457. <https://doi.org/10.1016/j.ijhydene.2008.11.090>
- [57] W. Silva, T.N. Truong, and F. Mondragon, “Electronic characterization and reactivity of bimetallic clusters of the  $\text{Ti}(\text{Mg}_n)$  type for hydrogen storage applications”, *J. Alloys Comp.*, **509(34)**, (2011), 8501-8509. <https://doi.org/10.1016/j.jallcom.2011.06.022>.
- [58] L.L. Wang, and D.D. Johnson, “Hydrogen Desorption from Ti-Doped  $\text{MgH}_2$  (110) Surfaces: Catalytic Effect on Reaction Pathways and Kinetic Barriers”. *J. Phys. Chem. C*, **116(14)**, (2012), 7874–7878. <https://doi.org/10.1021/jp300794x>
- [59] D. Kyoï, T. Sato, E. R oennebro, N. Kitamura, A. Ueda, M. Ito, S. Katsuyama, S. Hara, D. Nor eus, and T. Sakai, “A new ternary magnesium–titanium hydride  $\text{Mg}_7\text{TiH}_n$  with hydrogen desorption properties better than both binary magnesium and titanium hydrides”, *J. Alloys. Comp.*, **372(1-2)**, (2004), 213–217. <https://doi.org/10.1016/j.jallcom.2003.08.098>
- [60] M.J. Frisch, G.W. Trucks, H.B. Schlegel, G.E. Scuseria, M.A. Robb, J.R. Cheeseman, G. Scalmani, V. Barone, B. Mennucci, G.A. Petersson, H. Nakatsuji, M. Caricat, X. Li, H.P. Hratchian, A.F. Izmaylov, J. Bloino, G. Zheng, J.L. Sonnenberg, M. Hada, M. Ehara, K. Toyota, R. Fukuda, J. Hasegawa, M. Ishida, T. Nakajima, Y. Honda, O. Kitao, H. Nakai, T. Vreven, Jr J.A. Montgomery, J.E. Peralta, F. Ogliaro, M. Bearpark, J.J. Heyd, E. Brothers, K.N. Kudin, V.N. Staroverov, T. Keith, R. Kobayashi, J. Normand, K. Raghavachari, A. Rendell, J. C. Burant, S.S. Iyengar, J. Tomasi, M. Cossi, N. Rega, J.M. Millam, M. Klene, J. E. Knox, J.B. Cross, V. Bakken, C. Adamo, J. Jaramillo, R. Gomperts, R.E. Stratmann, O. Yazyev, A.J. Austin, R. Cammi, C. Pomelli, J.W. Ochterski, R.L. Martin, K. Morokuma, V.G. Zakrzewski, G.A. Voth, P. Salvador, J.J. Dannenberg, S. Dapprich, A.D. Daniels, O. Farkas, J.B. Foresman, J.V. Ortiz, J. Cioslowski, D.J. Fox (2013) Gaussian’09, Revision D.01, Gaussian, Inc., Wallingford C.
- [61] A.D. Becke, "Density-functional exchange-energy approximation with correct asymptotic behavior", *Phys. Rev. A*, **38(6)**, (1988), 3098–3100. <https://doi.org/10.1103/physreva.38.3098>

- [62] C. Lee, W. Yang, and R.G. Parr, “Development of the Colle-Salvetti correlation energy formula into a functional of the electron density”, *Phys. Rev. B.*, **37(2)**, (1988), 785. <https://doi.org/10.1103/PhysRevB.37.785>.
- [63] T. Lu, and F. Chen, “Multiwfn: A multifunctional wavefunction analyzer”, *J. Comp. Chem.*, **33(5)**, (2011), 580-592. <https://doi.org/10.1002/jcc.22885>
- [64] T. Diedrich, T. Döppner, Th. Fennel, J. Tiggesbäumker, and K.H. Meiwes-Broer, “Shell structure of magnesium and other divalent metal clusters”, *Phys. Rev. A.*, **72(2)**, (2005), 3203-3214. <https://doi.org/10.1103/PhysRevA.72.023203>
- [65] T. Diedrich, T. Döppner, J. Braune, J. Tiggesbaumker, and K.H.M. Broer “Electron Delocalization in Magnesium Clusters Grown in Supercold Helium Droplets”, *Phys. Rev. Lett.*, **86(21)**, (2001), 4807. <https://doi.org/10.1103/PhysRevLett.86.4807>
- [66] Computational Chemistry Comparison and Benchmark Data Base Std. Ref database 101, National Institute of Standards and Technology (NIST) USA (2020). <https://cccbdb.nist.gov>
- [67] B. Boruah, and B. Kalita, “Exploring enhanced hydrogen adsorption on Ti doped Al nanoclusters: A DFT study”, *J. Chem. Phys.*, **518**, (2019), 123-133. <https://doi.org/10.1016/j.chemphys.2018.04.018>



## CHAPTER-6

---

### HYDROGEN STORAGE ON MgO SUPPORTED $TiMg_n$ ( $n=2-6$ ) CLUSTERS: A FIRST PRINCIPLE INVESTIGATION

#### *6.1 Introduction*

Hydrogen is a promising clean energy source for a sustainable future because it is abundant, versatile, and produces no greenhouse gas emissions upon combustion. However, efficient and safe hydrogen storage remains a significant challenge in realizing its widespread adoption. Conventional storage methods, such as compressed gas and liquid hydrogen, have an energy density limit, safety and cost limitations. Therefore, the search for alternative hydrogen storage materials with high gravimetric and volumetric storage capacities has been the subject of intense research in recent years. One promising hydrogen storage approach is using supported clusters. A thin metal or metal oxide sheet as substrate forms a nanocluster support material. Usually, a nanocluster has a high surface-to-volume ratio and tunable electronic and chemical properties. The supported system provides stability to the nanocluster and enhances its stability. The system could be useful as a support to nanoclusters and to store hydrogen gas in atomic or molecular form. In this context, the MgO substrate is a platform to support a cluster. The enhanced stability of the cluster can efficiently help to adsorb hydrogen molecules (physisorption) and split hydrogen molecules to store them in an atomic form in the reactive sites of the clusters by diffusion (chemisorption).

Additionally, using such materials may offer benefits such as increased stability and reduced weight, making them attractive for practical hydrogen storage applications. Using supported clusters offers several advantages over other materials in hydrogen storage, such as high gravimetric and volumetric storage capacities, fast hydrogen adsorption and desorption kinetics, and low hydrogen dissociation energy barriers. Literature advocates numerous studies on hydrogen kinetics on pure and doped metal nanoclusters [1-3]. Transition metal-doped clusters are reported to show favorable electronic and chemical properties for hydrogen storage [4-8]. Enhancement of reactivity due to the catalytic effect of graphene support on metal clusters has been reported before. Intayot et al. [9] reported that  $Ti_4$  B-Gr could adsorb

eight H<sub>2</sub> molecules and six reversible hydrogen adsorption stages. Chen et al. [10] wrote the hydrogen storage capacity of Pt<sub>4</sub> clusters supported by B or N-doped graphene sheets is the most promising. Graphene-supported Pt<sub>n</sub> nanoclusters are an excellent system for hydrogen storage reported by several groups [11, 12]. Hussain et al. [13] studied Pd<sub>n</sub>/hexabenzocoronene system and noted that Pd<sub>8</sub> hexabenzocoronene has the highest adsorption energy, whereas supported Pd<sub>7</sub> and Pd<sub>10</sub> systems have favorable electronic properties. Fadlallah et al. [14] reported hydrogen storage properties of graphene-supported Ni<sub>6</sub> and Ni<sub>13</sub> clusters. After substrate support, the adsorption energy enhances from 0.1 eV of free groups to 0.36 eV for supported Ni<sub>6</sub> and 0.41 eV for supported Ni<sub>13</sub>. Hydrogenation and hydrogen kinetics of Cu<sub>n</sub> clusters on Cu (111) substrate reported that Cu<sub>5</sub> undergoes substantial structural changes in chemisorption and catalyzes H<sub>2</sub> dissociation [15]. Kantorovich et al. [16] reported an experimental and DFT study of the nucleation characteristics of Mg<sub>n</sub> clusters on the MgO surface; it is said that the adsorption energy of a single Mg atom is largest when they are adsorbed at the step edges. The study of MgO substrates, both rectangular and graphene-like sheets, has been reported by Zhang et al. [17]. Graphene, like MgO monolayer, is a well-established substrate reported by many authors in the past [18-21]. The studies on MgO substrate-supported Ti-doped Mg<sub>n</sub> clusters have yet to be reported. This chapter presents the DFT-based modeling of the possibility of the finite-sized MgO-supported TiMg<sub>n</sub> (n=2-6) clusters for hydrogen storage. In the later section of the chapter, we discuss the properties and advantages of supported nanoclusters for hydrogen storage compared to hydrogen storage by bare clusters.

## ***6.2 Computational Methodology***

Computational in the presented work is self-consistent-field (SCF) electronic structure calculations on all clusters within the density functional theory (DFT) framework. During the calculations, molecular orbitals (MO) are expressed as a linear combination of atom-centered basis functions for which the LanL2DZ inbuilt in the Gaussian'09 program package [22] is used. Spin-polarized calculations use the Becke three-parameter exchange and the Lee, Yang, and Parr generalized gradient approximation (GGA), popularly known as B3LYP functional [23, 24] is used. As a preliminary step, geometry optimization was performed, and harmonic

vibrational frequency calculations were computed for the clusters to ensure that the clusters were global minima in each size range. All geometries were optimized with unconstrained symmetry starting from the different initial configurations to avoid the minimum surface potential energy lock. For the evaluation of VIP, VEA, chemical hardness, and chemical potential, the Koopmans method [25] is adopted.

### **6.3 Results and Discussions**

We have reported before the catalytic effect of the  $\text{TiMg}_n$  cluster in the hydrogen adsorption-desorption process [26]. In the present study, we have used substrate-supported  $\text{Mg}_n$  and  $\text{TiMg}_n$  ( $n=2-6$ ) clusters as hydrogen storage systems. Rectangular finite size  $\text{Mg}_{18}\text{O}_{18}$  substrate ( $10.12\text{\AA} \times 10.12\text{\AA}$ ) is selected as the optimum size to support the  $\text{Mg}_n$  ( $n=2-6$ ) and  $\text{TiMg}_n$  ( $n=2-6$ ) nanoclusters. The optimized  $\text{Mg}_{18}\text{O}_{18}$  finite-size substrate gets optimized to a uniformly curved substrate. The study of curved graphene substrate-supported systems was reported earlier [27] as a better substrate for energy storage. We have chosen a non-hydrogen terminated rectangular- $\text{Mg}_{18}\text{O}_{18}$  (Fig. 6.1) substrate to support the  $\text{Mg}_n$  and  $\text{TiMg}_n$  ( $n=2-6$ ) clusters. In addition, we have also studied the other optimized rectangular substrates. It is to be noted that the optimized substrate with hydrogen termination does not have any regular smooth surface, as shown in Fig. 6.2. Therefore, we have considered  $\text{Mg}_{18}\text{O}_{18}$  as the substrate in the present substrate supported clusters for hydrogen storage. After complete optimization of the substrate, a uniform bend is observed without any bond length variation. Due to the finite size of the substrate, the edge effect produces unsaturated strain over the surface and causes bending. By periodic repetition of the surface, one could get rid of bending. However, to support the small nanocluster, the part of the surface used is much smaller than the total surface area. Hence, we can expect similar adsorption energies and other chemical and thermodynamic properties in the case of a large substrate. The optimized substrate-supported pure and hydrogenated cluster systems are shown in Fig. 6.3. The optimized substrate-supported Ti doped and Ti doped hydrogenated cluster systems are shown in Fig. 6.4. It is reported that the  $\text{TiMg}_5$  cluster is the most promising hydrogen storage cluster in the small size range [26, 28], and  $\text{TiMg}_8$  is the most stable magic cluster among  $\text{TiMg}_n$  ( $n=2-12$ ) clusters

[28]. In the present study, we have used a finite-sized MgO substrate ( $\text{Mg}_{18}\text{O}_{18}$ ) to enhance the stability of the bare cluster and use it for hydrogen adsorption reaction by

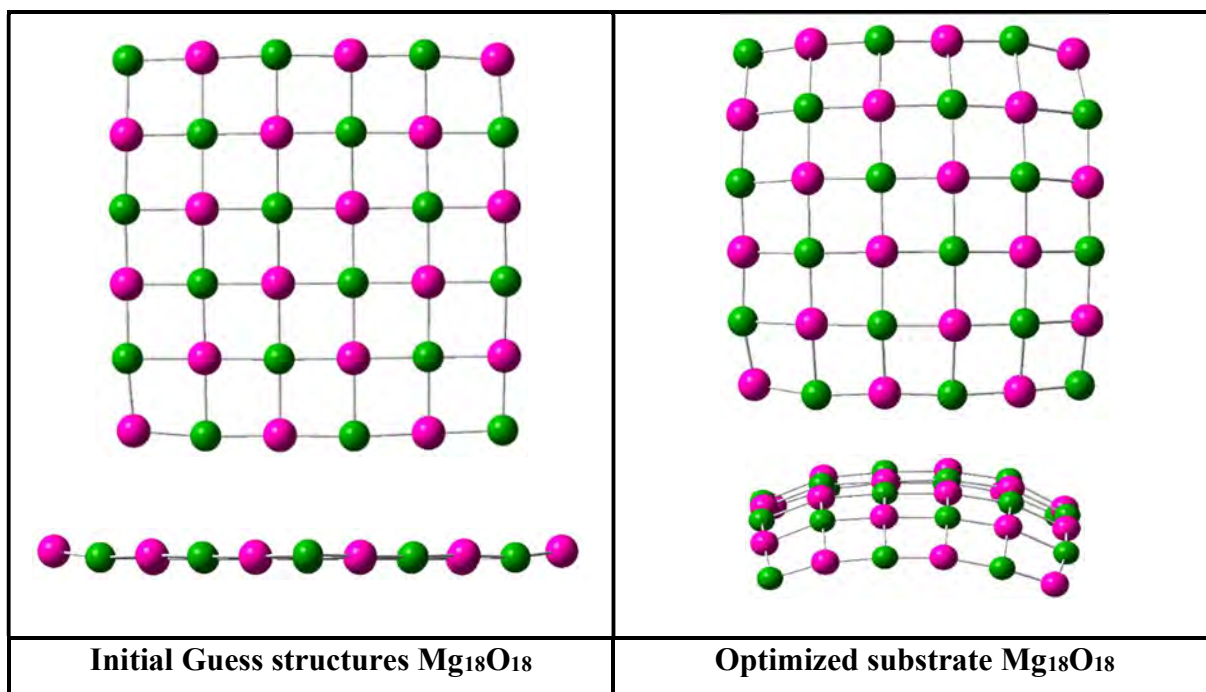


Fig. 6.1 Rectangular  $\text{Mg}_{18}\text{O}_{18}$  substrate. Here, Mg atoms are shaded as pink and oxygen atoms are shaded as green.

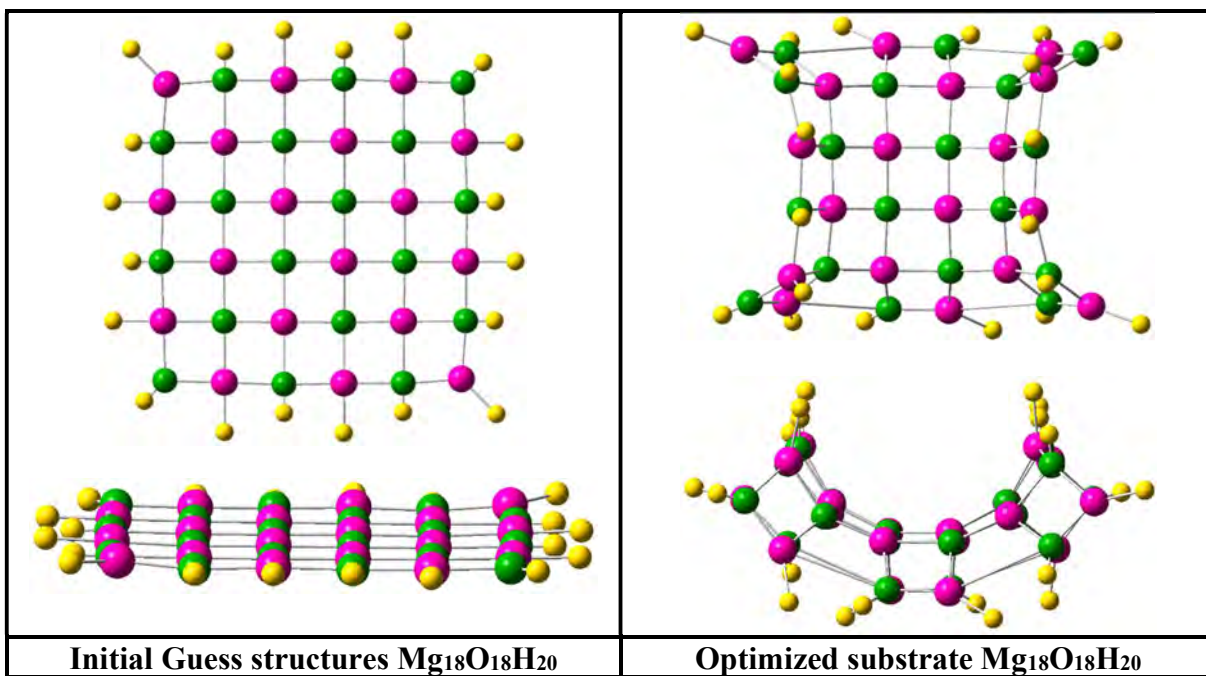


Fig. 6.2 Other substrates. Here, Mg atoms are shaded as pink, oxygen atoms are shaded as green and hydrogen atoms are shaded as yellow.

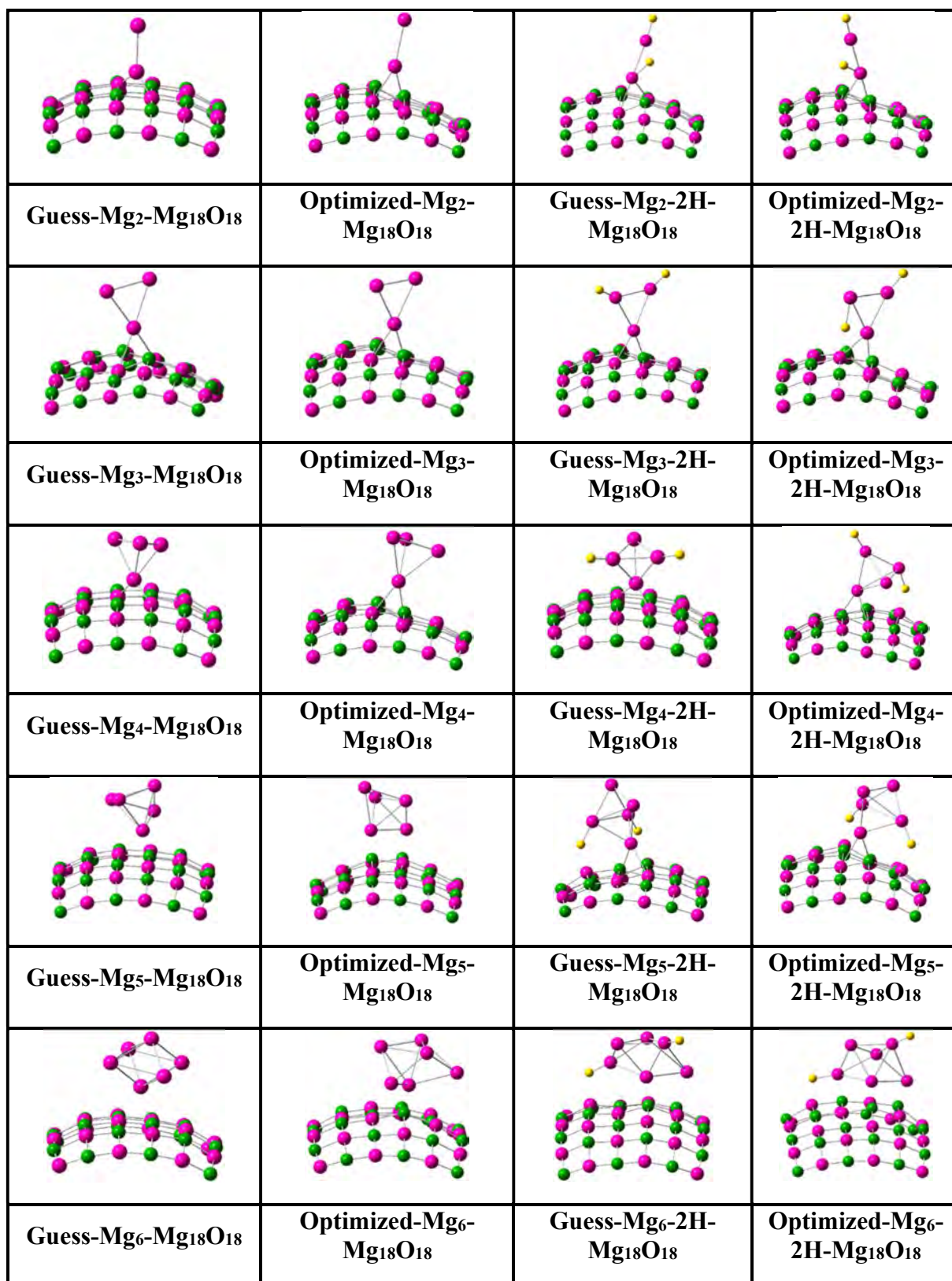


Fig. 6.3 Guess and optimized substrate supported pure Mg<sub>n</sub> and Mg<sub>n</sub>-2H clusters system.

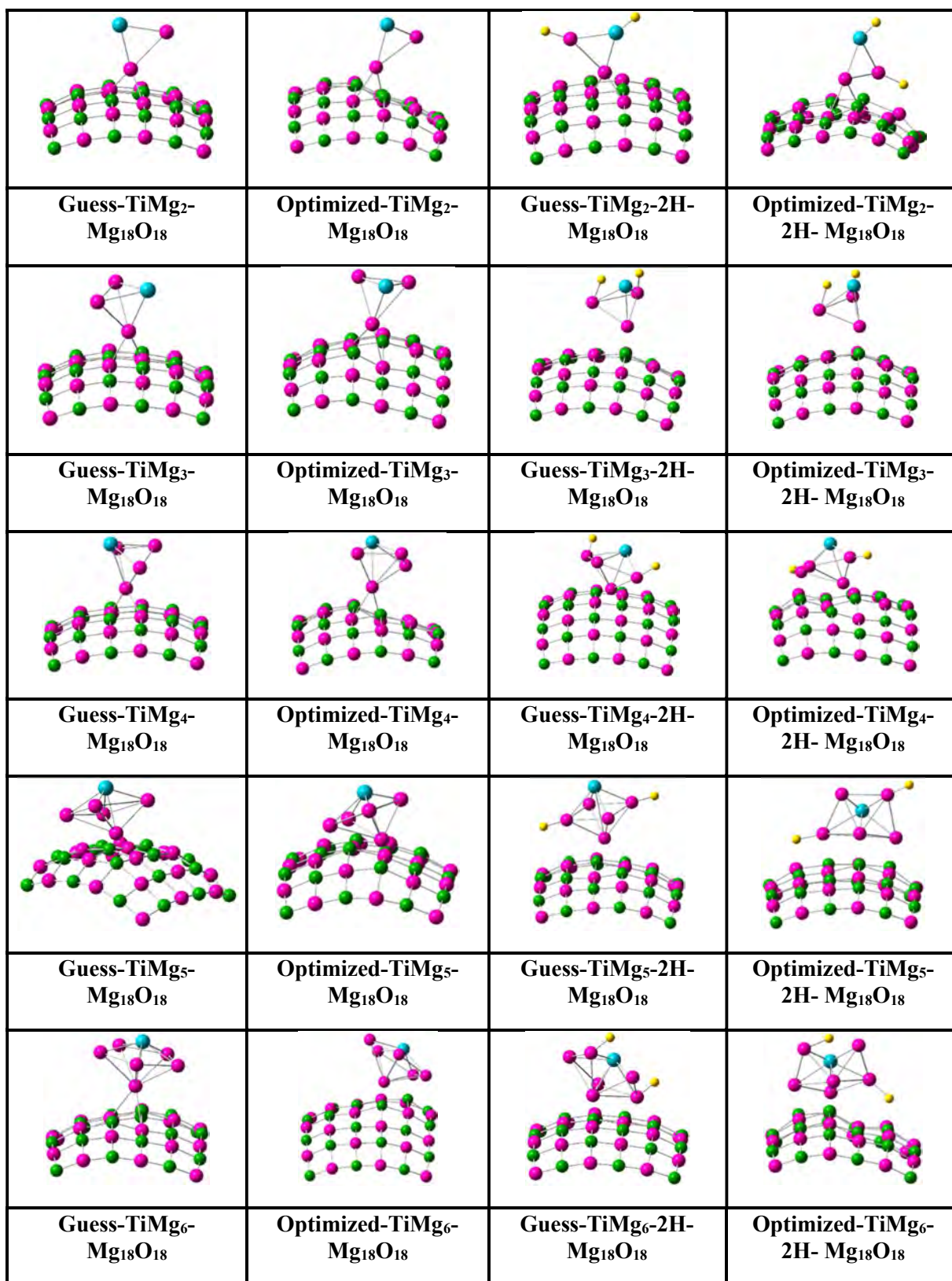


Fig. 6.4 Guess and optimized substrate supported pure TiMg<sub>n</sub> and TiMg<sub>n</sub>-2H clusters system.

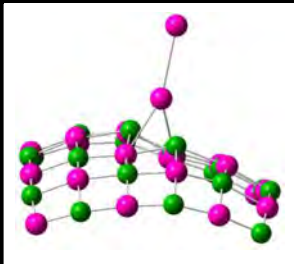
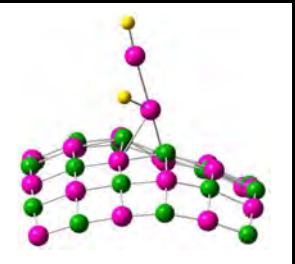
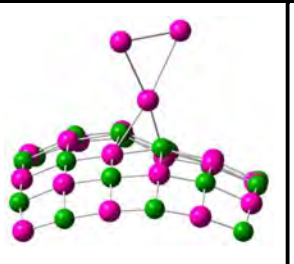

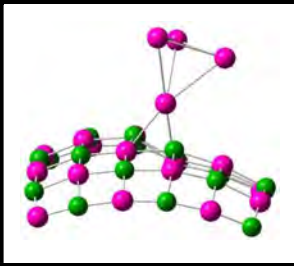
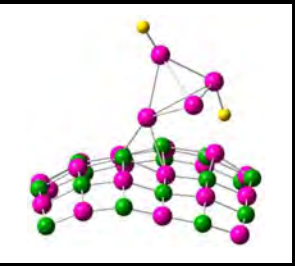
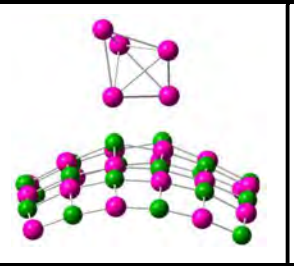
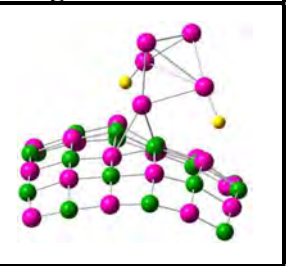
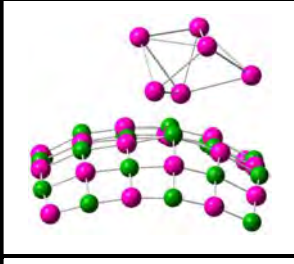
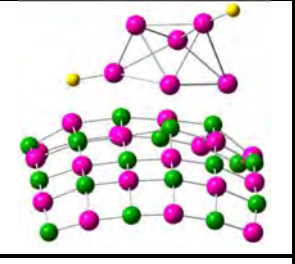
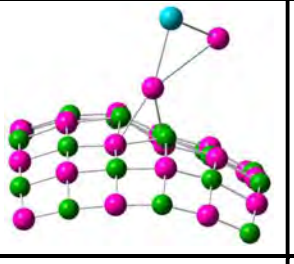
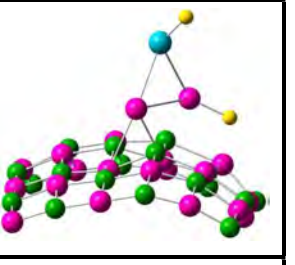
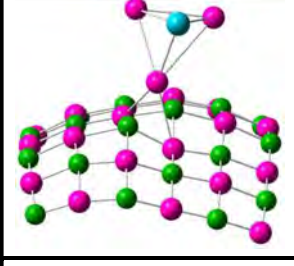
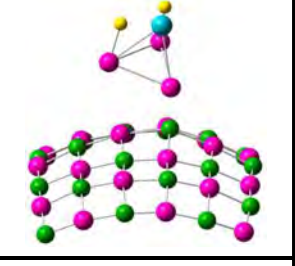
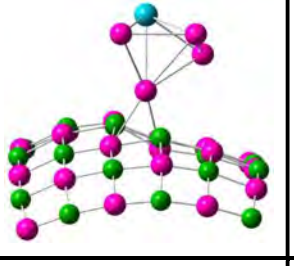
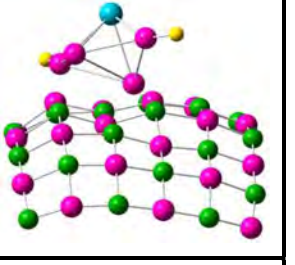
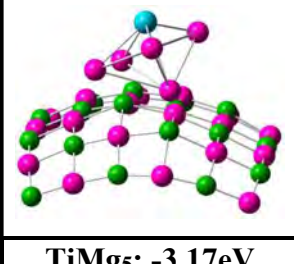
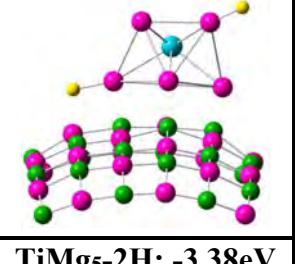
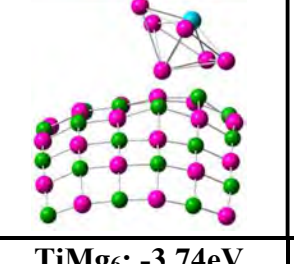
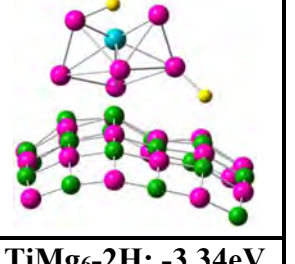
			
<b>Mg<sub>2</sub>: -0.59eV</b>	<b>Mg<sub>2</sub>-2H: -2.52eV</b>	<b>Mg<sub>3</sub>: -0.43eV</b>	<b>Mg<sub>3</sub>-2H: -2.97eV</b>
			
<b>Mg<sub>4</sub>: -0.51eV</b>	<b>Mg<sub>4</sub>-2H: -2.69eV</b>	<b>Mg<sub>5</sub>: -1.71eV</b>	<b>Mg<sub>5</sub>-2H: -2.87eV</b>
			
<b>Mg<sub>6</sub>: -1.23eV</b>	<b>Mg<sub>6</sub>-2H: -3.74eV</b>	<b>TiMg<sub>2</sub>: -2.42eV</b>	<b>TiMg<sub>2</sub>-2H: -3.06eV</b>
			
<b>TiMg<sub>3</sub>: -2.19eV</b>	<b>TiMg<sub>3</sub>-2H: -3.13eV</b>	<b>TiMg<sub>4</sub>: -2.15eV</b>	<b>TiMg<sub>4</sub>-2H: -3.25eV</b>
			
<b>TiMg<sub>5</sub>: -3.17eV</b>	<b>TiMg<sub>5</sub>-2H: -3.38eV</b>	<b>TiMg<sub>6</sub>: -3.74eV</b>	<b>TiMg<sub>6</sub>-2H: -3.34eV</b>

Fig. 6.5 Mg<sub>18</sub>O<sub>18</sub> substrate supported Mg<sub>n</sub>, TiMg<sub>n</sub>, Mg<sub>n</sub>-2H, TiMg<sub>n</sub>-2H clusters, E<sub>ads</sub> energy(eV) between the substrate and clusters Mg<sub>n</sub> and TiMg<sub>n</sub>; E<sub>ads-H</sub> energy between the supported clusters and adsorbed hydrogen. Here, Mg atoms are colored by pink, oxygen atoms are shaded as green, Ti as blue and hydrogen as yellow.

calculating different parameters, like, cluster-adsorption energy ( $E_{ads}$ ), hydrogen-adsorption in supported cluster system ( $E_{ads-H}$ ), stability, HOMO-LUMO gap, vertical ionization potential (VIP), vertical electron affinity (VEA), chemical hardness ( $\eta$ ), and chemical potential ( $\mu$ ). In addition, the gravimetric density for the maximum number of hydrogen adsorption in bare  $TiMg_5$  and substrate-supported  $TiMg_5$  clusters has also been presented. The activation barrier for successive  $H_2$  adsorption using the TS Bery transition state has been presented. Fig. 6.5 represents the substrate supported  $Mg_n$ ,  $TiMg_n$ ,  $Mg_n-2H$ ,  $TiMg_n-2H$  clusters,  $E_{ads}$  energy(eV) between the substrate and clusters  $Mg_n$  and  $TiMg_n$ ;  $E_{ads-H}$  energy between the supported clusters and adsorbed hydrogen.

### 6.3.1. Adsorption/ Desorption Energies

In the present report, we have studied two different adsorption energies. The first is the adsorption energy between the substrate and the cluster ( $E_{ads}$ ), and the 2<sup>nd</sup> one is the hydrogen adsorption energy to the supported-cluster system ( $E_{ads-H}$ ). The adsorption energy ( $E_{ads}$ ) is supplied to an adsorbed cluster to be desorbed from the substrate. With the above definition, different adsorption energies are presented in the equations (6.1-6.3).

$$E_{ads} = E_{cluster+substrate} - (E_{cluster} + E_{substrate}) \quad (6.1)$$

$$E_{ads-H} = E_{Mg_n-2H+substrate} - (E_{Mg_n+substrate} + E_{H_2}) \quad (6.2)$$

$$E_{ads-H} = E_{TiMg_n-2H+substrate} - (E_{TiMg_n+substrate} + E_{H_2}) \quad (6.3)$$

The variation of hydrogen adsorption energies of different substrate-supported cluster systems is shown in Fig. 6.6 with the variation of the cluster size  $n$ . As per the above definition, negative adsorption energy implies enhanced stability. The supported Ti-doped  $Mg_5$  cluster also shows a drastic decrease in adsorption energy, although it does not hold a dip in adsorption energy. These adsorption energies are much lower than those for supported  $Mg_4$ ,  $Mg_5$  and  $Mg_6$  clusters. The supported  $Mg_n-2H$  cluster system variation for hydrogenated groups shows a local dip on  $n=3$ . For  $n=4$  and 5, the adsorption energies decrease rapidly. The behavior of adsorption energy of supported  $TiMg_n-2H$  cluster system shows a typical decreasing nature of graph with a visible local dip on  $n=5$ .

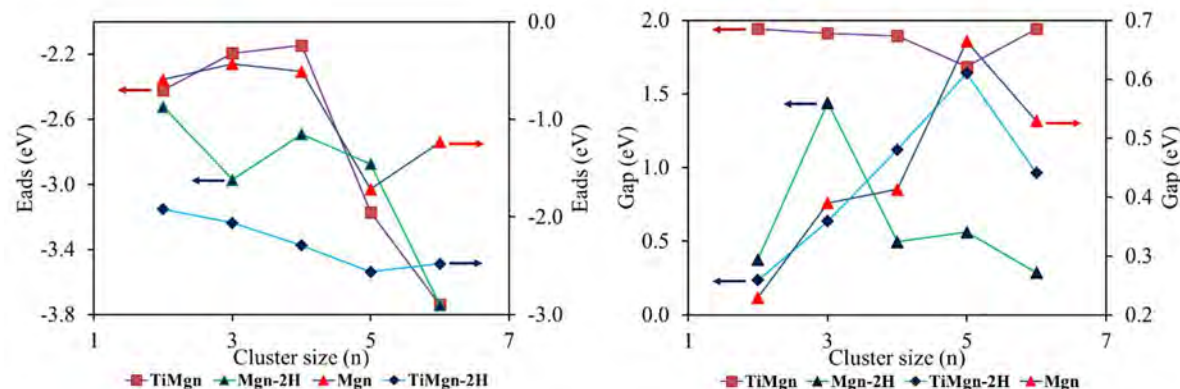


### 6.3.2 HOMO-LUMO Gap

HOMO- LUMO gap for supported clusters is calculated [13] using equation (6.4),

$$\Delta E_{gap} = (E_{LUMO} - E_{HOMO}) \quad (6.4)$$

Fig. 6.6 Shows the variation of the HOMO-LUMO gap of the substrate ( $Mg_{18}O_{18}$ ) supported  $Mg_n$ ,  $Mg_n$ -2H,  $TiMg_n$ , and  $TiMg_n$ -2H cluster with the increase of cluster size ( $n=2-6$ ).

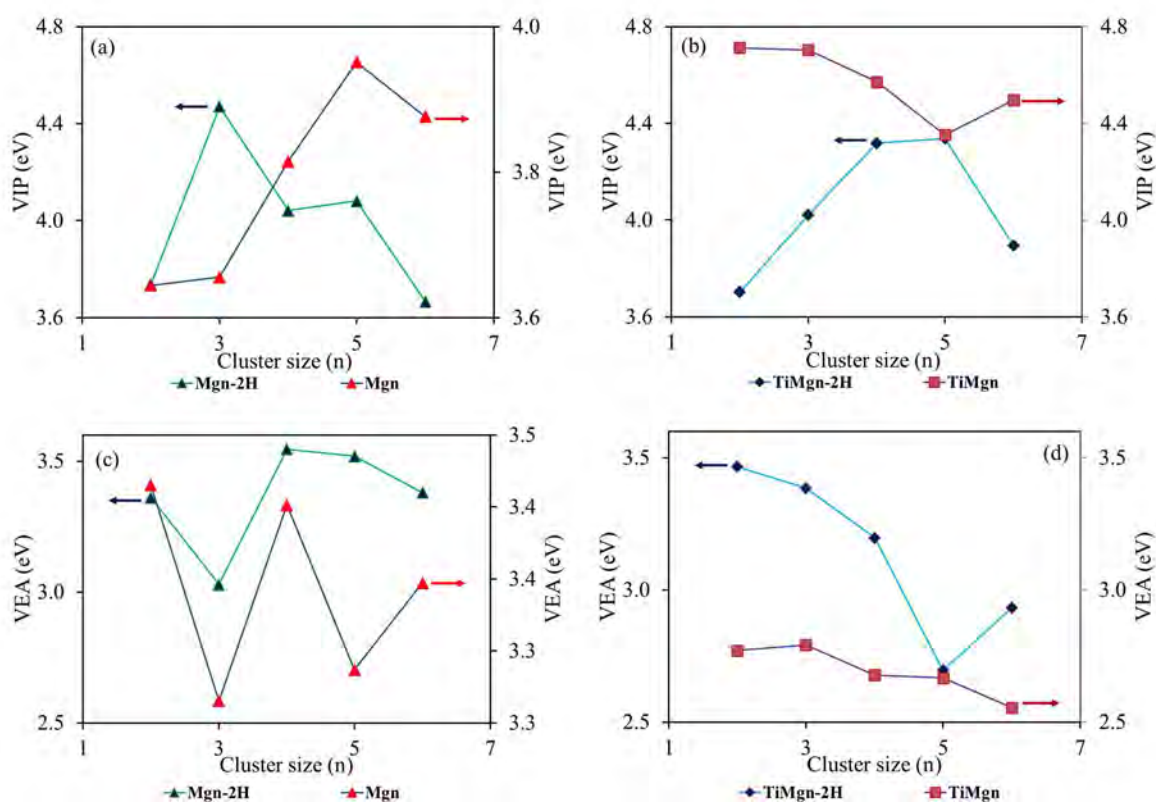


**Fig. 6.6** Variation of adsorption energy and HOMO-LUMO gaps of supported  $Mg_n$ ,  $Mg_n$ -2H,  $TiMg_n$  and  $TiMg_n$ -2H clusters system.

It is known that the higher the HOMO-LUMO gap, the higher the stability. Fig. 6.6 shows the variation of the HOMO-LUMO gap of supported  $Mg_n$  clusters. The local peak at  $n=5$  indicates the enhanced stability of this size. Next, the supported  $Mg_n$ -2H cluster system series has local maxima at  $n=3$  and  $5$ . Hence these two systems are stable. Variations of the HOMO-LUMO gap (H-L gap) of the supported  $TiMg_n$  ( $n=2-6$ ) systems show a decreasing nature and a local dip at  $n=5$ . It indicates that the H-L gap of supported  $TiMg_5$  before storing hydrogen possesses local minima, but the same holds local maxima just after storing hydrogen. Thus, the bare  $TiMg_5$  was reactive before hydrogen storage due to the presence of reactive sites, and hence it is very promising for hydrogen storage. After hydrogenation, the supported  $TiMg_5$ -2H system becomes more stable with fewer reactive sites. It indicates that the substrate-supported  $TiMg_5$  can store relatively higher doses of hydrogen. Sometimes with the increase in the number of atoms, the nature of variation of the H-L gap decreases because of the higher orbital overlapping. For this reason, the variation of the H-L gap may not be an excellent choice to understand the system property. For these systems, the study of VIP, VEA, chemical hardness, and chemical potential is recommended to get a clearer picture.

### 6.3.3 Vertical Ionization Potential (VIP), Vertical Electron Affinity (VEA), Chemical Hardness ( $\eta$ ) and Chemical Potential ( $\mu$ )

By definition, vertical ionization potential (VIP) is the energy needed when an electron is detached from the neutral system. Thus, the higher the value of the VIP, the higher the system's stability will be, as more energy is needed to detach an electron from the system. Again, vertical electron affinity (VEA) can be defined as the amount of energy liberated when an electron is added to the system. By definition, the higher the vertical electron affinity higher will be the electron affinity means the system will be less stable and more reactive. VIP and VEA can be defined following the Koopmans method [25]:  $VIP = -E_{HOMO}$  and  $VEA = -E_{LUMO}$



**Fig. 6.7** Variation of VIP and VEA of different supported clusters: (a) VIP of supported Mg<sub>n</sub> and Mg<sub>n</sub>-2H, (b) VIP of supported TiMg<sub>n</sub> and TiMg<sub>n</sub>-2H, (c) VEA of supported Mg<sub>n</sub> and Mg<sub>n</sub>-2H, (d) VEA of supported TiMg<sub>n</sub> and TiMg<sub>n</sub>-2H.

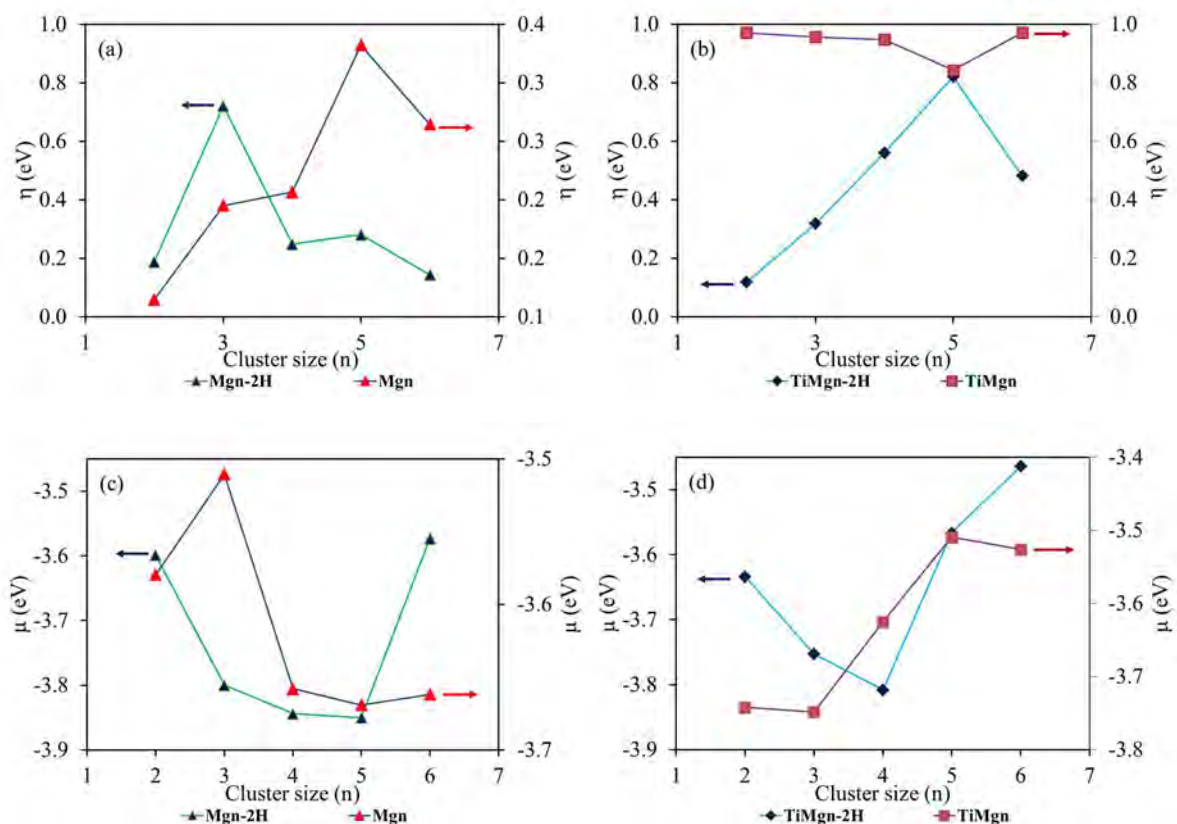
The variation of VIP of different substrate-supported clusters with the cluster size is shown in Fig. 6.7(a-b). The presence of local maxima in Fig. 6.7(a) supports the higher stability of supported Mg<sub>n</sub> and Mg<sub>n</sub>-2H clusters. However, there is a local dip at n=5 in supported TiMg<sub>n</sub> represents lower stability with better reactivity and is hence useful for hydrogen storage. We

found a local maxima in VIP after hydrogen adsorption in supported TiMg<sub>5</sub>-2H. Variation of VEA of supported Mg<sub>n</sub> and Mg<sub>n</sub>-2H shows the opposite nature at n=5 compared to VIP. The variation of VEA of supported TiMg<sub>n</sub>-2H shows local minima at n=5. As we know, the lower the VEA, means lower the electron affinity and the higher the chemical stability. Thus, the supported TiMg<sub>n</sub>-2H cluster system is showing higher stability. The supported TiMg<sub>n</sub> clusters show a decreasing trend in VEA. The supported TiMg<sub>n</sub>-2H is showing local dip in supported TiMg<sub>5</sub>-2H system with a decreasing nature of the VEA graph, indicates higher stability. This is because of the presence of reactive sites over the surface of the bare TiMg<sub>5</sub> cluster.

Next, we studied the supported systems' chemical potential and hardness. Using the Koopmans method [25], chemical potential ( $\mu$ ) and chemical hardness ( $\eta$ ) can be expressed as follows:

$$\mu = -(E_{HOMO} + E_{LUMO})/2; \eta = (E_{HOMO} - E_{LUMO})/2 \quad (6.5)$$

The higher the chemical potential value, the higher the reactivity and the lower the system's stability. Chemical hardness can be addressed as the resistance to exchange the number of electrons. The higher the chemical hardness value, the higher the chemical inertness, meaning higher system stability. After hydrogen adsorption onto both the supported Mg<sub>5</sub> and TiMg<sub>5</sub> clusters, there are local maxima in chemical hardness. Chemical hardness measures the resistance of a system to changes in electron density, or in other words, it measures the hardness of the electron clouds to penetrate it for reaction and the presence of local maxima or minima is the measure of the hardness. The local peak in chemical hardness could imply a more stable and less reactive state, indicating a certain level of chemical stability brought about by hydrogen adsorption. The variation of  $\mu$  and  $\eta$  with the cluster size is shown in Fig. 6.8. From Fig. 6.8(a) and 6.8(b), the local maxima of all supported clusters at n=5 except supported TiMg<sub>5</sub> show that it is relatively less chemically stable. The variation of chemical potential for Mg<sub>n</sub> and Mg<sub>n</sub>-2H also supports the results we obtained from the chemical hardness variation. However, the behavior of supported TiMg<sub>n</sub>-2H is not the same. A higher value of chemical potential (Fig. 6.8d) for supported TiMg<sub>n</sub>-2H represents more ability to adsorb hydrogens. After the hydrogenation of the substrate-supported TiMg<sub>5</sub> cluster i.e., supported TiMg<sub>5</sub>-2H got a local peak in chemical hardness and possessed higher stability. All calculated parameters are presented in Table 6.1.

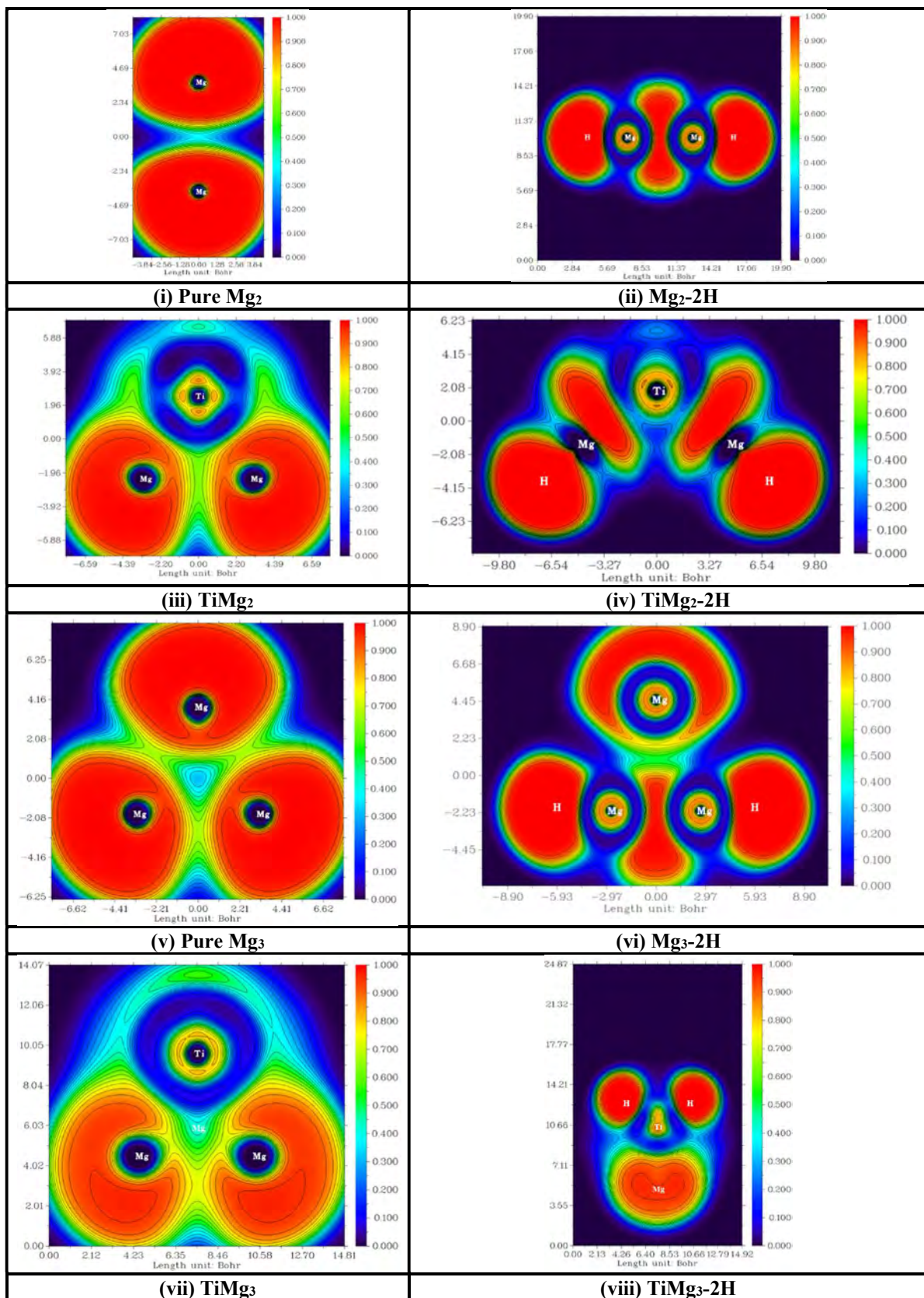


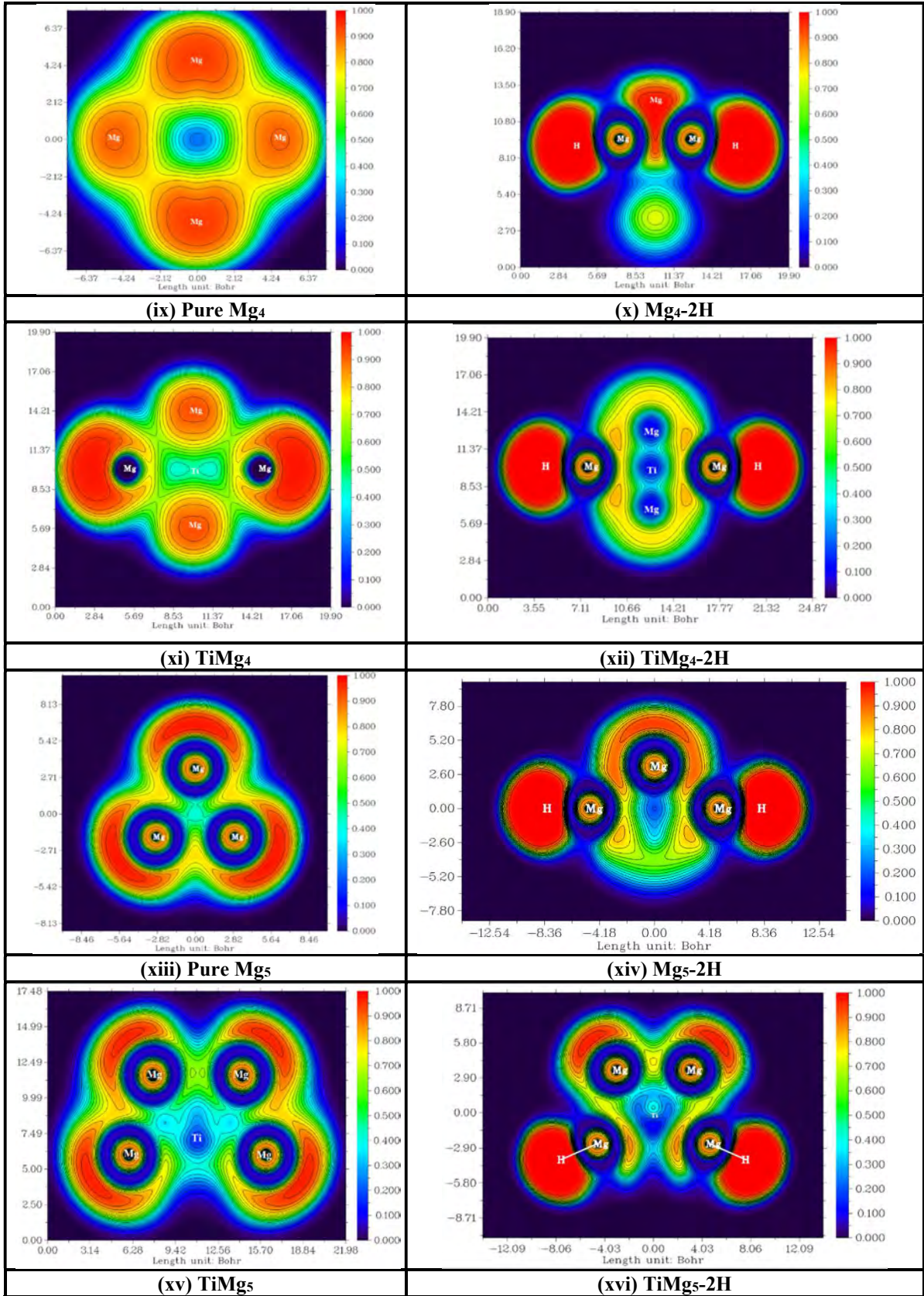
**Fig. 6.8** Variation of  $\mu$  and  $\eta$  of different supported clusters: (a)  $\eta$  of supported  $Mg_n$  and  $Mg_n-2H$ , (b)  $\eta$  of supported  $TiMg_n$  and  $TiMg_n-2H$ , (c)  $\mu$  of supported  $Mg_n$  and  $Mg_n-2H$ , (d)  $\mu$  of supported  $TiMg_n$  and  $TiMg_n-2H$ .

Now it can be seen clearly from the parameters' behavior after hydrogenation that the supported  $TiMg_5$  cluster system becomes stable. Since it has less reactivity, one may conclude that the number of reactive sites has decreased after hydrogenation. In the bare  $TiMg_5-2H$  cluster, a local minima was reported before [26, 28], and we found that the  $n=5$  size is a promising cluster as a hydrogen storage. When the substrate supports the cluster  $TiMg_5-2H$ , it holds local maxima in chemical hardness and becomes thermodynamically very stable with specific reactivity, which helps in further hydrogenation or extra hydrogenation. This is explained in the next section.

### 6.3.4 Electron Localization Functions (ELF)

Electron localization function (ELF) indicates the presence of localized electron pairs on the surface of the cluster or system. The calculated 2D-ELF maps of clusters are shown in Fig. 6.9. From the ELF study, one can have a clear picture of the probability of finding an electron pair with two opposite signs on the surface of the cluster or any molecular system.





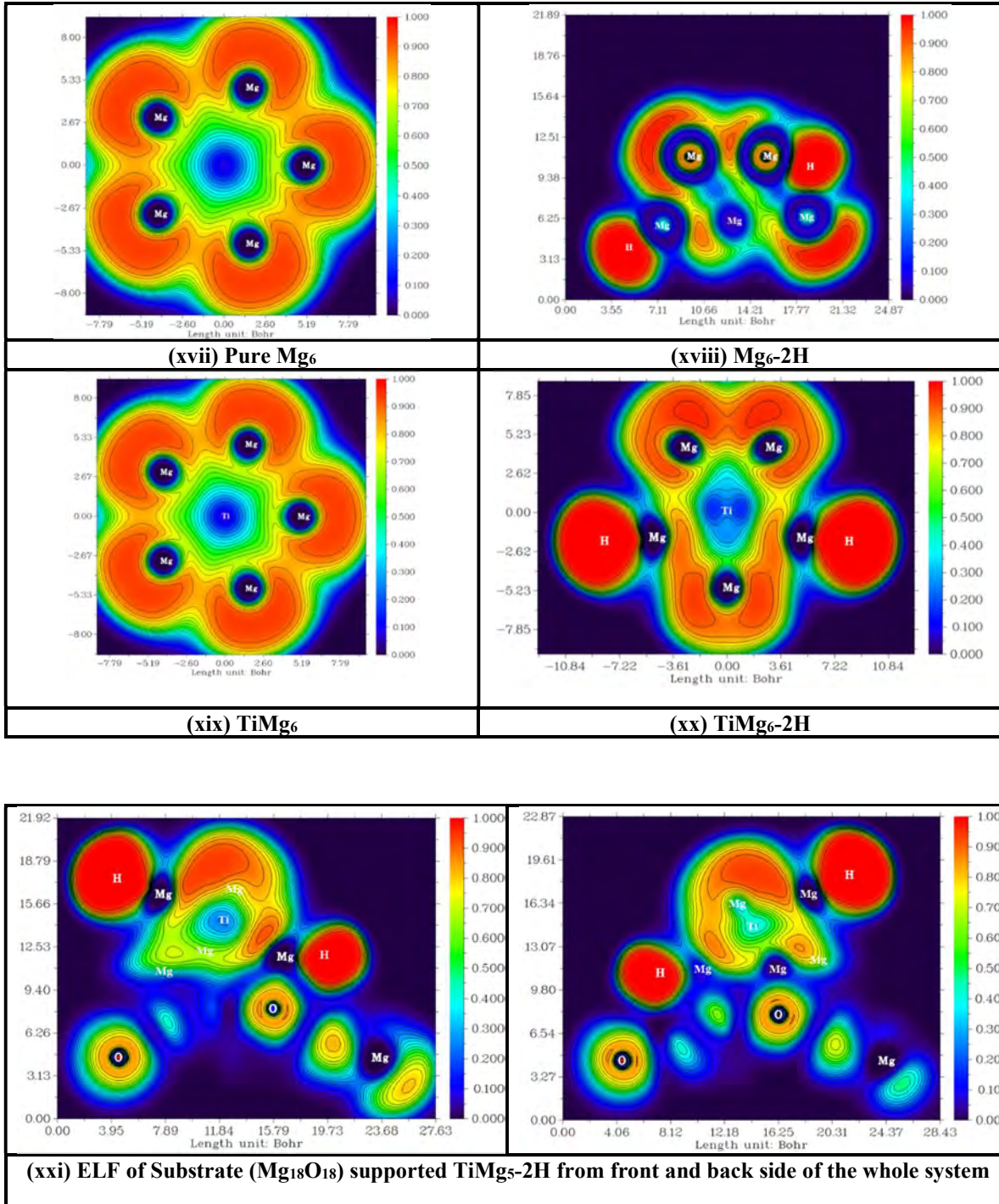


Fig. 6.9 The nature of electron Localization (ELF) of different pure  $Mg_n$ , hydrogenated pure  $Mg_n$ , Ti-doped  $Mg_n$  and hydrogenated Ti-doped  $Mg_n$  clusters ( $n=2-6$ ). Fig. 6.9 (i), (ii), (iii), (iv) represent the ELF of pure  $Mg_2$ ,  $Mg_2-2H$ ,  $TiMg_2$  and  $TiMg_2-2H$  clusters respectively. Fig. 6.9 (v), (vi), (vii), (viii) represent the ELF of pure  $Mg_3$ ,  $Mg_3-2H$ ,  $TiMg_3$  and  $TiMg_3-2H$  clusters respectively. Fig. 6.9 (ix), (x), (xi), (xii) represent the ELF of pure  $Mg_4$ ,  $Mg_4-2H$ ,  $TiMg_4$  and  $TiMg_4-2H$  clusters respectively. Fig. 6.9 (xiii), (xiv), (xv), (xvi) represent the ELF of pure  $Mg_5$ ,  $Mg_5-2H$ ,  $TiMg_5$  and  $TiMg_5-2H$  clusters respectively. Fig. 6.9 (xvii), (xviii),

(xix), (xx) represent the ELF of pure Mg<sub>6</sub>, Mg<sub>6</sub>-2H, TiMg<sub>6</sub> and TiMg<sub>6</sub>-2H clusters respectively. Fig. 6.9 (xxi) represent the ELF of the substrate supported TiMg<sub>5</sub>-2H from front and back side of the whole system.

These electron pairs present on the surface of the molecular system can interact with the other electrons outside of the surface region. Thus, the stronger the presence of an electron pair, the higher will be the reactivity at that particular site of a particular cluster or molecular system. ELF can be defined as

$$ELF(r) = \frac{1}{1 + \chi^2(r)}; \chi(r) = \frac{D(r)}{D_h(r)} \quad (6.6)$$

It can be seen that an ELF map contains different coloured regions as red, green, blue etc. Different colours in ELF map holds different meaning. The region where ELF value ranges 0-0.4 is shaded as blue it means there is absence of electron pair or very weak electron pair localization. The region shaded as green represent the region is with metallic bonding and here, the ELF value ranges from 0.5 to 0.8. Next, the reddish or prominent red region in the ELF map represents the presence of strong electron pair localization. This region is reactive in nature and here the ELF ranges from 0.9 to 1.0. These reactive regions are helpful for hydrogen storage. The 2D ELF map of different clusters and substrate-supported clusters is plotted using the open-source software/code Multiwfn.

### 6.3.5 Hydrogen Dissociation and Drifting of Hydrogen Atoms to the Reactive Sites

In this section, we have studied different steps of hydrogen splitting and diffusion of the hydrogen atoms to the reactive sites. These reactive sites are calculated based on the Electron Localization Function (ELF) using the Multiwfn program [29]. The reactive sites are represented in (Fig. 6.10). First, the hydrogen molecule adsorbed by the Ti atom in supported-cluster as shown in Fig. 6.10(a). Due to the interaction of adsorbed hydrogen with the reactive sites in TiMg<sub>5</sub> clusters, the H<sub>2</sub> molecule starts to dissociate. The bond length between the hydrogen atoms increases, as shown in Fig. 6.10(b-c). After complete dissociation, the hydrogen atoms drift towards the reactive sites of the clusters and make bonds, as shown in Fig. 6.10(d-f). Various sections of Fig. 6.10, including the ELF plot, explain that the H<sub>2</sub> molecule is first physisorbed in the cluster plane with Ti-atom by weak Van der Waals forces, then the molecule splits. In the next step, it gets diffused towards reactive Mg atoms of the



cluster, and chemisorbed, making bonding with the reactive cluster. The ELF plot of supported TiMg<sub>5</sub>-2H cluster after diffusion of hydrogen atoms at the reactive site is also shown in Fig 6.10. Thus, all steps of hydrogenation [30] were completed.

**Table 6.1 Calculated data of various parameters associated with the supported clusters. All units are in eV.**

Rectangular Mg <sub>18</sub> O <sub>18</sub> Substrate + Mg <sub>n</sub>							Rectangular Mg <sub>18</sub> O <sub>18</sub> Substrate+TiMg <sub>n</sub>					
n	E <sub>ads</sub>	Gap	VIP	VEA	μ	η	E <sub>ads</sub>	Gap	VIP	VEA	μ	η
2	-0.59	0.23	3.64	3.42	-3.53	0.11	-2.42	1.94	4.71	2.77	-3.74	0.97
3	-0.43	0.39	3.66	3.27	-3.46	0.20	-2.19	1.91	4.70	2.79	-3.75	0.96
4	-0.51	0.41	3.81	3.40	-3.61	0.21	-2.15	1.89	4.57	2.68	-3.63	0.95
5	-1.71	0.66	3.95	3.29	-3.62	0.33	-3.17	1.69	4.35	2.67	-3.51	0.84
6	-1.23	0.53	3.88	3.35	-3.61	0.26	-3.74	1.94	4.50	2.56	-3.53	0.97
Rectangular Mg <sub>18</sub> O <sub>18</sub> Substrate+Mg <sub>n</sub> -2H							Rectangular Mg <sub>18</sub> O <sub>18</sub> Substrate+TiMg <sub>n</sub> -2H					
n	E <sub>ads</sub>	Gap	VIP	VEA	μ	η	E <sub>ads</sub>	Gap	VIP	VEA	μ	η
2	-2.52	0.38	3.74	3.36	-3.55	0.19	-1.92	0.24	3.70	3.47	-3.58	0.12
3	-2.97	1.44	4.47	3.03	-3.75	0.72	-2.06	0.64	4.02	3.38	-3.70	0.32
4	-2.69	0.50	4.04	3.55	-3.79	0.25	-2.29	1.12	4.32	3.20	-3.76	0.56
5	-2.87	0.56	4.08	3.52	-3.80	0.28	-2.56	1.64	4.34	2.70	-3.52	0.82
6	-3.74	0.29	3.67	3.38	-3.52	0.14	-2.48	0.96	3.90	2.93	-3.41	0.48

### 6.3.6 Gravimetric Density Enhancement

The most important parameter for a hydrogen storage system is its gravimetric density. We have used the following relation to calculate the gravimetric density analysis only by considering the cluster, not the substrate. Because one may use a substrate of different kinds and sizes, the inclusion of the substrate in the calculation may give different results. Therefore, we have done the calculation without the inclusion of the substrate. Under this consideration, the relation can be given following the work reported by Boruah and Kalita [31]:

$$wt\% \text{ of } H_2 = \frac{N \times m_{H_2}}{(N \times m_{H_2} + m_{Ti} + n \times m_{Mg})} \times 100\% \quad (6.7)$$

N is the number of H<sub>2</sub> molecules adsorbed, n is the number of Mg atoms in the cluster,  $m_{H_2}$ ,  $m_{Ti}$ , and  $m_{Mg}$  are the masses of H<sub>2</sub> molecule, Ti atom, and Mg atoms.

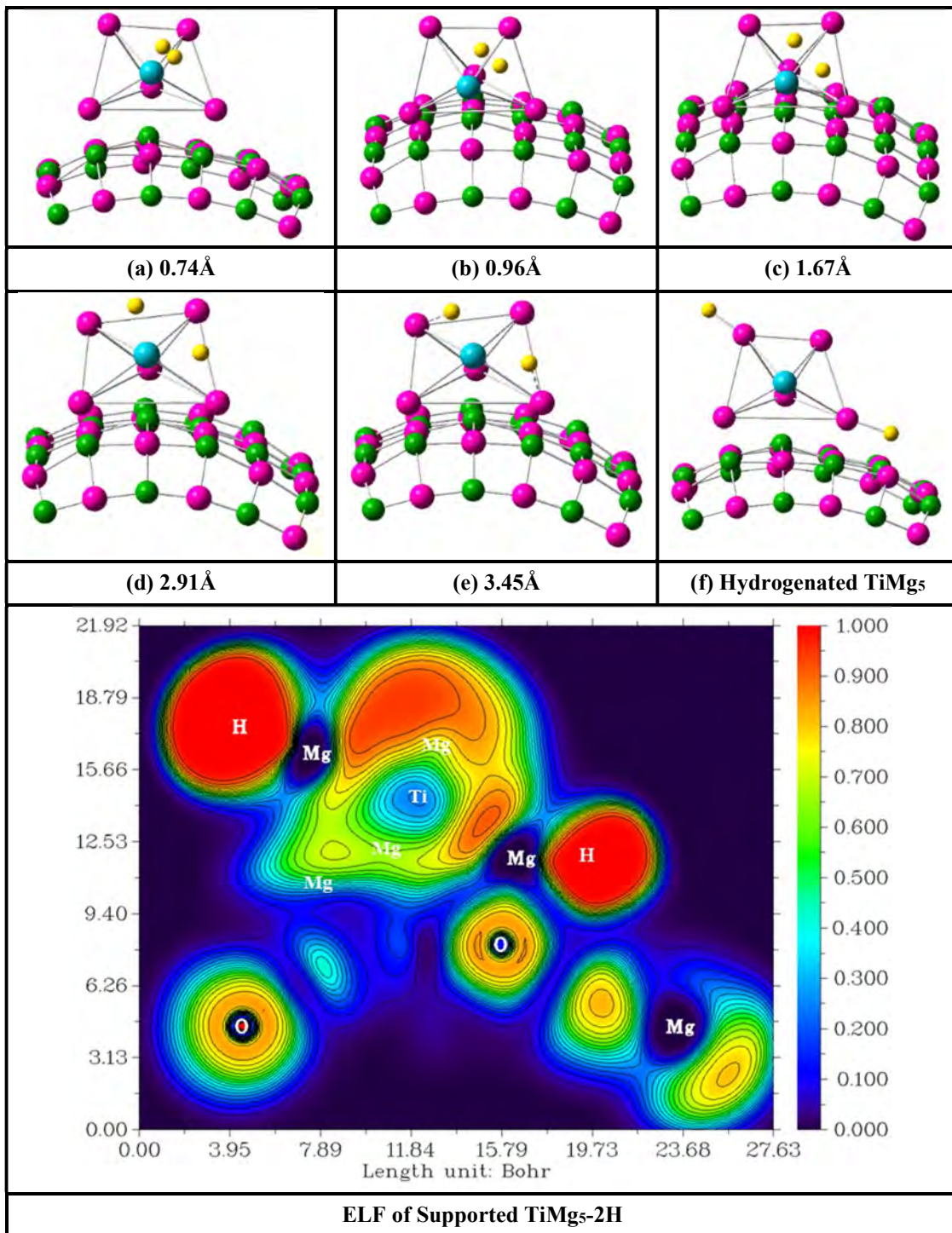
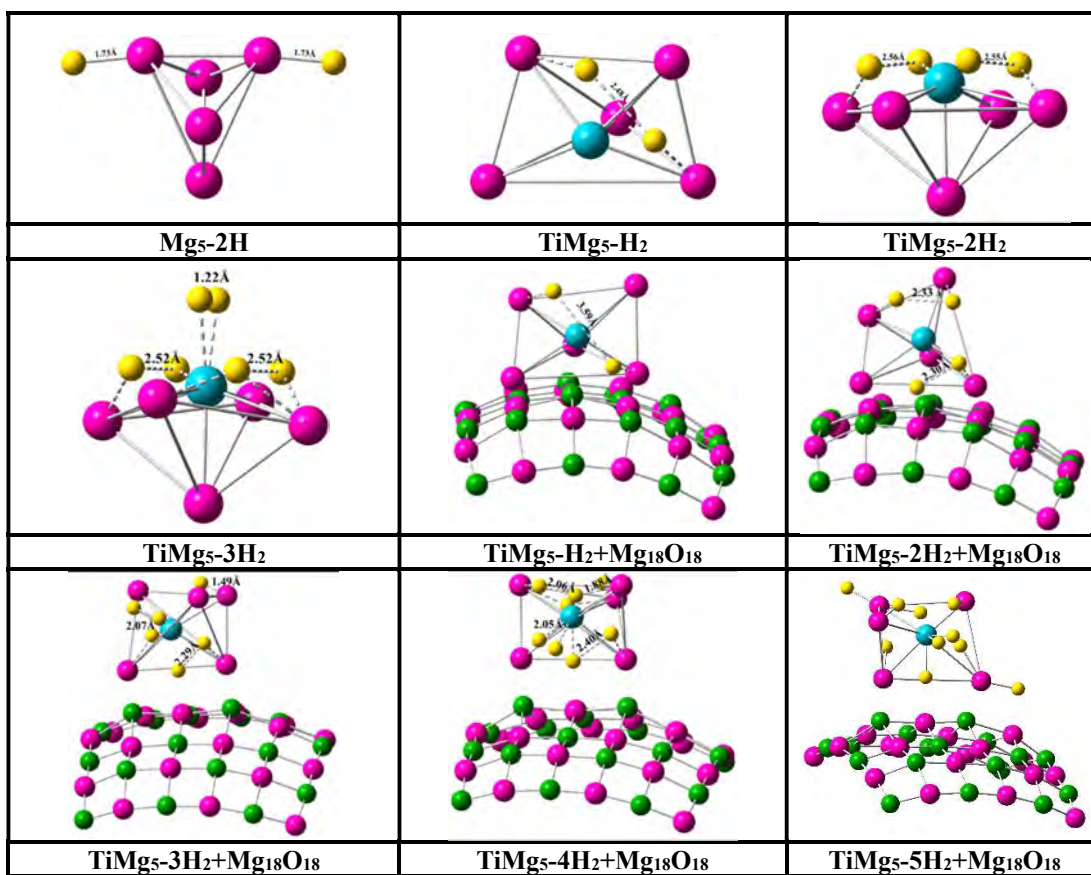


Fig. 6.10 Hydrogen adsorption and dissociation on the reactive surface of supported TiMg<sub>5</sub>. Different stages of drifting of the dissociated hydrogen atoms with atomic separation in Å are shown. ELF of supported TiMg<sub>5</sub>-2H at the final state. The colors in the figure are as per the vertical scale at the extreme right.



**Fig. 6.11** Highest possible H<sub>2</sub> adsorption in pure Mg<sub>5</sub>, TiMg<sub>5</sub>, and supported TiMg<sub>5</sub> cluster systems. Here, Mg atoms are colored by pink, oxygen atoms are shaded as green, Ti as blue and hydrogen as yellow.

It is seen from the study that a bare Mg<sub>5</sub> atom can adsorb only one hydrogen molecule, and after Ti doping, due to the catalytic effect of Ti, three hydrogen molecules can be adsorbed (TiMg<sub>5</sub>). After MgO substrate support, five hydrogen molecules get adsorbed by the system. The activation energy of substrate-supported TiMg<sub>5</sub>-H<sub>2</sub> is seen to be 2.15 eV. The gravimetric density enhances from 1.63 wt.% in bare Mg<sub>5</sub> to 3.45 wt.% in the TiMg<sub>5</sub> cluster. Finally, it reaches 5.62 wt.% in the supported system. So, it is clear that the dose increases from the pure Mg<sub>5</sub> cluster to the supported TiMg<sub>5</sub> system. The optimized Mg<sub>5</sub>-H<sub>2</sub>, TiMg<sub>5</sub>-3H<sub>2</sub>, and Substrate-supported TiMg<sub>5</sub>-5H<sub>2</sub> cluster systems are shown in Fig. 6.11. Fig. 6.12 shows that the pure Mg<sub>5</sub> cluster throws away the second hydrogen molecule, and the TiMg<sub>5</sub> cluster throws away the fourth hydrogen molecule after the saturation of the maximum ability to store hydrogen. Also, the bare TiMg<sub>5</sub> cluster gets highly distorted during this process. This confirms

that pure Mg<sub>5</sub> clusters can adsorb only one hydrogen molecule, and TiMg<sub>5</sub> clusters can adsorb up to three hydrogen molecules.

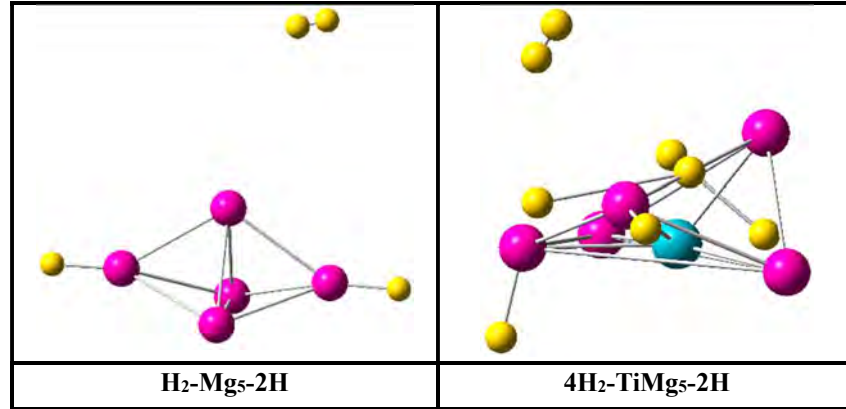


Fig. 6.12 Repelling of additional hydrogen molecule beyond the dose limit. Here, Mg atoms are colored by pink, Ti as blue and hydrogen as yellow.

### 6.3.7 Binding Energy

One can calculate the binding energy of a non-supported TiMg<sub>5</sub> cluster as

$$(BE)_{TiMg_5+mH_2} = \frac{[(E_{TiMg_5}) + (E_{mH_2}) - (E_{TiMg_5+mH_2})]}{(5 + 1 + m)} \quad (6.8)$$

Where m is the number of H<sub>2</sub> molecules adsorbed. For one H<sub>2</sub> molecule, the BE/H comes out to be 0.478 eV, for two H<sub>2</sub> molecules it comes 0.388 eV and for three H<sub>2</sub> molecules it is 0.314 eV. One can calculate the hydrogen binding energy of a supported TiMg<sub>5</sub> cluster as

$$(BE)_{Substrate+TiMg_5+mH_2} = \frac{[(E_{Substrate+TiMg_5}) + (E_{mH_2}) - (E_{Substrate+TiMg_5+mH_2})]}{(5 + 1 + m)} \quad (6.9)$$

Where, m is the number of H<sub>2</sub> molecules adsorbed.

In the calculation, the atoms of the substrate not considered since hydrogen adsorption occurs only at the reactive sites of the cluster. For one hydrogen molecule adsorption the BE/H becomes 1.088 eV, for two hydrogen molecules adsorption the value is 0.798 eV and for three hydrogen molecules adsorption it is 0.566 eV for four hydrogen molecule adsorption it becomes 0.471 eV, and for five hydrogen molecules adsorption it becomes 0.416 eV. Thus, binding energy falls as more and more H<sub>2</sub> molecules are adsorbed.

### 6.3.8 Relative Stability

During growth process the second-order change in energy is considered as the local thermodynamic stability parameter of the system by definition. The stability of the MgO (100) Mg<sub>18</sub>O<sub>18</sub> substrate-supported non-hydrogenated and hydrogenated cluster systems have been calculated from the relations equations (6.10-6.14) below.

$$\Delta_{2(\text{TiMg}_n)} = E_{\text{TiMg}_{n-1}} + E_{\text{TiMg}_{n+1}} - 2E_{\text{TiMg}_n} \quad (6.10)$$

$$\Delta_{2(\text{Mg}_n+\text{sub})} = E_{\text{Mg}_{n-1}+\text{sub}} + E_{\text{Mg}_{n+1}+\text{sub}} - 2E_{\text{Mg}_n+\text{sub}} \quad (6.11)$$

$$\Delta_{2(\text{TiMg}_n+\text{sub})} = E_{\text{TiMg}_{n-1}+\text{sub}} + E_{\text{TiMg}_{n+1}+\text{sub}} - 2E_{\text{TiMg}_n+\text{sub}} \quad (6.12)$$

$$\Delta_2 = E_{(\text{Mg}_{n-1}-2\text{H})+\text{sub}} + E_{(\text{Mg}_{n+1}-2\text{H})+\text{sub}} - 2E_{(\text{Mg}_n-2\text{H})+\text{sub}} \quad (6.13)$$

$$\Delta_{2(\text{TiMg}_n-2\text{H})+\text{sub}} = E_{(\text{TiMg}_{n-1}-2\text{H})+\text{sub}} + E_{(\text{TiMg}_{n+1}-2\text{H})+\text{sub}} - 2E_{(\text{TiMg}_n-2\text{H})+\text{sub}} \quad (6.14)$$

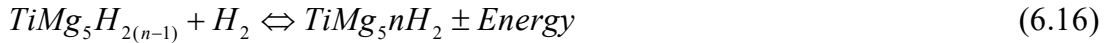
The variations of stability of free clusters and substrate-supported cluster systems are compared in Table 6.2.

<b>Table 6.2 Comparative stability study in (eV) of Mg<sub>n</sub> clusters. All units are in eV</b>		
Clusters	Without substrate	With rectangular Mg <sub>18</sub> O <sub>18</sub> substrate
Mg <sub>5</sub>	0.076	1.610
Mg <sub>5</sub> -2H	-0.551	1.060
TiMg <sub>5</sub>	-0.245	0.209
TiMg <sub>5</sub> -2H	-0.323	0.555

It is clear from the study that, after substrate support, the strength of the pure Mg<sub>5</sub> cluster increases noticeably, but after hydrogenation, the system becomes unstable. After substrate support, the Ti-doped Mg<sub>5</sub> (TiMg<sub>5</sub>) cluster system's stability is enhanced by 185%, i.e., the TiMg<sub>5</sub> cluster adsorbed suitably on the substrate. After hydrogenation, the system remains very stable, producing a highly durable hydrogen storage system.

### 6.3.9 Reaction Energy and Activation Barrier Energy calculation

The reaction energy is the minimum energy required to start a reaction. The reactions of hydrogenation of the systems can be written as



Reaction energy can be calculated from the difference of total energy of reactants and product as

$$E_{reaction} = E(Mg_5) + E(H_2) - E(Mg_5H_2) \quad (6.18)$$

$$E_{reaction} = E(TiMg_5H_{2(n-1)}) + E(H_2) - E(TiMg_5H_{2n}) \quad (6.19)$$

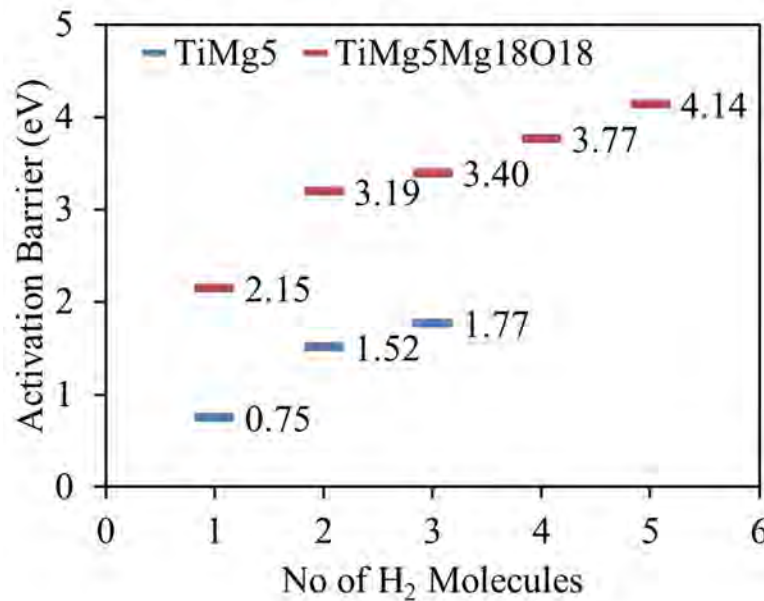
$$E_{reaction} = E(TiMg_5Mg_{18}O_{18}H_{2(n-1)}) + E(H_2) - E(TiMg_5Mg_{18}O_{18}H_{2n}) \quad (6.20)$$

The activation Barrier can be calculated as

$$E_{Activation\ barrier}(bare\ TiMg_5) = E(TiMg_5H_{2(n-1)}) + E(H_2) - E_{TS}(TiMg_5H_{2n}) \quad (6.21)$$

$$E_{Activation\ barrier} = E(TiMg_5Mg_{18}O_{18}H_{2(n-1)}) + E(H_2) - E_{TS}(TiMg_5Mg_{18}O_{18}H_{2n}) \quad (6.22)$$

Due to computational limitations, the transition state of the systems is calculated using TS-Berny and the activation energy is calculated using the above equation (6.21) and (6.22). It is seen that the activation barrier energy tallies well with the values from reaction energy values calculated using equation (6.18) to (6.20).



**Fig. 6.13** The activation barrier energy for successive H<sub>2</sub> adsorption in bare TiMg<sub>5</sub> (blue) and substrate-supported TiMg<sub>5</sub> cluster systems (red).

It is seen that a bare TiMg<sub>5</sub> cluster can adsorb a maximum of three H<sub>2</sub> molecules and for one H<sub>2</sub> molecule adsorption the activation barrier becomes 0.75 eV and for successive 2H<sub>2</sub> and 3H<sub>2</sub> adsorption an extra 1.52 eV and 1.77 eV is required respectively. For substrate-supported TiMg<sub>5</sub> clusters the activation energy for one H<sub>2</sub> molecule is found to be 2.15 eV and an extra energy of 3.19 eV, 3.40 eV, 3.77 eV and 4.14 eV are required for 2H<sub>2</sub>, 3H<sub>2</sub>, 4H<sub>2</sub>, and 5H<sub>2</sub> molecule adsorption respectively (Fig. 6.13).

## ***6.4 Summary and Conclusions***

We have conducted the study of electronic and chemical properties, adsorption energy and stability for different cluster systems on a substrate, particularly focusing on the interaction between clusters and hydrogen molecules from the variation of different thermodynamic (VIP) and chemical parameters (HOMO-LUMO Gap,  $\mu$ , and  $\eta$ ) with the cluster size. The existence of local minima at n=5 size in the variation in VIP indicates the cluster's higher reactivity for this size. Further, we found the same system (supported TiMg<sub>n</sub>) gains stability at n=5 after hydrogen adsorption. There is a local dip in VIP for supported TiMg<sub>5</sub> and local peak after hydrogenation. After hydrogen adsorption onto both the supported Mg<sub>5</sub> and TiMg<sub>5</sub> clusters, there are local maxima in chemical hardness. In the case of chemical potential, the supported Mg<sub>5</sub> and Mg<sub>5</sub>-2H hold local minima and supported TiMg<sub>5</sub> holds local maxima which implies higher chemical reactivity. After hydrogenation, supported TiMg<sub>5</sub> holds local maxima in chemical hardness, indicating higher stability, but there is no local maxima or minima in chemical potential. However, the nature of chemical potential shows increasing nature for supported TiMg<sub>5</sub>-2H system as it also holds a certain reactivity. From the variation of the HOMO-LUMO gap of the systems, we found that after hydrogen adsorption, the gap decreases in the supported Mg<sub>5</sub> cluster. However, it is essential to note that the gap is always very high compared to other supported clusters in supported TiMg<sub>n</sub>, with a local dip of n=5. After hydrogen adsorption, the supported TiMg<sub>5</sub>-2H shows a local peak in the HOMO-LUMO gap. This type of behavior of each and every parameter indicates that the chemical reactivity of supported TiMg<sub>5</sub> is very high, as because the bare TiMg<sub>5</sub> cluster holds very good chemical reactivity and higher number of reactive sites. After supporting the TiMg<sub>5</sub> by the substrate

also it holds higher reactivity. After the hydrogen adsorption, the supported  $\text{TiMg}_5$ , i.e., supported  $\text{TiMg}_5\text{-2H}$  holds good stability, as because the number reactive sites get reduced and the reactivity get reduced after the hydrogenation. This indicates that the supported  $\text{TiMg}_5\text{-2H}$  system is the most promising hydrogen storage material. At the end, concerning Fig. 6.10, we can easily conclude that the supported  $\text{TiMg}_5$  cluster is the most efficient size and composition for hydrogen storage and dissociation. We also found that the ability of hydrogen adsorption by the supported  $\text{TiMg}_5$  is higher than the other sizes because of the presence of more reactive site over the cluster surface. The gravimetric density of hydrogen in the bare  $\text{TiMg}_5$  cluster is 3.45 wt.% which gets enhanced to 5.62 wt.% after substrate support. The ELF study of the supported  $\text{TiMg}_5\text{-2H}$  indicates that, even after hydrogenation, the supported  $\text{TiMg}_5\text{-2H}$  can adsorb more hydrogen molecules. So, we could expect the improved gravimetric density in supported  $\text{TiMg}_5$ . Our observations suggest that the interaction between the clusters, substrate, and hydrogen molecules results in a more stable system compared to isolated clusters. Complete study suggests the system could have implications for potential applications as hydrogen storage.



## References

- [1] M.R. Usman, “Hydrogen storage methods: Review and current status”, *Renewable and Sustainable Energy Reviews*, **167**, (2022), 112743. <https://doi.org/10.1016/j.rser.2022.112743>.
- [2] A. Kumar, P. Muthukumar, P. Sharma, and E.A. Kumar, “Absorption-based solid-state hydrogen storage system: A review”, *Sustainable Energy Technologies and Assessments*, **52**, (2022), 102204. <https://doi.org/10.1016/j.seta.2022.102204>
- [3] J. Zheng, C.G. Wang, H. Zhou, E. Ye, J. Xu, Z. Li, and X.J. Loh, “Current Research Trends and Perspectives on Solid-State Nanomaterials in Hydrogen Storage”, *Research*, **2021**, (2021), 39 pages. <https://doi.org/10.34133/2021/3750689>
- [4] D. Bandyopadhyay, “Study of pure and doped hydrogenated germanium cages: a density functional investigation,” *Nanotechnology*, **20(27)**, (2009), 275202(1-12). <http://doi.org/10.1088/0957-4484/20/27/275202>
- [5] B. Bogdanovi, and M. Schwickardi, “Ti-doped alkali metal aluminum hydrides as potential novel reversible hydrogen storage materials”, *J Alloys Compd*, **253–254**, (1997), 1-9. [https://doi.org/10.1016/S0925-8388\(96\)03049-6](https://doi.org/10.1016/S0925-8388(96)03049-6)
- [6] F. Zuliani, L. Bernasconi and E.J. Bacrends, “Titanium as a Potential Addition for High-Capacity Hydrogen Storage Medium”, *Journal of Nanotechnology*, **2012**, (2012), 831872-9. <https://doi.org/10.1155/2012/831872>
- [7] R. Trivedi, and D. Bandyopadhyay, “Hydrogen storage in small size Mg<sub>n</sub>Co clusters: A density functional study”, *Int. J. Hydrogen Energy*, **40(37)**, (2015), 12727-12735. <https://doi.org/10.1016/j.ijhydene.2015.07.122>
- [8] R. Trivedi, and D. Bandyopadhyay, “Study of adsorption and dissociation pathway of H<sub>2</sub> molecule on Mg<sub>n</sub>Rh (n=1-10) clusters: A first principle investigation”, *Int. J. Hydrogen Energy*, **41(44)**, (2016), 20113-20121. <https://doi.org/10.1016/j.ijhydene.2016.09.007>
- [9] R. Intayot, C. Rungnim, S. Namuangruk, N. Yodsin, and S. Jungstittiwong, “Ti<sub>4</sub>-Decorated B/N-doped graphene as a high-capacity hydrogen storage material: a DFT study”, *Dalton Trans*, **50(33)**, (2021), 11398-11411. <http://dx.doi.org/10.1039/D1DT01498F>

- [10] I.N. Chen, S.Y. Wu, and H.T. Chen, "Hydrogen storage in N- and B-doped graphene decorated by small platinum clusters: A computational study", *Applied Surface Science*, **441**, (2018), 607-612. <https://doi.org/10.1016/j.apsusc.2018.02.106>.
- [11] H. Shi, M.A. Scott, and A. Ramasubramaniam, "First-Principles Predictions of Structure–Function Relationships of Graphene-Supported Platinum Nanoclusters", *J. Phys. Chem. C*, **120(22)**, (2016), 11899-11909. <http://dx.doi.org/10.1021/acs.jpcc.6b01288>
- [12] S. Nigam, and C. Majumder, "Substrate induced reconstruction and activation of platinum clusters: A systematic DFT study", *Applied Surface Science*, **422**, (2017), 1075-1081. <https://doi.org/10.1016/j.apsusc.2017.06.041>
- [13] R. Hussain, M. Saeed, M.Y. Mehboob, S.U. Khan, M.U. Khan, M. Adnan, M. Ahmed, J. Iqbal, and K. Ayub, "Density functional theory study of palladium cluster adsorption on a graphene support", *RSC Adv*, **10(35)**, (2020), 20595-20607. <http://doi.org/10.1039/D0RA01059F>
- [14] M.M. Fadlallah, A.G. Abdelrahman, U. Schwingenschlögl, and A.A. Maarouf, "Graphene and Graphene nanomesh supported nickel clusters: electronic, magnetic, and hydrogen storage properties", *Nanotechnology*, **30(8)**, (2019), 085709. <https://doi.org/10.1088/1361-6528/aace3c>
- [15] L. Núria, I. Francesc, and P. Gianfranco, "Electronic Effects in the Activation of Supported Metal Clusters: Density Functional Theory Study of H<sub>2</sub> Dissociation on Cu/SiO<sub>2</sub>", *J. Phys. Chem. B*, **103(40)**, (1999), 8552-8557. <https://doi.org/10.1021/jp991655t>
- [16] L.N. Kantorovich, A.L. Shluger, P.V. Sushko, J. Günster, P. Stracke, D.W. Goodman, and V. Kemper, "Mg clusters on MgO surfaces: study of the nucleation mechanism with MIES and abinitio calculations", *Faraday Discuss*, **114**, (1999), 173-194. <https://doi.org/10.1039/A903241J>
- [17] Y.G. Zhang, H.Y. He, and B.C. Pan, "Structural Features and Electronic Properties of MgO Nanosheets and Nanobelts", *J. Phys. Chem. C*, **116(43)**, (2012), 23130-23135. <https://doi.org/10.1021/jp3077062>

- [18] B. Luo, Y. Yao, E. Tian, H. Song, X. Wang, G. Li, H. Xi, B. Li, H. Song, and L. Li, “Graphene like monolayer monoxides and monochlorides”, *PNAS*, **116(35)**, (2019), 17213-17218. <https://doi.org/10.1073/pnas.1906510116>
- [19] V.V. On, J.G. Sanchez, and D.M. Hoat, “Tuning the electronic and magnetic properties of MgO monolayer by nonmetal doping: A First Principles investigation”, *Material today Commum*, **34**, (2023), 105422. <https://doi.org/10.1016/j.mtcomm.2023.105422>
- [20] V.V. On, J.G Sanchez, R.P. Perez, T.V. Vu, J.F.R. Silva, G.H. Cocolletzi, and D.M. Hoat, “Defective and Doped MgO monolayer as promising 2D materials for optoelectronic and spinotronics applications”, *Material Science in Semiconductor Processing*, **149**, (2022), 106876. <https://doi.org/10.1016/j.mssp.2022.106876>
- [21] R. Hazarika, and B. Kalita, “Electronic structure alteration in MgO monolayer through alkali metal doping”, *Materials Today proc*, (2023) (available online on 11 May 2023). <https://doi.org/10.1016/j.matpr.2023.04.619>
- [22] M.J. Frisch, G.W. Trucks, H.B. Schlegel, G.E. Scuseria, M.A. Robb, J.R. Cheeseman, G. Scalmani, V. Barone, G.A. Mennucci Petersson, H. Nakatsuji, M. Caricat, X. Li, H.P. Hratchian, A.F. Izmaylov, Bloino, J.G. Zheng, J.L. Sonnenberg, M. Hada, M. Ehara, K. Toyota, R. Fukuda, J. Hasegawa, M. Ishida, T. Nakajima, Y. Honda, O. Kitao, H. Nakai, Jr. T. Vreven,, J.A. Montgomery, F. Peralta, J.E. Ogliaro, M. Bearpark, J.J. Heyd, E. Brothers, K.N. Kudin, V.N. Staroverov, T. Keith, R. Kobayashi, J. Normand, K. Raghavachari, A. Rendell, J.C. Burant, S.S. Iyengar, J. Tomasi, M. Cossi, N. Rega, J.M. Millam, M. Klene, J.E. Knox, J.B. Cross, V. Bakken, C. Adamo, J. Jaramillo, R. Gomperts, R.E. Stratmann, O. Yazyev, A.J. Austin, R. Cammi, C. Pomelli, J.W. Ochterski, R.L. Martin, K. Morokuma, V.G. Zakrzewski, G.A. Voth, P. Salvador, J.J. Dannenberg, S. Dapprich, A.D. Daniels, O. Farkas, J.B. Foresman, J.V. Ortiz, J. Cioslowski, D.J. Fox. ; 2013 Gaussian’09, Revision D.01, Gaussian, Inc., Wallingford C.
- [23] A.D. Becke, “Density-functional exchange-energy approximation with correct asymptotic behavior”, *Phys. Rev. A*, **38(6)**, (1988), 3098–3100. <https://doi.org/10.1103/PhysRevA.38.3098>

- [24] C. Lee, W. Yang, and R.G. Parr, "Development of the Colle-Salvetti correlation energy formula into a functional of the electron density", *Phys. Rev. B*, **37(2)**, (1988), 785-789. <http://aps.org/doi/10.1103/PhysRevB.37.785>.
- [25] T. Koopmans, "About the assignment of wave functions and eigenvalues to the individual electrons of an atom", *Physica*, **1**, (1934), 104-113. [https://doi.org/10.1016/S0031-8914\(34\)90011-2.4410](https://doi.org/10.1016/S0031-8914(34)90011-2.4410)
- [26] D. Bandyopadhyay, S. Chatterjee, R. Trivedi, and K. Dhaka, "Insights into catalytic behavior of TiMg<sub>n</sub> (n=1–12) nanoclusters in hydrogen storage and dissociation process: A DFT investigation", *Int. J. of Hydrogen Energy*, **47(27)**, (2022), 13418-13429. <https://doi.org/10.1016/j.ijhydene.2022.02.091>
- [27] C. Liu, Z. Yu, D. Neff, A. Zhamu, and B.Z Jang, "Graphene-Based Supercapacitor with an ultrahigh energy density", *Nano Letters*, **10(12)**, (2010), 4863-4868. <https://doi.org/10.1021/nl102661q>
- [28] S. Chatterjee, and D. Bandyopadhyay, "Insights into the Electronic Structure and Stability of TiMg<sub>n</sub> (n=1-12) Clusters: Validation of Electron Counting Rule", *Materials Today Communications*, **32**, (2022), 103860. <https://doi.org/10.1016/j.mtcomm.2022.103860>
- [29] T. Lu, and F. Chen, "Multiwfn: A multifunctional wave function analyzer", *J. Comp. Chem.*, **33(5)**, (2012), 580-592. <https://doi.org/10.1002/jcc.22885>
- [30] P. Pal, J.M. Ting, S. Agarwal, T. Ichikawa, and A. Jain, "The Catalytic Role of D-block Elements and Their Compounds for Improving Sorption Kinetics of Hydride Materials: A Review", *Reactions*, **2(3)**, (2021), 333-364. <https://doi.org/10.3390/reactions2030022>
- [31] B. Boruah, and B. Kalita, "Exploring enhanced hydrogen adsorption on Ti-doped Al nanoclusters: A DFT study", *J. Chem. Phys.*, **518**, (2019), 123-133. <https://doi.org/10.1016/j.chemphys.2018.04.018>.

## CHAPTER-7

---

### CONCLUSIONS AND SCOPE FOR FUTURE WORK

#### 7.1 CONCLUSIONS

In the present study, Magnesium clusters have been modeled and investigated. In order to design and study a hydrogen storage material, the thesis work is planned to complete in two parts. In the first part, the electronic, thermodynamic, chemical properties of pure and transition metal (TM) doped magnesium clusters are studied. In the second part, the hydrogenation, dehydrogenation and other properties of the free clusters as well as substrate-supported clusters are studied.

At first (Chapter 3), pure Magnesium (Mg) clusters and their isomers of size  $n=2-20$  atoms are modeled with B3LYP functionals and 6-311G(d) basis set using Gaussian'09. Taking global minimum structures bond lengths, the electronic, thermodynamic, and chemical properties like binding energy, HOMO-LUMO, vertical electron affinity (VEA), vertical ionization potential (VIP), chemical hardness ( $\eta$ ), chemical potential ( $\mu$ ), electrostatic potential map (MEP), etc., are studied. Molecular surfaces, natural bond orbitals, charge transfer from Mg atoms, dipole moment, Polarizability and reactive sites are studied.

Next, Transition metal (TM=Ti) has been encapsulated /doped endohedrally as well as exohedrally with pure  $Mg_n$  clusters (Chapter 4) and all the properties mentioned above have been studied for TM-doped  $Mg_n$  ( $n=2-20$ ) clusters. In addition to the energy parameters mentioned above, the electron localization function (ELF), Nucleus independent chemical shift (NICS), and critical points (CPs) of the  $TiMg_8$  cluster are studied. IR and Raman of all the clusters also have been studied and it has been found that the  $TiMg_8$  cluster is a highly stable cluster which holds closed shell configuration and can be considered as jellium-clusters as well as a “magic cluster”.

After, studying  $TiMg_n$  clusters, the hydrogenation of  $TiMg_n$  clusters has been studied (Chapter 5). After adding hydrogen to the  $TiMg_n$  clusters, all the above properties like binding energy, HOMO-LUMO, stability, VIP, VEA, chemical hardness, chemical potential, NBO (Natural

bond orbitals), electron localization function (ELF), IRC (Intrinsic reaction coordinate) of these hydrogenated clusters have been studied. Results reveals that pure  $Mg_n$  clusters are not very impressive hydrogen storage material. It cannot split a gaseous  $H_2$  molecule for adsorption. Only it can adsorb hydrogen atoms. Intensive investigation it shows that the  $TiMg_5$  cluster is the most promising hydrogen storage cluster. The catalytic effects of Ti on  $Mg_n$  clusters also are studied. It also has been found that the  $TiMg_5$  cluster can adsorb up to 3  $H_2$  molecules. Here, the  $H_2$  molecules are first physisorbed, then splitting of hydrogen molecule to hydrogen atoms occur due to catalytic effect of TM molecule. The hydrogen atoms then diffuse to reactive sites of the cluster and get chemisorbed. During dissociation, the hydrogen atoms get detached from the reactive sited and diffused to form hydrogen molecule. From the IRC curves (Fig. 5.12), the IRC of  $Mg_5-2H$  and  $TiMg_5-2H$ , it can be seen that the potential barrier reduces by 32.8% due to catalytic effect of Ti doping. The gravimetric density goes up to 3.45 wt.% at NTP. In respect of desorption due to the catalytic effect of Ti the bond length between Mg-H increases, which means that the H atoms a more loosely bound with the Mg atoms and can be detached applying lower energy.

Generally, the clusters, which are good for hydrogen storage, possess good chemical reactivity and less thermodynamic and chemical stability. An atomic cluster holds less stability means the cluster may be good for hydrogen storage but the cluster may break or get distorted during the hydrogenation/ de-hydrogenation process, which is not good. Thus, we need a system that should hold good thermodynamic stability as well as good chemical reactivity so that it can store hydrogen with good efficiency.

In the work, MgO rectangular substrate has been modeled (Chapter 6) Next, after supporting the cluster with the substrate, the hydrogenation of the substrate-supported system has been performed and all the electronic, thermodynamic, and chemical properties like binding energy, HOMO-LUMO, stability, VIP, VEA, chemical hardness, and chemical potential have been studied. Extra hydrogen intake capacity of the substrate-supported  $TiMg_5$  clusters is also studied. Attainment of DOE criteria and height of barrier potential studied and verified consequently. Finally, it is found that, after supporting the clusters with MgO, the supported  $TiMg_5$  cluster holds good chemical reactivity and good thermodynamic stability. After hydrogenation, the supported hydrogenated  $TiMg_5$  i.e., substrate-supported  $TiMg_5-2H$  system shows both good thermodynamic stability and good chemical stability. Not only that it also

has been found that Substrate supported  $\text{TiMg}_5$  cluster can store 5  $\text{H}_2$  molecules whereas free  $\text{TiMg}_5$  cluster can store up to 3 $\text{H}_2$  molecules. Thus, one can claim that the hydrogen storage efficiency increased by 62.89 % after supporting the  $\text{TiMg}_5$  cluster with MgO substrate. The highest gravimetric density of Ti-doped  $\text{Mg}_5$  clusters is found to be 3.45 wt.% which get enhanced due to MgO support to 5.62 wt.%. Thus, the target of the thesis work successfully achieved as, finally a well-capable hydrogen storage system found that holds good thermodynamic stability and recyclability up to three cycles. It is noticed that in Ti doped Magnesium clusters the bond length Mg-H increases in presence of MgO from 1.73Å to 1.93Å. So, it can be said that Ti doping and MgO support effectively weakens Mg-H bond as a result desorption energy and temperature will be less.

## 7.2 FUTURE SCOPE OF WORK

The current research has extensively explored the electronic, thermodynamic, and chemical properties of pure  $\text{Mg}_n$ , Ti-doped  $\text{Mg}_n$ , and substrate-supported Ti encapsulated  $\text{Mg}_n$  clusters, along with the hydrogenation of these systems. Looking ahead, several future directions emerge:

- 1. Experimental Validation:** This work is theoretical; thus, the logical next step is conducting experimental investigations corresponding to the theoretical studies. Experimental verification is crucial to validate the practical applicability of the findings. This step is imperative for translating theoretical insights into tangible applications.
- 2. Applications of  $\text{TiMg}_8$  Cluster:** The study identifies  $\text{TiMg}_8$  as the most stable cluster with a closed-shell configuration and a HOMO-LUMO energy gap of 1.45 eV, placing it within the ideal range for solar absorption band gaps. Given its exceptional stability,  $\text{TiMg}_8$  holds potential applications in photovoltaic cells, fluorescent-bio imaging, various electronic devices, and industrial applications. Future experimental investigations on  $\text{TiMg}_8$  could unveil practical, real-life applications.
- 3. Extended Investigation on Larger Clusters:** While this thesis reports on the hydrogen storage properties of  $\text{TiMg}_n$  clusters for  $n=2-20$ , future research should extend this investigation to clusters with  $n>20$ . Exploring larger clusters is crucial for understanding the scalability and potential limitations of the proposed hydrogen storage materials.

**4. Exploration of Alternative Substrates:** The thesis introduces a specific substrate-supported system for hydrogen storage. However, future research should delve into the exploration of alternative substrates, both 2D and 3D. A broader investigation into various substrates will likely reveal additional hydrogen storage materials, contributing to the ongoing efforts to address current energy and air pollution challenges.

In summary, the future scope of this research encompasses experimental validation, further exploration of specific clusters, investigation into larger clusters, and the exploration of alternative substrates. These endeavors will enhance the understanding of the studied systems and contribute to developing practical solutions for pressing energy and environmental issues.



## LIST OF PUBLICATIONS OF THE AUTHOR

1. D. Bandyopadhyay, **Soham Chatterjee**, R. Trivedi, and K. Dhaka, “Insights into catalytic behavior of  $\text{TiMg}_n$  ( $n=1-12$ ) nanoclusters in hydrogen storage and dissociation process: A DFT investigation”, *Int. J. of Hydrogen Energy*, **47(27)**, (2022), 13418-13429. <https://doi.org/10.1016/j.ijhydene.2022.02.091>.
2. **Soham Chatterjee**, and D. Bandyopadhyay, “Insights into the electronic structure and stability of  $\text{TiMg}_n$  ( $n=1-12$ ) clusters: validation of electron counting rule”, *Materials Today Communications*, **32**, (2022), 103860. <https://doi.org/10.1016/j.mtcomm.2022.103860>
3. **Soham Chatterjee**, and Debashis Bandyopadhyay, “Further Studies on Hydrogenation/Dehydrogenation characteristics of Ti doped  $\text{Mg}_n$  ( $n=2-8$ ) nanoclusters: A density functional study”, Communicated.
4. **Soham Chatterjee**, and Debashis Bandyopadhyay, “Hydrogen Storage on MgO Supported  $\text{TiMg}_n$  ( $n=2-6$ ) Clusters: A First Principle Investigation”, *Int. J. of Hydrogen Energy*, **62**, (2024). <https://doi.org/10.1016/j.ijhydene.2024.03.081>

## LIST OF PRESENTATIONS

1. “A Brief Introduction to Density Functional Theory”, Research scholar day presentation, BITS Pilani, 5<sup>th</sup> March 2019.
2. “Supported  $\text{Ti@Mg}_n$  Clusters: Novel way to Model Hydrogen storage system”, Research scholar day presentation, BITS Pilani, 8<sup>th</sup> Feb. 2020.
3. “Electronic Properties and Applications of the Supported Clusters, Nanotubes and Graphene: A Density Functional Investigation”, on 5<sup>th</sup> May, 2020 BITS Pilani.
4. “Exploring High Energy Hydrogen Storage with Ti-doped doped Mg Clusters: A Density Functional Approach” on 5<sup>th</sup> May 2021, BITS Pilani.
5. “Electronic Structures and Stability of  $\text{TiMg}_n$  Clusters and Their Hydrogenation: A Density Functional Approach”, Research scholar day presentation, 2022, BITS Pilani.

6. “Influence of MgO support on stability and electronic properties of pure and Ti-doped  $Mg_n$  ( $n=2-6$ ) clusters: A Density Functional Study”, Research scholar day presentation, March 2023, BITS Pilani.

### **SEMINAR /WORKSHOP PARTICIPATED**

- 1) Participated in the “National Conference on Nanotechnology and advanced materials 2016” organized by BIT, Mesra on 26-27 Sept 2016.
- 2) Participated in “Teaching Learning workshop for next-generation Academicians” at BITS Pilani on 7<sup>th</sup> September 2019.

## Biography of the Author

After completion of Schooling at Hindu School, Kolkata in the year 2013 the author completed 5 year Integrated Masters degree (IMSc) in Physics in first class with distinction from Birla Institute of Technology, Mesra, Ranchi, Jharkhand with specialization Condensed Matter Physics in the year 2018. He worked as a JRF on a DST-SERB research project from December 2018 to December 2021. He worked as BITS Pilani Institute fellow (JRF) from January 2022 and SRF from September 2022.

He has performed experimental research work on Nb:TiO<sub>2</sub> thin film using DC Magnetron and RF Magnetron Sputtering unit in BIT, Mesra during IMSc. Now, his research interest centers on the computational study of solid-state nanoclusters using Density Functional Theory. His prime interest centers in developing non-conventional, clean environment friendly sustainable energy source and catalytic materials. He has expertise and intensive hand-on work experience on Gaussian' 09, Gaussview, Vienna Ab-initio Simulation Package (VASP), LAMMPS, SAMSON connect, BoltzTrap, Multifunctional Wavefunction Analyzer (Multiwfn) program, VMD, VESTA, Quantum Espresso (QE) program, MATLAB etc. He has two peer-reviewed publications in International Journals of repute. He has communicated other two research works to international peer review journals.

## Biography of the Supervisor

Professor Debashis Bandyopadhyay is an experimental and theoretical condensed matter physicist. He obtained his Ph.D. degree from the Indian Institute of Technology (I.I.T.), Kanpur, under the guidance of Professor R.M. Singru, in the field of experimental condensed matter physics. After spending a couple of years in I.I.T. Kanpur as a post-doctoral fellow, he joined Emory University, Atlanta, U.S.A., for his second post-doctoral work. There, he worked on studying the reaction kinetics of several proteins at low temperatures. Then, returning to India, he joined the physics department of BITS, Pilani, Pilani campus. He has a wide range of research experiences in fields like low-temperature physics, gamma-ray spectroscopy, magnetism, industrial material, mineral processing, fuel, alloy phase diagrams, reaction kinetics in biological systems, etc. His primary research focuses on using the Vienna Ab-initio Simulation Package (VASP) to investigate various aspects of the electronic and optical properties, hydrogen storage, phonon dispersion, thermodynamic properties, etc., in 2D and 3D materials. He is engaged as a reviewer for a range of prestigious international journals (more than 25) across multiple fields. Recently, he has been featured in the "World Ranking of Top 2% Scientist" database published by Stanford University in two successive years, 2021 and 2022. He authorized several research papers published in reputed international journals in experimental and theoretical fields. At present, he is a professor in the Department of Physics at BITS Pilani, Pilani campus, Rajasthan, India.